EU Fifth Framework Programme 1998-2002
Energy, Environment and Sustainable Development

Environmental Design of Low Crested Coastal Defence Structures

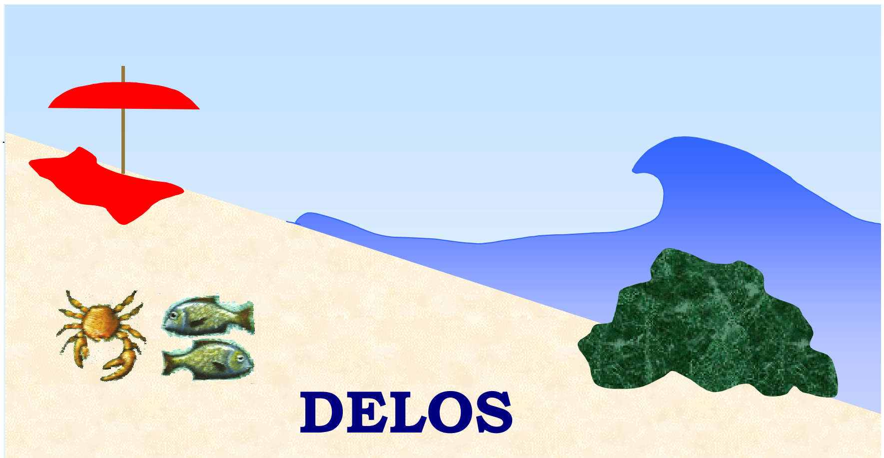

D31
Wave basin experiment final form

Date of preparation: 30.06.2003 **Contract EVK3-CT-2000-00041**

EU Fifth Framework Programme 1998-2002
Energy, Environment and Sustainable Development

Environmental Design of Low Crested Coastal Defence Structures

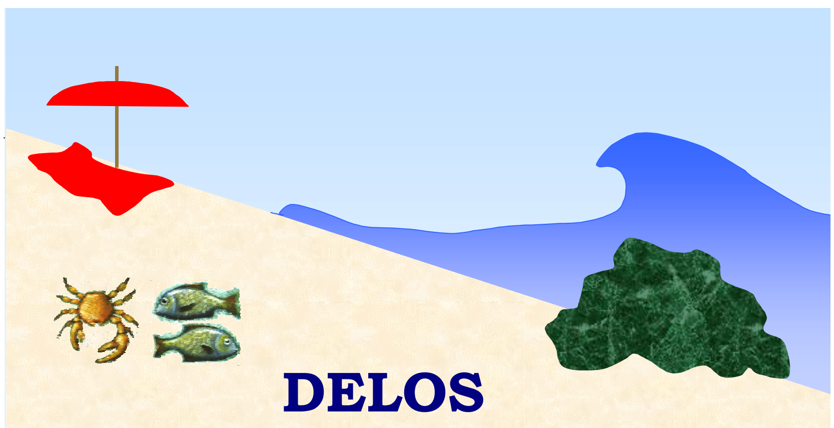

D31
Wave basin experiment final form

- 3D Stability tests at AAU -

By Morten Kramer & Hans Burcharth

DELOS EVK-CT-2000-00041

Contents

1 Introduction

Low-Crested structures (LCS's) are typically built in shallow water as detached breakwaters for coastal protection purposes. The structures are usually parallel to the shoreline with wave attack almost perpendicular to the structure. However under special environmental conditions more oblique waves can occur. Groin systems or breakwaters for harbours where structures are not parallel to shore line are other examples in which oblique wave attack occur.

Numerical models are still too inaccurate to describe the stability phenomenon especially in case of 3D-waves: Therefore numerical models cannot be used in establishment of design formulae.

Several 2D laboratory experiments on trunk armour layer stability of LCS's have been performed in wave channels; see e.g. Ahrens 1987, Van der Meer 1990/1996, Loveless and Debski 1997. To our knowledge only one 3D test series with long crested waves has been carried out on complete LCS's, see Vidal et al. 1992. These tests were carried out in the wave basin at NRC, Canada, 1991-1992 on a 4.7m long structure exposed to irregular head-on waves. The results showed that in some situations the rear head was prone to damage. Only one structure geometry was tested with cross-section slopes 1V:1.5H. The results could therefore only quantify influence of freeboard on the stability for that specific geometry.

The objective of the new LCS stability tests (mainly roundhead but also trunk) was to supplement existing tests in order to identify the influence on rubble stone stability of:

1) Obliquity of short crested waves
2) Wave height and steepness
3) Crest width
4) Freeboard
5) Structure slope

The stability tests were carried out in the short-crested wave basin at Aalborg University in Denmark during the summer 2002.

1.1 Wave basin layout

The wave basin used in the tests has dimensions as shown in Figure 2. The maximum water depth in front of the wavemakers is approximately 0.5 meter (the wavemakers are 0.7 meters high).

Regular and irregular short crested waves with peak periods up to approximately a maximum of 3 seconds can be generated with acceptable result. Oblique 2D and 3D waves can be generated.

Figure 1 Crate filled with sea stones

The absorbing sidewalls are made of crates (121x121cm, 70cm deep) filled with sea stones with D_{n50} of approximately 5cm. The area outside the crates were left empty in all the tests.

The beach was made of quarry rock with D_{n50}=1.5cm.

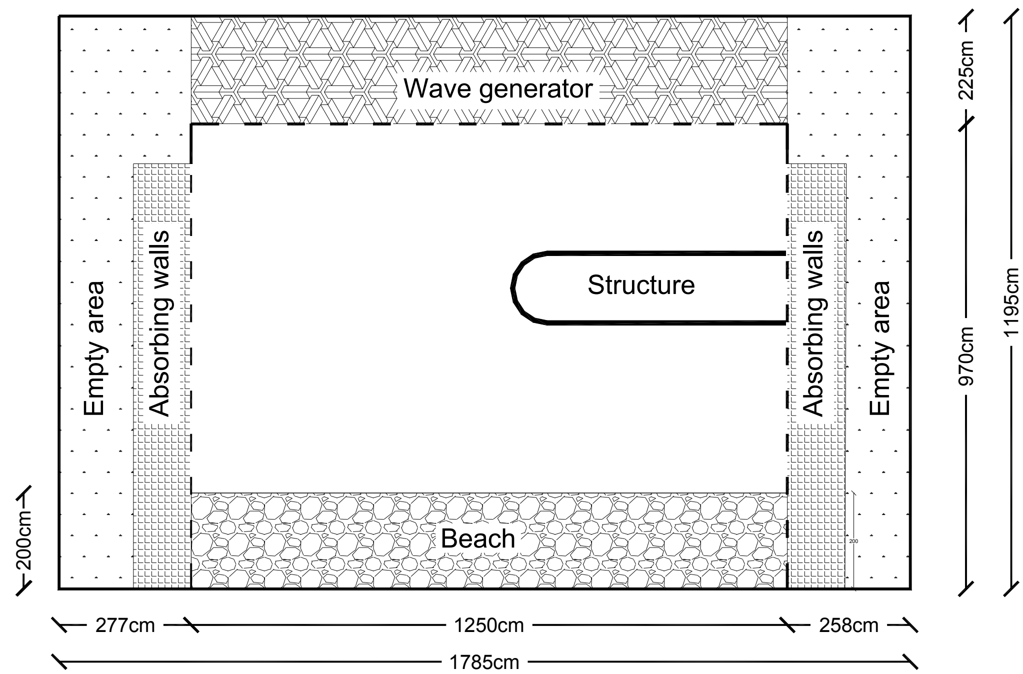

Figure 2 Wave basin layout with position of structure

2 Structural layout and cross sections

The trunk and the roundhead were constructed by carefully selected quarry stones with density 2.65t/m^3. The stones were painted in different colours to identify and quantify damage using digital photos. Two different cross sections were tested at different water levels; see Table 1 and Figure 3. The length of the structure was 5m.

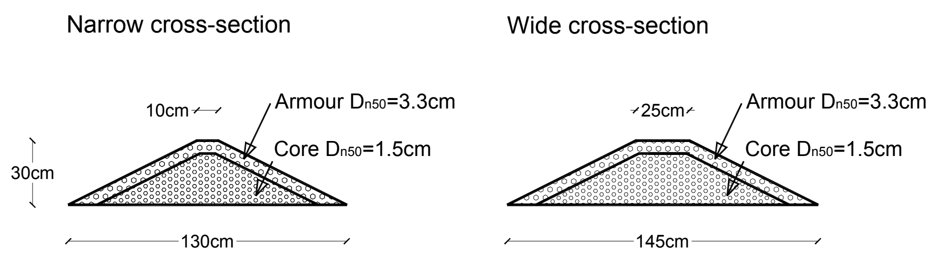

Figure 3 Cross-section geometry

Table 1 Cross-section details

Crest width	0.1m and 0.25m (3D_{n50} and 8D_{n50})
Crest height	0.30m
Front and back slope	1V : 2H
Freeboards	-0.10m, -0.05m, 0.0m and +0.05m
Armour stone size	D_{n50}=0.033m
Core stone size	D_{n50}=0.015m
Thickness of armour layer	0.66m (2D_{n50})

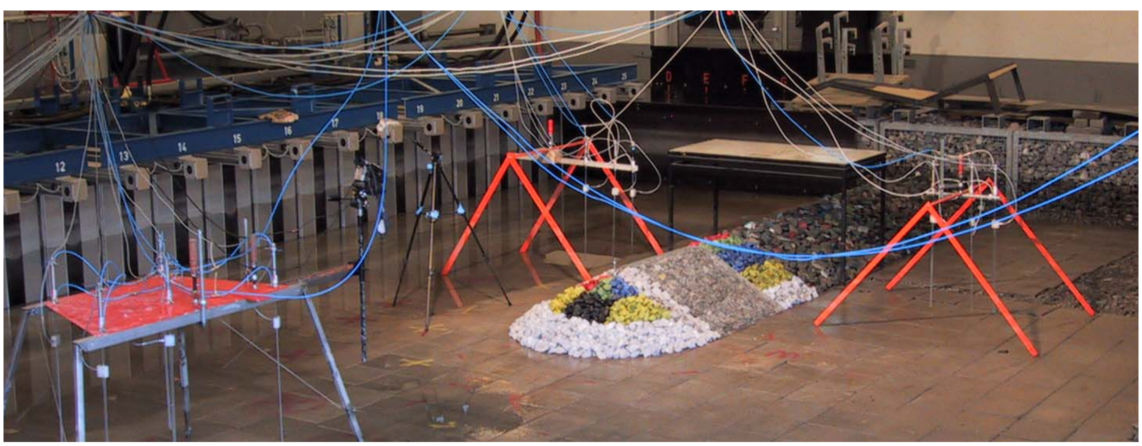

Figure 4 Photo of model

A circular roundhead with crest radius equal to half the trunk crest width was chosen. The structure was located at a plateau 8cm above the seabed at the paddles. The plateau was built by flagstones, and the foreshore slope was poured in concrete. The water level in deep water was varied from 33cm to 48cm, which gives water depths at the structure of 0.25m and 0.40m. This is shown on the following sketch.

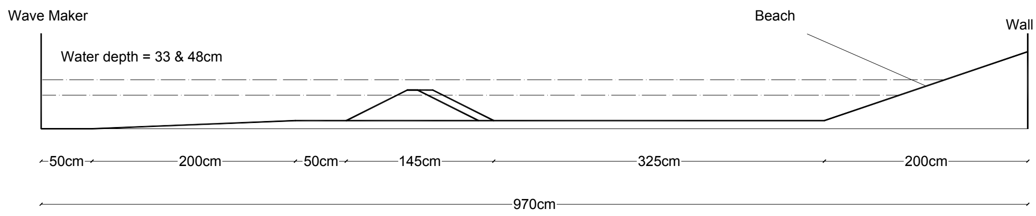

Figure 5 Bottom topography and location of structures in stability tests.

Three types of armour stones were used in model. Carefully selected stones (Type A) were used in the test sections where damage was measured, see Figure 6. Between the trunk and roundhead test section a net with large masks (2x2cm) was covering the surface to avoid damage in that area. This made rebuilding easier and gave less strict specifications for the armour material (Type B). For the dummy section between the side-wall (to the right on Figure 6) and the trunk test section, larger stones (Type C) were used to avoid damage. Type A was used in 15cm ($5 \cdot D_{n50}$) strips on each side of the test sections to ensure correct boundary conditions.

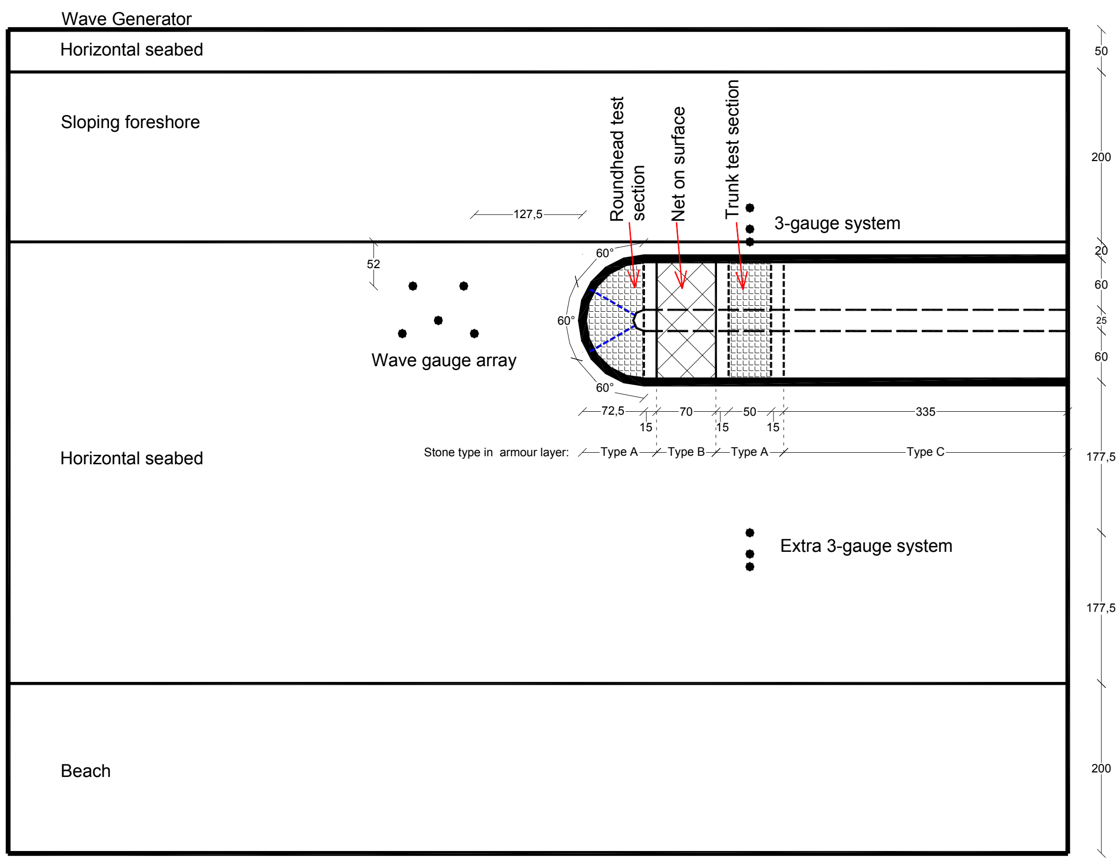

Figure 6 Layout of stability tests, wide structure is shown. Measures in cm.

3 Materials

The rubble stones used for armour layers in the test sections (Type A) were quarry rock with mass density $\rho_s = 2650$ kg/m^3. In order to get well graded armour material in the test sections and to avoid very flat or long stones all the stones were carefully selected manually one-by-one.

All Type A stones were spread out on the floor, mixed, and a random sample containing 169 stones was extracted. Each individual stone was weighed, and the length (X), width (Y) and height (Z) was measured. The length was taken as the longest dimension, and the height as the shortest dimension. Figure 7 (right) shows that 80% of the Type A stones have X/Z<2, and that all stones have X/Z<3. This means that Type A contains no flat or long stones.

The Type B stones contained some flat and long stones but was only used for the dummy trunk section shown in Figure 6. The Type C stones used for the main dummy part of the trunk contained sizes large enough to avoid displacements during the tests.

Stone types A, B and C were narrow graded, cf. Table 2 and Figure 8. For the core was used more wide graded stones (Type D), cf. Table 2 and Figure 8.

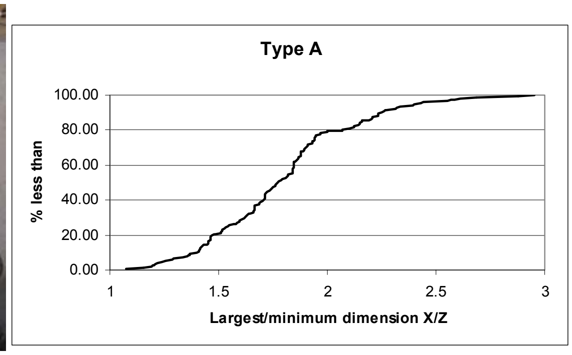

Figure 7 Left: Manual measurements in lab. Right: Curve describing the length/height-ratio.

From each type of material a sample was taken, and the nominal diameter D_n of each individual stone was calculated from the weight W and the mass density ρ_s.

$$D_n = \sqrt[3]{\frac{W}{\rho_s}}$$

Table 2 Nominal diameters for materials

	D_{n50} [cm]	D_{n85} [cm]	D_{n15} [cm]	D_{n85}/D_{n15} -
Type A	3.25	3.60	3.01	1.20
Type B	3.07	3.43	2.68	1.28
Type C	4.74	5.24	4.32	1.21
Type D	1.44	1.83	1.11	1.64

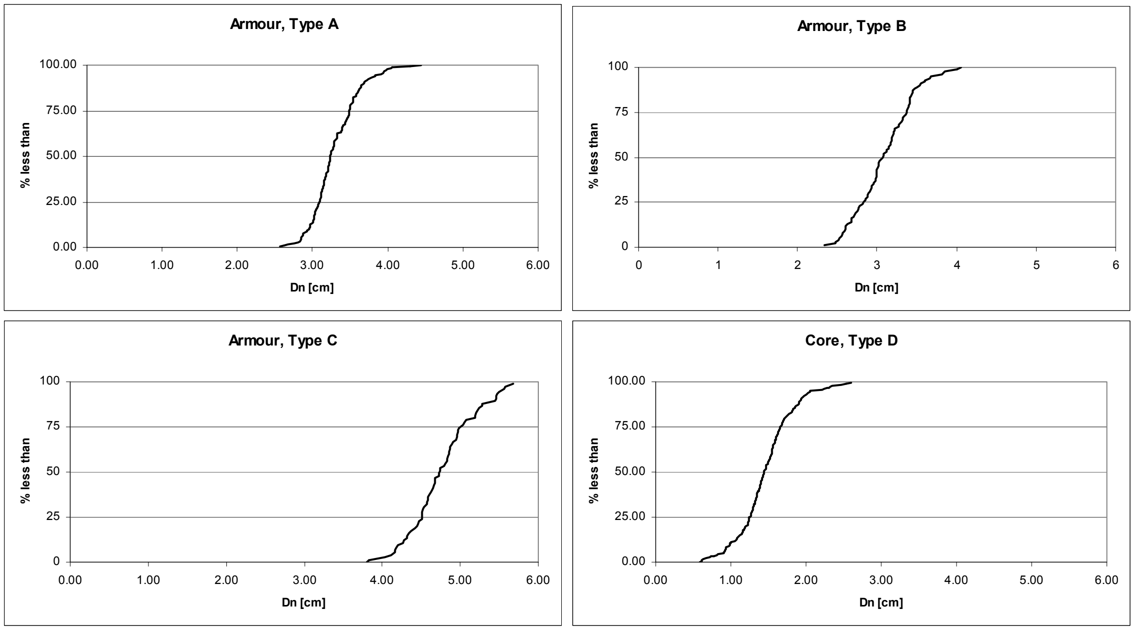

Figure 8 Grading of materials

The porosity (n) for armour Type A and core Type D was calculated in the following way. A sample of stones with bulk volume V was weighed without water in the pores (W_s). The corresponding volume of the voids V_v was measured by adding water to the sample. The porosity was calculated as follows:

Porosity (directly by volume of voids) $= V_v/V$
Porosity (by weight of stone) $= (V - W_s/\rho_s)/V$

A sample size was chosen such that the two estimates gave the same porosity. For Type A V=14 litres was chosen, and for Type D V=2 litres was chosen. The result was $n_{(\text{Type A})} = 0.44$ and $n_{(\text{Type D})} = 0.43$.

To identify damage and to follow each individual stone's path Type A stones were painted in different colours. The stones were immersed in thin paint for a short time and spread out on the floor to dry. In that way only a thin layer of paint was added and the surface roughness of the material was only slightly altered. Seven colour codings were used: Red (R), green (G), blue (B), black (K), white (W), yellow (Y) and no colour (N).

3.1 Building of the breakwater model

Without water in the basin the position of the breakwater was marked with chalk on the seabed. Core material was spread out and a templet constructed in wood was used to ensure correct height and slopes. Armour material was then spread out randomly on the core by pouring the stones from buckets. A templet was used to ensure target slopes and thickness of the armour layer. Manual adjustment of the profile was necessary.

The basin was filled with water such that the water depth was equal to target zero freeboard. The crest height was then given a final adjustment by moving and adding stones such that a precise freeboard was obtained.

4 Wave conditions

In all tests a Jonswap spectra with peak enhancement factor 3.3 and a spreading parameter s=50 was used as input to the wave generator.

4.1 Calibration tests

Initially 34 calibration tests without the model structure in place were performed with irregular 3D waves. The purpose was to ensure that correct wave conditions were reproduced, and to investigate the influence of the sloping foreshore on the wave breaking. Two deepwater wave steepness' s_0=0.02 and s_0=0.04 were tested with four to five wave heights (ranging from no wave breaking to a lot of wave breaking). Four water depths were investigated corresponding to the depths used in the subsequent tests. A wave gauge array consisting of 5 individual gauges was positioned where the roundhead of the breakwater was to be placed in the subsequent experiments. It was confirmed that in case of non breaking waves the wave generator produced a wave spectrum very close to the target. In general most waves started to break on the top edge of the foreshore slope. When a lot of wave breaking took place (more than 50% of the waves were breaking) a significant wave height to water depth ratio of $H_s/h \simeq 0.5$ was observed at the investigated location. In the actual tests with the structure present the waves were depth limited. Wave breaking was therefore important and is described in more detail in chapter 5.

4.2 Actual tests

The target length of each series was 1000 waves. A test block was defined by fixed water level, wave direction, wave steepness, and spreading. In each test block the significant wave height was increased in steps until severe damage was observed. It was attempted to get four tests in each block. However, this was not possible in all blocks due to the progress of the damage. Target conditions were therefore continuous adjusted according to target damage during a tests block. After each block the breakwater was rebuilt. The following describes the procedure applied in a test block.

- Built/rebuilt the structure
- Fix water level, wave direction, steepness and spreading
- Perform test with 1000 waves with small wave height
- Measure damage
- Increase significant wave height and run 1000 waves
- Measure damage
- ...continue to increase the wave height and measure damage until severe damage was observed

Table 3 Target conditions for the narrow-crest structure

Test no.	Test day	Test name	Time [sec]	[°]	Crest width [m]	Free-board [m]	Wave steepness	Hs deep [m]	Tp deep [s]
1	9 July	Test001	1140 (19min)	90	0.1	0.05	0.02	0.05	1.27
2		Test002	1380 (23min)	90	0.1	0.05	0.02	0.075	1.55
3		Test003	1500 (25min)	90	0.1	0.05	0.02	0.1	1.79
4	10 July	Test004	1680 (28min)	90	0.1	0.05	0.02	0.125	2.00
5		Test005	840 (14min)	90	0.1	0.05	0.04	0.05	0.90
6		Test006	1020 (17min)	90	0.1	0.05	0.04	0.075	1.10
7		Test007	1140 (19min)	90	0.1	0.05	0.04	0.1	1.27
8		Test008	1260 (21min)	90	0.1	0.05	0.04	0.125	1.42
9		Test009	1140 (19min)	90	0.1	0	0.02	0.05	1.27
10		Test010	1380 (23min)	90	0.1	0	0.02	0.075	1.55
11		Test011	1500 (25min)	90	0.1	0	0.02	0.1	1.79
12	11 July	Test012	1680 (28min)	90	0.1	0	0.02	0.125	2.00
13		Test013	840 (14min)	90	0.1	0	0.04	0.05	0.90
14		Test014	1020 (17min)	90	0.1	0	0.04	0.075	1.10
15		Test015	1140 (19min)	90	0.1	0	0.04	0.1	1.27
16		Test016	1260 (21min)	90	0.1	0	0.04	0.125	1.42
17		Test017	1380 (23min)	90	0.1	0	0.04	0.15	1.55
18		Test018	1380 (23min)	90	0.1	-0.05	0.02	0.075	1.55
19		Test019	1500 (25min)	90	0.1	-0.05	0.02	0.1	1.79
20		Test020	1680 (28min)	90	0.1	-0.05	0.02	0.125	2.00
21		Test021	1740 (29min)	90	0.1	-0.05	0.02	0.15	2.19
22		Test022	1860 (31min)	90	0.1	-0.05	0.02	0.175	2.37
23	13 July	Test023	1140 (19min)	90	0.1	-0.05	0.04	0.1	1.27
24		Test024	1260 (21min)	90	0.1	-0.05	0.04	0.125	1.42
25		Test025	1380 (23min)	90	0.1	-0.05	0.04	0.15	1.55
26		Test026	1500 (25min)	90	0.1	-0.05	0.04	0.175	1.67
27		Test027	1560 (26min)	90	0.1	-0.05	0.04	0.2	1.79
28		Test028	1680 (28min)	90	0.1	-0.1	0.02	0.125	2.00
29	14 July	Test029	1740 (29min)	90	0.1	-0.1	0.02	0.15	2.19
30		Test030	1860 (31min)	90	0.1	-0.1	0.02	0.175	2.37
31		Test031	1920 (32min)	90	0.1	-0.1	0.02	0.2	2.53
32		Test032	1260 (21min)	90	0.1	-0.1	0.04	0.125	1.42
33		Test033	1380 (23min)	90	0.1	-0.1	0.04	0.15	1.55
34		Test034	1500 (25min)	90	0.1	-0.1	0.04	0.175	1.67
35		Test035	1560 (26min)	90	0.1	-0.1	0.04	0.2	1.79
36		Test036	1620 (27min)	90	0.1	-0.1	0.04	0.225	1.90

Table 4 Target conditions for the wide-crest structure

Test no.	Test day	Test name	Time [sec]	[°]	Crest width [m]	Free-board [m]	Wave steepness	Hs deep [m]	Tp deep [s]
37	16 July	Test037	1140 (19min)	90	0.25	0.05	0.02	0.05	1.27
38		Test038	1380 (23min)	90	0.25	0.05	0.02	0.075	1.55
39		Test039	1500 (25min)	90	0.25	0.05	0.02	0.1	1.79
40		Test040	1680 (28min)	90	0.25	0.05	0.02	0.125	2.00
41		Test041	1140 (19min)	70	0.25	0.05	0.02	0.05	1.27
42		Test042	1380 (23min)	70	0.25	0.05	0.02	0.075	1.55
43		Test043	1500 (25min)	70	0.25	0.05	0.02	0.1	1.79
44		Test044	1680 (28min)	70	0.25	0.05	0.02	0.125	2.00
45		Test045	1140 (19min)	80	0.25	0.05	0.02	0.05	1.27
46		Test046	1380 (23min)	80	0.25	0.05	0.02	0.075	1.55
47	19 July	Test047	1500 (25min)	80	0.25	0.05	0.02	0.1	1.79
48		Test048	1680 (28min)	80	0.25	0.05	0.02	0.125	2.00
49		Test049	1140 (19min)	100	0.25	0.05	0.02	0.05	1.27
50		Test050	1380 (23min)	100	0.25	0.05	0.02	0.075	1.55
51		Test051	1500 (25min)	100	0.25	0.05	0.02	0.1	1.79
52		Test052	1140 (19min)	110	0.25	0.05	0.02	0.05	1.27
53		Test053	1380 (23min)	110	0.25	0.05	0.02	0.075	1.55
54		Test054	1500 (25min)	110	0.25	0.05	0.02	0.1	1.79
55		Test055	1680 (28min)	110	0.25	0.05	0.02	0.125	2.00
56		Test056	1140 (19min)	60	0.25	0.05	0.02	0.05	1.27
57	22 July	Test057	1380 (23min)	60	0.25	0.05	0.02	0.075	1.55
58		Test058	1500 (25min)	60	0.25	0.05	0.02	0.1	1.79
59		Test059	1680 (28min)	60	0.25	0.05	0.02	0.125	2.00
60		Test060	1140 (19min)	90	0.25	0	0.02	0.05	1.27
61		Test061	1380 (23min)	90	0.25	0	0.02	0.075	1.55
62		Test062	1500 (25min)	90	0.25	0	0.02	0.1	1.79
63		Test063	1680 (28min)	90	0.25	0	0.02	0.125	2.00
64		Test064	1500 (25min)	90	0.25	-0.05	0.02	0.1	1.79
65		Test065	1680 (28min)	90	0.25	-0.05	0.02	0.125	2.00
66		Test066	1740 (29min)	90	0.25	-0.05	0.02	0.15	2.19
67		Test067	1680 (28min)	90	0.25	-0.1	0.02	0.125	2.00
68		Test068	1740 (29min)	90	0.25	-0.1	0.02	0.15	2.19
69		Test069	1860 (31min)	90	0.25	-0.1	0.02	0.175	2.37

Note on wave direction:

>90° : Most of the back head is sheltered from direct wave attack
90° : Normal incidence waves perpendicular to structure
<90° : A large part of the head is exposed to direct wave attack

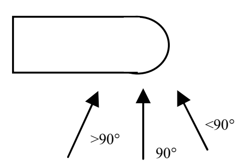

5 Measurements

Three kinds of measurements were performed:

- Waves were recorded continuous during the tests.
- Wave breaking was described from visual observations.
- Damage in terms of displacement of stones was measured after each test by use of digital photos. Damage was classified in categories. Digital video recordings were taken during a few tests of special interest.

5.1 Wave recordings

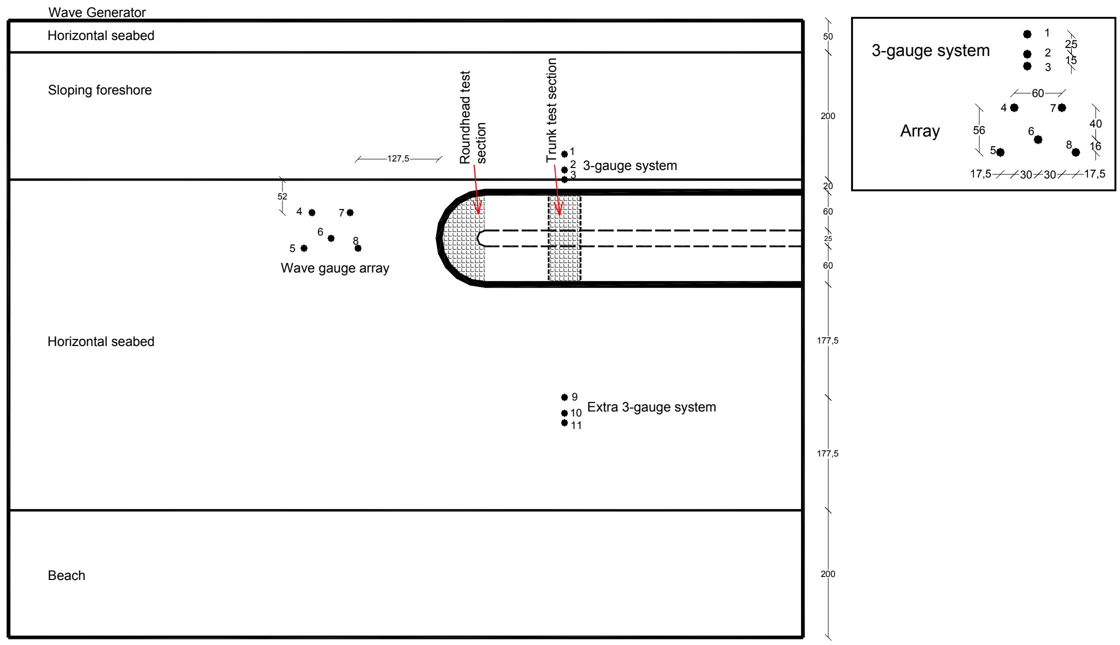

Figure 9 Position of wave gauges. Measures in cm.

Recordings by an array of five wave gauges can be used to estimate incoming and reflected wave spectra. At the position of the array almost 1.5 metres from the roundhead the influence of the roundhead (reflection and diffraction) on the incoming waves is believed to be negligible. However, the trunk reflects some wave energy which is re-reflected by the paddles. Therefore the waves in front of the trunk might in reality be slightly higher (and/or more wave breaking) than at the array. Measurements from the 3-gauge system were performed to quantify that effect. In some wave situations a lot of waves were expected to be breaking in front of the structure, and the measurements were therefore possibly very dependent on the gauge position. The 3-gauge system was placed close to the structure with distances 60, 35 and 20cm to the foot of the trunk. As 3D waves were generated these gauges cannot be used in a traditional reflection analysis.

The purpose of the measurements from the extra 3-gauge system (located on the leeward side of the structure) was to be able to compare with possible future numerical wave calculations. It was not the intention to use these measurements in the stability considerations.

Data files were stored in ASCII text format, one file for each test, with test number as filename. Each column in a file corresponds to a wave gauge such that data in column no 1 are sampled from wave gauge no 1, etc. In that way every file has 11 columns.
Measured surface elevation data is in cm generally with zero at still water level. However all wave gauges might not be precisely adjusted to zero at still water level. Positive surface elevation indicates a wave crest passing.
All data were sampled at 20Hz from start of wave generation.

5.2 Wave breaking

Wave breaking on the foreshore slope or on/over the structure was carefully monitored. In general the following was observed during a test block of four tests with increasing significant wave height.

1) Smallest waves that gave no damage:
   - Gentle lapping of waves against trunk crest only
   - Very few waves (<10%) were breaking over trunk crest

2) Second smallest waves that in some part of the structure moved a few stones:
   - Some waves were breaking (approx 50%) over the trunk crest
   - Very few waves were breaking on top edge of foreshore slope

3) Second largest waves that in some part of the structure gave significant damage:
   - Most waves were breaking over the trunk crest
   - Few waves were breaking on top edge of the foreshore slope

4) Largest waves that in most part of the structure gave severe damage:
   - Almost all waves were breaking over the trunk crest
   - A lot of the waves were breaking on the top edge of the foreshore slope
   - Very few waves were breaking on foreshore slope before reaching the top edge

In some cases the wave breaking was concentrated at the roundhead forming a jet of water and air slamming down on the top part of leeward head (between blue and green stone shown subsequent on Figure 11). This led frequently to severe damage of the leeward part of the roundhead.

5.3 Measurement of damage

Four pictures were taken in between each test. Three pictures were taken of the roundhead and one of the trunk. Picture 1 shows the seaward side of the roundhead, picture 2 the roundhead seen from the gap, picture 3 the leeward side of the roundhead, and picture 4 the trunk seen from a position vertically above the centre of the trunk section. Digital video () of selected tests were recorded from the gap.

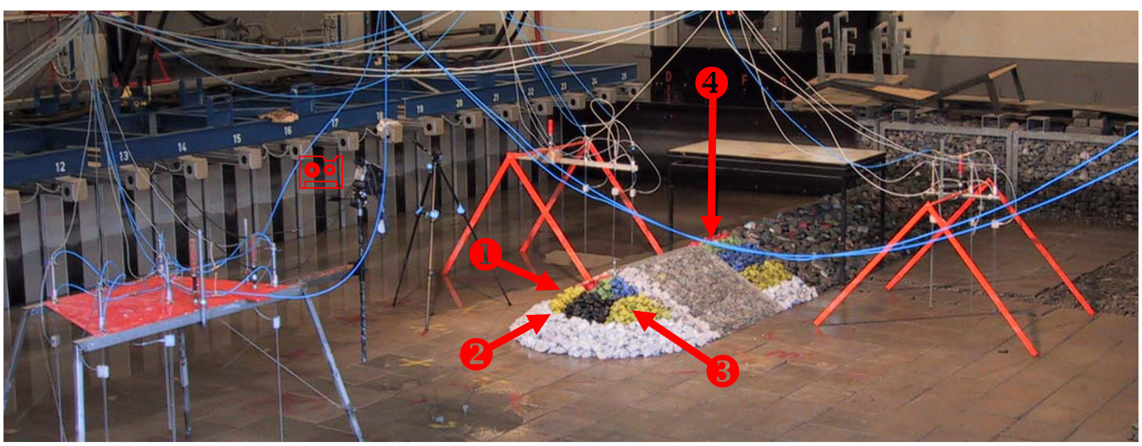

Figure 10 Position of pictures for measurement of damage

The colouring of the roundhead was split in three sections of 60° each. The three sections were called: Seaward Head (SH), Middle Head (MH) and Leeward Head (LH). The trunk was split in three parts called: Seaward Slope (SS), Crest (C), and Leeward Slope (LS).

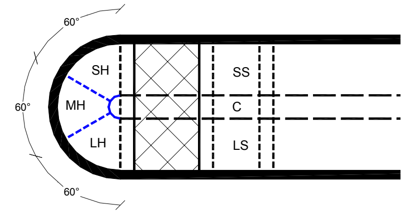

The precise colouring is shown in the following figures.

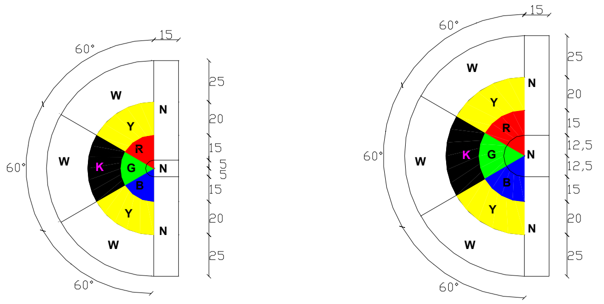

Figure 11 Colouring of roundhead. Left: Narrow structure. Right: Wide structure. Measures in cm.

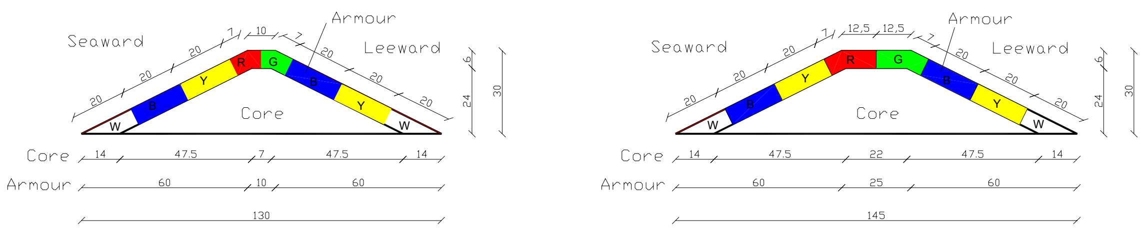

Figure 12 Colouring of trunk. Left: Narrow structure. Right: Wide structure. Measures in cm.

The digital pictures were imported into a program for photo viewing, and by switching back and forth between pictures before and after a test it was possible to follow the path of every individual stones and to count the number of stones that moved in that particular test. A stone was defined to have moved, when it moved more than one D_{n50} away from its original position. The following example, Figure 13 and Figure 14, shows how to count the number of stones. After test number 19 no stones had moved from the original position in the roundhead. After test number 20 four stones had moved.

Figure 13 Picture from position 2. Left: Before test 20. Right: After test 20.

The number of stones that have moved is easily counted from Figure 13:

- Seaward Head (SH): 3R (three red stones have moved)
- Middle Head (MH): 1G (one green stone has moved)
- Leeward head (LH): 0 (no movement)

Figure 14 Tracking the stone movements

When more than approximately 20 stones moved, the actual number had to be roughly estimated. This was generally only the case when the structure was heavily damaged or close to total destruction (filter layer often exposed to direct wave attack).

The degree of damage was also assessed visually and categorized as follows (according to definitions by Losada et al., 1986):

- ND: No damage (maybe one or two loose stones starts rotating)
- ID: Initiation of damage (a few stones starts to move)
- IR: Iribarren damage (big holes in the outer armour layer, but the filter layer is not visible).
- D: Destruction (filter layer is exposed to direct wave attack)

The example on Figure 13 and Figure 14 is for the roundhead categorized as: ID for seaward head and ND for middle head and leeward head. The categorisation is described further in chapter 8.2 subsequent.

6 CD file contents

One CD contains source data and other information about the stability tests. The CD is categorized in the following folders:

- "Data" contains recorded wave data in ASCII text format. Wave data are compressed in the file "Data.zip". The wave data files contain surface elevation measured in cm at 20Hz.
- "Documents" contains documents describing the tests plus databanks with analysed waves, analysed damage and stone gradings. Documents are in Microsoft Word 2002 format and databanks in Microsoft Excel 2002 format.
- "Drawings" contains AutoDesk AutoCAD 2002 drawings of detailed layout and cross-sections in the tests.
- "Pictures" contains jpeg pictures for damage estimation and some general pictures from the experiments.

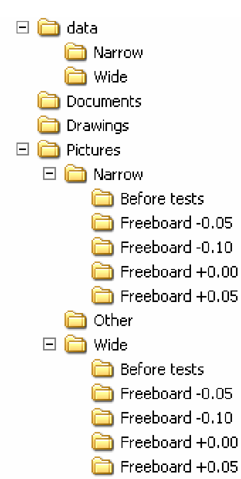

7 Video recordings

Digital video of selected tests were recorded from the gap (for position of camera see on Figure 10). The video is stored on mini DV-tapes and are kept at:

Hydraulics & Coastal Engineering Laboratory
Aalborg University
Department of Civil Engineering
Sohngaardsholmsvej 57
9000 Aalborg
Denmark

To borrow the tapes or get copies of selected sequences please contact Morten Kramer (i5mkr@civil.auc.dk) from Aalborg University.

Table 5 Available video recordings

Tape number	Test number
1	4
2	12
3	17
4	22
5	40
6	54 and 55

8 Results of AAU experiments

The following is a presentation of the test results and explanations of how the results have been derived. The definition of wave height to be used in the stability considerations is fundamental; therefore the wave heights are described in detail.

8.1 Target and actual wave conditions

In general target and actual significant wave heights were approximately the same also for the breaking waves. However some remarks on which wave heights to use in the stability considerations are appropriate.

8.1.1 Wave heights

The structure was expected to produce slightly higher waves in front of the trunk than what was measured with the wave gauge array, see Figure 6. For the array H_{mo} was calculated with directional wave analysis by the Bayesian Direct Method (Hashimoto and Kobune1987). H_s was calculated by time domain analysis for the three individual wave gauges in the 3-gauge system. These H_s' were expected to be larger than the actual incoming H_s due to wave reflection and re-reflections. On Figure 15 the wave heights from the 3-gauge system are compared to the results from the array. "Hs1" in Figure 15 corresponds to Hs for gauge number 1 (gauge farthest from structure, see Figure 9 for position of wave gauges), etc.

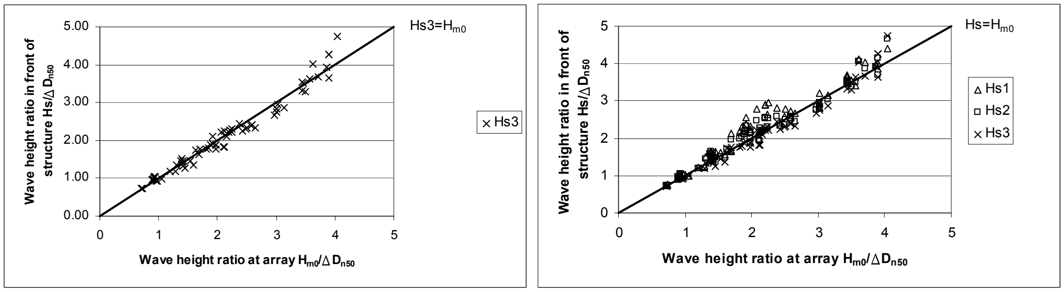

Figure 15 Comparison of waves in front of structure (left: Hs for gauge 3, right: Hs for the 3 individual gauges) with waves at array (H_{m0}). Hs3 is closest to structure.

From Figure 15 (left) it is seen that points follow the line Hs3=H_{m0}, Hs from gauge 3 in the 3-gauge system is therefore approximately equal to H_{m0} from the array. This indicates that the influence of reflected and re-reflected waves between the structure and the paddles is marginal.

At Figure 15 right is seen that the waves closest to the structure (Hs3) are a bit smaller than the average, and that the waves farthest to the structure (Hs1) are a bit larger than the average. In most tests the largest waves were depth limited. Wave gauge number 1 and 2 were located on the foreshore slope at a larger water depth than the structure. As larger water depth allows larger waves it is obvious that Hs1 should be larger than Hs3. Hs, $H_{2\%}$ (wave height with probability of exceedance 2%) and $H_{1\%}$ were calculated for the gauges in the 3-gauge system, and the average values for all tests were found as given in Table 6. In Table 6 it is seen that the wave height ratio based on Hs decreases from $Hs/\Delta D_{n50}$ = 2.31 (at gauge no. 1) to 2.20 (at gauge no. 2) to 2.12 (at gauge no. 3). This corresponds to an average significant wave height 4% larger at gauge 2 compared to gauge 3, and a 9% larger significant wave height at gauge 1 compared to gauge 3. The same decrease in wave height is found for the average $H_{2\%}$ and $H_{1\%}$.

Table 6 Average wave height ratios in front of structure

	Gauge 1	Gauge 2	Gauge 3
$Hs/\Delta D_{n50}$	2.31	2.20	2.12
$H_{2\%}/\Delta D_{n50}$	3.03	2.89	2.76
$H_{1\%}/\Delta D_{n50}$	3.20	3.04	2.91

It is clear that the wave height distribution changes as the waves approach the structure. This is shown further in the following example. Test number 4 was a test with large breaking waves, which lead to severe damage of the structure in all sections.

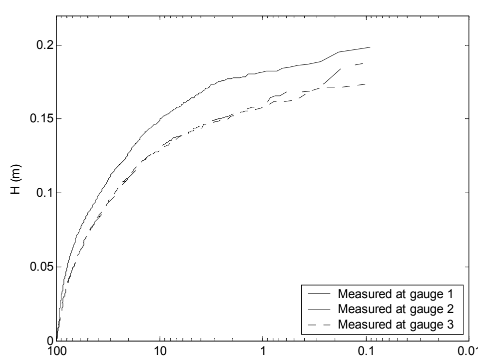

Figure 16 Measured wave height distribution for the 3-gauge system, test number 4

From Figure 16 it is clear, that especially the highest waves are higher at gauge number 1 than at gauge 3. In test number 4 the water depth at gauge 3 was 0.25m and at gauge 4 it was 0.266m, i.e. 6.5% larger water depth at gauge 1. The $H_{2\%}$ was measured to 0.178m at gauge 1 and 0.152m at gauge 3, i.e. a 17% larger wave height at gauge 1.

The change in wave height distribution is investigated in more detail in Figure 17. The measured wave height distribution is compared to the Rayleigh distribution and to the point model proposed by Battjes and Gronendijk, 2000. Battjes and Gronendijks model is developed for wave height distributions on shallow foreshores, and it takes account for water depth and foreshore slope.

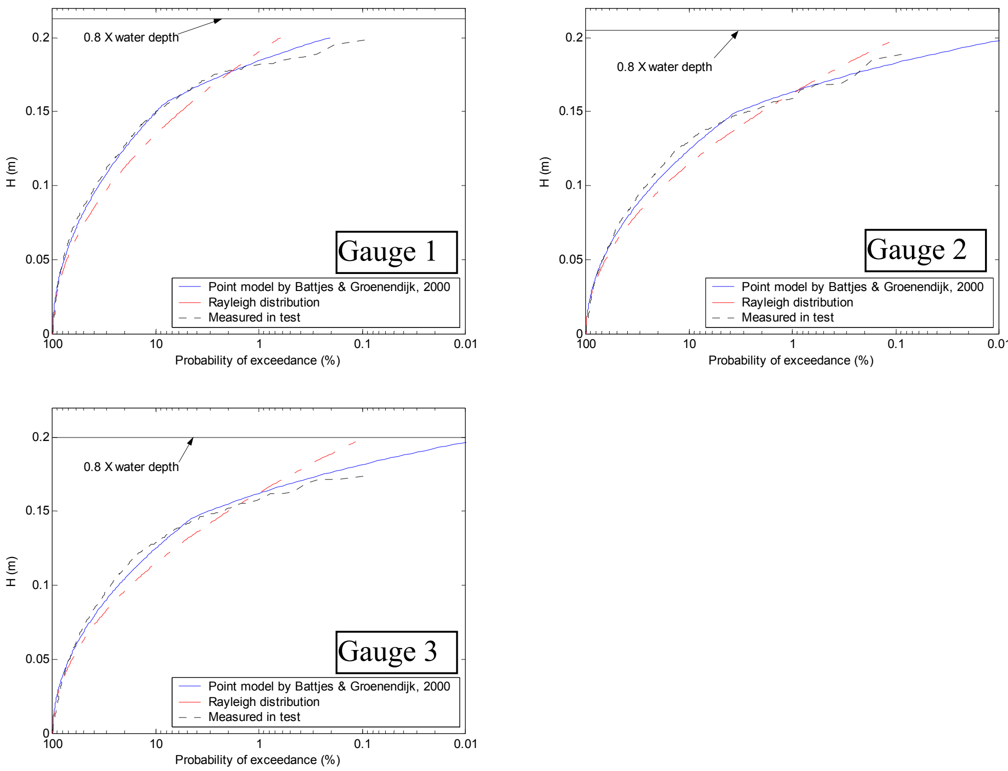

Figure 17 Measured wave height distribution compared to calculated, test number 4

From Figure 17 it is seen that the measured wave height distribution deviates from the Rayleigh distribution. Further it is seen that the point model fits the measured distribution from test number 4 outstandingly well. As LCS's are built in shallow waters the point model seems to be a good tool in describing wave height distributions at a given location.

Wave heights, concluding remarks

Wave height measurements from gauge 3 are appropriate in describing Hs for all wave directions. It is therefore chosen to use a stability number based on measurements from gauge 3 in the stability considerations subsequent.

Because the highest waves lead to damage of the structure, and because the waves are depth limited leading to changes in wave height distribution, it could be reasonable to use a more infrequent wave height than the significant wave height in the damage descriptions. However, the experimental results can be converted by a multiplication factor, which is clarified in the following. From Table 6 the average measured $H_{2\%}$ and $H_{1\%}$ at gauge 3 is 30% and 37% larger than Hs respectively. In Figure 18 measured Hs' in all tests are compared to $H_{2\%}$ and $H_{1\%}$. The measured relation between $H_{1\%/2\%}$ and Hs is constant, but it differs from the Rayleigh distribution. According to the Rayleigh distribution $H_{2\%}$ = 1.49*Hs and $H_{1\%}$ = 1.51*Hs.

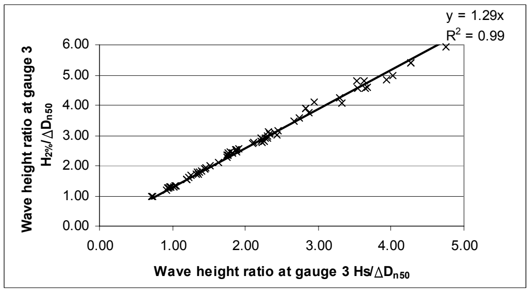

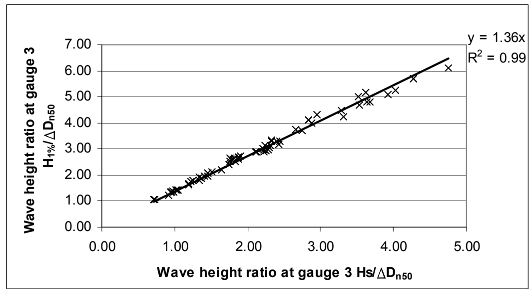

Figure 18 Wave height ratios at gauge 3 and linear fit by use of $H_{2\%}$ (left) and $H_{1\%}$ (right)

It is seen that the plotted values on Figure 18 fits the straight lines very well. In the following it is chosen to use Hs in the damage description. In case it is needed to make a damage description based on $H_{2\%}$ or $H_{1\%}$ Figure 18 can be used for conversion. Wave heights with other exceedance probability are available in the Excel databank on the CD (see chapter 6).

8.1.2 Peak period

Target and actual peak periods were in all cases approximately the same, also for cases with wave breaking.

8.1.3 Wave steepness

In the main part of the tests the target deepwater wave steepness was Hs_{deep}/L_{0p} = 0.02, and in the remaining part of the tests the target deepwater wave steepness was Hs_{deep}/L_{0p} = 0.04. For all the tests the actual wave steepness' defined by $s_{0p}=2\pi Hs/gT_p^2$ are calculated and plotted in Figure 19. Measurements from wave gauge 3 are used to define Hs.

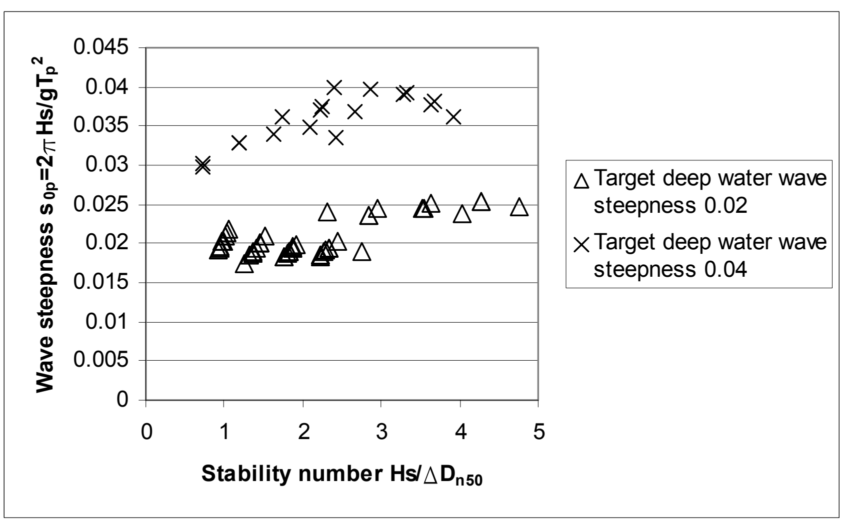

Figure 19 Target and actual wave steepness' in all tests

The average for all tests with target deepwater wave steepness 0.02 and 0.04 is s_{0p}=0.020 and s_{0p}=0.035 respectively. On Figure 19 it is seen that s_{0p} is slightly increasing for higher stability numbers. However, in all tests the wave steepness' are close to the average values s_{0p}=0.02 and s_{0p}=0.035.

8.1.4 Number of waves

The target number of waves was 1000. The average numbers of waves for all tests were:

Gauge 1:	1012
Gauge 2:	1031
Gauge 3:	1037
Average:	1027

The actual number of waves was found as an average from the 3-gauge system. In all tests except for 2 the actual number of waves was 1000 ± 10%, however in 72% of the tests the number of waves was 1000 ± 5%.
The actual number of waves is considered to be in agreement with the target.

8.1.5 Main incoming wave direction

Normal incidence waves was defined the angle 90° (wave direction perpendicular to structure). Analysis showed that only two cases of normal incident waves were outside 90° ± 3°. The difference is only considered to be due to the statistical uncertainty in the analysis. Oblique waves with obliquity up to ± 20° (70° to 110° waves) were also produced correct. In one test block (test no 56 to 59) it was attempted to generate 30° oblique waves. Analysis showed that the actual main direction was only 90°±23°. Test no 56-59 should therefore only be used with care, see chapter 8.1.6 for more detail.

For wave directions less than 90° (when a large part of the head was exposed to direct wave attack) the waves tend to get trapped between the structure, and the paddles and sidewall causing slightly larger waves in front of the structure than at the array. It is therefore important that wave heights from the 3-gauge system are used in the damage description, especially in case of oblique waves.

8.1.6 Spreading of incoming waves

In 86% of the cases the standard deviation on the wave direction was in the range 9°-15° (corresponding to s-values in Mitsuyasu spreading function s=34 to s=109). Wave situations with the largest significant wave heights had the largest spreading and wave situations with the lowest significant wave heights had the lowest spreading. In average the standard deviation was 12.1° (corresponding to s=55). The input to the wave generator was s=50. As e.g. refraction and wave breaking will change the spreading, the actual measured conditions are considered to be in agreement with the target conditions.

Example of 3D wave spectra

It is chosen to show results from tests number 40 and 59 on the wide-crest structure. Tests 40 and 59 were tests with the largest tested wave heights at the lowest water depth. During the testing the wave breaking was described with the words *"A lot of the waves break on top edge of foreshore slope, almost all waves break over trunk crest"*. These tests led to severe damage in all sections of the structure.

In both tests the freeboard was F=+0.05m (emerged crest), and the target deep water wave steepness corresponded to 0.02. In test number 40 waves with main direction head-on (90°) were generated, and in test number 59 it was attempted to generate 60° waves (30° oblique, a large part of the head exposed to direct wave attack). In Table 7 the target wave is specified by the input to the wave generator. H_{m0}, spreading and main direction θ are measured from the array. The number of waves is from gauge number 3.

Table 7 Wave conditions in test number 40 and 59 at the wave gauge array

	Setup		Target wave			Measured wave			
Test	**Water depth [m]**	**Freeboard [m]**	**Hs [m]**	**Tp [sec]**	**θ [°]**	**H_{m0} [m]**	**Number of waves**	**Spreading [°]**	**θ [°]**
40	0.25	+0.05	0.125	2.0	90	0.114	1073	16	91
59	- ‖ -	- ‖ -	- ‖ -	- ‖ -	60	0.100	1129	15	70

Directional wave analysis by the Bayesian Direct Method (Hashimoto and Kobune1987) leads to the polar plot in Figure 20. In Figure 20 the energy content from 0 to $3.5 \cdot 10^{-5}$ $m^2s/°$ is marked with red colour meaning high energy, and with blue colour meaning low energy. The direction of wave propagation 0:360° is shown along the circumference, and the frequencies 1, 2, and 3Hz are shown as the radii from origo.

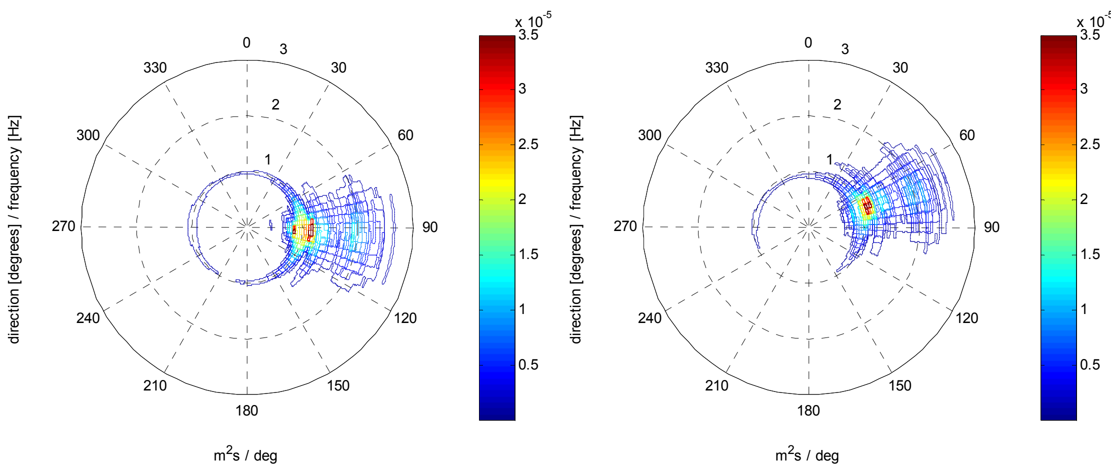

Figure 20 3D wave spectra for test number 40 (left) and 59(right)

In Figure 20 the effect of wave breaking is identified as a secondary peak at the double peak frequency, i.e. at 2Hz. Due to oblique wave direction the waves in test no. 59 travel a longer distance in shallow water before hitting the structure and the wave gauges. Consequently wave breaking becomes more pronounced in test no. 59, and H_{m0} decreases. In Table 7 it is seen that H_{m0} in test number 59 is 0.100m, and in test number 40 it is 0.114m.

In Figure 20 (left) it is seen that a small amount of energy is present in the range 180° to 360°. This is due to reflections from the beach. The reflection is in average (for all tests) less than 15% (reflected wave height compared to incoming wave height), largest for the largest waves in the deepest water. The reflection from the beach is generally very low, and the influence on the wave climate in front of the structure is therefore marginal.

Waves with main direction 60° (30° oblique) were generated in test no. 59, but when the waves reached the array the main direction was only 70° (20° oblique). As the waves travel into shallow water refraction will change the obliquity and force the wave orthogonals to become more parallel to the foreshore and structure. For this reason the spreading of the oblique waves decreases slightly. Results from tests in series with main wave direction 60° are omitted in the following.

8.2 Stability under actual wave conditions

The freeboard and the wave height are the most important parameters in describing the stability of the structural sections. The normalized freeboard Rc/D_{n50} has therefore been used as one primary parameter, and the wave height ratio or stability number $Ns = Hs/\Delta D_{n50}$ as another primary parameter. As explained in chapter 8.1.1 measurements from wave gauge 3 are used to define Hs.

8.2.1 Definition of Initiation of Damage

In order to establish a relationship between the number of displaced stones and the degree of damage the model was inspected visually after each test. After the tests the relationship between the categories (defined in chapter 5.3 according to definitions by Losada et al., 1986) and the number of displaced stones was estimated as given in Table 8.

*Table 8 Visual judgement of degree of damage related to the number of displaced stones. The * indicates that the values are judged visually.*

	Narrow structure						Wide structure					
	Trunk			Roundhead			Trunk			Roundhead		
	SS	C	LS	SH	MH	LH	SS	C	LS	SH	MH	LH
ND*	2	2	2	2	2	2	2	2	2	2	2	2
ID*	3	3	3	3	3	3	3	3	3	3	3	3
IR*	8	9	10	6	6	6	8	15	12	10	10	10
D*	-	30	30	20	20	20	-	50	-	20	20	20

Usually only marginal damage is accepted when designing a structure. Therefore it is chosen to investigate and compare results only for the category ID (Initiation of Damage). In the following it is chosen to define ID as the level where 1% of the stones in the armour layer of a section are displaced. In Table 9 N is the number of displaced armour stones in a section that equals 1%.

Table 9 Number of displaced stones that equals 1% displaced stones in armour layer

	Narrow structure						Wide structure					
	Trunk			Roundhead			Trunk			Roundhead		
	SS	C	LS	SH	MH	LH	SS	C	LS	SH	MH	LH
N	3.2	1.3	3.2	1.6	1.6	1.6	3.2	2.1	3.2	2.2	2.2	2.2

In some sections 1% equals less than 3 displaced stones. However in the experiments it was necessary to have at least 3 displaced stones in a section to describe the damage progress as *Initiation of Damage*. **Initiation of damage on the following figures therefore equals 3 displaced stones in any section.**

The following example is for tests no. 5-8 (narrow structure, normal incidence waves, s_{0p}=0.035, Rc=+0.05m). In Figure 21 (right) it is seen that ID corresponds to Ns=1.74 (tree stones are displaced during test no. 7). In tests where the number of displaced stones didn't exactly correspond to initiation of damage the stability number was slightly corrected by linear fitting, see Figure 21 (left). In Figure 21 (left) ID corresponds to Ns=1.81.

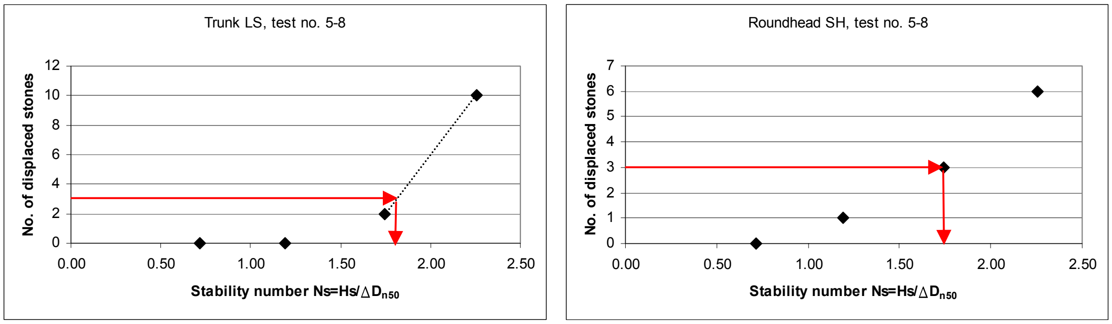

Figure 21 Damage in test 5-8 to leeward slope (left), and seaward head (right).

This analysis was done for all the test-series. The results are shown in Appendix A, Table 23.

8.2.2 Stability related to wave steepness and structural section

The investigation of the influence of wave steepness on stability was performed only for the narrow structure for normal incidence waves (main direction perpendicular to structure). For each section of the breakwater the results are compared, see Figure 22. From the graphs it is seen that the data for s_{0p}=0.02 and s_{0p}=0.035 are fairly close in case of Initiation of Damage. However, the series with s_{0p}=0.02 (long waves) tend to give slightly more damage than series with s_{0p}=0.035 (short waves). This means the structure is more stable for s_{0p}=0.035. It is also clear that the data fits the regression lines reasonably well.

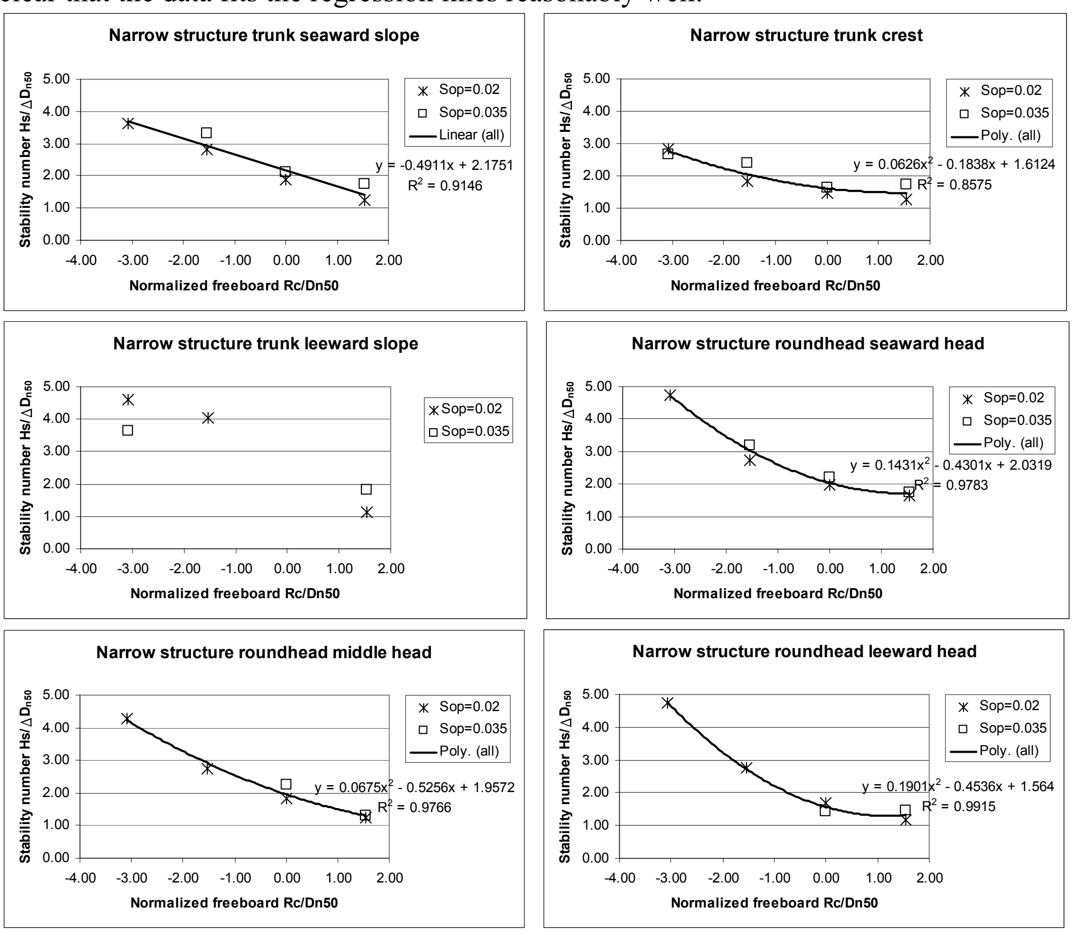

Figure 22 Stability of narrow structure sections. Influence of wave steepness. Initiation of damage.

Further, the regression lines for different sections of the breakwater are compared in Figure 23. For the trunk it is seen that the crest is the least stable section and that the leeward slope is the most stable part. For the roundhead the leeward head is the least stable part, and the stability of the middle head and seaward head is approximately the same.

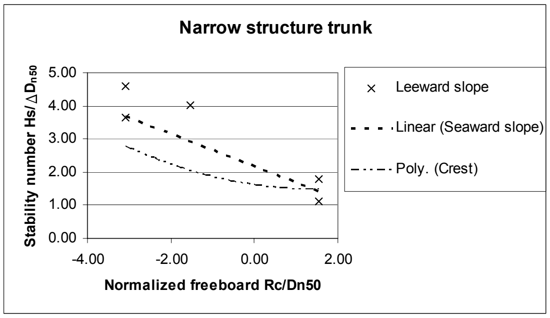

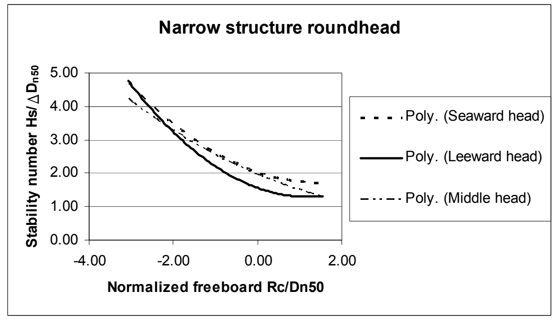

Figure 23 Stability of narrow structure sections. Trunk (left) and roundhead (right). Initiation of damage.

The stability of the head is further compared to the stability of the crest in Figure 24. It is seen that the trunk crest is the least stable part under submerged conditions, and that for zero or emerged conditions the leeward head is the least stable.

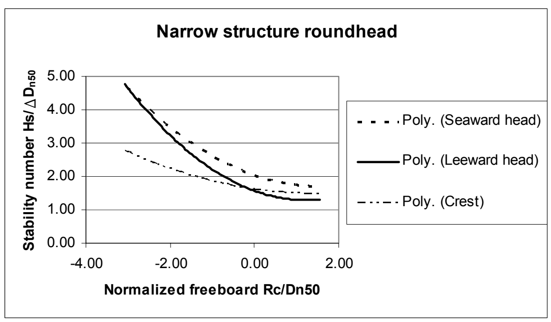

Figure 24 Stability of narrow structure sections. Initiation of damage.

8.2.3 Stability related to crest width

Two structures with crest widths 0.1m and 0.25m (equal to $3D_{n50}$ for the narrow crest and $8D_{n50}$ for the wide crest) were tested in normal incidence waves with s_{0p}=0.02. In Figure 25 the stability of the structures is compared. No significant clear difference in response can be identified for the tested crest widths. Further it is seen that the influence of crest width is small.

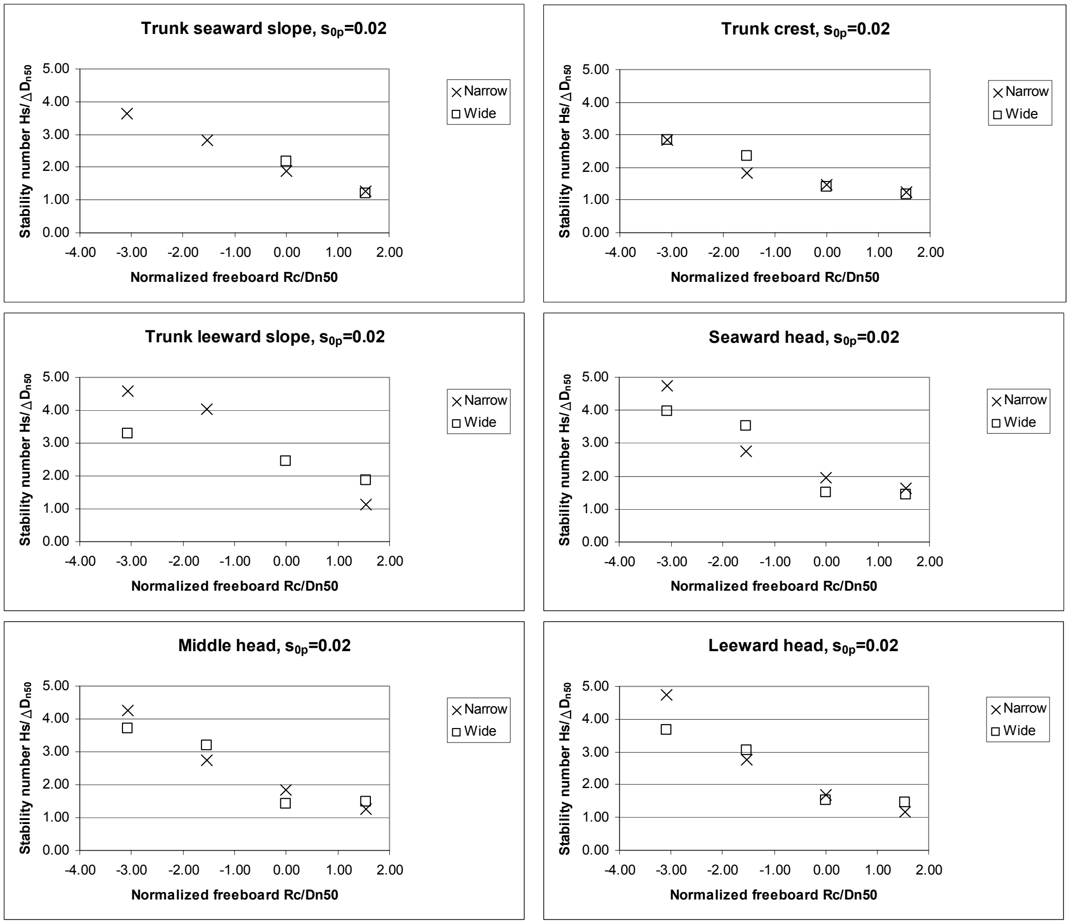

Figure 25 Stability related to crest width. Initiation of damage

8.2.4 Stability related to obliquity

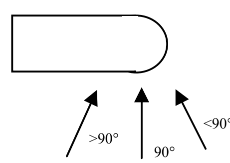

The wide structure was tested in waves with oblique main directions. Obliquities -20°,-10°, +10°, and +20° are compared to normal incidence waves (90°) in Figure 26.

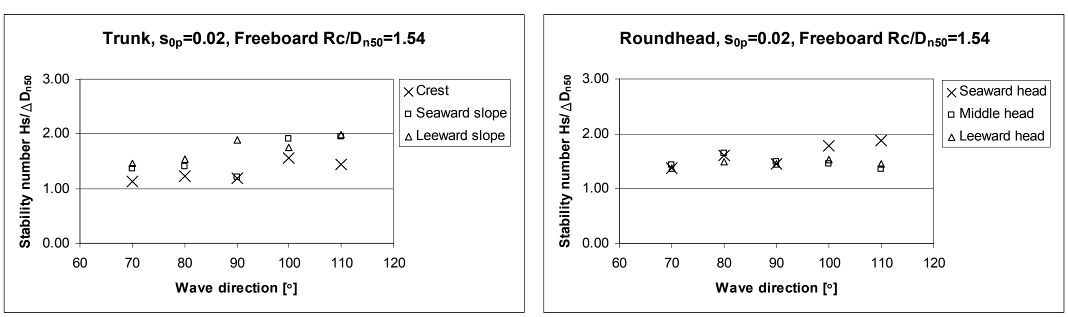

Figure 26 Stability related to wave direction. Initiation of damage. Left: Trunk. Right: Roundhead.

The trunk is the least stable under normal incidence waves. The crest is the least stable part of the trunk under all wave directions. Figure 26 (left) is not completely symmetric. The reason is that the layout in the basin is not symmetric. When waves with main direction <90° are

generated, waves are getting trapped between structure, side walls and paddles. This causes a less accurate description of the incoming waves.
When waves with main direction >90° are generated the seaward head is becoming significantly more stable (see Figure 26, right). The stability of the leeward and middle head is only slightly altered, but the middle head is becoming slightly less stable than the leeward head. During the experiments it was experienced (as described in chapter 5) that wave breaking tend to focus at the roundhead forming a jet of water and air slamming down on the top part of leeward head. This effect shifted towards the middle head in case of oblique waves causing the middle head more prone to damage.

9 Experimental data compared to existing formulae

In the following the test results from the AAU tests are compared to the formulae by Powell and Allsop (1985), Van der Meer (1990), and Vidal et al. (1992, 1995, 2000). Formulae and explanations are given in Appendix B.

9.1 Powell and Allsop (1985), trunk front slope

Only two test series in the AAU tests can be compared to the formula by Powell and Allsop. In the AAU experiments the largest freeboard to water depth ratio was Rc/h=0.2 (freeboard +0.05m, water depth 0.25m). In tests 1-4 (narrow structure) and 37-40 (wide structure) normal incidence waves with s_{0p}=0.02 were generated.
The first row in Table 24 (Appendix B) with Rc/h=0.29 corresponds to a slightly more emerged structure than Rc/h=0.2 in the AAU test. However values for Rc/h=0.29 are used for comparison. Therefore the stability according to the Powell and Allsop formula in Equation 1 should be the same or slightly smaller than for the front slope in the AAU experiments. a and b in the first row of Table 24 are used together with s_{0p}=0.02, and the curve on Figure 27 is established. It is seen that the Powell and Allsop formula follows the experimental data up to $N_{od}/N_a \cong 0.03$ (corresponding to 3% displaced armour units). For higher damage levels the formula predicts lower stability than what was measured.

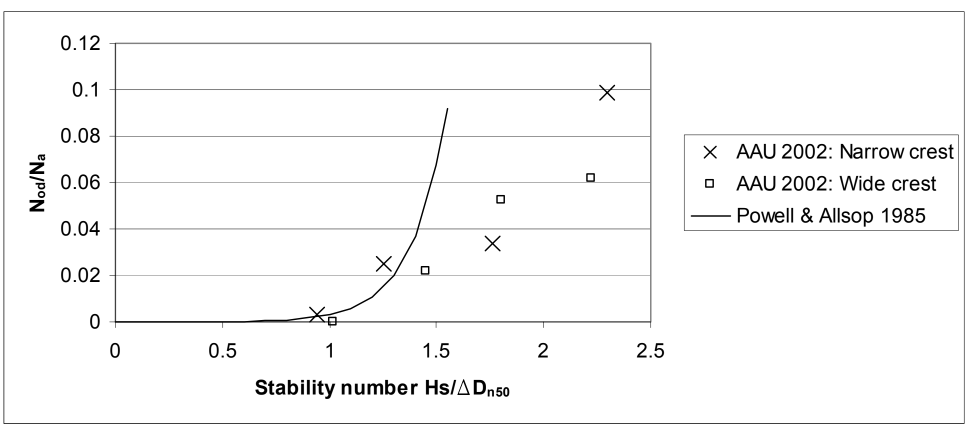

Figure 27 Test results compared to formulae by Powell & Allsop (1985)

At initiation of damage N_{od}/N_a=0.01 (1% displaced stones) the Powell & Allsop formula gives $Hs/\Delta D_{n50}$ = 1.19. This result is very close to the values obtained in the AAU experiments (1.20 and 1.26).

9.2 Van der Meer (1990), trunk front slope, emerged structure

The Van der Meer formula (1990) for low crest slopes given in Equation 2 is valid for positive freeboard. The following tests are available for comparison of seaward slope.

Table 10 Tests to be compared with Van der Meer formula

Test	Crest width	s_{0p}	Freeboard
1-4	0.10m	0.02	+0.05m
5-8	0.10m	0.035	+0.05m
9-12	0.10m	0.02	0.00
13-17	0.10m	0.035	0.00
37-40	0.25m	0.02	+0.05m
60-63	0.25m	0.02	0.00

In the Van der Meer 1990 formula the parameter S is used to quantify the damage. Broderick (1983) defined the damage parameter $S = A_e / D_{n50}^2$ given in Appendix C. For the AAU tests the relationship between damage parameter S and number of displaced units in Broderick's equation is $S = 0.11 \cdot N$ (see Appendix C). The S-values corresponding to the number of displaced units in the AAU tests are calculated from this equation.

Table 11 Parameters used in Van der Meer's 1990 formula for comparison

Parameter in van der Meer's formula	**Value used for comparison**	**Explanation**
P	0.5	For two layer structure
$\tan(\alpha)$	0.5	Structure slope
N_z	1000	Number of waves
s_{0p}=Hs/L_{0p}	0.02/0.035	Wave steepness' s_{0p}=0.02 or s_{0p}=0.035 are used depending on experiment. The actual s_{0p}'s varies a little in the tested wave conditions but are close to these values.
s_m=Hs/L_{0m}	$1.5 \cdot s_{0p}$ (0.03/0.05)	Wave steepness' s_m=0.03 or s_m=0.05 are used depending on experiment. The actual s_m's varies a little in the tested wave conditions but are close to these values.

Van der Meer suggests replacing Hs by $H_{2\%}$/1.4 in case of depth-limited waves. The actual significant wave heights in the experiments are close to this value (Hs $\cong$ $H_{2\%}$/1.3, see Figure 18) and no replacement has therefore been performed.

The reduction factors f_i are first calculated from Equation 2. The reduction factors are then used in Equation 4 to calculate the damage S, see Figure 28 and Figure 29. All tests were in the plunging wave regime, i.e. $\xi_m < \xi_{mc}$.

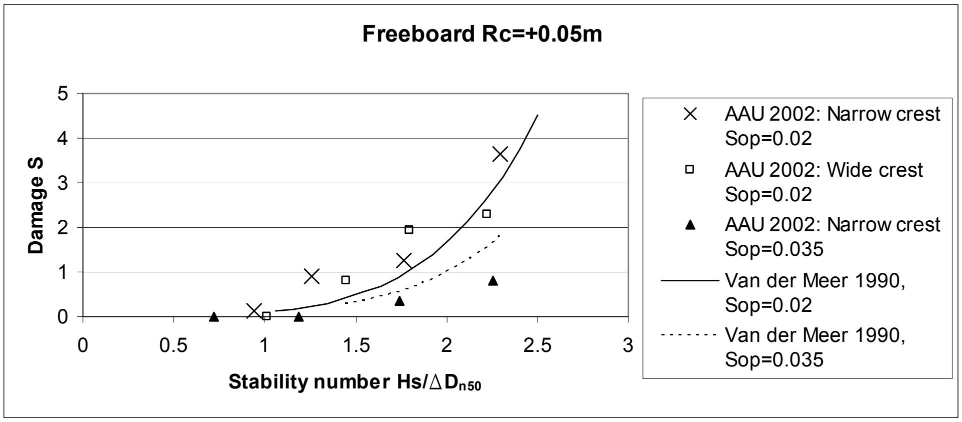

Figure 28 Tests for front slope compared to Van der Meer's 1990 formula, positive freeboard

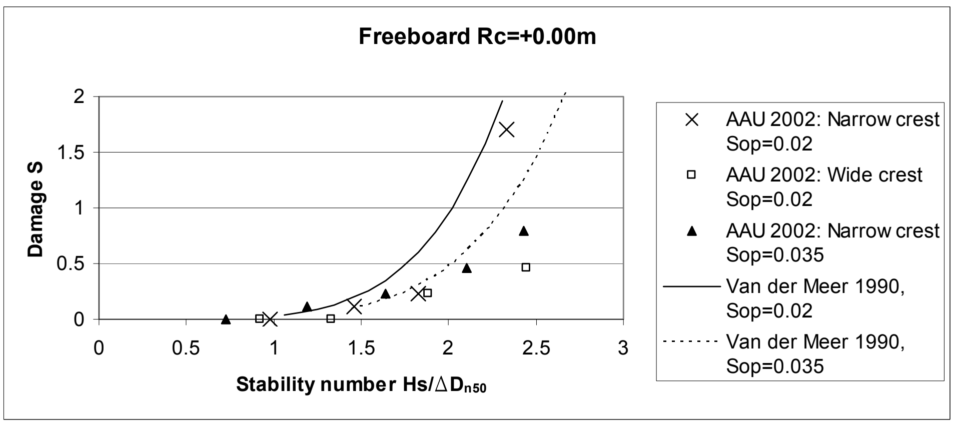

Figure 29 Tests for front slope compared to Van der Meer's 1990 formula, zero freeboard

The Van der Meer 1990 formula for low crest slopes gives approximately the same stability numbers for initiation of damage as measured in the experiments, and the curves follows the trend of the data.

9.3 Van der Meer (1990), trunk, submerged structure

The Van der Meer 1990 formula given in Appendix B, Equation 6, is used for comparison with the tests with zero or negative freeboard. The procedure is the same as used in chapter 9.2. The following tests are available for comparison.

Table 12 Tests to be compared with Van der Meer 1990 formula

Test	Crest width	s_{0p}	Freeboard
9-12	0.10m	0.02	0.00
13-17	0.10m	0.035	0.00
18-22	0.10m	0.02	-0.05m
23-27	0.10m	0.035	-0.05m
28-31	0.10m	0.02	-0.10m
32-36	0.10m	0.035	-0.10m
60-63	0.25m	0.02	0.00
64-66	0.25m	0.02	-0.05m
67-69	0.25m	0.02	-0.10m

Damage S in the AAU tests is calculated from the modified Broderick equation $S = 0.11 \cdot N$ (see Appendix C), where the number of displaced stones N is found as the sum of the number of displaced stones on the seaward slope, the crest and the leeward slope. In the following figures h is the water depth and $h_c^{'}$ is the height of the structure over the sea bed level ($h_c^{'}$=0.3m in all AAU tests).

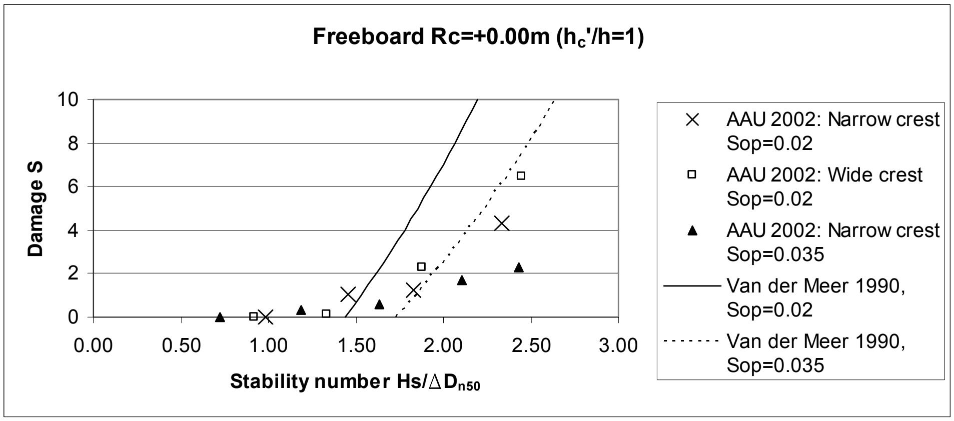

Figure 30 Tests for trunk compared to Van der Meer's 1990 formula, zero freeboard

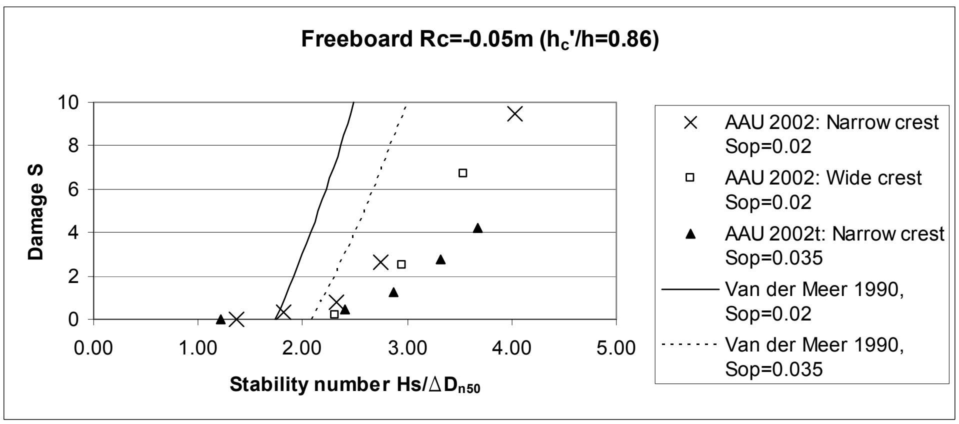

Figure 31 Tests for trunk compared to Van der Meer's 1990 formula, freeboard Rc=-0.05m

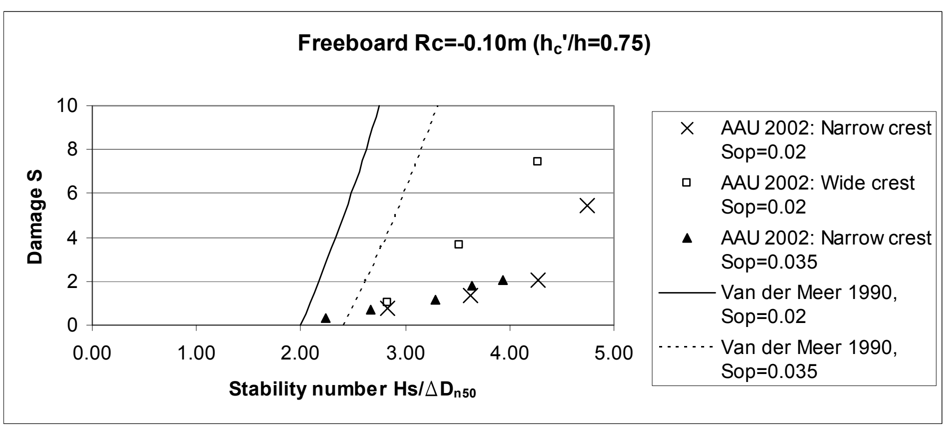

Figure 32 Tests for trunk compared to Van der Meer's 1990 formula, freeboard Rc=-0.10m

The formula does not fit the data very well especially for the most submerged structure. In general the curves are too steep predicting too much damage. For zero freeboard (Figure 30) the predicted stability number for start of damage (S=0-2) is close to the test results but for larger submergence (Figure 31 and Figure 32) the predicted stability number for start of damage is lower than found in the AAU test results.

9.4 Vidal et al. (1992, 1995, 2000), head and trunk stability

Vidal et al. (2000) proposed parameterized curves corresponding to initiation of damage of the trunk and the head of low-crested and submerged breakwaters. The formula is given in Appendix B, Equation 7. Vidal et al. 1995 defined the damage S corresponding to initiation of damage in Equation 7 as S=1 for the trunk crest and the seaward slope, and S=0.5 for the trunk leeward slope. Vidal divided the roundhead in two sections; the front head and the back head. The front head covered 60° of the seaward part of the roundhead (corresponding to the seaward head in the AAU tests) and the back head covered the remaining 120° (corresponding to the combined middle and leeward head in the AAU tests). A methodology to calculate damage S for the roundhead sections was proposed by Vidal et al. 1995 in which initiation of damage for the head was defined as S=1 for the back head and the front head.

In the present tests initiation of damage was defined as the damage level where 1% of the stones in a section are displaced. This degree of damage corresponds to a lower damage level than the level used by Vidal et al. However, the formula proposed by Vidal et al. 2000 is compared directly to the test results in the following figures without any corrections of the damage level.

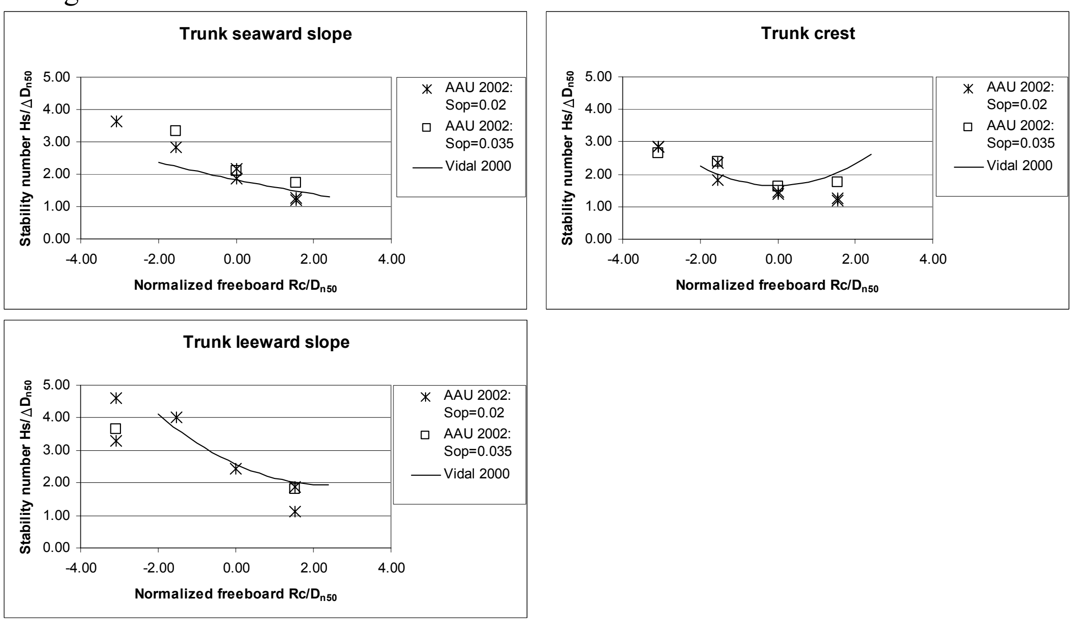

Figure 33 Tests for trunk compared to Vidal's 2000 parameterized formula

It is seen that Vidal's 2000 formula for the trunk fits the data quite well. However, the trunk seaward slope under submerged conditions tends to be a bit more stable in the AAU tests.

The test results for both the leeward and the middle head are plotted on Figure 34 (right).

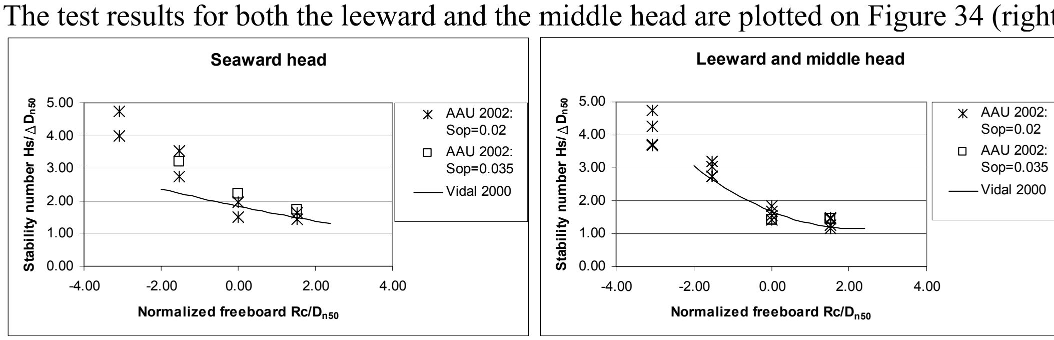

Figure 34 Tests for roundhead compared to Vidal's parameterized formula

Vidal's formula for the roundhead fits the data well. However, the seaward head under submerged conditions tends to be a bit more stable in the AAU tests. This will be described in more detail in chapter 10.3, in which Vidal's tests will be compared to the AAU tests with the same definition of damage.

10 Experimental data compared to existing datasets

In the following the test results from the AAU tests are compared to tests performed at UCA (2001), Delft (1995), NRC (1992), and Delft (1988). Details about all tests are given in Appendix D.

10.1 UCA 2001

In February 2001 stability tests were carried out in the wave flume at University of Cantabria. Details about the tests are given in Appendix D. A homogeneous cross section with crest height hc = 0.25m was tested subject to 16 irregular wave conditions. Water depths h was 0.2m and 0.3m corresponding to freeboards -0.05m and +0.05m. The crest height to water depth ratios hc/h were approximately the same as for the AAU tests, see Table 13.

Table 13 Differences in crest height for UCA and AAU tests

	UCA tests			AAU tests for comparison		
	Freeboard Rc	Rc/D_{n50}	hc/h	Freeboard Rc	Rc/D_{n50}	hc/h
Submerged crest	-0.05m	-4.17	0.83	-0.05m	-1.54	0.86
Emerged crest	+0.05m	4.17	1.25	+0.05m	1.54	1.20

Damage S in the AAU tests have been calculated from the modified Broderick equation $S = 0.11 \cdot N$ (see Appendix C), where the number of displaced stones N is found as the sum of displaced stones on the seaward slope, the crest and the leeward slope. The following AAU tests are available for comparison:

Table 14 AAU tests available for comparison with UCA tests

Test	Crest width	s_{0p}	Freeboard
1-4	0.10m	0.02	+0.05m
5-8	0.10m	0.035	+0.05m
37-40	0.25m	0.02	+0.05m
18-22	0.10m	0.02	-0.05m
23-27	0.10m	0.035	-0.05m
64-66	0.25m	0.02	-0.05m

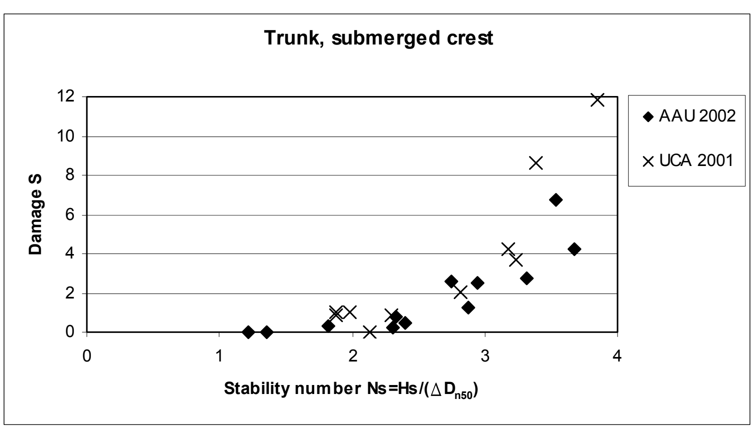

Figure 35 AAU and UCA tests with freeboard Rc=-0.05m

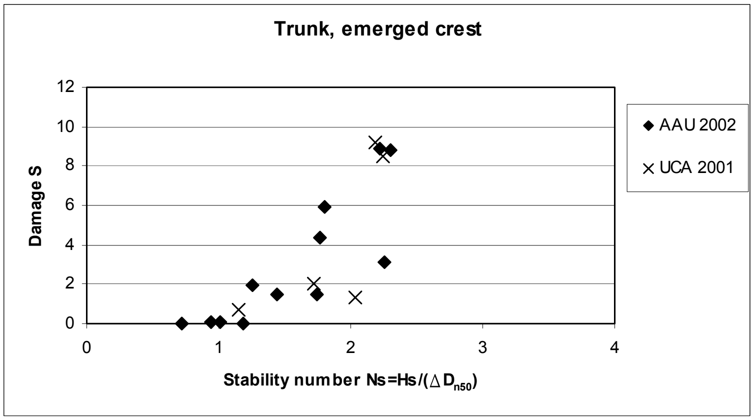

Figure 36 AAU and UCA tests with freeboard Rc=+0.05m

The two data sets are in agreement as the points on Figure 35 and Figure 36 follow the same trend. However, very small stones were used in the UCA tests (D_{n50}=0.012m), which indicates that viscous scale effects were present in the tests. On the other hand the UCA structure was homogeneous without core. These two deviations from the AAU structures counteracts each other. Caution should therefore be taken when drawing conclusions based on the comparisons.

10.2 Delft 1995

Burger (1995) tested the influence of rock shape and grading on the stability of front, crest and rear slope of low-crested structures. Results are presented by Burger (1995) and Van der Meer et al. (1996).

	Delft 1995			**AAU tests for comparison**		
	Freeboard Rc	Rc/D_{n50}	hc/h	Freeboard Rc	Rc/D_{n50}	hc/h
Emerged crest	+0.05m	2.0	1.12	+0.05m	1.54	1.2

The Delft 1995 results are available for two wave steepness's s_{0p}=0.02 and s_{0p}=0.04, which is approximately the same as used in the AAU tests. Damage S in the AAU tests have been calculated from the modified Broderick equation $S = 0.11 \cdot N$ (see Appendix C), where the number of displaced stones N is found as the sum of displaced stones on the seaward slope, the crest and the leeward slope. The following AAU tests are available for comparison:

Table 15 AAU tests available for comparison with Delft 1995 tests

Test	Crest width	s_{0p}	Freeboard
1-4	0.10m	0.02	+0.05m
5-8	0.10m	0.035	+0.05m
37-40	0.25m	0.02	+0.05m

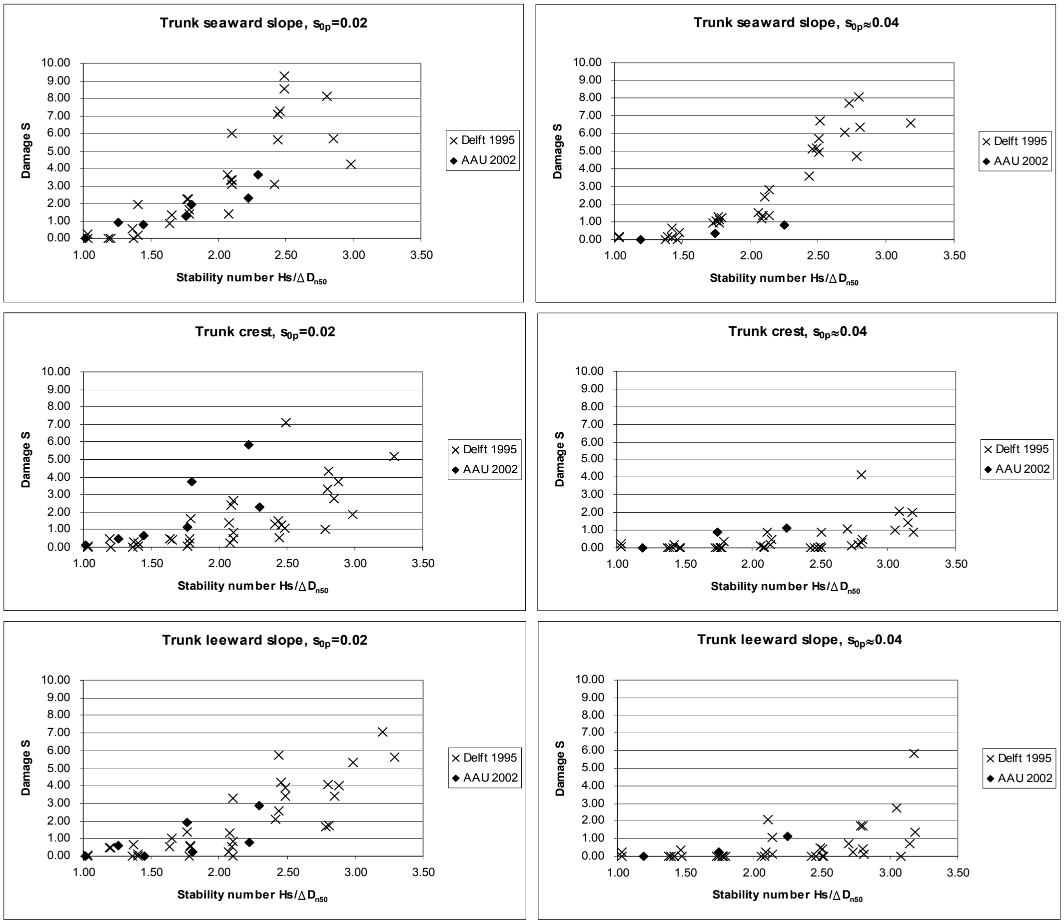

Figure 37 Stability of trunk sections, Delft 1995 tests compared to AAU tests

In Figure 37 it is seen that the two datasets are in agreement with respect to trends. However the crest seems to be slightly more prone to damage in the AAU tests, and the seaward slope seems to be slightly less prone to damage in the AAU tests. This could be due to different definition of the areas covered by the trunk sections. In the AAU tests the definition of sections in Figure 12 (on page 12) was adopted, whereas in the Delft 1995 tests the seaward and the leeward slopes were extended to the surface of the crest. To investigate whether this could influence the results the total damage for the trunk was calculated as the sum of damage to the seaward slope, crest, and leeward slope.

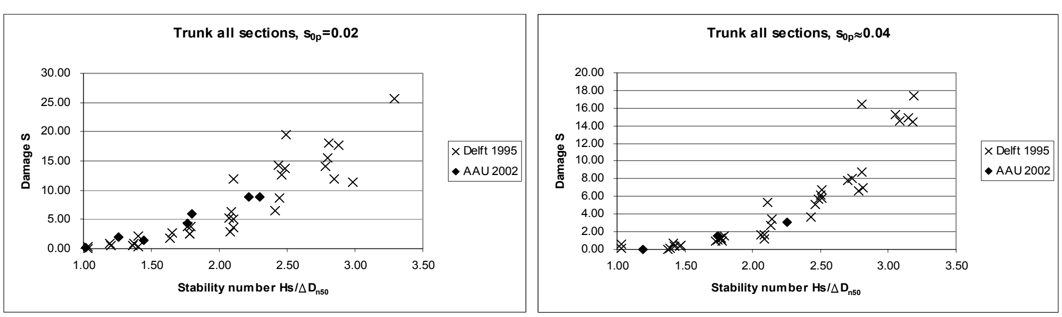

Figure 38 Stability of total trunk section, Delft 1995 tests compared to AAU tests

In Figure 38 it is seen that the two datasets are in almost perfect agreement. The differences in Figure 37 are therefore believed to be due to the different definitions of sections.

10.3 NRC 1992

Vidal et al. performed 3D stability tests at the Hydraulics Laboratory of the National Research Council Canada (NRC) in Ottawa, Canada, 1991-1992 on a complete 4.7m long structure in irregular head on waves. Detailed description of setup is found in Vidal et al. (1995) and in Appendix D.

Structure heights and freeboards were different in the AAU tests and the NRC tests. However the following three test series are compared in the following. In the first test series in Table 16 Rc/D_{n50} = -2.0 (NRC tests) and Rc/D_{n50} = -1.54 (AAU tests). This means that the AAU tests on submerged structure will be compared to a relatively more submerged structure in the NRC tests. According to this less damage for the same stability number is expected for the submerged NRC structure.

Table 16 NRC test series to be compared to the AAU tests

	NRC tests			AAU tests for comparison		
	Freeboard Rc	Rc/D_{n50}	hc/h	Freeboard Rc	Rc/D_{n50}	hc/h
Submerged crest	-0.05m	-2.0	0.89 / 0.92	-0.05m	-1.54	0.86
Zero freeboard	0	0	1	0	0	1
Emerged crest	+0.04m	1.61	1.07	+0.05m	1.54	1.2

Table 17 AAU tests available for comparison with NRC tests

Test	Crest width	s_{0p}	Freeboard
1-8	0.10m	0.02/0.035	+0.05m
9-17	0.10m	0.02/0.035	0
18-27	0.10m	0.02/0.035	-0.5m
37-40	0.25m	0.02	+0.5m
60-63	0.25m	0.02	0
64-66	0.25m	0.02	-0.05m

For the trunk it is chosen only to compare results for the crest stability.

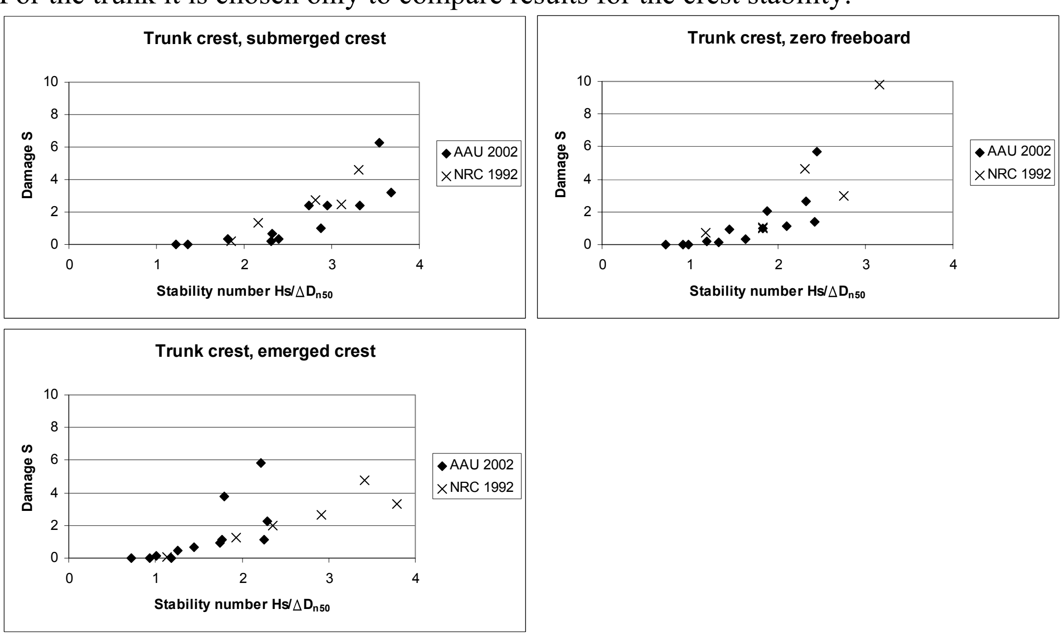

Figure 39 Trunk crest stability, NRC tests compared to AAU tests.

In Figure 39 it is seen that the points for the two data sets follow the same trend. However, the crest under submerged conditions does not seem to be less prone to damage for the NRC tests. This indicates that the crest seems to be slightly more stable in the AAU tests under submerged conditions.

To compare damage to the roundhead the numbers of displaced stones in the AAU sections have been converted to the damage S-value as used in the NRC tests. The methodology described in Appendix D, given by *Equation 9* and *Equation 10* has been used. On the following figures the leeward head corresponds to the same section for the leeward head as used in the NRC tests. The leeward head on the following figures therefore corresponds to the combined area of the middle and leeward head in the AAU tests. Please note the different scaling of the axes on the following figures.

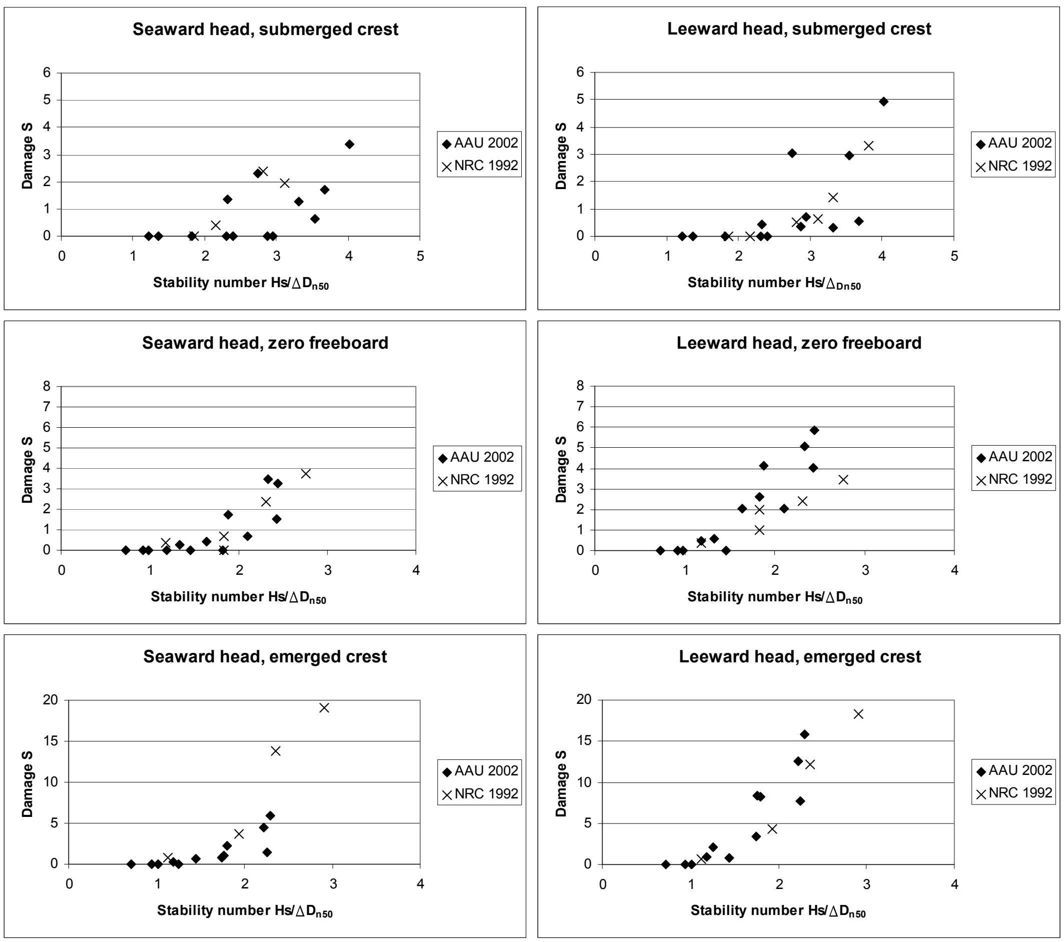

Figure 40 Roundhead stability, NRC tests compared to AAU tests.

The data points on Figure 40 are in agreement. However, as for the trunk crest, the NRC structure does not seem to be less prone to damage under submerged conditions. There can be several explanations for that. The main differences to the present tests are (in subjectively estimated order of priority) described in the following and the influence of the parameters that are believed to be of most importance is explained further.

- The structure slopes were 1:1.5 in the NRC tests (1:2 in AAU tests)
    - o A steeper slope is less stable. This indicates that the NRC structure should be less stable than the AAU structure.
- No foreshore slope was present in NRC tests
    - o In the NRC tests a horizontal seabed was used. On a horizontal seabed it is not possible to produce as steep waves as on a sloping foreshore. This can make the structure on the horizontal seabed more stable. Therefore the stability of the NRC structure could be larger than the AAU structure.
- 2D irregular waves were generated in NRC tests (3D in AAU tests)
- Higher structure in NRC tests (40-60cm in NRC tests and 30cm in AAU tests)
- Slightly smaller stones in NRC tests (D_{n50}=2.5cm in NRC tests and D_{n50}=3.3cm in AAU tests)

10.4 Delft 1988

Van der Meer (1988) performed LCS stability tests in the wave flume at Delft Hydraulics. Water depth was kept constant and structure height was changed.

Table 18 Delft 1988 test series to be compared to the AAU tests

	Delft 1988			AAU tests for comparison		
	Freeboard Rc	Rc/D_{n50}	hc/h	Freeboard Rc	Rc/D_{n50}	hc/h
Submerged crest	-0.10m	-2.91	0.75	-0.10m	-3.08	0.75
Zero freeboard	0	0	1	0	0	1
Emerged crest	+0.125m	3.63	1.31	+0.05m	1.54	1.2

Damage S in the AAU tests have been calculated from the modified Broderick equation $S = 0.11 \cdot N$ (see Appendix C), where the number of displaced stones N is found as the sum of displaced stones on the seaward slope, the crest and the leeward slope. The following AAU tests are available for comparison:

Table 19 AAU tests available for comparison with Delft 1988 tests

Test	Crest width	s_{0p}	Freeboard
1-8	0.10m	0.02/0.035	+0.05m
9-17	0.10m	0.02/0.035	0
28-36	0.10m	0.02/0.035	-0.10m
37-40	0.25m	0.02	+0.05m
60-63	0.25m	0.02	0
67-69	0.25m	0.02	-0.10m

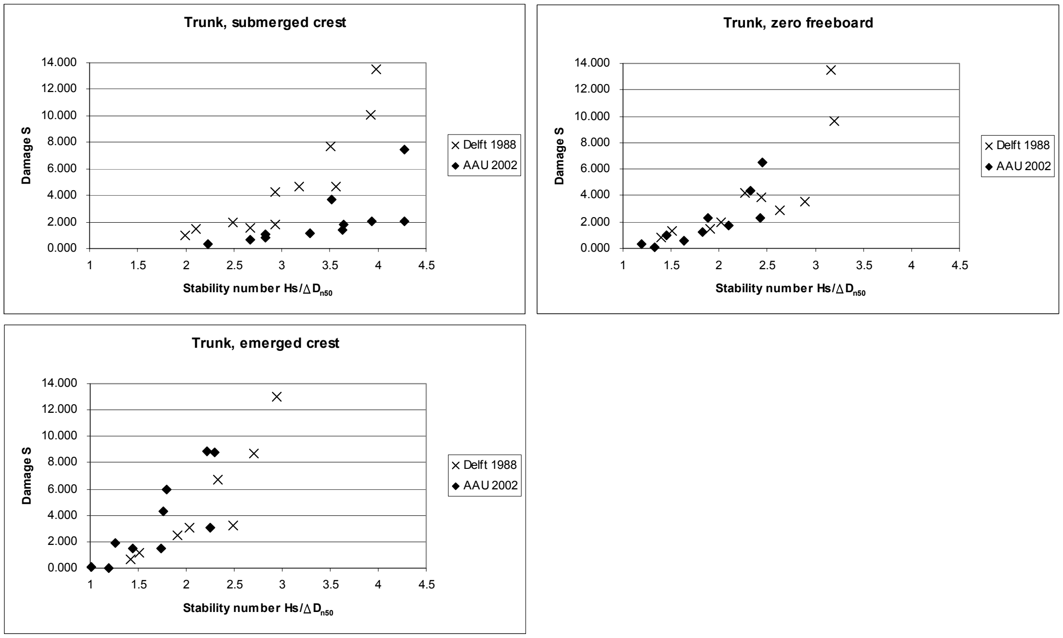

Figure 41 Trunk stability, Delft 1988 tests compared to AAU tests.

The two datasets are in agreement for zero freeboard and emerged crest. However, under submerged conditions the Delft 1988 structure was more prone to damage.
In Table 18 it is seen that for submerged crest the relative submergence $Rc/D_{n50} = -3.08$ in the AAU test and $Rc/D_{n50} = -2.91$ as target in the Delft 1988 test. In the Delft 1988 tests the actual crest height as built was slightly different from the target. For the submerged crest the actual crest height as built was measured to 0.31m (taken as the average for the tests with submerged crest). Hereby the actual relative submergence in the Delft 1988 tests was $Rc/D_{n50} = -2.62$, which is somewhat different from the compared AAU tests.

When the difference in relative freeboard is taken into account the two datasets are considered in agreement.

11 Conclusions

The AAU test results have been compared to four different test series performed by other researchers. Structure geometries, wave basin/flume layouts, stone characteristics and types of waves generated were different in all five datasets. Because of this some deviations between the results is expected and also observed. However, when the differences are kept in mind all four datasets are considered to be in reasonable agreement with the AAU tests.
The AAU test results were compared to the formula shown in Table 20. Even though there are differences between tests and formulae, the existing formulae are able to predict the damage in the AAU tests to some extend. As very few tests have been available for comparisons Table 20 should not be used to check the validity of a certain formula.

Table 20 Overview of stability formula compared to AAU tests

Author	**Formula valid for**	**How well does the formula fit the AAU test?**	
		For start of damage	**For progress of damage**
Powell and Allsop (1985)	Trunk front slope	Well	Formula overestimates the progress of damage
Van der Meer (1990)	Trunk front slope, emerged structure	Well	Well
Van der Meer (1990)	Trunk, submerged structure	Formula underestimates the stability in case of large submergence	Formula overestimates the progress of damage
Vidal et al. (1992, 1995, 2000)	Head and trunk stability	Well	Well

11.1 Conclusions on AAU experiments related to initiation of damage

The following main conclusions about the AAU tests related to initiation of damage can be drawn:

Influence of	Importance	Comments
Freeboard	Large	A submerged structure is significantly more stable than an emerged low crested structure. The more submerged the more stable. For larger emergence than tested in the AAU tests the overtopping will reduce and consequently the trunk leeward slope and crest will become more stable.
Crest width	Small	The stability of much wider structures than the tested ones might be larger compared to the tested relatively narrow structures.
Wave steepness	Small	Long waves (s_{0p}=0.02) cause only slightly larger damage to the structure than steeper waves (s_{0p}=0.035) for low damage levels. However for higher damage levels the structure becomes relatively more stable in steep waves.
Obliquity of waves	Small	All parts of the trunk are slightly more stable under oblique wave attack than under normal incidence wave attack. The stability of the roundhead sections in case of oblique waves <90° (a large part of the head exposed to direct wave attack) is the same as for normal incidence waves. The stability of the leeward and middle part of the roundhead in case of oblique waves >90° (when a large part of the head is in lee of direct wave attack) is the same as for normal incidence waves, but the area of damage shifts towards the middle part of the head. However the seaward part of the head is becoming significantly more stable.

The conclusions can only be applied within the tested range of parameters.

11.2 Planned future publications

An abstract about the results has been submitted to Coastal Structures 2003 Conference (organized by ASCE, August 26 - 29, 2003, Embassy Suites, Portland, Oregon). The abstract has been accepted, and deadline for the paper is December 15, 2003. The title of the paper will be "Head and Trunk Stability of Low-Crested Breakwaters in Short Crested Waves" by Morten Kramer and Hans Burcharth.

The results will also be treated in Morten Kramer's PhD thesis, which is expected to be published autumn 2004.

12 References

Ahrens, J.P. (1987). *Characteristics of Reef Breakwaters*, Technical report CERC-87-17, Waterways Experiment Station, US Army Corps of Engineers.

Allsop, N.W. (1983). *Low-Crest Breakwaters, Studies in Random Waves*, Proceedings of Coastal Structures '83, American Society of Civil Engineers, pp 94-107.

Battjes, J.A. and Groenendijk, H.W. (2000). *Wave height distribution on shallow foreshores*, Journal of Coastal Engineering, Vol. 40, pp 161-182.

Burger, G. (1995). *Stability of low-crested breakwaters*. MSc. Thesis Delft University, report H1878/H2415 and Final Proceedings, EU research project Rubble mound breakwater failure modes, MAST 2 contract MAS2-CT92-0042.

Broderick, L.L. (1983). *Riprap Stability A Progress Report,* Proceedings of Coastal Structures '83, American Society of Civil Engineers, pp 320-330.

Givler, L.D., and Sorensen, R.M. (1986). *An Investigation of the Stability of Submerged Homogeneous Rubble-Mound Structures Under Wave Attack*, Report IHL 110-86, H.R. IMBT Hydraulics, Lehigh University, Philadelphia, PA.

Goda, Y. (1985). *Random Seas and Design of Marine Structures*, University of Tokyo Press.

Hashimoto,N. and Kobune,K. (1988) *Estimation of directional spectrum from a Bayesian approach*. Proc.21st ICCE, Vol 1, ASCE, pp.62-72.

Losada, M.A., Desire, J.M., and Alejo, L.M. (1986). *Stability of Rock Breakwaters Armour Units*, ASCE, Journal of Structural Engineering, Vol. 112, No. 11, pp. 2392-2401

Loveless, J. and Debski, D. (1997). *The Design and Performance of Submerged Breakwaters*, Ministry of Agriculture Fisheries and Food, contract CSA 2606, Department of Civil Engineering, University of Bristol.

Mitsuyasu, H. et. al. (1975). *Observations of the Directional Spectrum of Ocean Waves using a Cloverleaf Buoy*, Journal of Physical Oceanography, Vol. I, pp. 750-760.

Powell, K.A., and Allsop, N.W. (1985). *Low-Crest Breakwaters, Hydraulic Performance and Stability*, Report No. SR 57, Hydraulics Research Station, Wallingford, England.

Van der Meer, J.W., Tutuarima, W.H. and Burger, G. (1996). *Influence of Rock Shape and Grading on Stability of Low-Crested Structures*, Proc. 25th International Conference on Coastal Engineering, chapter 152, pp 1957-1970, Orlando, Florida.

Van der Meer, J. W. (1990). *Low-crested and reef breakwaters*, Delft Hydraulics Publication H986, Delft Hydraulics Laboratory, The Netherlands.

Van der Meer, J. W. (1991). *Stability and Transmission at Low-Crested Structures*, Delft Hydraulics Publication No. 453, Delft Hydraulics Laboratory, The Netherlands.

Van der Meer, J.W. and Pilarczyk, K.W. (1990). *Stability of Low-crested and Reef Breakwaters*, Proc. 22nd International Conference on Coastal Engineering, Vol. 2, pp. 1375-1388, Delft, The Netherlands.

Van der Meer, J.W. (1988). *Rock Slopes and Gravel Beaches under Wave Attack*, PhD-thesis Delft University of Technology.

Vidal, C., Medina, R., and Martín, F.L. (2000). *A Methodology to Assess the Armour Unit Stability of Low-Crested and Submerged Rubble-Mound Breakwaters*, Pooceedings of the Coastal Structures ´99 Conference, Balkema, Rotterdam, pp 721-725.

Vidal, C, Losada, M.A. and Mansard, E.P.D (1995). *Stability of Low-Crested Rubble-Mound Breakwater heads*, Journal of Waterway, port, coastal and Ocean Engineering, vol. 121, No. 2, pp 114-122.

Vidal, C., Losada, M.A., Medina, R., Mansard, E.P.D. and Gomez-Pina, G. (1992). *A Universal Analysis for the Stability of both Low-Crested and Submerged Breakwaters,* Proc. 23rd International Conference on Coastal Engineering, pp. 1679-1692, Venice, Italy.

Appendix A: Test schedule and results of AAU tests

More detailed information can be found in the databank for the tests. The following parameters are used in the tables:

θ target incoming wave direction (90°=normal incidence waves)

B crest width

Rc freeboard

wave steep., Hs and *Tp* target deepwater wave characteristics

h water depth

Hs(3) significant wave height from gauge 3 in the 3-wavegauge system

H_{moI} incident significant wave height from the array

No waves is the average number of waves from the 3-wavegauge system

Spr. and θ *(Hi)* spreading and direction of the incoming waves from the array, respectively.

N number of displaced stones counted from the photos

Table 21 Details about stability tests with narrow cross-section

Target								Measured waves					Damage, trunk			Damage, roundhead		
Test no.	θ [°]	B [m]	Rc [m]	Wave steep.	Hs [m]	Tp [s]	h at LCS [m]	Hs (3) [m]	Hmo_l [m]	No waves	Spr. [°]	θ (Hi) [°]	SS N	C N	LS N	SH N	MH N	LH N
1	90	0.1	0.05	0.02	0.05	1.27	0.25	0.049	0.051	1034	10	87	1G	0	0	0	0	0
2	90	0.1	0.05	0.02	0.075	1.55	0.25	0.065	0.076	1082	12	89	8Y	4G	5B	0	2G+1K	3B+1G
3	90	0.1	0.05	0.02	0.1	1.79	0.25	0.092	0.103	1052	13	89	9Y+2B	5R+5G	16B+1Y	3R+1Y	11G+3K	7B+9Y
4	90	0.1	0.05	0.02	0.125	2.00	0.25	0.120	0.117	1129	15	88	2W+7B+23Y	10R+10G	24B+1Y	10Y+14R	19G+9K+2W	18B+16Y
5	90	0.1	0.05	0.04	0.05	0.90	0.25	0.037	0.037	1055	9	89	0	0	0	0	0	0
6	90	0.1	0.05	0.04	0.075	1.10	0.25	0.062	0.062	981	9	89	0	0	0	1R	2G	1B
7	90	0.1	0.05	0.04	0.1	1.27	0.25	0.091	0.084	987	11	91	1B+2Y	5R+3G	2B	2R+1Y	4G+3K	4B+1Y
8	90	0.1	0.05	0.04	0.125	1.42	0.25	0.117	0.110	971	13	89	4B+3Y	6R+4G	10B	5R+1Y	4G+4K	13B+10Y
9	90	0.1	0	0.02	0.05	1.27	0.3	0.051	0.055	970	9	90	0	0	0	0	0	0
10	90	0.1	0	0.02	0.075	1.55	0.3	0.076	0.080	1003	10	91	1Y	6R+2G	0	0	0	0
11	90	0.1	0	0.02	0.1	1.79	0.3	0.095	0.109	994	11	92	1B+1Y	7R+2G	0	0	2G	4B+1Y
12	90	0.1	0	0.02	0.125	2.00	0.3	0.121	0.130	1044	14	92	1W+2B+12Y	16R+7G	0	11R	6G	6B+4Y
13	90	0.1	0	0.04	0.05	0.90	0.3	0.038	0.038	991	9	90	0	0	0	0	0	0
14	90	0.1	0	0.04	0.075	1.10	0.3	0.062	0.067	991	9	89	1Y	2R	0	0	0	1B
15	90	0.1	0	0.04	0.1	1.27	0.3	0.085	0.088	978	10	91	2Y	2R+1G	0	1R	0	4B+1Y
16	90	0.1	0	0.04	0.125	1.42	0.3	0.109	0.112	986	11	93	1B+3Y	6R+4G	1B	2R	1G	4B+1Y
17	90	0.1	0	0.04	0.15	1.55	0.3	0.126	0.135	1016	12	90	1B+6Y	7R+5G	1B	5R	3G	6B+4Y
18	90	0.1	-0.05	0.02	0.075	1.55	0.35	0.071	0.083	1004	10	89	0	0	0	0	0	0
19	90	0.1	-0.05	0.02	0.1	1.79	0.35	0.095	0.111	1004	10	90	0	3R	0	0	0	0
20	90	0.1	-0.05	0.02	0.125	2.00	0.35	0.121	0.138	1058	13	91	1Y	4R+2G	0	3R	1G	0
21	90	0.1	-0.05	0.02	0.15	2.19	0.35	0.143	0.157	1055	13	89	2Y	13R+8G	0	6R	1W+3G+1K	3B
22	90	0.1	-0.05	0.02	0.175	2.37	0.35	0.209	0.188	1053	14	90	1W+4B+13Y	31R+31G	2Y+1B	2Y+11R	1W+1K+8G	6B+3Y
23	90	0.1	-0.05	0.04	0.1	1.27	0.35	0.063	0.105	999	11	89	0	0	0	0	0	0
24	90	0.1	-0.05	0.04	0.125	1.42	0.35	0.125	0.134	1008	10	91	1W	1R+2G	0	0	0	0
25	90	0.1	-0.05	0.04	0.15	1.55	0.35	0.149	0.163	1033	11	92	1W	6R+3G	1Y	0	1G	0
26	90	0.1	-0.05	0.04	0.175	1.67	0.35	0.173	0.179	1055	11	89	1W+1B+2Y	10R+11G	1Y	4R	1G	0
27	90	0.1	-0.05	0.04	0.2	1.79	0.35	0.191	0.193	1005	13	89	1W+2B+5Y	13R+15G	1Y	1W+1Y+4R	2G	0
28	90	0.1	-0.1	0.02	0.125	2.00	0.4	0.147	0.157	1060	12	92	1Y	5R+1G	0	1R	2G	0
29	90	0.1	-0.1	0.02	0.15	2.19	0.4	0.189	0.185	1025	14	91	3Y	8R+1G	0	1R	2G	1Y
30	90	0.1	-0.1	0.02	0.175	2.37	0.4	0.222	0.203	1057	15	91	5Y	11R+1G	1B	1R	4G+1K	1B+1Y
31	90	0.1	-0.1	0.02	0.2	2.53	0.4	0.247	0.210	1000	17	92	5Y	25R+14G	2B+1Y+1W	3R	4K+5G	3B
32	90	0.1	-0.1	0.04	0.125	1.42	0.4	0.116	0.126	1012	10	91	0	2R	1B	0	1G	0
33	90	0.1	-0.1	0.04	0.15	1.55	0.4	0.139	0.155	1028	10	92	1Y	2R+1G	2B	0	1G	0
34	90	0.1	-0.1	0.04	0.175	1.67	0.4	0.171	0.182	1058	11	93	1Y	5R+1G	2B+1Y	0	1G	0
35	90	0.1	-0.1	0.04	0.2	1.79	0.4	0.189	0.203	1049	12	93	1Y	7R+4G	2B+2Y	0	1G	0
36	90	0.1	-0.1	0.04	0.225	1.90	0.4	0.204	0.201	1027	13	92	1Y	9R+4G	2B+2Y	0	3G+1K	0

Table 22 Details about stability tests with wide cross-section

Target								Measured waves					Damage, trunk			Damage, roundhead		
Test no.	θ [°]	B [m]	Rc [m]	Wave steep.	Hs [m]	Tp [s]	h at LCS [m]	Hs (3) [m]	Hmo_I [m]	No waves	Spr. [°]	θ (Hi) [°]	SS N	C N	LS N	SH N	MH N	LH N
37	90	0.25	0.05	0.02	0.05	1.27	0.25	0.053	0.048	990	10	89	0	1R	0	0	0	0
38	90	0.25	0.05	0.02	0.075	1.55	0.25	0.075	0.072	1043	12	91	1W+3B+3Y	6G	0	1R+2Y	0	4Y
39	90	0.25	0.05	0.02	0.1	1.79	0.25	0.094	0.096	1029	13	92	1W+5B+11Y	11R+22G	2B	10R+1Y	20G+2K	13B+6Y
40	90	0.25	0.05	0.02	0.125	2.00	0.25	0.116	0.114	1073	16	91	1W+6B+13Y	19R+32G	7B	1W+6Y+17R	6K+26G	21B+14Y
41	70	0.25	0.05	0.02	0.05	1.27	0.25	0.049	0.046	996	10	72	0	0	0	0	0	0
42	70	0.25	0.05	0.02	0.075	1.55	0.25	0.071	0.073	1031	12	71	1B+2Y	2R+5G	2B	3R	0	3B+2Y
43	70	0.25	0.05	0.02	0.1	1.79	0.25	0.091	0.094	1039	13	74	1W+2B+7Y	8R+10G	6B	3Y+9R	16G	16B+5Y
44	70	0.25	0.05	0.02	0.125	2.00	0.25	0.115	0.108	1100	15	76	2W+6B+13Y	13R+19G	17B	2W+8Y+22R	6K+22G	22B+6Y
45	80	0.25	0.05	0.02	0.05	1.27	0.25	0.051	0.047	1021	10	80	0	0	0	0	0	0
46	80	0.25	0.05	0.02	0.075	1.55	0.25	0.073	0.074	1027	12	80	3Y	5G	1B	0	0	0
47	80	0.25	0.05	0.02	0.1	1.79	0.25	0.097	0.098	1018	14	82	1B+6Y	3R+16G	8B	1Y+6R	6G	9B+6Y
48	80	0.25	0.05	0.02	0.125	2.00	0.25	0.119	0.115	1076	16	82	3B+10Y	4R+18G	13B	1W+2Y+19R	2K+13G	13B+8Y+1W
49	100	0.25	0.05	0.02	0.05	1.27	0.25	0.054	0.049	993	10	98	0	0	0	0	0	0
50	100	0.25	0.05	0.02	0.075	1.55	0.25	0.079	0.072	1017	14	98	0	2G	0	1R	6G	2B
51	100	0.25	0.05	0.02	0.1	1.79	0.25	0.099	0.100	1005	15	101	4Y	5R+6G	5B	4R	3K+15G	13B+8Y
52	110	0.25	0.05	0.02	0.05	1.27	0.25	0.055	0.048	973	11	107	0	0	0	0	0	0
53	110	0.25	0.05	0.02	0.075	1.55	0.25	0.075	0.074	1024	13	109	0	1R+2G	0	1R	7G	2B+1Y
54	110	0.25	0.05	0.02	0.1	1.79	0.25	0.098	0.103	1018	15	111	2Y	3R+4G	2B	1Y+2R	14G	16B+8Y
55	110	0.25	0.05	0.02	0.125	2.00	0.25	0.116	0.117	1077	16	111	3B+4Y	3R+5G	5B	1y+13R	4K+21G	26B+13Y
56	60	0.25	0.05	0.02	0.05	1.27	0.25	0.050	0.047	980	8	64	0	0	0	0	0	0
57	60	0.25	0.05	0.02	0.075	1.55	0.25	0.069	0.068	1014	13	67	0	2R	0	0	1K+1G	2B
58	60	0.25	0.05	0.02	0.1	1.79	0.25	0.092	0.088	1034	12	67	1B+2Y	5R+3G	4B	1R	2K+4G	10B+2Y
59	60	0.25	0.05	0.02	0.125	2.00	0.25	0.110	0.100	1129	15	70	1B+7Y	9R+17G	17B	1Y+8R	4K+18G	21B+4Y
60	90	0.25	0	0.02	0.05	1.27	0.3	0.048	0.050	1025	9	90	0	0	0	0	0	0
61	90	0.25	0	0.02	0.075	1.55	0.3	0.069	0.074	1023	11	91	0	1R	0	1R	2G	0
62	90	0.25	0	0.02	0.1	1.79	0.3	0.098	0.103	992	13	92	2Y	8R+10G	0	7R	9G	8B
63	90	0.25	0	0.02	0.125	2.00	0.3	0.127	0.124	1023	15	94	4Y	34R+16G	3B	1Y+14R	14G	13B
64	90	0.25	-0.05	0.02	0.1	1.79	0.35	0.120	0.129	985	11	93	0	2R	0	0	0	0
65	90	0.25	-0.05	0.02	0.125	2.00	0.35	0.153	0.157	1075	13	93	0	17R+4G	1B	0	1K	2B
66	90	0.25	-0.05	0.02	0.15	2.19	0.35	0.184	0.179	1031	13	92	2Y	39R+16G	2B	3R	1K+5R	5B+3Y
67	90	0.25	-0.1	0.02	0.125	2.00	0.4	0.147	0.157	1060	12	92	0	5R+3G	1B	0	1G	0
68	90	0.25	-0.1	0.02	0.15	2.19	0.4	0.183	0.180	1026	13	92	0	21R+7G	3B+1Y	0	2G	1Y
69	90	0.25	-0.1	0.02	0.175	2.37	0.4	0.222	0.203	1057	15	91	1B+1Y	37R+19G	4B+1Y	1Y+4R	6G	10B+1G

Table 23 Stability numbers related to initiation of damage for all tests

Test		Crest	Free-	Norm. Rc	Wave	Ns (ID) for trunk			Ns (ID) for roundhead		
no.	[°]	width [m]	board [m]	Rc/D_{n50}	steepness	SS	C	LS	SH	MH	LH
1-4	90	0.1	0.05	1.54	0.02	1.26	1.26	1.13	1.64	1.26	1.18
5-8	90	0.1	0.05	1.54	0.035	1.74	1.74	1.81	1.74	1.30	1.47
9-12	90	0.1	0	0.00	0.02	1.87	1.46	-	1.97	1.83	1.68
13-17	90	0.1	0	0.00	0.035	2.10	1.64	-	2.21	2.27	1.41
18-22	90	0.1	-0.05	-1.54	0.02	2.83	1.82	4.03	2.75	2.75	2.75
23-27	90	0.1	-0.05	-1.54	0.035	3.32	2.40	-	3.21	-	-
28-31	90	0.1	-0.1	-3.08	0.02	3.63	2.83	4.59	4.75	4.27	4.75
32-36	90	0.1	-0.1	-3.08	0.035	-	2.67	3.64	-	-	-
37-40	90	0.25	0.05	1.54	0.02	1.20	1.19	1.88	1.45	1.50	1.45
41-44	70	0.25	0.05	1.54	0.02	1.37	1.13	1.47	1.37	1.44	1.37
45-48	80	0.25	0.05	1.54	0.02	1.40	1.23	1.54	1.60	1.64	1.50
49-51	100	0.25	0.05	1.54	0.02	1.91	1.56	1.75	1.78	1.45	1.54
52-55	110	0.25	0.05	1.54	0.02	1.95	1.45	1.99	1.88	1.36	1.45
56-59	60	0.25	0.05	1.54	0.02	1.77	1.41	1.77	1.85	1.33	1.38
60-63	90	0.25	0	0.00	0.02	2.16	1.40	2.44	1.51	1.41	1.54
64-66	90	0.25	-0.05	-1.54	0.02	-	2.34	-	3.54	3.18	3.05
67-69	90	0.25	-0.1	-3.08	0.02	-	2.83	3.29	3.97	3.71	3.67

Appendix B: Existing stability formulae

Powell and Allsop (1985), low crested slopes

Powell and Allsop (1985) analyzed the data by Allsop (1983) and proposed the following stability formula for two-layer armoured overtopped, low-crested slopes:

$$\frac{N_{od}}{N_a} = a\exp\left[b\, s_p^{-1/3}\, H_s/(\Delta D_{n50})\right] \quad \text{or} \quad \frac{H_s}{\Delta D_{n50}} = \frac{s_p^{1/3}}{b}\ln\left(\frac{1}{a}\frac{N_{od}}{N_a}\right) \qquad \text{Equation 1}$$

where values of the empirical coefficients a and b are given in the table as functions of freeboard R_c and water depth h. N_{od} and N_a are the number of units displaced out of the armour layer and the total number of armour layer units respectively.

Table 24 Values of coefficients a and b in Equation 1

R_c/h	$a \cdot 10^4$	b	wave steepness H_s/L_p
0.29	0.07	1.66	<0.03
0.39	0.18	1.58	<0.03
0.57	0.09	1.92	<0.03
0.38	0.59	1.07	>0.03

Van der Meer (1990), low crested slopes

Van der Meer (1988, 1990 and 1991) suggested the van der Meer stability formulae for non-overtopped rock slope, Equation 4 and Equation 5, to be used with D_{n50} replaced by $f_i D_{n50}$. The reduction factor f_i is in Van der Meer (1990) given as

$$f_i = \left(1.25 - 4.8\frac{R_c}{H_s}\sqrt{\frac{s_{op}}{2\pi}}\right)^{-1} \qquad \text{Equation 2}$$

where R_c is the freeboard $s_{op} = H_s/L_{op,}$ and L_{op} is deep water wave length corresponding to the peak wave period. Limits of Equation 2 are given by

$$0 < \frac{R_c}{H_s}\sqrt{\frac{s_{op}}{2\pi}} < 0.052 \qquad \text{Equation 3}$$

Irregular, head-on waves were used to establish the following formulae for **non-overtopped slopes** (van der Meer 1988)

$$\frac{H_s}{\Delta D_{n50}} = 6.2 \cdot S^{0.2} P^{0.18} N_z^{-0.1} \xi_m^{-0.5} \qquad \text{plunging waves: } \xi_m < \xi_{mc} \qquad \text{Equation 4}$$

$$\frac{H_s}{\Delta D_{n50}} = 1.0 \cdot S^{0.2} P^{-0.13} N_z^{-0.1} (\cot\alpha)^{0.5} \xi_m^{P} \quad \text{surging waves: } \xi_m > \xi_{mc} \qquad \text{Equation 5}$$

$$\xi_m = s_m^{-0.5}\tan\alpha \qquad \xi_{mc} = \left(6.2\, P^{0.31}(\tan\alpha)^{0.5}\right)^{1/(P+0.5)}$$

where H_s significant wave height in front of breakwater
D_{n50} Equivalent cube length of medium rock
ρ_s Mass density of rocks
ρ_w Mass density of water

Δ $(\rho_s/\rho_w) - 1$
S relative eroded area
P notional permeability; for three layer conventional breakwater P=0.4, two layer structure P=0.5, and homogeneous structure P=0.6.
N_z number of waves
α slope angle
s_m wave steepness, $s_m = H_s/L_{om}$
L_{om} deep water wave length corresponding to mean wave period

Validity:

1) Equation 4 and Equation 5 are valid for non-depth limited waves. For depth-limited waves H_s is replaced by $H_{2\%}/1.4$.
2) For cot $\alpha \geq 4.0$ only Equation 4 should be used.
3) $N_z \leq 7{,}500$ after which number equilibrium damage is more or less reached.
4) $0.1 \leq P \leq 0.6$, $0.005 \leq s_m \leq 0.06$, $2.0 t/m^3 \leq \rho \leq 3.1 t/m^3$
5) For the 8 test run with depth-limited waves, breaking conditions were limited to spilling breakers which are not as damaging as plunging breakers. Therefore Equation 4 and Equation 5 may not be conservative in some breaking wave conditions.

Uncertainty of the formula: The coefficients of variation on the factor 6.2 in Equation 4 and on the factor 1.0 in Equation 5 are estimated to be 6.5% and 8%, respectively.

van der Meer (1990), submerged breakwaters

The following formula was established for submerged breakwaters with two-layer armour on front, crest and rear slope. Irregular, head-on waves.

$$\frac{h_c'}{h} = (2.1 + 0.1S)\exp(-0.14\,N_s^*) \qquad \text{Equation 6}$$

where h water depth
h_c' height of structure over sea bed level
S relative eroded area
N_s^* spectral stability number, $N_s^* = \frac{H_s}{\Delta D_{n50}} s_p^{-1/3}$

Uncertainty of the formula: The uncertainty of Equation 6 can be expressed by considering the factor 2.1 as a Gauss distributed stochastic variable with the mean 2.1 and a standard deviation of 0.35, i.e. a coefficient of variation of 17%.

data source: Givler and Sorensen (1986): Regular head-on waves, slope 1:1.5
van der Meer: Irregular head-on waves, slope 1:2

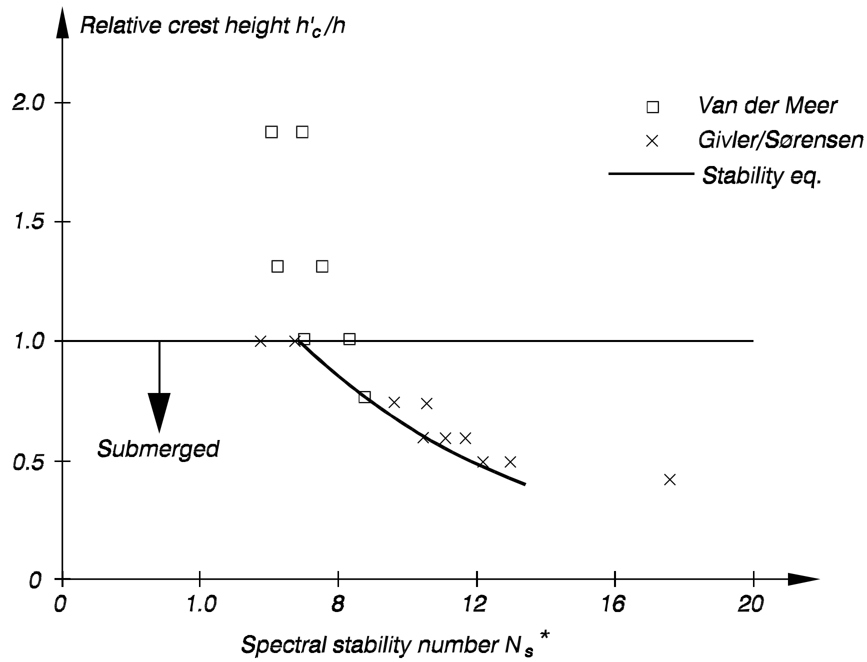

Vidal et al. (1992, 1995, 2000), head and trunk stability

Vidal et al. 1992 performed 3D small scale laboratory tests at NRC, Canada and proposed stability graphs for trunk corresponding to initiation of damage. In 1995 stability graphs for head damage for different damage levels were proposed. In 2000 a general methodology to calculate stability of LCS's was proposed and parameterized stability curves for initiation of damage were given for all structural sections. The tests are described in more detail in Appendix D.

Vidal et al. 1992, trunk damage

Two-Layer Armoured Low-Crested and Submerged Breakwaters

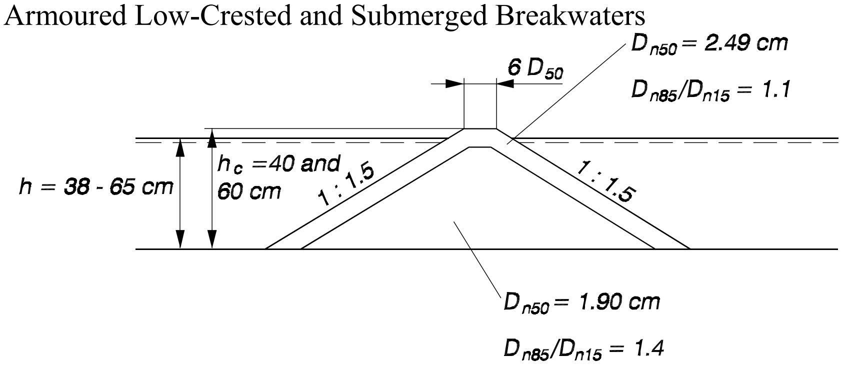

Figure 42 Tested trunk cross section in tests by Vidal et al. 1992

Tested ranges:

Irregular, head-on waves

H_s = 5-19cm, T_p =1.4 and 1.8 sec

Freeboard: -5cm ≤ $R_c = h_c$-h ≤ 6cm

Dimensionless freeboard -2 ≤ R_c/D_{n50} ≤ 2.4

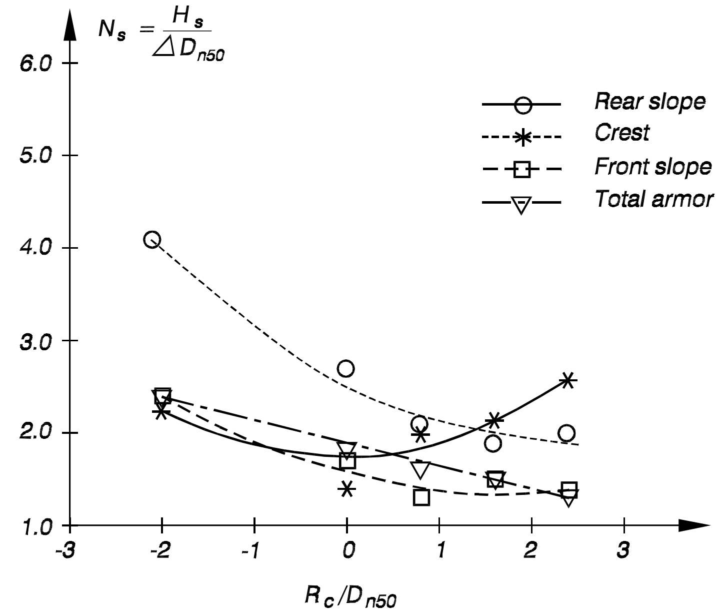

Figure 43 Stability of trunk corresponding to initiation of damage, S=0.5-1.5

Vidal et al. (1995), head

Vidal et al. (1995) proposed the following stability curves to be used for LCS roundheads.

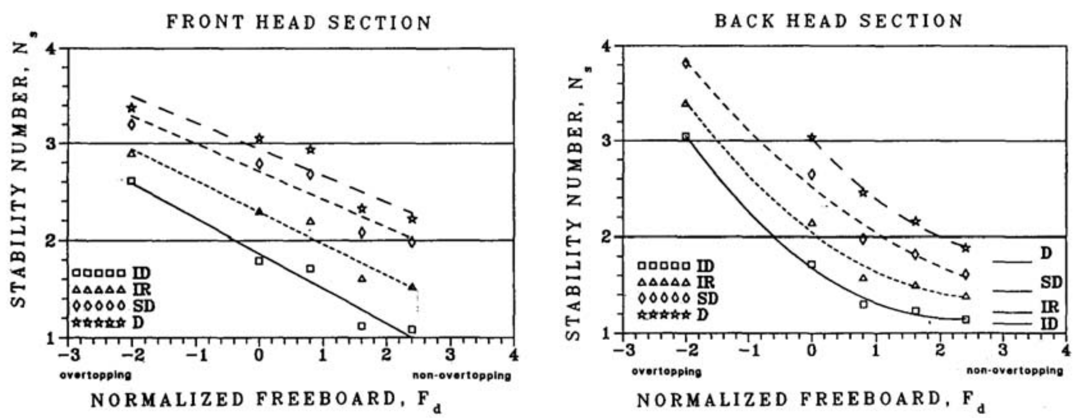

Figure 44 Breakwater head stability curves for different levels of damage

Damage level: ID, Initiation of Damage
IR, Iribarren's damage
SD, Start of Destruction
D, Destruction

Normalized freeboard: $F_d = F / D_{n50}$
F is used for freeboard

Vidal et al. (2000), head and trunk

Vidal et al. (2000) proposed a more general methodology to evaluate stability for various low-crested breakwater geometries. Reduction factors were introduced including existing knowledge about conventional breakwaters. Parameterized curves corresponding to initiation of damage of trunk and head were given as:

$$N_s = A + B F_d + C F_d^2 \qquad \text{Equation 7}$$

Equation 7 is valid in the range: $-2.01<F_d<2.41$

Table 25 Values of coefficients A, B and C in Equation 7

Sector	**A**	**B**	**C**
Front slope and front head	1.831	-0.2450	0.0119
Crest	1.652	0.0182	0.1590
Back slope	2.575	-0.5400	0.1150
Back head	1.681	-0.4740	0.1050

Appendix C: Calculation of eroded area S

Broderick (1983) defined the damage parameter $S = A_e / D_{n50}^2$. A_e is the average eroded area in a section of width X. S is often used to quantify damage of rubble structures.

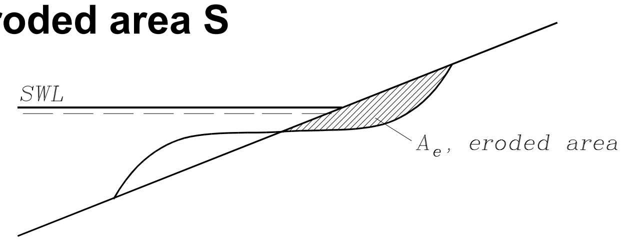

Broderick used the equation to determine damage on a riprap slope. Broderick's equation can be written in terms of number of displaced units (N). The number of displaced stones N in the test section is assumed to equal the eroded volume $V_e = N \cdot D_{n50}^3 /(1-n)$. The average eroded area in the test section can then be calculated as $A_e = V_e / X$, and Broderick's equation becomes:

$$S = \frac{N \cdot D_{n50}}{(1-n) \cdot X} \qquad \text{Equation 8}$$

n: Porosity of armour (n=0.43 in the present experiments)
X: Width of test section (X=50cm for the trunk)
D_{n50}: Nominal diameter of armour (D_{n50}=3.25cm)

For the trunk the relationship between damage parameter S and number of displaced units in *Equation 8* becomes $S = 0.11 \cdot N$, which corresponds to S=0.34 for N=3.

Appendix D: Existing stability data

UCA, 2001

Tests were carried out at the wave flume of the University of Cantabria (68.9 x 2 x 2 m). The cross section given in Table 26 was tested in regular waves (52 tests) and irregular waves (16 tests). However, the stone size of the armour indicates that viscous scale effects were present in the tests.

Table 26 Test conditions in UCA tests

Number of tests	16 with irregular waves
Structure height	0.25m
Crest width	0.25m
Structure slope	1V:2H
Foreshore slope	1:20
Water depth	0.20m and 0.30m
Freeboard	-0.05m and +0.05m
Type of breakwater	Reef type
Materials	Quarry crushed limestone, W_{50}=4.3g, D_{n50}=0.012m
Hs	0.02m to 0.07m
Tp	1.8sec to 3.4sec
Test duration	1 hour (1300 to 2400 waves)

References: None. Document describing the tests and digital data have been provided by Cesar Vidal, UCA.

Table 27 UCA test results for irregular waves

TEST	$H_{1/3}$	$H_{1/10}$	$H_{1/100}$	H_{max}	H_{50}	H_{100}	H_{200}	T_p	Rc	D	S
9	0.022	0.029	0.041	0.058	0.038	0.035	0.031	1.8	0.05	3600	0.70
10	0.042	0.057	0.080	0.093	0.077	0.070	0.063	1.8	0.05	3600	9.17
20	0.053	0.073	0.102	0.126	0.096	0.088	0.079	2.6	0.05	3600	50.70
21	0.039	0.054	0.077	0.099	0.071	0.064	0.057	2.6	0.05	3600	1.36
29	0.043	0.058	0.081	0.096	0.072	0.065	0.058	3.4	0.05	3600	8.47
30	0.033	0.044	0.063	0.101	0.054	0.049	0.043	3.4	0.05	3600	2.00
38	0.036	0.047	0.055	0.085	0.061	0.055	0.050	1.8	-0.05	3600	0.89
39	0.062	0.081	0.096	0.153	0.106	0.096	0.087	1.8	-0.05	3600	3.68
46	0.044	0.058	0.067	0.091	0.073	0.067	0.060	2.2	-0.05	3600	0.87
47	0.061	0.081	0.096	0.153	0.106	0.096	0.087	2.2	-0.05	3600	4.22
52	0.054	0.072	0.082	0.131	0.089	0.082	0.073	2.6	-0.05	3600	2.02
53	0.038	0.050	0.057	0.089	0.061	0.057	0.050	2.6	-0.05	3600	1.04
58	0.065	0.088	0.098	0.146	0.108	0.098	0.087	3.0	-0.05	3600	8.59
59	0.036	0.048	0.047	0.085	0.053	0.050	0.045	3.0	-0.05	3600	0.99
67	0.074	0.098	0.108	0.157	0.117	0.108	0.097	3.4	-0.05	3600	11.85
68	0.041	0.054	0.058	0.107	0.064	0.058	0.052	3.4	-0.05	3600	0.01

$H_{1/n}$: Incident average of the N/n biggest waves in the test of N waves in m.
H_n : Incident average of the n biggest waves in the test of N waves in m
H_{max} : Incident maximum wave height in the test of N waves in m
Tp: Incident peak period
Rc: Freeboard in m
D: Duration in seconds
S: Damage according to Broderick (Appendix C)

To investigate the influence of wave period all data are plotted in Figure 45. It is seen that all data follows the same trend in damage pregress.

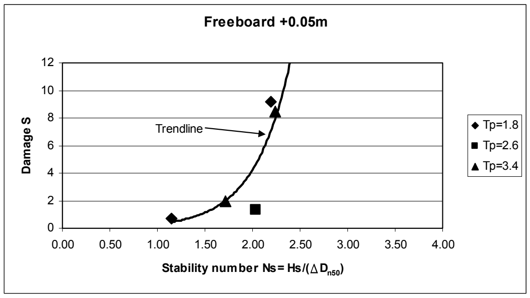

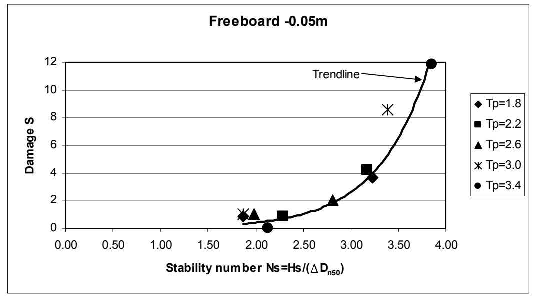

Figure 45 Damage in UCA tests

Delft, 1995

Burger (1995) tested the influence of rock shape and grading on the stability of front, crest and rear slope of low-crested structures. No or very small influences were found. Tests were performed at Delft Hydraulics in the "Shelde basin" at the "De Voorst". Results are presented by Burger (1995) and Van der Meer et al. (1996).

Figure 46 Test details for Delft 1995 tests

Number of tests	76
Structure height	0.67m
Crest width	?
Structure slope	Seaward 1:2, and rear 1:1.5
Foreshore slope	Horizontal
Water depth	0.6m
Freeboard	+0.07m
Type of breakwater	2 layer conventional type
Materials	Rock D_{n50}=0.035m
Hs	0.07 to 0.18m
Tp	Two different steepness' s_p=0.02 and s_p=0.04. Tp= 1.5s to 2.4s.
Test duration	1000 waves

Table 28 Selected results from Delft tests

serie	test	Hs	Dn50	rho	Tp	s	S front	S crest	S rear
		(m)	(m)	(kg/m3)	(s)	(-)			
1a	1	0.071	0.0351	2700	1.586	0.02	0.00	0.51	0.46
	2	0.098	0.0351	2700	1.7986	0.02	0.85	0.48	0.54
	3	0.124	0.0351	2700	2.0276	0.02	1.41	0.22	1.33
	4	0.144	0.0351	2700	2.1686	0.02	3.08	1.31	2.08
	5	0.170	0.0351	2700	2.3844	0.02	5.70	2.75	3.42
	6	0.178	0.0351	2700	2.4292	0.02	4.27	1.84	5.33
1b	1	0.082	0.0351	2700	1.1382	0.04	0.00	0.00	0.00
	2	0.103	0.0351	2700	1.2822	0.04	0.95	0.00	0.00
	3	0.123	0.0351	2700	1.3744	0.04	1.52	0.12	0.00
	4	0.145	0.0351	2700	1.5008	0.04	3.61	0.00	0.00
	5	0.161	0.0351	2700	1.6106	0.04	6.05	1.05	0.74
	6	0.182	0.0351	2700	1.7194	0.04	11.55	1.00	2.74
2a	1	0.071	0.0347	2700	1.586	0.02	0.00	0.00	0.49
	2	0.098	0.0347	2700	1.7986	0.02	1.32	0.44	1.00
	3	0.124	0.0347	2700	2.0276	0.02	3.32	0.85	0.86
	4	0.144	0.0347	2700	2.1686	0.02	5.65	0.53	2.57
	5	0.170	0.0347	2700	2.3844	0.02	10.04	3.76	3.99
	6	0.178	0.0347	2700	2.4292	0.02	32.22	24.79	12.19

2b	1	0.082	0.0347	2700	1.1382	0.04	0.15	0.00	0.00
	2	0.103	0.0347	2700	1.2822	0.04	1.06	0.02	0.00
	3	0.123	0.0347	2700	1.3744	0.04	1.15	0.00	0.00
	4	0.145	0.0347	2700	1.5008	0.04	5.13	0.00	0.00
	5	0.161	0.0347	2700	1.6106	0.04	7.72	0.11	0.26
	6	0.182	0.0347	2700	1.7194	0.04	12.52	2.07	0.00
3a	1	0.078	0.0335	2700	1.6292	0.02	0.00	0.32	0.64
	2	0.101	0.0335	2700	1.7758	0.02	2.22	0.25	0.00
	3	0.119	0.0335	2700	1.9896	0.02	3.36	2.43	0.56
	4	0.140	0.0335	2700	2.0936	0.02	7.30	1.25	4.19
	5	0.160	0.0335	2700	2.3282	0.02	11.93	4.33	1.75
	6	0.184	0.0335	2700	2.4296	0.02	25.67	26.42	12.00
3b	1	0.084	0.0335	2700	1.1338	0.04	0.43	0.00	0.00
	2	0.102	0.0335	2700	1.2746	0.04	1.22	0.36	0.00
	3	0.120	0.0335	2700	1.3778	0.04	2.39	0.87	2.09
	4	0.143	0.0335	2700	1.4954	0.04	6.70	0.00	0.00
	5	0.160	0.0335	2700	1.6082	0.04	6.36	0.47	0.11
	6	0.181	0.0335	2700	1.71	0.04	6.61	1.99	5.83
4a	1	0.078	0.0338	2700	1.6292	0.02	0.54	0.00	0.00
	2	0.101	0.0338	2700	1.7758	0.02	2.22	0.09	1.40
	3	0.119	0.0338	2700	1.9896	0.02	3.62	1.37	0.21
	4	0.140	0.0338	2700	2.0936	0.02	7.07	1.49	5.76
	5	0.160	0.0338	2700	2.3282	0.02	11.39	1.02	1.69
	6	0.184	0.0338	2700	2.4296	0.02	10.98	18.43	7.04
4b	1	0.084	0.0338	2700	1.1338	0.04	0.00	0.00	0.33
	2	0.102	0.0338	2700	1.2746	0.04	0.97	0.00	0.00
	3	0.120	0.0338	2700	1.3778	0.04	1.38	0.08	0.23
	4	0.143	0.0338	2700	1.4954	0.04	5.18	0.02	0.49
	5	0.160	0.0338	2700	1.6082	0.04	4.72	0.15	1.74
	6	0.181	0.0338	2700	1.71	0.04	12.75	1.40	0.73
5a	1	0.059	0.0336	2700	1.3736	0.02	0.00	0.00	0.00
	2	0.080	0.0336	2700	1.6426	0.02	1.95	0.24	0.00
	3	0.102	0.0336	2700	1.7788	0.02	1.42	0.50	0.59
	4	0.120	0.0336	2700	2.0146	0.02	3.10	0.49	0.00
	5	0.142	0.0336	2700	2.1218	0.02	9.30	1.09	3.43
	6	0.160	0.0336	2700	2.338	0.02	8.10	3.32	4.09
	7	0.188	0.0336	2700	2.4038	0.02	14.80	5.16	5.63
5b	1	0.059	0.0336	2700	0.9768	0.04	0.20	0.22	0.22
	2	0.081	0.0336	2700	1.1354	0.04	0.67	0.00	0.00
	3	0.101	0.0336	2700	1.282	0.04	1.31	0.00	0.00
	4	0.122	0.0336	2700	1.3746	0.04	1.38	0.20	1.10
	5	0.143	0.0336	2700	1.5046	0.04	5.69	0.08	0.40
	6	0.160	0.0336	2700	1.6096	0.04	8.03	0.28	0.44
	7	0.182	0.0336	2700	1.6924	0.04	15.17	0.89	1.36
6a	1	0.059	0.0368	2550	1.3736	0.02	0.27	0.06	0.03
	2	0.080	0.0368	2550	1.6426	0.02	0.16	0.05	0.12
	3	0.102	0.0368	2550	1.7788	0.02	1.65	1.62	0.56
	4	0.120	0.0368	2550	2.0146	0.02	6.02	2.63	3.29
	5	0.142	0.0368	2550	2.1218	0.02	8.57	7.11	3.89
	6	0.160	0.0368	2550	2.338	0.02	>50	>50	>50
	7	0.188	0.0368	2550	2.4038	0.02	>50	>50	>50
6b	1	0.059	0.0368	2550	0.9768	0.04	0.10	0.04	0.00
	2	0.081	0.0368	2550	1.1354	0.04	0.12	0.19	0.00
	3	0.101	0.0368	2550	1.282	0.04	1.14	0.00	0.00

	4	0.122	0.0368	2550	1.3746	0.04	2.84	0.50	0.12
	5	0.143	0.0368	2550	1.5046	0.04	4.95	0.90	0.00
	6	0.160	0.0368	2550	1.6096	0.04	10.58	4.12	1.70
	7	0.182	0.0368	2550	1.6924	0.04	>50	>50	>50

NRC, 1992

Details on setup are found in Vidal et al. (1995) and in Table 29. Tests were performed on a complete 3D structure, and damage was measured in trunk and roundhead. The trunk was divided in front slope (FS), back slope (BS), crest (C), and total slope (TS). The roundhead was divided in front head (FH) covering an area of 60° in the seaward part, and back head (BH), which covered the remaining 120° of the leeward part of the roundhead.

Table 29 Test details for NRC tests

Number of tests	35
Structure length	4.7m
Structure height	40cm and 60cm
Crest width	0.15m ($6 \cdot D_{n50}$)
Structure slope	1:1.5
Foreshore slope	Horizontal bed
Water depth	38cm to 65cm
Freeboard	-0.05, 0.0, 0.02, 0.04, 0.06
Type of breakwater	2 layer conventional type
Materials	Gravel armour: D_{50}=2.5cm, D_{85}/D_{15}=1.1cm, r_s=2650kg/m^3, n=0.44. Gravel core: D_{50}=1.9cm, D_{85}/D_{15}=1.4cm, r_s=2650kg/m^3, n=0.44.
Hs	0.05m to 0.15m
Tp	1.4s and a few 1.8s

Damage S to the trunk was calculated according to Broderick (Appendix C) but for the roundhead the methodology described in Vidal et al. (1995) was use. The mean head radius R is calculated from *Equation 9*.

$$R = \frac{b}{2} + \frac{\cot\alpha\,(Hs + F)}{2}, \text{ for } F \le \frac{Hs}{2}$$
$$R = \frac{b}{2} + \cot\alpha\left(\frac{Hs}{4} + F\right), \text{ for } F > \frac{Hs}{2} \qquad \text{Equation 9}$$

In *Equation 9*, b is the crest width, α is the structure slope, and F is the freeboard. Further the arc length $A_{l\theta}$ is calculated as $A_{l\theta} = R\theta$, where θ is the angle covered by the actual section of the roundhead, e.g. θ = π/3 equal to 60° for the seaward head. It is now possible to calculate a damage parameter according to *Equation 10*.

$$S_{head} \frac{N \cdot D_{n50}}{(1-n) \cdot A_{l\theta}} \qquad \text{Equation 10}$$

In *Equation 10* N is the number of displaced stones in the section, and n is the porosity of the armour.

Table 30 Selected results from NRC tests

TEST	Hs	Tp	Rc	S(BH)	GD	S(FH)	GD	S(TS)	GD	S(C)	GD	S(BS)	GD	S(FS)	GD
1	0.047	1.39	0	0.39	ND	0.39	ND	0.45	ND	0.72	ND	0	ND	0.45	ND
4	0.073	1.4	0	1.97	ID	0	ND	1.27	ND	1	ID	0.09	ND	0.81	ID
5	0.073	1.4	0	0.98	ID	0.66	ND	2.08	ID	1.09	ID	0.18	ND	0.36	ND
2	0.092	1.41	0	2.38	IR	2.38	ID	4.74	IR	4.64	IR	0.45	ND	2.87	IR
3	0.11	1.41	0	3.47	IR	3.73	IR	5.15	IR	2.97	IR	0.18	ND	3.31	IR
13	0.126	1.4	0	12.12	D	13.73	D	17.61	D	9.83	SD	0.82	ID	9.19	D
9	0.074	1.39	-0.05	0	ND	0	ND	0	ND	0.18	ND	0	ND	0.27	ND
6	0.086	1.41	-0.05	0	ND	0.4	ND	1.63	ID	1.36	ID	0.09	ND	0.63	ND
7	0.112	1.41	-0.05	0.51	ND	2.4	ID	2.53	IR	2.72	IR	0.18	ND	1.81	ID
8	0.124	1.41	-0.05	0.64	ND	1.93	ID	4.54	IR	2.44	IR	0.27	ND	4.21	SD
14	0.132	1.4	-0.05	1.42	ID	10.13	D	5.35	IR	4.6	IR	0.09	ND	2.72	IR
15	0.152	1.41	-0.05	3.3	IR	14.33	D	10.72	SD	10.22	SD	0.54	ND	5.03	SD
16	0.054	1.4	0.02	1.16	ND	0	ND	1.36	ND	0.09	ND	0.18	ND	0.27	ND
12	0.073	1.41	0.02	3.55	IR	1.48	ID	3.54	IR	1.09	ID	0.27	ND	2.44	IR
10	0.092	1.41	0.02	6.35	SD	1.63	ID	6.43	IR	1.27	ID	0.27	ND	4	SD
11	0.103	1.41	0.02	8.62	SD	5.34	IR	8.8	SD	3.57	IR	0.63	ND	5.31	SD
17	0.146	1.4	0.02	15.38	D	23.18	D	43.76	D	8.63	SD	1.54	ID	11.83	D
18	0.045	1.41	0.04	0.71	ND	0.85	ND	0.45	ND	0.09	ND	0	ND	0.27	ND
19	0.077	1.4	0.04	4.36	SD	3.68	IR	4.13	IR	1.27	ID	0.36	ND	2.78	IR
20	0.094	1.4	0.04	12.18	D	13.78	D	6.68	SD	1.99	ID	0.54	ND	4.72	SD
21	0.116	1.4	0.04	18.24	D	19.14	D	22.31	D	2.62	ID	1.27	ID	11.22	D
22	0.136	1.41	0.04	_	_	_	_	_	_	4.76	IR	0.91	ID	_	_
23	0.151	1.41	0.04	_	_	_	_	_	_	3.28	IR	3.17	IR	_	_
24	0.052	1.41	0.06	1.41	ID	1.41	ID	1.09	ND	0	ND	0	ND	0.91	ID
25	0.077	1.42	0.06	8.32	SD	5.1	IR	4.08	IR	0.18	ND	0	ND	2.98	IR
26	0.09	1.41	0.06	16.43	D	8.92	SD	5.16	IR	0.36	ND	1	ND	5.62	SD
27	0.109	1.41	0.06	_	_	12.58	D	19.56	D	1.18	ID	2.26	IR	11.09	D
28	0.122	1.41	0.06	_	_	_	_	_	_	1.81	ID	3.08	IR	_	_
29	0.132	1.41	0.06	_	_	_	_	_	_	2.35	IR	3.3	SD	_	_
30	0.05	1.82	0.02	0.51	ND	0	ND	0.91	ND	0.36	ND	0	ND	0.36	ND
31	0.078	1.82	0.02	4.22	SD	4.64	IR SD	4.7	IR	1.81	ID	0.45	ID	3.54	IR
32	0.105	1.81	0.02	13.28	D	11.63	D	16.49	D	3.69	IR	0.54	ND	6.79	SD
33	0.131	1.81	0.02	_	_	16.84		_		3.7	IR	0.27	ND	16.12	D
34	0.07	1.82	0.06	2.48	IR	0.91	ND	4.46	IR	0.27	ND	0	ND	2.99	IR
35	0.096	1.82	0.06	15.59	D	6.44	SD	26.55	D	0.36	ND	0.72	ND	8.87	D

Delft, 1988

Van der Meer (1988) performed 31 LCS stability tests in the wave flume (1.0m wide, 1.2m deep and 50m long) at Delft Hydraulics. All tests were performed with 1000 waves and 3000 waves. Water depth was kept constant and structure height was varied.

Table 31 Test details for Delft 1988 tests

Number of tests	31
Structure height	0.3m, 0.40m and 0.525m
Crest width	$8D_{n50}$
Structure slope	1:2
Foreshore slope	1:30
Water depth	0.4m
Freeboard	-0.1m, 0, +0.125m
Type of breakwater	Two layer conventional type
Materials	Armour D_{n50}=0.0344m, Core D_{n50}=0.019m. ρ_s=2600kg/m^3
Hs	0.08m to 0.22m
Tp	1.96sec and 2.56sec
Test duration	Test with both 1000 and 3000 waves

Table 32 Selected results from Delft 1988 tests

Test	Structure height (m)	Tp (s)	Hs (m)	$Hs/\Delta D_{n50}$ (-)	Tz (s)	Damage S (N=1000)	(N=3000)
PA001	0.4	1.96	0.105	1.9077	1.70	1.480	2.47
PA002	0.4	1.96	0.125	2.27108	1.72	4.200	4.40
PA003	0.4	1.98	0.145	2.63445	1.72	2.870	8.63
PA004	0.4	1.96	0.174	3.16134	1.72	13.530	20.54
PA005	0.4	1.96	0.083	1.50799	1.70	1.280	1.72
PA006	0.4	2.56	0.134	2.43459	2.21	3.850	4.66
PA007	0.4	2.56	0.159	2.88881	2.22	3.520	5.52
PA008	0.4	2.56	0.196	3.56105	2.19	16.910	46.38
PA009	0.4	2.56	0.111	2.01672	2.22	2.010	2.92
PA010	0.4	2.53	0.077	1.39898	2.21	0.860	1.02
PA011	0.4	2.56	0.176	3.19767	2.21	9.620	17.87
PA012	0.525	2.60	0.137	2.4891	2.21	3.270	5.64
PA013	0.525	2.60	0.162	2.94331	2.20	13.040	21.98
PA014	0.525	2.56	0.112	2.03488	2.19	3.050	3.39
PA015	0.525	2.50	0.078	1.41715	2.21	0.680	0.75
PA016	0.525	2.56	0.149	2.70712	2.22	8.660	14.54
PA017	0.525	1.94	0.128	2.32558	1.70	6.690	12.27
PA018	0.525	1.96	0.105	1.9077	1.68	2.450	3.54
PA019	0.525	1.94	0.083	1.50799	1.68	1.160	1.84
PA020	0.525	1.96	0.148	2.68895	1.70	14.070	45.86
PA021	0.3	1.96	0.147	2.67078	1.72	1.590	2.53
PA022	0.3	1.94	0.175	3.17951	1.72	4.640	7.02
PA023	0.3	1.96	0.196	3.56105	1.72	4.630	6.77
PA024	0.3	1.96	0.216	3.92442	1.74	10.100	13.54
PA025	0.3	1.94	0.116	2.10756	1.70	1.450	1.71
PA026	0.3	1.98	0.161	2.92515	1.72	1.810	2.05
PA027	0.3	2.53	0.193	3.50654	2.18	7.660	11.60
PA028	0.3	2.56	0.161	2.92515	2.18	4.230	7.43
PA029	0.3	2.56	0.137	2.4891	2.18	2.000	3.11
PA030	0.3	2.56	0.11	1.99855	2.18	0.970	1.20
PA031	0.3	2.60	0.219	3.97892	2.16	13.470	16.96

EU Fifth Framework Programme 1998-2002
Energy, Environment and Sustainable Development

Environmental Design of Low Crested Coastal Defence Structures

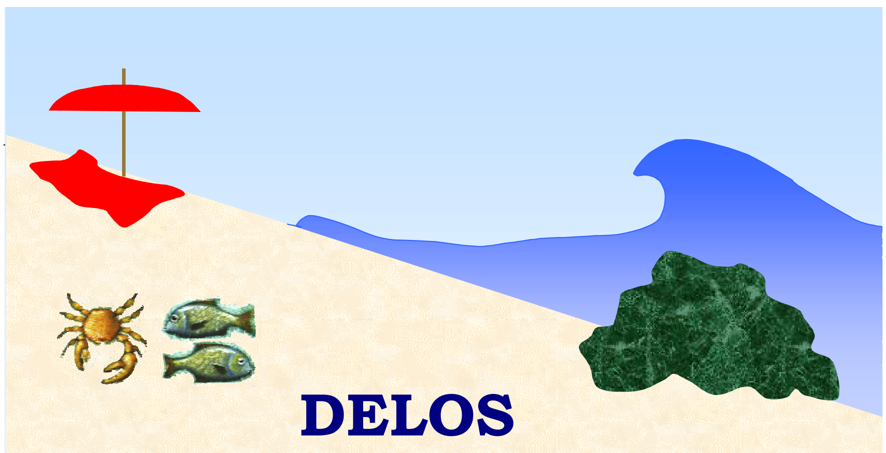

Wave basin hydrodynamic tests

Internal Report

Date of preparation: 15.06.2003 **Contract EVK3-CT-2000-00041**

List of Contents

List of Figures

List of Tables

3D Hydrodynamic tests at Aalborg University, DK

by Barbara Zanuttigh & Alberto Lamberti

1. Introduction

Typical existing structures

In this subsection, some typical cross sections of existing structures built-up in different part of the world are presented in Fig.s 1.1-1.5.

$h_s/Dn_{50}=3.2$

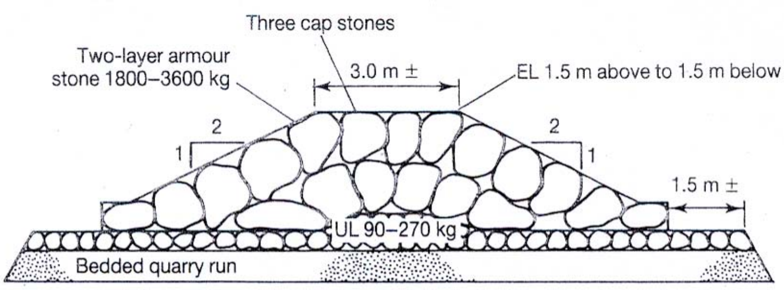

Fig. 1.1 Example of groin cross-section from Atlantic Coast, North Carolina, USA.

$h_s/Dn_{50}=3.6$

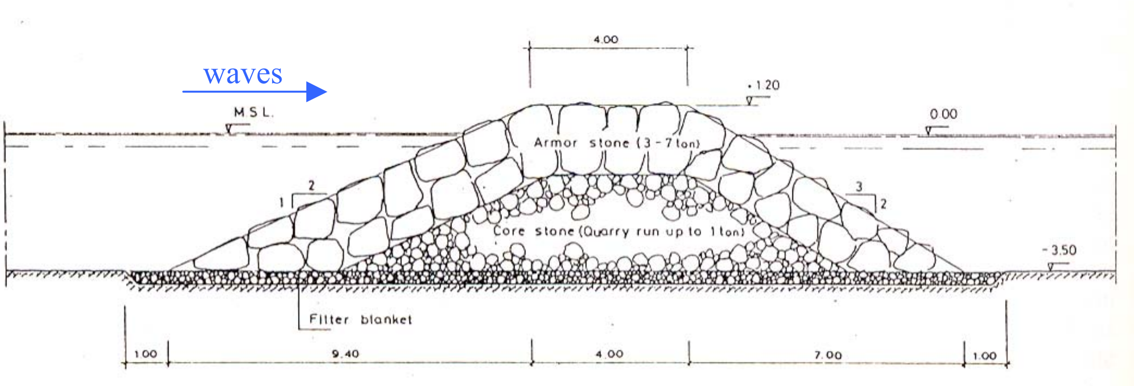

Fig. 1.2 Section of a typical detached (emerging) breakwater used in the Emilia Romagna, IT.

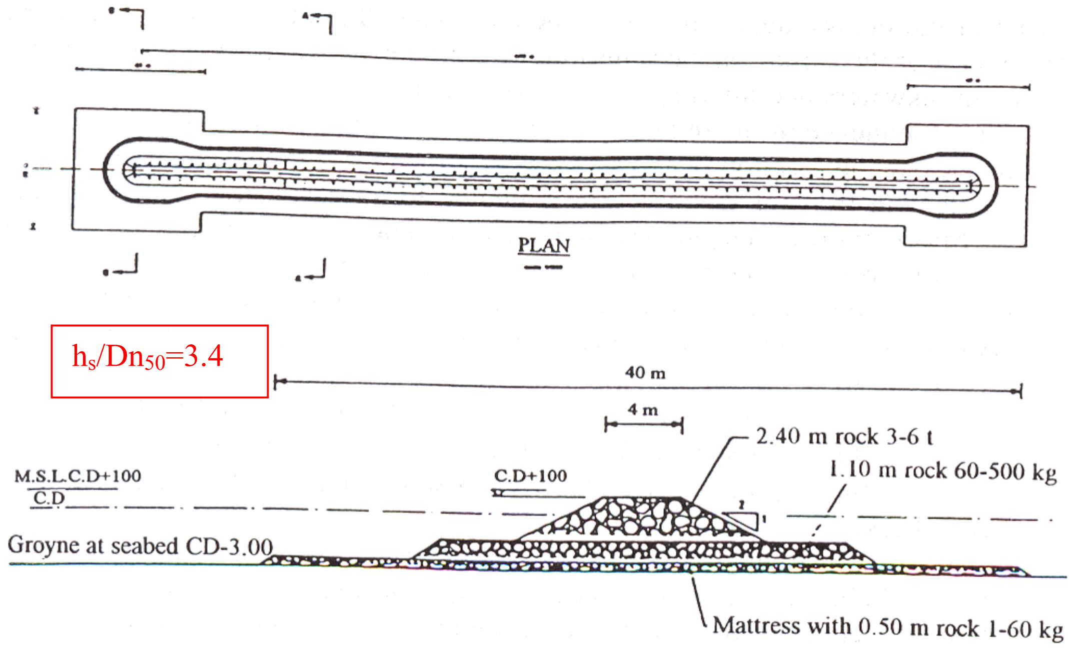

Fig. 1.3 Layout of breakwater scheme proposed for Kerteh (top) and typical cross-section of offshore breakwater (bottom) from Lindo et al., 1993.

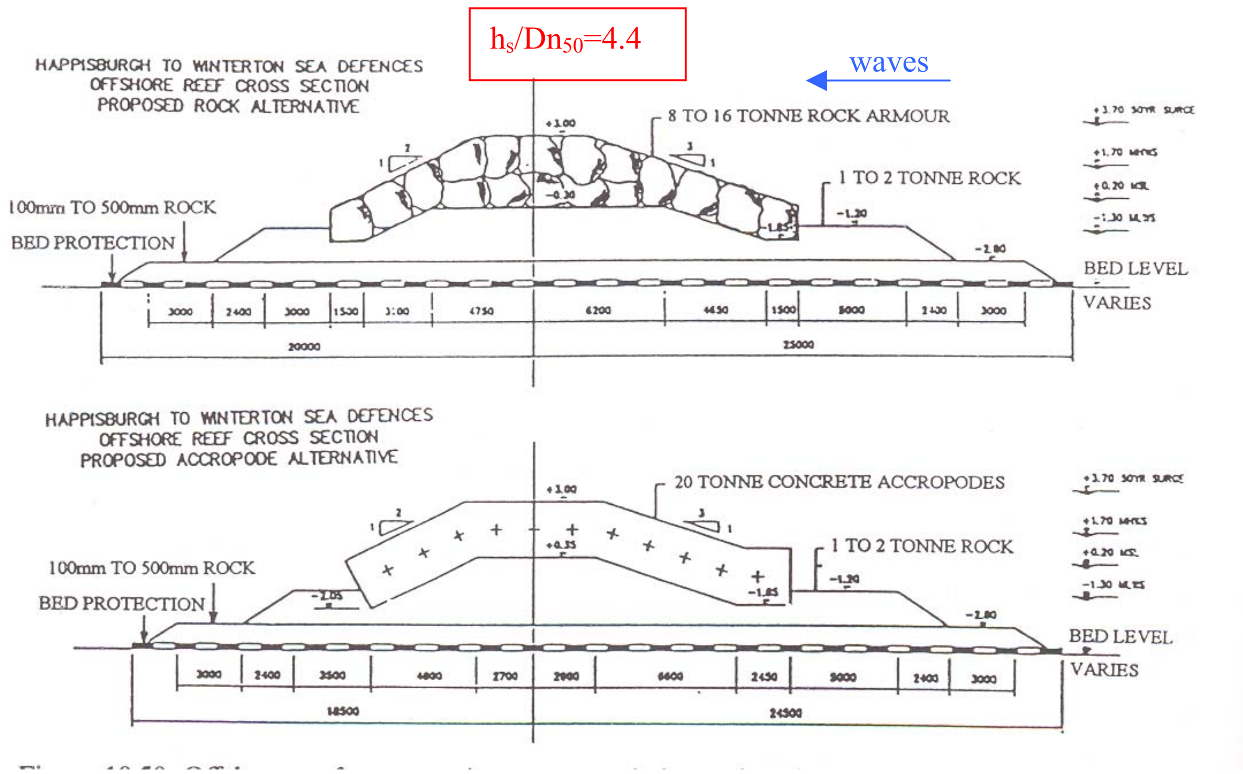

Fig. 1.4 Nappisburgh to Wintertone sea defences, UK.

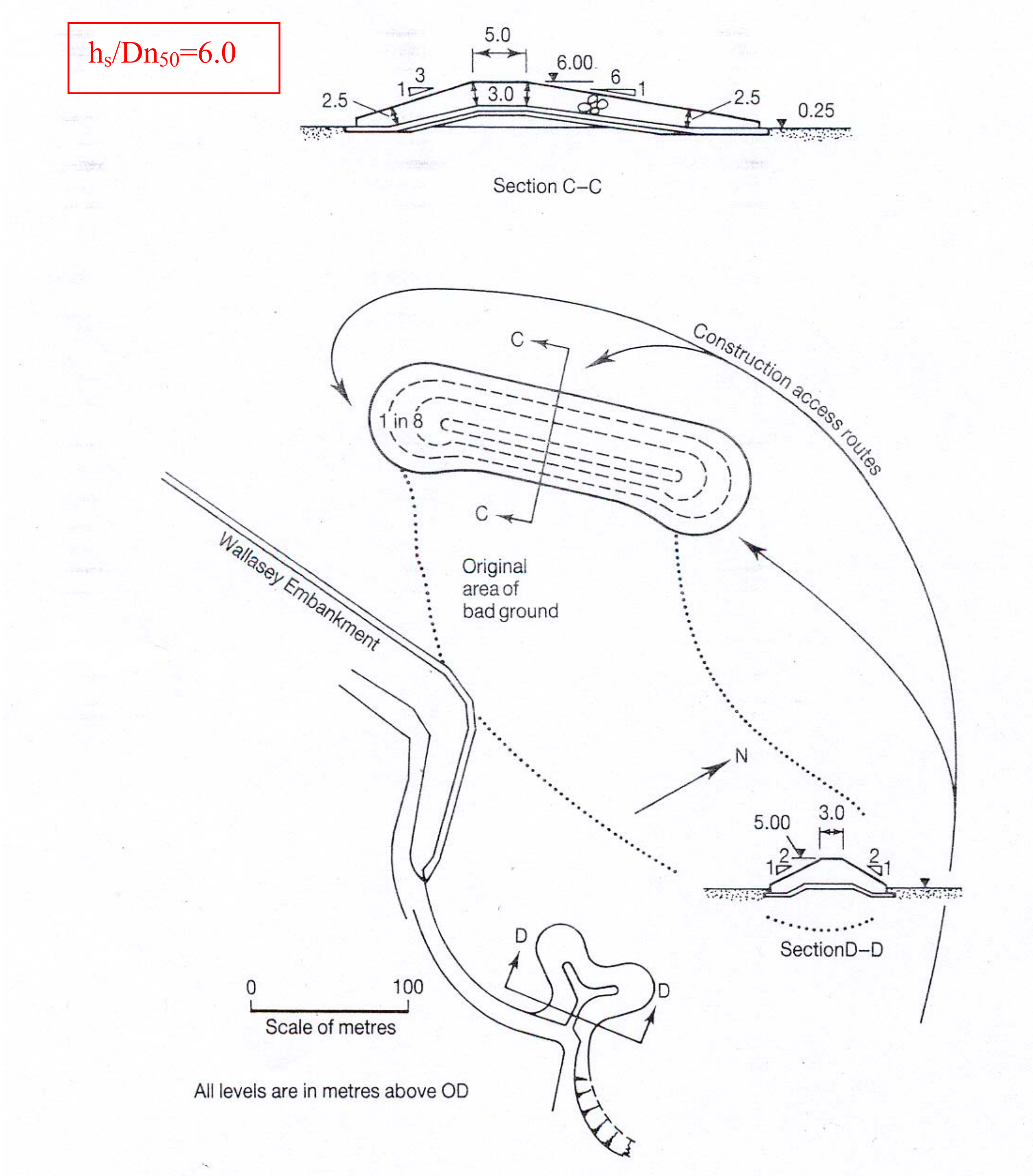

Fig. 1.5 Offshore breakwater, Leasowe Bay, UK. H_s=3.0 m, T_p=5-7 s, Dn_{50}=1.0 m.

In conclusion, the ratio h_s/Dn_{50} is in the range 3.0-6.0. The lower limit is related to the layered structure of the mound, whereas the upper limit is related to depth limited wave conditions, which always control design wave height for coastal defence structures. Actually, the ratio is always below 4.0 when the slope is 1:2 and increases up to 6.0 only in the extreme mild slope case of Fig. 1.5.

Available wave basin laboratory test

This subsection contains a brief review of 3D hydrodynamic tests.

Gourlay (1974)
The purpose of these experiments was to analyse the alongshore current generation by breaker height gradients. The *layout* adopted (Fig. 1.6) consisted of a semi-infinite breakwater parallel to wave crests, behind which a beach was built up in concrete. This beach was parallel to undiffracted wave crests in the exposed zone, outside the geometric shadow of the breakwater, while in the sheltered zone behind the breakwater it wascurved with a constant radius centred on the breakwater tip.

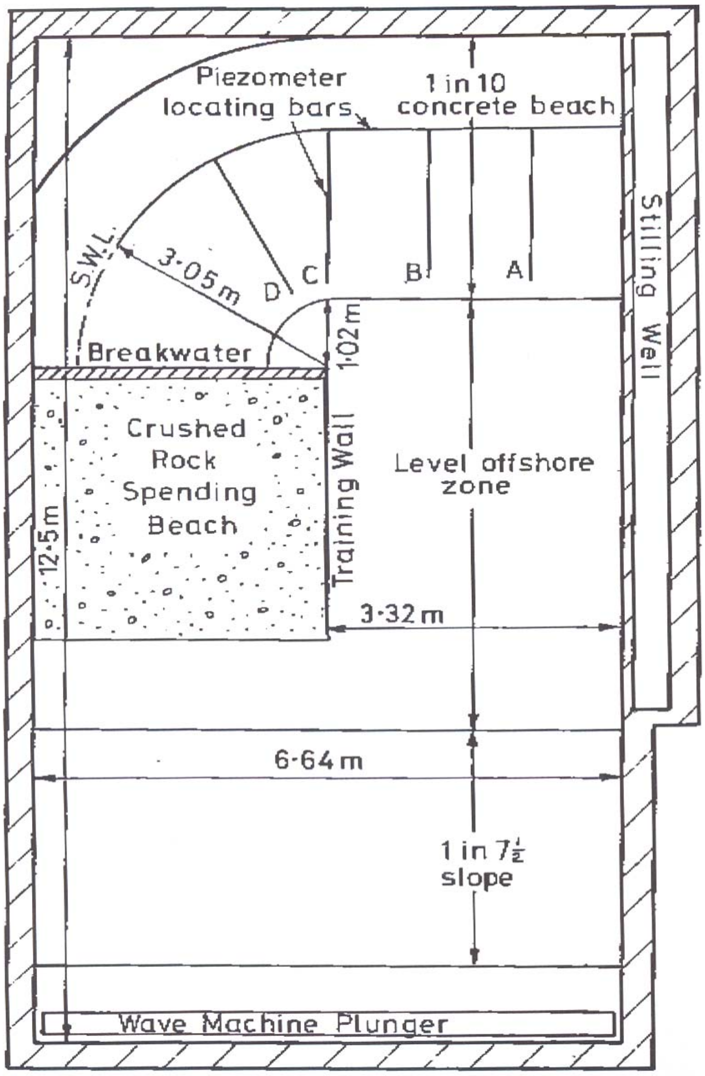

Fig. 1.6 Experimental set-up. The sea bed consists of a plane beach sloping at 1:30
with a rip channel excavated in the centre.

Wave conditions considered regular wves, with wave periods in the range 1-1.5 s. Water depth offshore was 0.20 m, constant for all tests.

Measurements were performed with 39 piezometers, to obtain wave set-up; capacitance wave height meters of the insulated wire type, to obtain wave heights; a movie camera, to analyse flow circulation. The camera was suspended above the basin, pointing vertically downwards, and the paths of coloured floats were recorded during a period of few minutes.
Remarks. Accuracy and consistency of the measurements were influenced by the fact that the test basin was located outdoors and was thus subjected to weather changes.

Hamm (1993)
Tests were carried out in a multidirectional wave tank, aiming to analyse wave propagation on a beach and near shore circulation produced by breakers in presence of a rip channel. The *layout* for the experiments prepared at the Laboratoire d'Hydraulique in Grenoble is presented in Fig. 1.7.

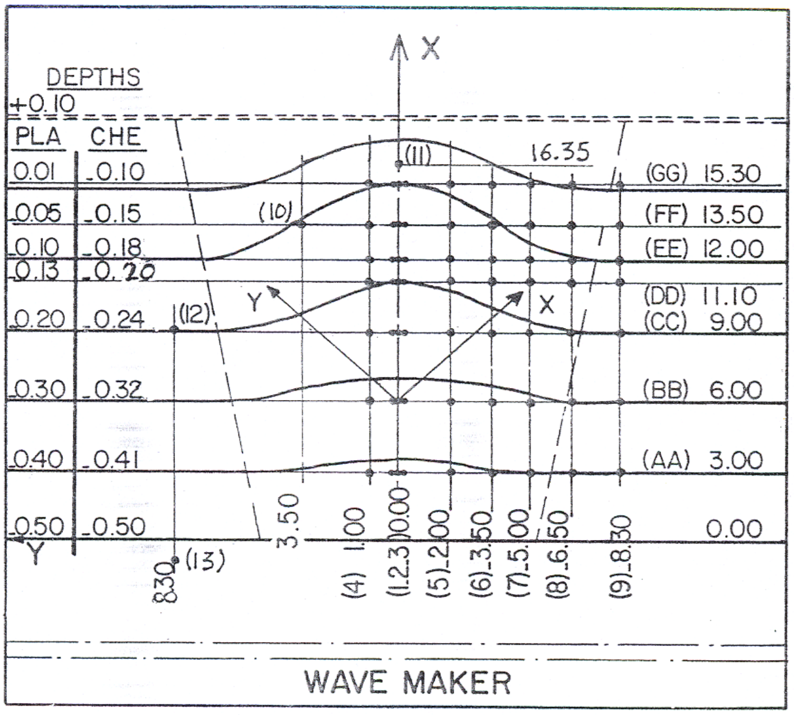

Fig. 1.7 Experimental set-up. The sea bed consists of a plane beach sloping at 1:30 with a rip channel excavated in the centre.

17 *Wave conditions* were selected in order to cover a wide range of wave steepness values, frequency spectrum and directional spreading (Tab. 1.1). A stable rip-current pattern was achieved 15 minutes after the starting up of the generator.
Measurements were performed with two groups of wave gauges and wave direction gauges, with video-recordings and an EMC.
Remarks. The instability of the rip current could be visually observed in most of the tests, but a denser measuring network would have been needed to quantify this instability.

	Hs (mm)	Tp (s)		n		Hs (mm)	Tp (s)		n
Monochromatic	40	1.25			Unidirectional	80	1.25	7	
Unidirectional	40	1.25	3.3		Multidirectional	80	1.25	7	6
Multidirectional	40	1.25	3.3	2	Monochromatic	100	1.25		
Unidirectional	40	1.976	3.3		Unidirectional	100	1.25	3.3	
Multidirectional	40	1.976	3.3	6	Unidirectional	100	1.25	7	
Monochromatic	70	1.25			Multidirectional	100	1.25	3.3	2
Unidirectional	70	1.25	3.3		Unidirectional	100	1.976	3.3	
Multidirectional	70	1.25	3.3	6	Unidirectional	130	1.60	3.3	
					Multidirectional	130	1.60	3.3	2

Tab. 1.1 Hamm tests: wave conditions.

Borthwick et al. (1997)
Nearshore currents due to a sinusoidal multi-cusped beach were analysed at the UK Coastal Research Facility. The *layout* consisted of sinusoidal cusps (Fig. 1.8), fabricated with a cement mortar skim moulded over granular fill placed on an existing concrete beach, in a working area of 20x15 m.

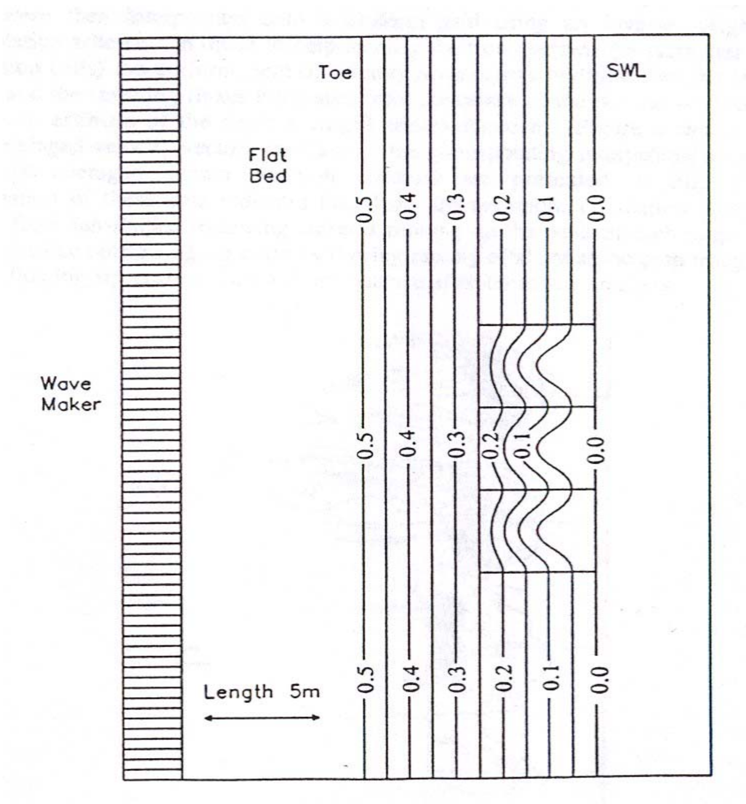

Fig. 1.8 Still water depth contours (in m) and outline of the multi-cusped beach within the UKCRF basin.

Wave conditions cover 4 different cases: regular waves, period 1.0 s, height 0.1 m, 0° incident angle; regular waves, period 1.2 s, height 0.125 m, 0° incident angle; oblique waves, period

1.2 s, height 0.125 m, 20° incident angle; random waves, peak period 1.2 s, significant wave height 0.125 m, 0° incident angle.
Measurements were performed with wave gauges, to determine the wave height field; ADVs, to obtain detailed description of vertical profiles of rip and meandering; 2 video cameras, to visualise flow patterns and current velocities following 10-cm diameter neutrally buoyant markers.
Remarks. Measurements were carried out into 2 phases, to avoid effects of measuring devices on flow patterns recorded by video cameras. The same type of markers were used in both cases of regular and random waves.

Mory & Hamm (1997)
Tests were carried out in the 3D wave basin in the Laboratoire d'Hydraulique in Grenoble. Wave height, set-up and currents were measured around a detached breakwater erected on a 1 in 50 plane beach, *layout* in Fig. 1.9.

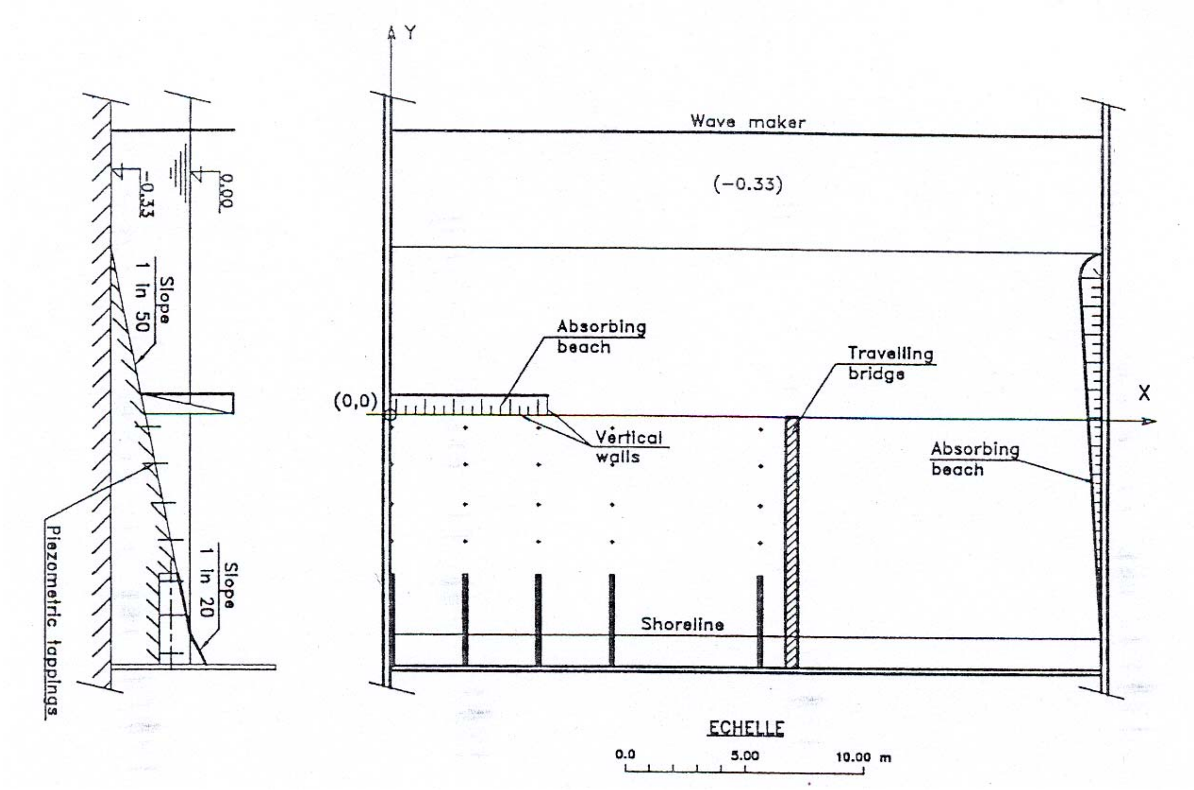

Fig. 1.9 Layout of experimental set-up.

Considering the symmetry of the flow, the *structure* consisted of half a breakwater, 6.66 m long an 0.87 m wide, perpendicular to a lateral wall of the basin (see Fig. 1.9). The breakwater is limited inshore by a wall; the offshore side consisted of a 50% sloping beach covered with a 5 cm thick synthetic mattress serving to absorb to incident waves.
Wave conditions, listed in Table 1.2, included regular unidirectional, random unidirectional and directional random waves .
Measurements of mean free surface elevation were collected by measuring the mean piezometric levels using tappings (following Battjes & Janssen, 1978) in the sea bed connected to stilling wells, in which the water level is determined by an ultrasonic probe. Current measurements were obtained by a two component LDA and an EMC. Locations of

instrumentation are shown in Fig. 1.10. Visualisations with videocamera were performed, moving the camera to cover the whole surface of the basin. For regular wave conditions, the images were analysed to determine the position of the breaking line. Tracking of dye clouds, injected at several locations, was also employed to visualise the general current circulation.
Remarks. Light conditions were critical and strongly influenced the quality of flow visualisations. The grid 1x1 m in a 30x30 m was found very useful and an even denser grid would have been appreciated.

Incident wave conditions measured offshore ($y = -7.2$ m)

Wave type	$H_{m,d}$	H_{mo}	$H_E = H_{mo}/\sqrt{2}$	Period
Regular Reg1	0.075 m			1.69 s
Regular Reg2	0.117 m			1.69 s
URW		0.115 m	0.081 m	1.69 s [a]
DRW		0.115 m	0.081 m	1.69 s [a]

[a] Peak period of Jonswap Spectrum.

Tab. 1.2 Mory & Hamm tests: wave conditions.

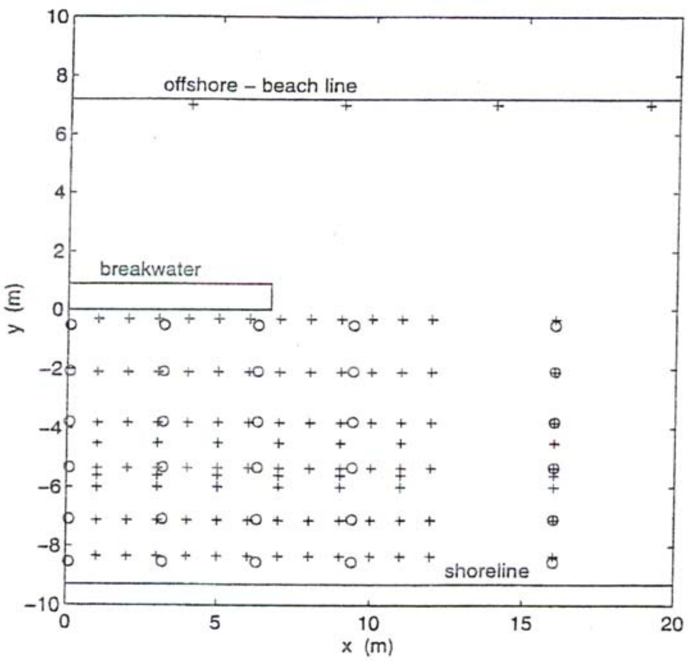

Fig. 1.10 Locations of wave height and set-up measurements in basin:
+, wave gauges; o, piezometric tappings.

Chapman, Ilic et al. (2000)
A large scale (1:28) physical model representing 5 of the 8 Elmer breakwater was analysed at UK Coastal Research Facility. A plan of the *layout* is reported in Figure 1.11.
The *structures* (215 mm height) were built up using scaled limestone blocks (Dn=50 mm) and a Dn=13 mm gravel for the exposed bedstone.
Wave conditions, listed in Tab. 1.3, included regular, short-crested and multi-directional waves. All tests were equivalent in terms of wave energy. Depth at the paddles was 0.32 m.

Measurements of surface elevation were collected using dual resistance wire wave gauges, mounted on an aluminium beam to enable multiple positions to be measured simultaneously minimising hydrodynamic disturbance. Arrays of wave gauges were used to measure breakwater reflection, breakwater transmission and inshore directional wave properties.
For the measurements of currents, two methods were adopted: 2D and 3D ADV, to obtain instantaneous variation in the xyz local velocities; digital imaging (one-hour tape for each condition), to obtain, by analysing movements of neutrally dense floats, information on the Lagrangian flow characteristics. The measurement system is presented in Fig. 1.12.

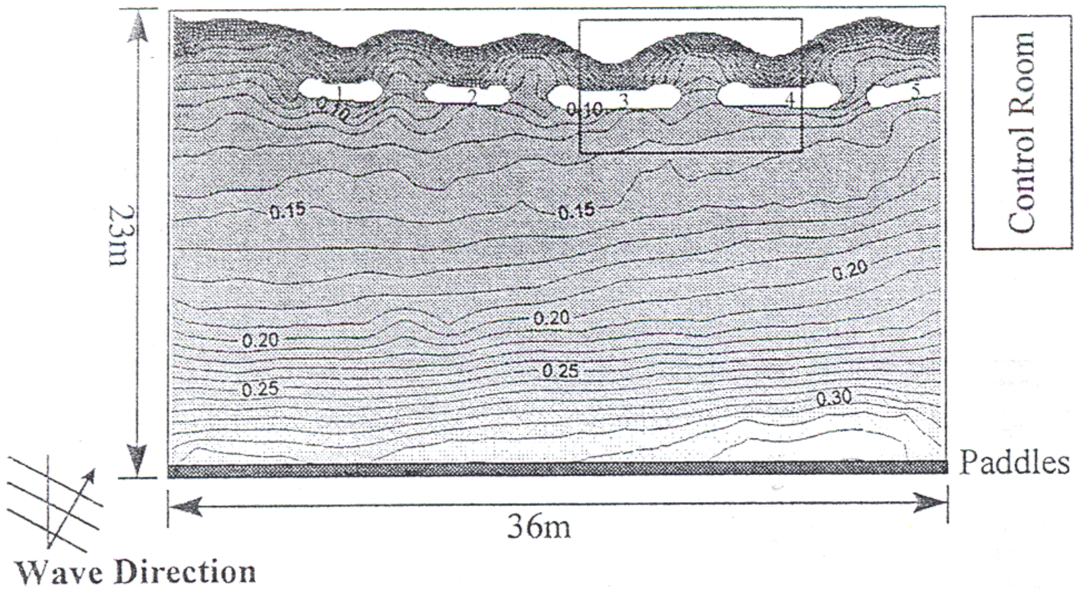

Fig. 1.11 Plan of the physical model layout. Box indicates position of main bay (between breakwaters 3 and 4) and contours show still water depth.

Condition	Hs	Wave Period	Wave Angle	Energy Spectrum
	(m)	(s)	(Degrees)	
Regular Normal (RN)	0.038	1.1	0	-
Regular Oblique (RO)	0.038	1.1	10	-
Random Normal (IRN)	0.054	1.1	0	JONSWAP
Field Condition 1 (FC1)	0.047	1.3	0	Field Measured
Field Condition 2 (FC2)	0.054	1.8	12	Field Measured

Tab. 1.3 Tested wave conditions.

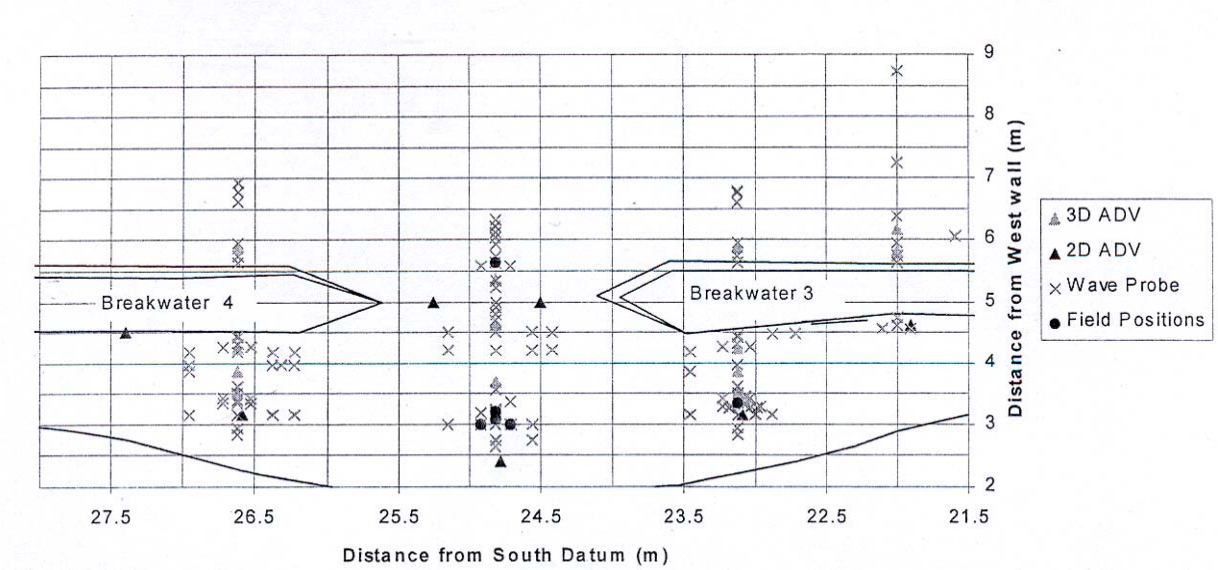

Fig. 1.12 Location of wave gauges and ADV measuring positions within the main bay.

Remarks. The construction of breakwaters with a single layer of armourstone means that a greater transmission takes place than if the construction was made with a core. No overtopping occur in these tests; therefore, transmission in this sense is only through the structure. When using transmissive breakwaters, wave breaking on the front of the structure forces mass flux through the breakwater, which in turn causes water to pile up in the lee of the breakwater.

Ilic, Chapman et al. (2000)
Layout, Structures and *Measurements* are the same reported in the previous experiment. Regarding the layout, it has been tested in both cases of fixed and mobile bed.
Wave conditions, listed in Tables 1.4 and 1.5 below for fixed and mobile bed respectively, included monochromatic, random and multi-directional waves for both normal and oblique incidence. Depth at the paddles was 0.32 m for all tests.
Remarks. Salient growth was strongly affected by wave transmission; also, no longshore transport occurred either during beach evolution or subsequently.

	Wave Type	*Wave Height (m)*	*Wave Period (s)*	*Wave direction (deg)*
Test 1	Regular	0.07	1.2	20
Test 2	Regular	0.06	1.6	20
Test 3	Random - unidirectional	0.05	1.2	20
Test 4	Regular	0.038	1.1	0
Test 5	Regular	0.038	1.1	10
Test 6	Random – multidirectional	0.054	1.1	0

Tab. 1.4 Ilic et al.: wave conditions for fixed bed.

	Wave Type	*Bed Type*	*Water Depth at the paddles (m)*	*Wave Height (m)*	*Wave Period (s)*	*Wave direction (deg)*
Test 1	Regular	Sand	0.32	0.07	1.2	20
Test 2	Random - unidirectional	Sand	0.32	0.05	1.2	20
Test 3	Random - unidirectional	Sand	0.29	0.05	1.2	20
Test 4	Random - unidirectional	Sand	0.35	0.05	1.2	20
Test 5	Regular	Anthracite	0.32	0.07	1.2	20
Test 6	Regular	Anthracite	0.35	0.07	1.2	20
Test 7	Regular	Anthracite no transmission	0.32	0.07	1.2	20

Tab. 1.5 Ilic et al.: wave conditions for mobile bed.

Sutherland et al. (2000)

Experimental measurements of hydrodynamics, scour and deposition around a detached breakwater were performed at UK Coastal Research Facility. The tested *layout* is presented in Fig. 1.13.

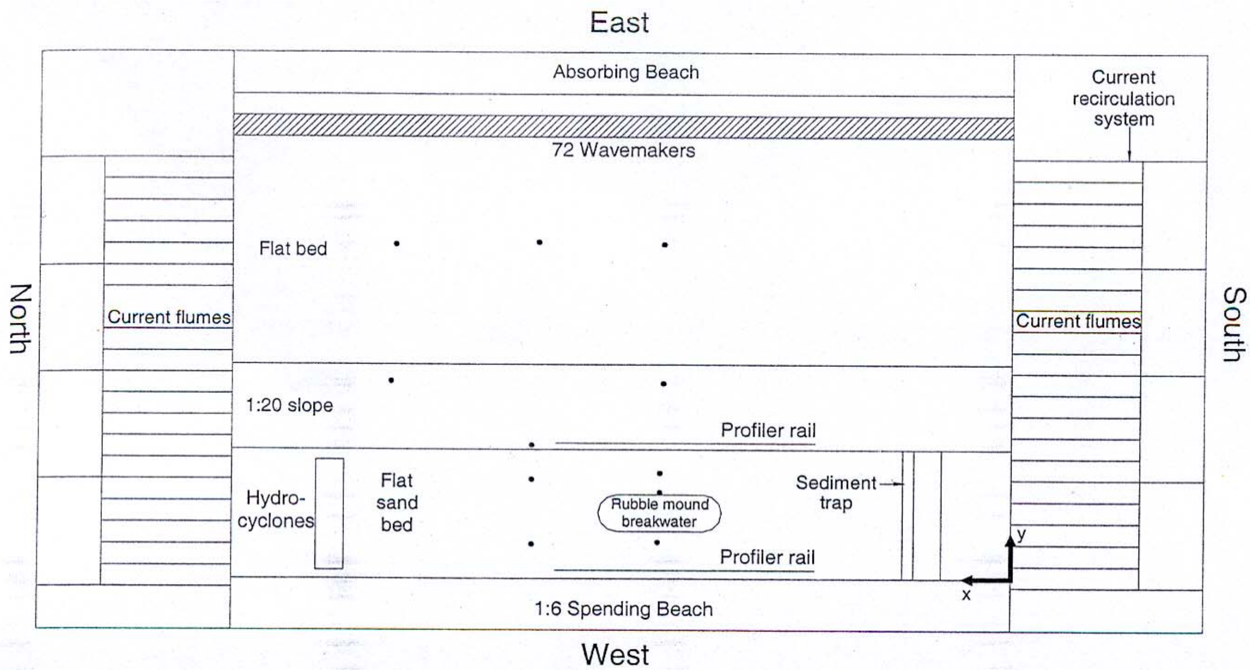

Fig. 1.13 Plan of the experimental set-up.

The *structure* had a 4 m long and 1.75 m wide straight central section and semicircular heads, which extended for almost 0.8 m beyond the trunk. It was constructed with 1:2 front and rear slopes, with a core of 6 to 10 mm diameter gravel that extended up to mean water level with 0.1 m of armour stone (Dn_{50}= 58 mm) above.

Wave conditions are listed in Table 1.6 (where P is the width of scour protection layer); for all tests, depth at the paddles is 0.5 m.

Test	H_{m0} m	T_p s	α deg	U ms^{-1}	P m	N_{waves}
A	0.1	2.8	0	0	0	30000
B	0.1	2.8	20	0.1	0	30000
C	0.1	2.8	20	0	0	30000
D	0.1	2.8	20	0	0.5	30000
E	0.12	1.5	20	0	0.5	3000

Tab. 1.6 Sutherland et al.: target test program.

Measurements (see Fig. 1.14 to view the displacement map of the instrumentation) were performed using wave gauges, to measure wave field; inshore and offshore arrays of wave gauges, to measure incident, reflected, transmitted and diffracted waves; ADVs to measure local xyz velocities around the structure. At the end of each test, the bed was profiled using 50 cross-shore line with 100 mm spacing.

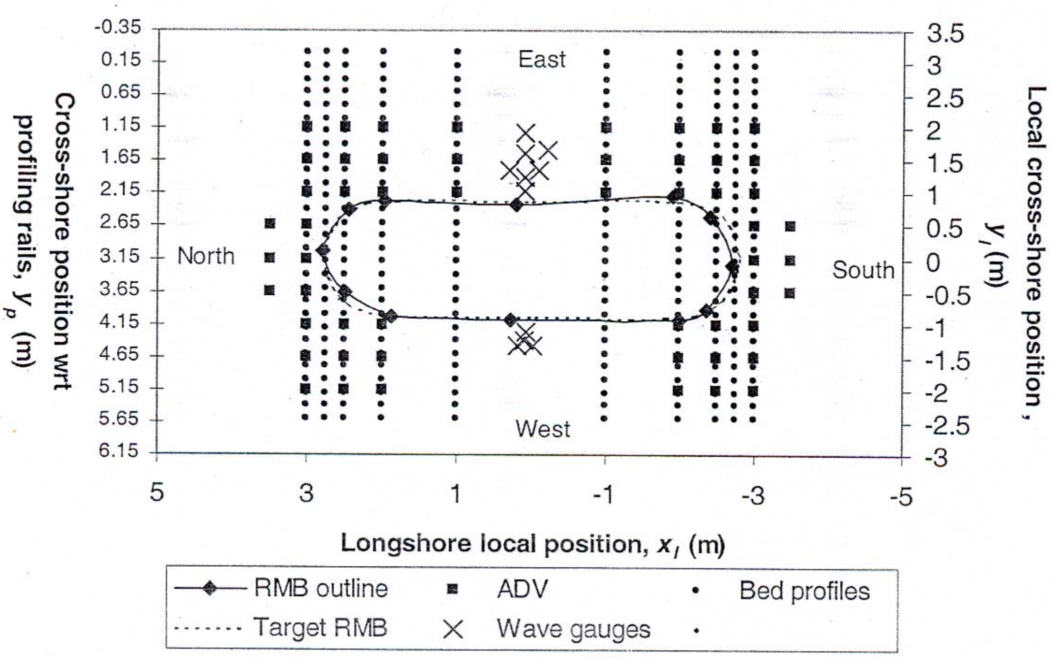

Fig. 1.14 Local co-ordinate system and position of acquisition devices.

Remarks. The results presented clearly the 3D effects even for small incidence case; for instance, the interaction of the roundhead and trunk scour was suppressed by Fredsøe & Sumer (1997) but is allowed here.

Drønen et al. (2002)

A laboratory study of the flow over a bar with a single rip channel was performed in a 4 m wide and 30 m long wave tank at ISVA, DK. The tested *layout* is presented in Fig. 2.10. The *structure* was a 4.8 m wide and 0.13 m high; the width of the trough was 1.15 m. The rip

channel was 1 m wide. These scales have not been selected to represent a real topography but rather to schematise some typical features associated with bar/rip channel systems.
Wave conditions are listed in the tables below (Tab. 1.7), where H_{rms} is deep-water-root-mean-square, H is wave height, D_c is the still-water depth at the bar crest and T is the peak period of the surface elevation. For all tests, the wave generator was run for at least 50 waves before a given test series was started.

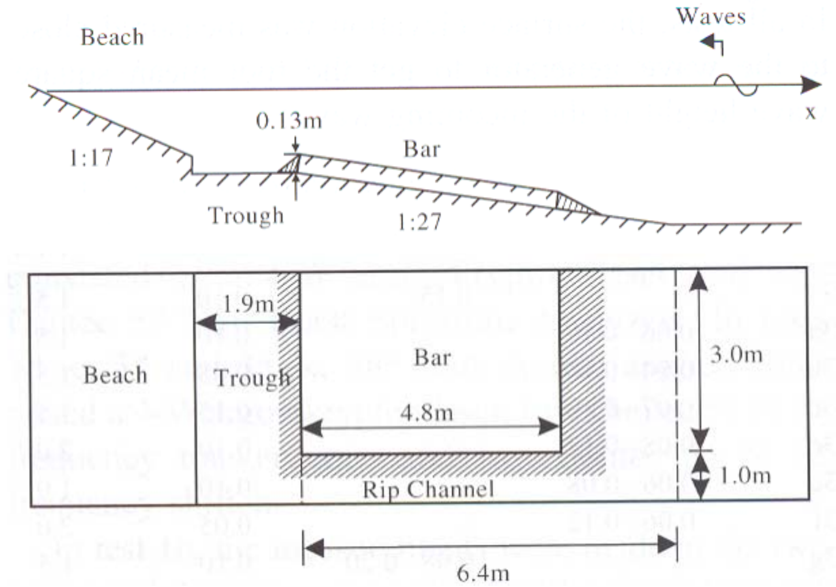

Fig. 1.15 Plan of the experimental set-up.

Measurements (see Fig. 1.16 to view the displacement map of the instrumentation) were performed using high-precision resistance wave gauges and a LDA system composed by a 4-W argon/krypton laser and two Burst Spectrum Analyzers or two frequency trackers plus two frequency shifters. Particle tracking was performed following the trajectories of a drifter launched at selected positions.
Remarks. The results reveal the importance of 3D effects, so that a depth-integrated viewpoint may not always be sufficient for predicting the flow in the near bed region. The overall trajectory pattern changes as a function of the wave breaking distance from the bar crest. For different wave climate and water level conditions, the rip current intensity and the wave height result to be strongly correlated.

Table 1
Test conditions, test 1: 2DH circulation and 3D

Test	H_{rms} (m)	H (m)	D_c (m)	T (s)	Test summary
1a	–	0.19	0.15	1.5	Surface elevation
1b	–	0.19	0.15	1.5	Velocity at one depth ($z = D/3$)
1c	–	0.19	0.15	1.5	Velocity profiles over bar/rip/trough
1d	–	0.15	0.10	1.5	Velocity profiles in rip channel
1e	–	0.15	0.10	1.5	Velocity in rip channel close to bed

Table 2
Test conditions, test 2: particle trajectories

Test	H_{rms} (m)	H (m)	D_c (m)	T (s)
2a	–	0.19	0.15	1.5
2b	–	0.13	0.15	1.5
2c	0.09	–	0.10	1.5
2d	0.09	–	0.05	1.5

Table 3
Test conditions, test 3: rip current intensity

Test	H_{rms} (m)	H (m)	D_c (m)	T (s)
3 *	–	0.15	0.10	1.5
3a	0.06–0.10	–	0.10	1.5
3b	0.04–0.10	–	0.05	1.5
3c	0.07–0.10	–	0.15	1.5
3d	0.08–0.13	–	0.10	2.0
3e	0.06–0.08	–	0.10	1.0
3f	0.06–0.12	–	0.05	2.0
3g	–	0.08–0.20	0.10	1.5
3h	–	0.07–0.17	0.10	2.0
3i	–	0.12–0.14	0.10	1.0
3j	–	0.06–0.15	0.05	1.5
3k	–	0.11–0.19	0.15	1.5

Tab. 1.7 Drønen et al.: test conditions.

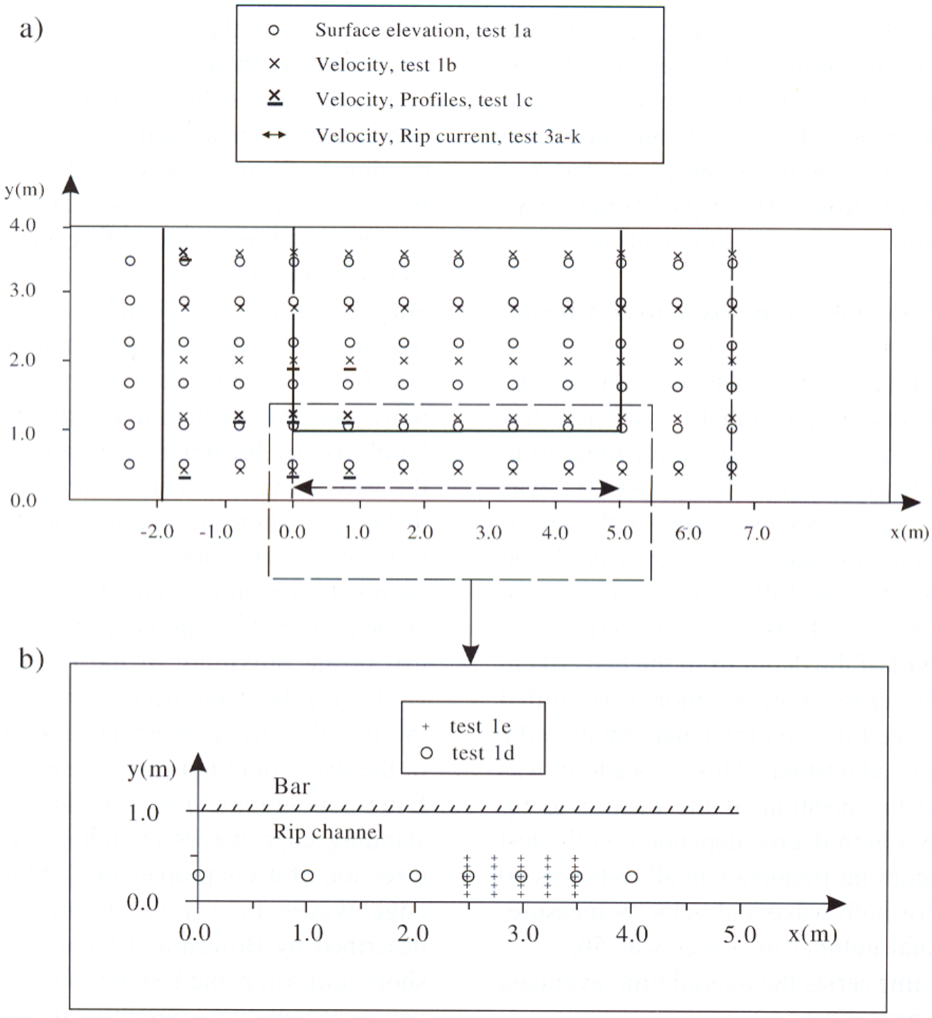

Fig. 1.16 Plan view of the measurement locations (a) for tests 1a-c and 3a-k; (b)for tests 1d-e and 3.

2. Structural layout and cross sections

Two different types of structure were tested:

- a narrow berm structure (Structure 1, Fig. 2.1), for which the critical features are: wave breaking point, crest and rear stability, wave pumping;
- a wide berm structure (Structure 2, Fig. 2.2), for which the critical features are: emergence/submergence, wave transmission, front and crest stability.

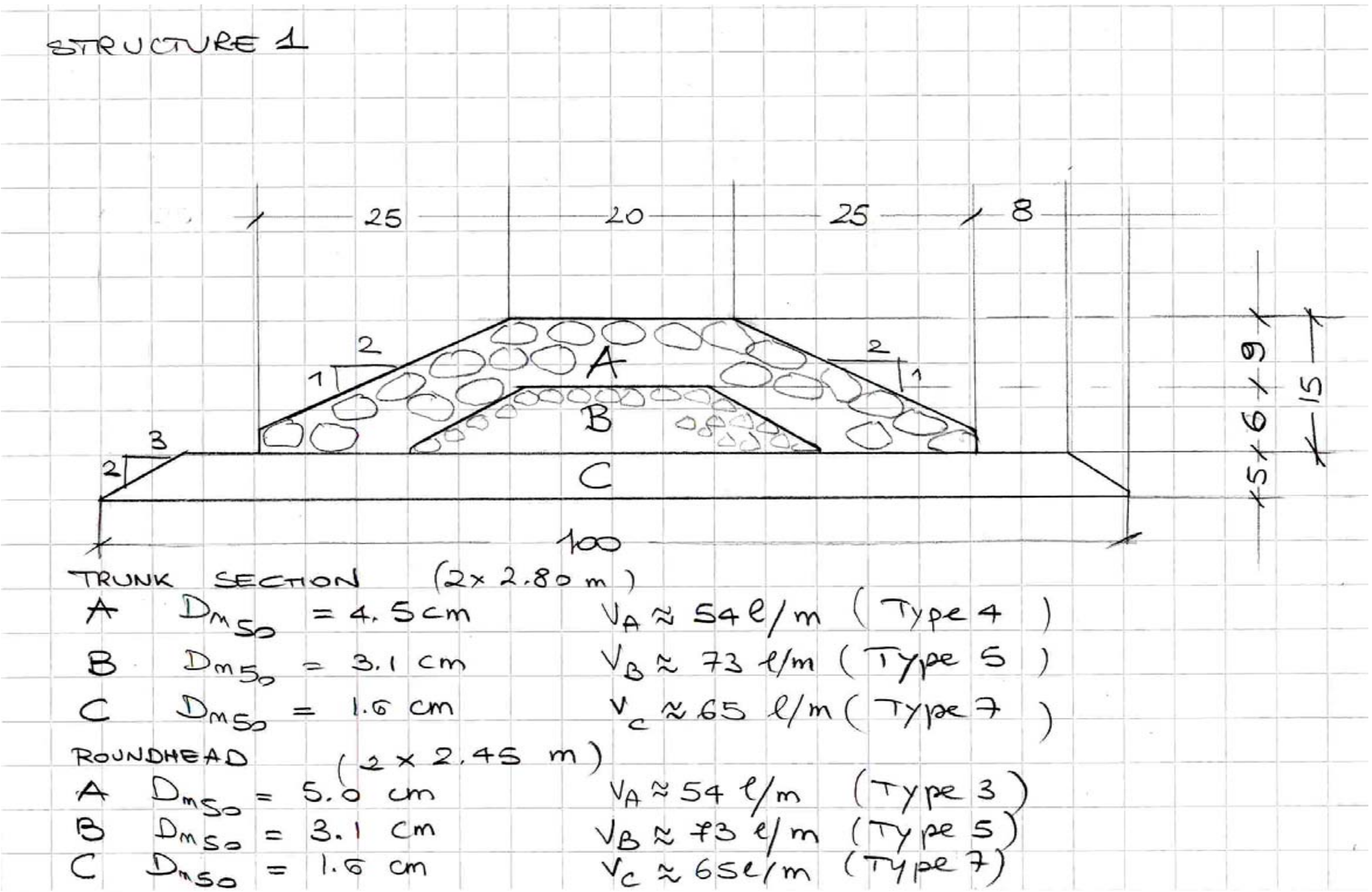

Fig. 2.1 Structure 1, narrow berm. Section and materials.

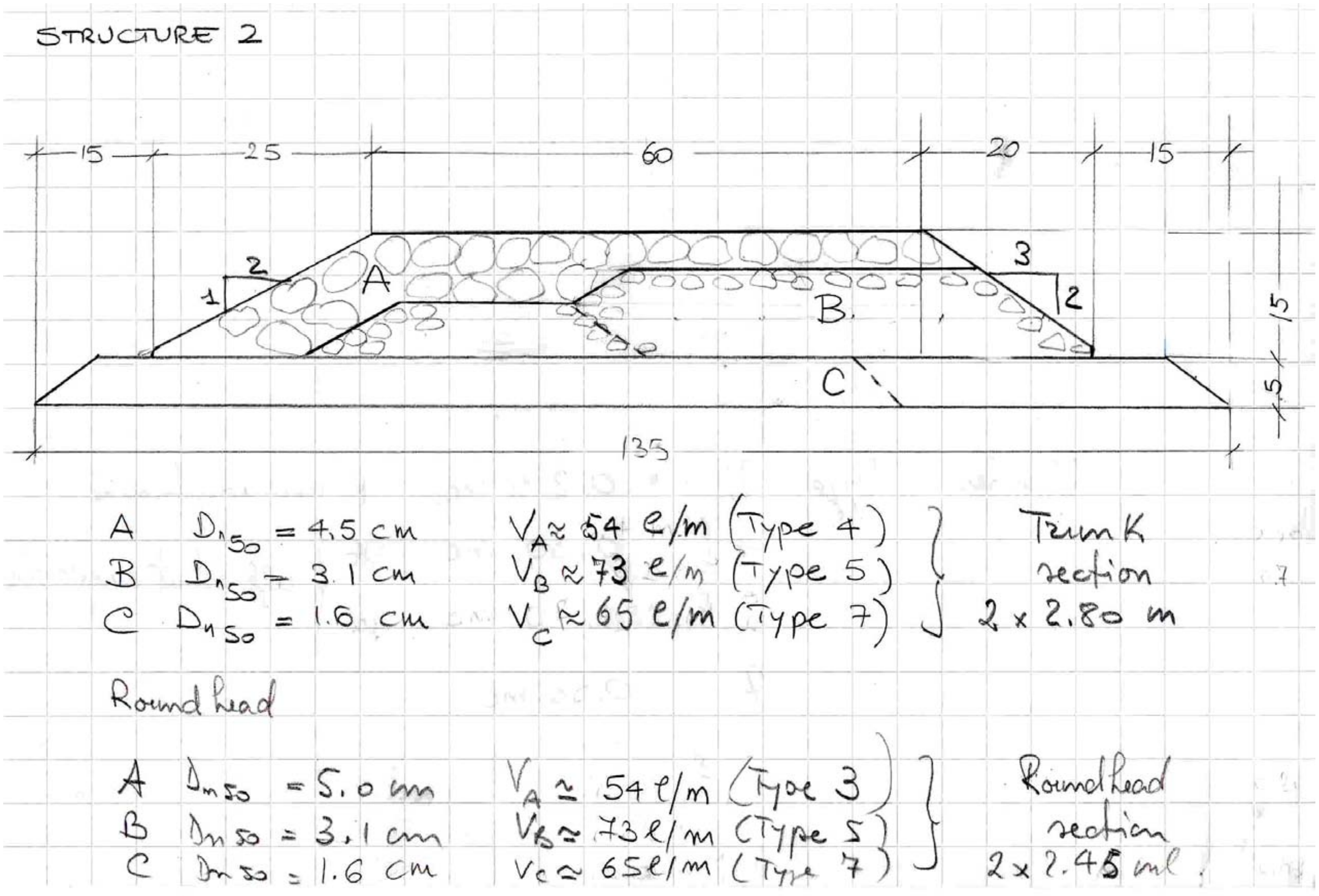

Fig. 2.2 Structure 2, narrow berm. Section and materials.

Two layouts were considered in scale 1:20 with respect to prototype.

Layout 1 (picture in Fig. 2.3, plan views in Fig.s 2.5 and 2.6 for narrow and wide berm respectively) consisted of two detached breakwaters with a gap in between. This layout allowed to examine flow characteristics at the roundheads and particularly inside the rip channel. Breakwaters were parallel to wave paddles; wave guides (two extending from wave paddles to the mid basin) allowed to obtain a wider reliable area.
Layout 2 (picture in Fig. 2.4, plan views in Fig.s 2.7 and 2.8 for narrow and wide berm respectively) consisted of one single breakwater inclined at 30° with respect to the beach. A wave guide from wave paddles to the mid basin, in front of the roundhead, allowed to obtain a larger reliable area.

Fig. 2.3 Layout 1, side view of the instrumented basin, narrow berm.

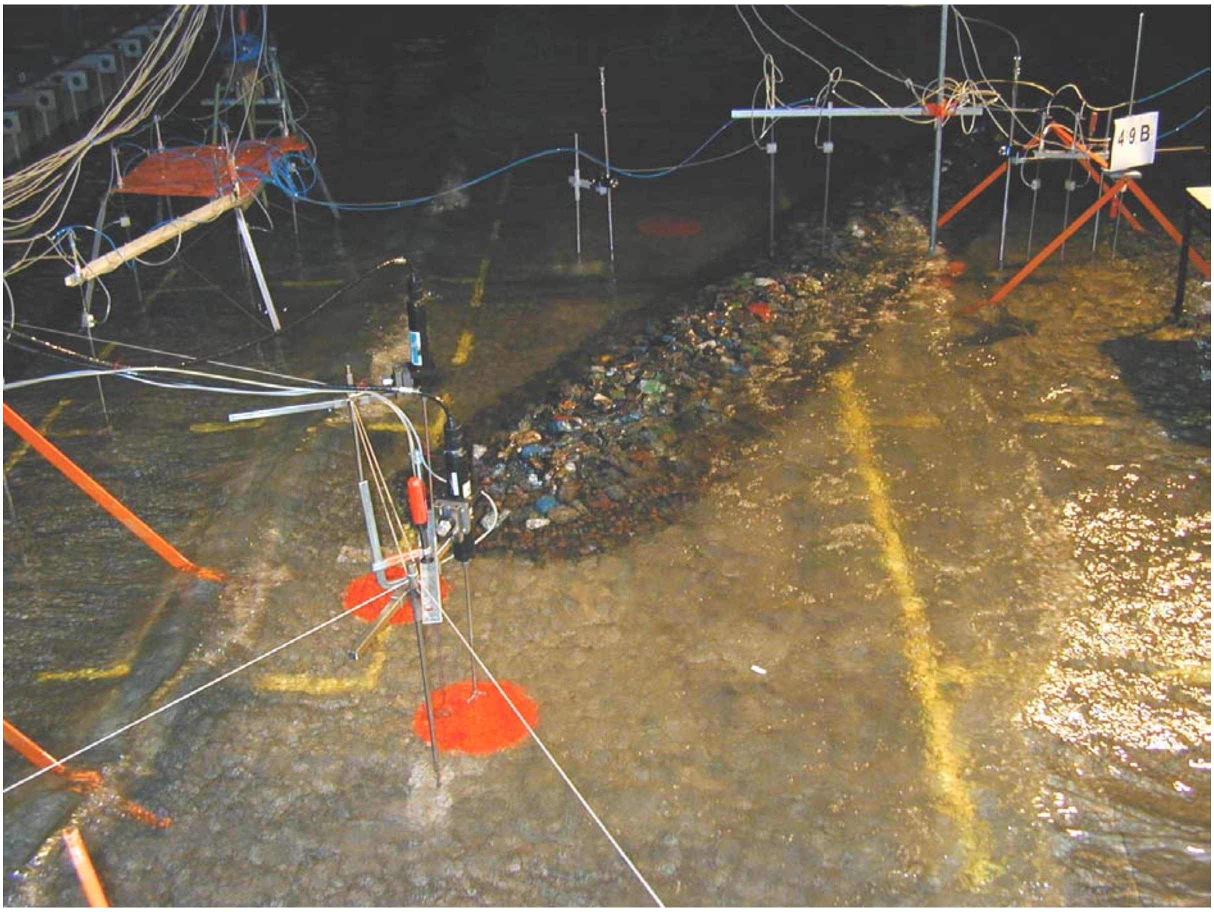

Fig. 2.4 Layout 2 side view of the instrumented basin, narrow berm.

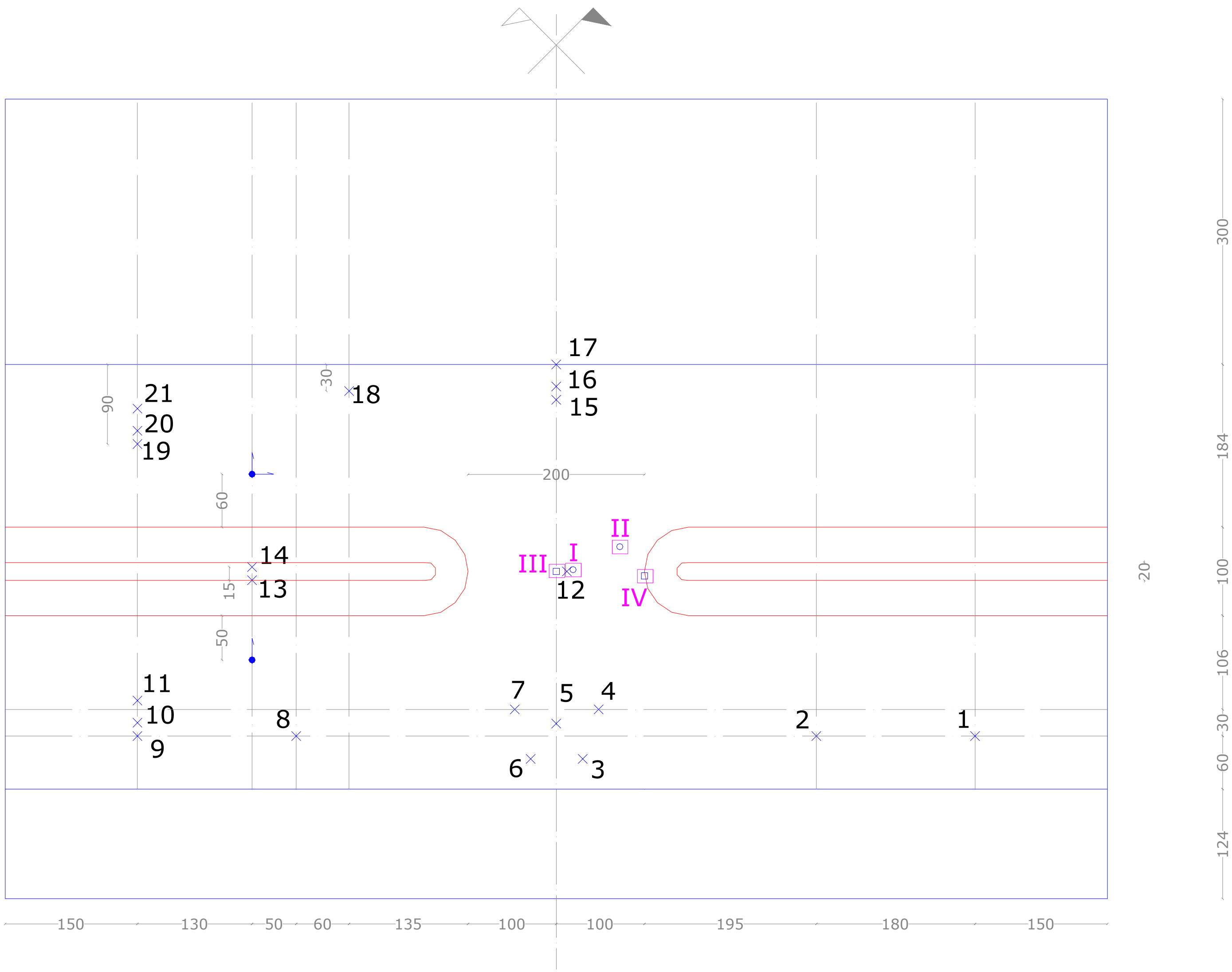

Fig. 2.5 Layout 1, plan view of the instrumented basin, narrow berm.

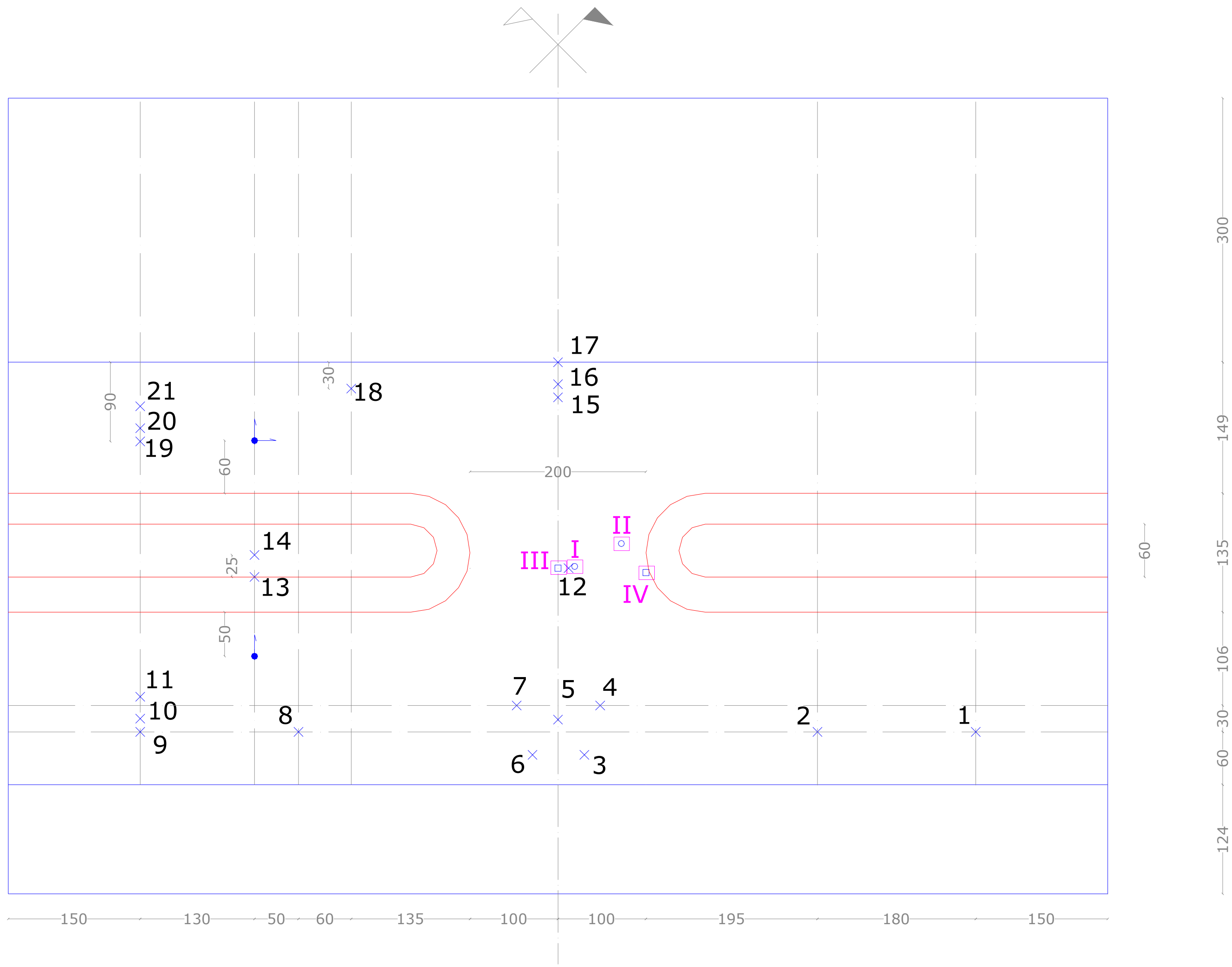

Fig. 2.6 Layout 1, plan view of the instrumented basin, wide berm.

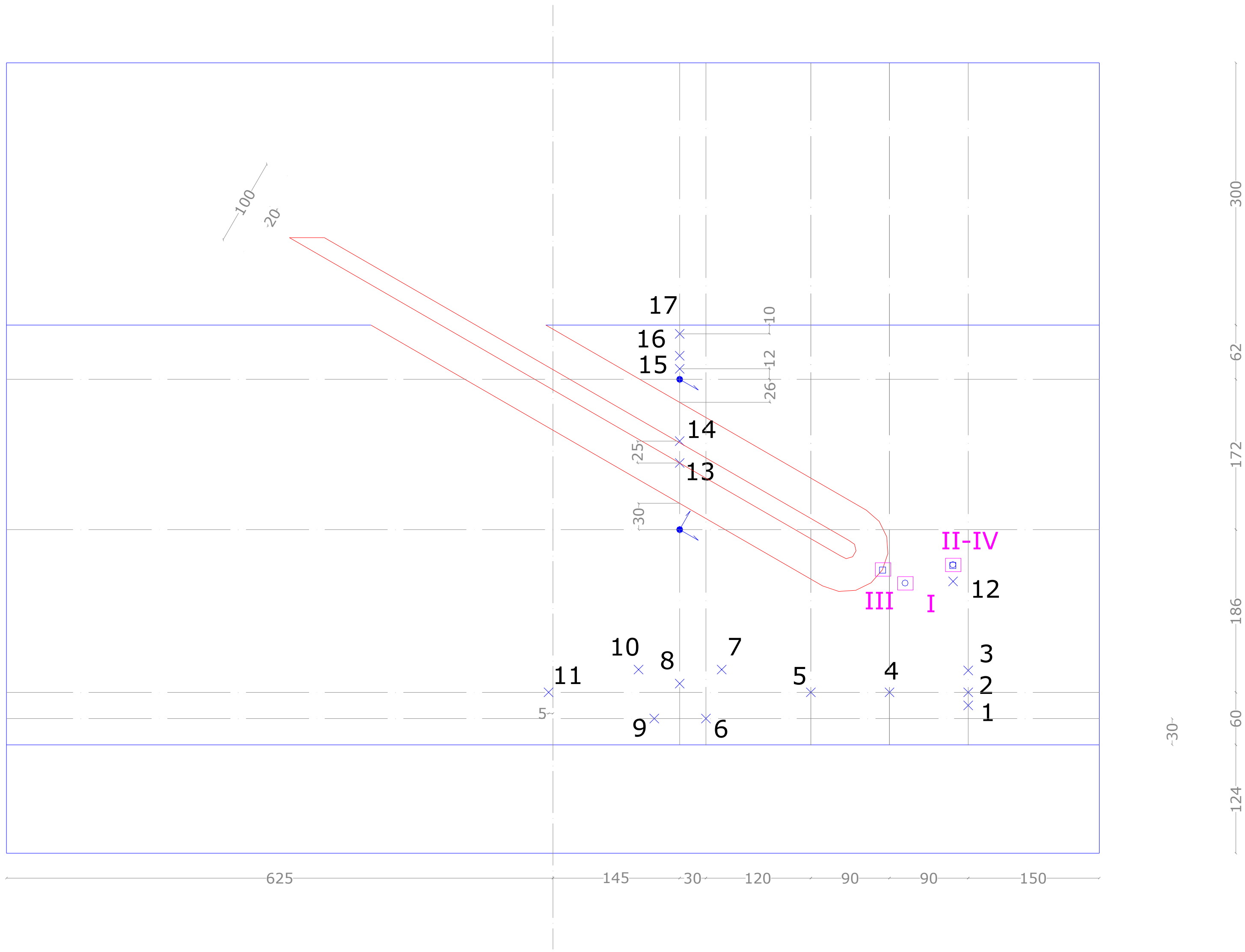

Fig. 2.7 Layout 2, plan view of the instrumented basin, narrow berm.

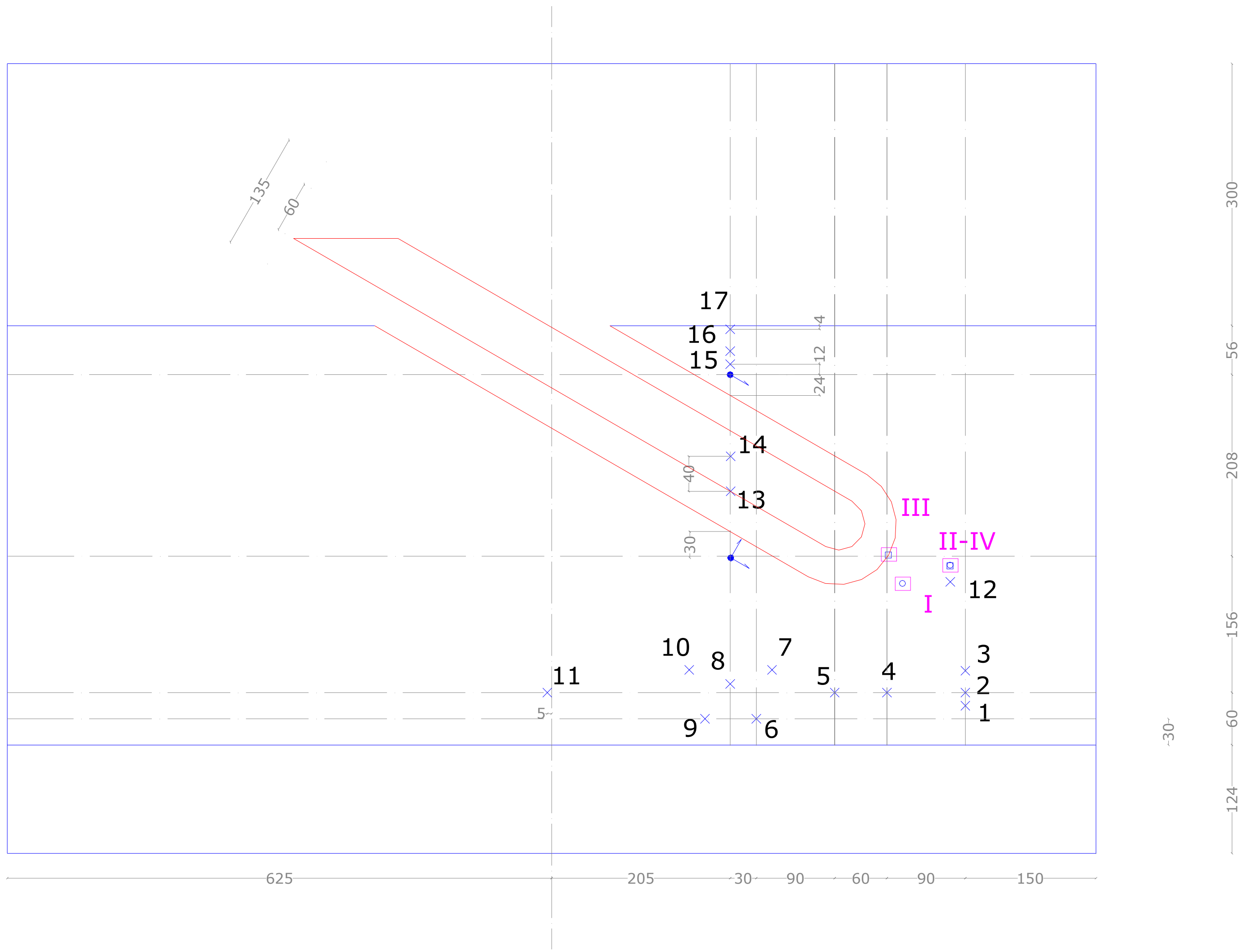

Fig. 2.8 Layout 2, plan view of the instrumented basin, wide berm.

3. Materials

For hydrodynamic tests, the following material characteristics composing the structures are proposed:
A, Dn_{50} = 4.5 cm;
B, Dn_{50} = 1.5 cm;
C, Dn_{50} = 5.2 cm.

Criterion used to define stone size is armour stone stability index equal to 1.8 in the trunk and double weight in the roundhead.
This choice of structures and materials gives a ratio $h_s/Dn_{50} \approx$ 5.5, higher than those usually adopted.
The design of the structures (see the sketches reported in section 2, Fig.s 2.5-2.8) was adapted to the quantity of different size stones available at the AAU laboratory.

4. Wave conditions

Wave conditions are reported in Tab. 4.1.
Wave attacks included regular, 2D (long crest) irregular and 3D (short crest) irregular waves and zero, positive (+3 cm) and negative (-7 cm) freeboard, for a total of 22 different attacks repeated on both structures, for a total of 44 tests. Wave direction was for each test 90°, wave spreading was 22.7° for Jonswap 3D spectrum. Tested wave heights H_s were in the range 3.4÷12.15 cm (H_s/h=0.17-0.45 where h is the depth at the structure) and peak periods within 0.74÷1.97 s.
According to DELOS objectives, the '0' freeboard case can be assumed as the reference freeboard condition (Rank 1).For this case, a complete set of wave attacks was generated, whereas in the other cases, a more or less reduced set was used. The choice of the priority of wave attacks for narrow and wide berm must reflect the different functionalities of these structures. Narrow berm structures are mainly used for emerged structures, wide berm for submerged; therefore the positive freeboard (+0.03 m) is Rank 2 for the narrow berm and Rank 3 for the wide berm, whereas the negative freeboard (-0.07 m) is Rank 2 for the wide berm and Rank 3 for the narrow berm
The effect of wave obliquity is represented by different layouts; there is thus no need to generate oblique waves with the induced problems due to reflection. For such reason, no oblique waves were generated in layout 1.

Tab. 4.1 Tested wave conditions.

Test no.	Test day	Structure	Layout	Test type	Free-board [m]	h at deep water [m]	h at structure [m]	Wave type	Wave steepness	H(s) deep [m]	T(p) deep [s]	L deep [m]	Dir. [°]	Spread S	H/h
	RANK 1							Mean sea level							
1	01-ago	1 (narrow)	1 (gap)	P	0	0,36	0,2	Jonswap 3D irregular	0,02	0,09	1,70	4,5	90	50	0,45
2	01-ago	1 (narrow)	1 (gap)	P	0	0,36	0,2	Jonswap 3D irregular	0,04	0,09	1,20	2,25	90	50	0,45
3	01-ago	1 (narrow)	1 (gap)	P	0	0,36	0,2	Jonswap 3D irregular	0,02	0,04	1,13	2	90	50	0,20
4	01-ago	1 (narrow)	1 (gap)	P	0	0,36	0,2	Jonswap 3D irregular	0,04	0,04	0,80	1	90	50	0,20
5	01-ago	1 (narrow)	1 (gap)	P	0	0,36	0,2	Regular	0,02	0,076	1,56	3,8	90	-	0,38
6	01-ago	1 (narrow)	1 (gap)	P	0	0,36	0,2	Regular	0,04	0,076	1,10	1,9	90	-	0,38
7	01-ago	1 (narrow)	1 (gap)	S	0	0,36	0,2	Regular	0,02	0,034	1,04	1,7	90	-	0,17
8	01-ago	1 (narrow)	1 (gap)	S	0	0,36	0,2	Regular	0,04	0,034	0,74	0,85	90	-	0,17
9	01-ago	1 (narrow)	1 (gap)	S	0	0,36	0,2	Jonswap 2D irregular	0,02	0,09	1,70	4,5	90	-	0,45
10	01-ago	1 (narrow)	1 (gap)	S	0	0,36	0,2	Jonswap 2D irregular	0,04	0,09	1,20	2,25	90	-	0,45
	RANK 2							Emerged narrow structure							
11	02-ago	1 (narrow)	1 (gap)	P	0,03	0,33	0,17	Jonswap 3D irregular	0,02	0,0765	1,57	3,825	90	50	0,45
12	02-ago	1 (narrow)	1 (gap)	P	0,03	0,33	0,17	Jonswap 3D irregular	0,04	0,0765	1,11	1,9125	90	50	0,45
13	02-ago	1 (narrow)	1 (gap)	P	0,03	0,33	0,17	Jonswap 3D irregular	0,02	0,034	1,04	1,7	90	50	0,20
14	02-ago	1 (narrow)	1 (gap)	P	0,03	0,33	0,17	Jonswap 3D irregular	0,04	0,034	0,74	0,85	90	50	0,20
15	02-ago	1 (narrow)	1 (gap)	S	0,03	0,33	0,17	Regular	0,02	0,0646	1,44	3,23	90	-	0,38
16	02-ago	1 (narrow)	1 (gap)	S	0,03	0,33	0,17	Regular	0,04	0,0646	1,02	1,615	90	-	0,38
	RANK 3							Submerged narrow structure							
17	02-ago	1 (narrow)	1 (gap)	P	-0,07	0,43	0,27	Jonswap 3D irregular	0,02	0,1215	1,97	6,075	90	50	0,45
18	02-ago	1 (narrow)	1 (gap)	P	-0,07	0,43	0,27	Jonswap 3D irregular	0,04	0,1215	1,40	3,0375	90	50	0,45
19	02-ago	1 (narrow)	1 (gap)	S	-0,07	0,43	0,27	Regular	0,02	0,1026	1,81	5,13	90	-	0,38
20	02-ago	1 (narrow)	1 (gap)	S	-0,07	0,43	0,27	Regular	0,04	0,1026	1,28	2,565	90	-	0,38
21	02-ago	1 (narrow)	1 (gap)	S	-0,07	0,43	0,27	Jonswap 3D irregular	0,02	0,054	1,32	2,7	90	50	0,20
22	02-ago	1 (narrow)	1 (gap)	S	-0,07	0,43	0,27	Jonswap 3D irregular	0,04	0,054	0,93	1,35	90	50	0,20

Test no.	Test day	Structure	Layout	Test type	Free-board [m]	h at deep water [m]	h at structure [m]	Wave type	Wave steepness	H(s) deep [m]	T(p) deep [s]	L deep [m]	Dir. [°]	Spread S	H/h
	RANK 1							Mean sea level							
23	06-ago	2 (wide)	1 (gap)	P	0	0,36	0,2	Jonswap 3D irregular	0,02	0,09	1,70	4,5	90	50	0,45
24	06-ago	2 (wide)	1 (gap)	P	0	0,36	0,2	Jonswap 3D irregular	0,04	0,09	1,20	2,25	90	50	0,45
25	06-ago	2 (wide)	1 (gap)	P	0	0,36	0,2	Jonswap 3D irregular	0,02	0,04	1,13	2	90	50	0,20
26	06-ago	2 (wide)	1 (gap)	P	0	0,36	0,2	Jonswap 3D irregular	0,04	0,04	0,80	1	90	50	0,20
27	06-ago	2 (wide)	1 (gap)	P	0	0,36	0,2	Regular	0,02	0,076	1,56	3,8	90	-	0,38
28	06-ago	2 (wide)	1 (gap)	P	0	0,36	0,2	Regular	0,04	0,076	1,10	1,9	90	-	0,38
29	06-ago	2 (wide)	1 (gap)	S	0	0,36	0,2	Regular	0,02	0,034	1,04	1,7	90	-	0,17
30	06-ago	2 (wide)	1 (gap)	S	0	0,36	0,2	Regular	0,04	0,034	0,74	0,85	90	-	0,17
31	06-ago	2 (wide)	1 (gap)	S	0	0,36	0,2	Jonswap 2D irregular	0,02	0,09	1,70	4,5	90	-	0,45
32	06-ago	2 (wide)	1 (gap)	S	0	0,36	0,2	Jonswap 2D irregular	0,04	0,09	1,20	2,25	90	-	0,45
	RANK 2							Submerged wide structure							
33	07-ago	2 (wide)	1 (gap)	P	-0,07	0,43	0,27	Jonswap 3D irregular	0,02	0,1215	1,97	6,075	90	50	0,45
34	07-ago	2 (wide)	1 (gap)	P	-0,07	0,43	0,27	Jonswap 3D irregular	0,04	0,1215	1,40	3,0375	90	50	0,45
35	07-ago	2 (wide)	1 (gap)	P	-0,07	0,43	0,27	Jonswap 3D irregular	0,02	0,054	1,32	2,7	90	50	0,20
36	07-ago	2 (wide)	1 (gap)	P	-0,07	0,43	0,27	Jonswap 3D irregular	0,04	0,054	0,93	1,35	90	50	0,20
37	07-ago	2 (wide)	1 (gap)	S	-0,07	0,43	0,27	Regular	0,02	0,1026	1,81	5,13	90	-	0,38
38	07-ago	2 (wide)	1 (gap)	S	-0,07	0,43	0,27	Regular	0,04	0,1026	1,28	2,565	90	-	0,38
	RANK 3							Emerged wide structure							
39	07-ago	2 (wide)	1 (gap)	P	0,03	0,33	0,17	Jonswap 3D irregular	0,02	0,0765	1,57	3,825	90	50	0,45
40	07-ago	2 (wide)	1 (gap)	P	0,03	0,33	0,17	Jonswap 3D irregular	0,04	0,0765	1,11	1,9125	90	50	0,45
41	07-ago	2 (wide)	1 (gap)	S	0,03	0,33	0,17	Regular	0,02	0,0646	1,44	3,23	90	-	0,38
42	07-ago	2 (wide)	1 (gap)	S	0,03	0,33	0,17	Regular	0,04	0,0646	1,02	1,615	90	-	0,38
43	07-ago	2 (wide)	1 (gap)	S	0,03	0,33	0,17	Jonswap 3D irregular	0,02	0,034	1,04	1,7	90	50	0,20
44	07-ago	2 (wide)	1 (gap)	S	0,03	0,33	0,17	Jonswap 3D irregular	0,04	0,034	0,74	0,85	90	50	0,20
	RANK 1							Mean sea level							
45	10-ago	1 (narrow)	2 (30 deg)	P	0	0,36	0,2	Jonswap 3D irregular	0,02	0,09	1,70	4,5	90	50	0,45
46	10-ago	1 (narrow)	2 (30 deg)	P	0	0,36	0,2	Jonswap 3D irregular	0,04	0,09	1,20	2,25	90	50	0,45

Test no.	Test day	Structure	Layout	Test type	Free-board [m]	h at deep water [m]	h at structure [m]	Wave type	Wave steepness	H(s) deep [m]	T(p) deep [s]	L deep [m]	Dir. [°]	Spread S	H/h
47	10-ago	1 (narrow)	2 (30 deg)	P	0	0,36	0,2	Jonswap 3D irregular	0,02	0,04	1,13	2	90	50	0,20
48	10-ago	1 (narrow)	2 (30 deg)	P	0	0,36	0,2	Jonswap 3D irregular	0,04	0,04	0,80	1	90	50	0,20
49	10-ago	1 (narrow)	2 (30 deg)	P	0	0,36	0,2	Regular	0,02	0,076	1,56	3,8	90	-	0,38
50	10-ago	1 (narrow)	2 (30 deg)	P	0	0,36	0,2	Regular	0,04	0,076	1,10	1,9	90	-	0,38
51	10-ago	1 (narrow)	2 (30 deg)	S	0	0,36	0,2	Regular	0,02	0,034	1,04	1,7	90	-	0,17
52	10-ago	1 (narrow)	2 (30 deg)	S	0	0,36	0,2	Regular	0,04	0,034	0,74	0,85	90	-	0,17
53	10-ago	1 (narrow)	2 (30 deg)	S	0	0,36	0,2	Jonswap 2D irregular	0,02	0,09	1,70	4,5	90	-	0,45
54	10-ago	1 (narrow)	2 (30 deg)	S	0	0,36	0,2	Jonswap 2D irregular	0,04	0,09	1,20	2,25	90	-	0,45
	RANK 2							Emerged narrow structure							
55	11-ago	1 (narrow)	2 (30 deg)	P	0,03	0,33	0,17	Jonswap 3D irregular	0,02	0,0765	1,57	3,825	90	50	0,45
56	11-ago	1 (narrow)	2 (30 deg)	P	0,03	0,33	0,17	Jonswap 3D irregular	0,04	0,0765	1,11	1,9125	90	50	0,45
57	11-ago	1 (narrow)	2 (30 deg)	P	0,03	0,33	0,17	Jonswap 3D irregular	0,02	0,034	1,04	1,7	90	50	0,20
58	11-ago	1 (narrow)	2 (30 deg)	P	0,03	0,33	0,17	Jonswap 3D irregular	0,04	0,034	0,74	0,85	90	50	0,20
59	11-ago	1 (narrow)	2 (30 deg)	S	0,03	0,33	0,17	Regular	0,02	0,0646	1,44	3,23	90	-	0,38
60	11-ago	1 (narrow)	2 (30 deg)	S	0,03	0,33	0,17	Regular	0,04	0,0646	1,02	1,615	90	-	0,38
	RANK 3							Submerged narrow structure							
61	12-ago	1 (narrow)	2 (30 deg)	P	-0,07	0,43	0,27	Jonswap 3D irregular	0,02	0,1215	1,97	6,075	90	50	0,45 *
62	12-ago	1 (narrow)	2 (30 deg)	P	-0,07	0,43	0,27	Jonswap 3D irregular	0,04	0,1215	1,40	3,0375	90	50	0,45 *
63	12-ago	1 (narrow)	2 (30 deg)	S	-0,07	0,43	0,27	Regular	0,02	0,1026	1,81	5,13	90	-	0,38
64	12-ago	1 (narrow)	2 (30 deg)	S	-0,07	0,43	0,27	Regular	0,04	0,1026	1,28	2,565	90	-	0,38
65	12-ago	1 (narrow)	2 (30 deg)	S	-0,07	0,43	0,27	Jonswap 3D irregular	0,02	0,054	1,32	2,7	90	50	0,20
66	12-ago	1 (narrow)	2 (30 deg)	S	-0,07	0,43	0,27	Jonswap 3D irregular	0,04	0,054	0,93	1,35	90	50	0,20
	RANK 1							Mean sea level							
67	16-ago	2 (wide)	2 (30 deg)	P	0	0,36	0,2	Jonswap 3D irregular	0,02	0,09	1,70	4,5	90	50	0,45
68	16-ago	2 (wide)	2 (30 deg)	P	0	0,36	0,2	Jonswap 3D irregular	0,04	0,09	1,20	2,25	90	50	0,45
69	16-ago	2 (wide)	2 (30 deg)	P	0	0,36	0,2	Jonswap 3D irregular	0,02	0,04	1,13	2	90	50	0,20

Test no.	Test day	Structure	Layout	Test type	Free-board [m]	h at deep water [m]	h at structure [m]	Wave type	Wave steepness	H(s) deep [m]	T(p) deep [s]	L deep [m]	Dir. [°]	Spread S	H/h
70	16-ago	2 (wide)	2 (30 deg)	P	0	0,36	0,2	Jonswap 3D irregular	0,04	0,04	0,80	1	90	50	0,20
71	18-ago	2 (wide)	2 (30 deg)	P	0	0,36	0,2	Regular	0,02	0,076	1,56	3,8	90	-	0,38
72	18-ago	2 (wide)	2 (30 deg)	P	0	0,36	0,2	Regular	0,04	0,076	1,10	1,9	90	-	0,38
73	18-ago	2 (wide)	2 (30 deg)	S	0	0,36	0,2	Regular	0,02	0,034	1,04	1,7	90	-	0,17
74	18-ago	2 (wide)	2 (30 deg)	S	0	0,36	0,2	Regular	0,04	0,034	0,74	0,85	90	-	0,17
75	18-ago	2 (wide)	2 (30 deg)	S	0	0,36	0,2	Jonswap 2D irregular	0,02	0,09	1,70	4,5	90	-	0,45
76	18-ago	2 (wide)	2 (30 deg)	S	0	0,36	0,2	Jonswap 2D irregular	0,04	0,09	1,20	2,25	90	-	0,45
	RANK 2							Submerged wide structure							
77	19-ago	2 (wide)	2 (30 deg)	P	-0,07	0,43	0,27	Jonswap 3D irregular	0,02	0,1215	1,97	6,075	90	50	0,45
78	19-ago	2 (wide)	2 (30 deg)	P	-0,07	0,43	0,27	Jonswap 3D irregular	0,04	0,1215	1,40	3,0375	90	50	0,45
79	19-ago	2 (wide)	2 (30 deg)	P	-0,07	0,43	0,27	Jonswap 3D irregular	0,02	0,054	1,32	2,7	90	50	0,20
80	19-ago	2 (wide)	2 (30 deg)	P	-0,07	0,43	0,27	Jonswap 3D irregular	0,04	0,054	0,93	1,35	90	50	0,20
81	19-ago	2 (wide)	2 (30 deg)	S	-0,07	0,43	0,27	Regular	0,02	0,1026	1,81	5,13	90	-	0,38
82	19-ago	2 (wide)	2 (30 deg)	S	-0,07	0,43	0,27	Regular	0,04	0,1026	1,28	2,565	90	-	0,38
	RANK 3							Emerged wide structure							
83	19-ago	2 (wide)	2 (30 deg)	P	0,03	0,33	0,17	Jonswap 3D irregular	0,02	0,0765	1,57	3,825	90	50	0,45 *
84	19-ago	2 (wide)	2 (30 deg)	P	0,03	0,33	0,17	Jonswap 3D irregular	0,04	0,0765	1,11	1,9125	90	50	0,45 *
85	19-ago	2 (wide)	2 (30 deg)	S	0,03	0,33	0,17	Regular	0,02	0,0646	1,44	3,23	90	-	0,38
86	19-ago	2 (wide)	2 (30 deg)	S	0,03	0,33	0,17	Regular	0,04	0,0646	1,02	1,615	90	-	0,38
87	19-ago	2 (wide)	2 (30 deg)	S	0,03	0,33	0,17	Jonswap 3D irregular	0,02	0,034	1,04	1,7	90	50	0,20
88	19-ago	2 (wide)	2 (30 deg)	S	0,03	0,33	0,17	Jonswap 3D irregular	0,04	0,034	0,74	0,85	90	50	0,20

* test repeated to check repetitiveness

5. Measurements

Objectives

Objective of the measurements is to provide data to verify and calibrate littoral circulation numerical models. Evaluation of armour stone stability is assumed as a secondary objective and aims to analyse only the influence of layout shape and special location on stability.
Measurements should describe boundary conditions and some of the fields characterising wave and current flow.

Methodology

Field variables are
- Wave ⇒ wave amplitude, wave number, (possibly breaking).
- Current ⇒ intensity and direction.
- Set-up ⇒ intensity.

Boundary conditions that must be checked are:
- Offshore wave condition;
- Reflection at the shoreline;
- Wave condition at absorbing boundaries.

Measurements regard the mentioned field variables and were carried out with:
- n. 4 ADV, to obtain local xyz velocities;
- n. 1ADVP with 6 1MHz probes, to obtain velocity profiles at fixed points;
- n. 21 for Layout 1, n. 17 for Layout 2 wave gauges to measure local free surface elevation;
- n. 2 digital cameras, to visualise flow patterns, following drifters or dye clouds, and to monitor the breaking.

Instrumentation setup is shown in the drawings reported at the end of this paragraph.

Regular and Irregular waves

Measurements with irregular waves are aimed to evaluate effects of the actual shape of wave spectra and of variability of wave height (effects on stability) for the same global wave parameters (H_{rms}, T_s and wave direction).
Measurements with regular waves are aimed to describe the shape of wave and current fields.

Performance of Tests

Regular wave tests:
t=0: Start-up
t=0-3 minutes:
    Side-camera Video Recording
t=3-10 minutes: Sleeping time
t=10 minutes: Flow regime
t=10-20 minutes:
    Launch of floats
    Acquisition with ADVs, ADVPs, WGs
    Side-camera Video Recording
    Central-camera Video Recording

Irregular wave tests:
t=0: Start-up
t=0-3 minutes:
 Acquisition with ADVs, ADVPs, WGs
 Side-camera Video Recording
t=3-10 minutes: Sleeping time
t=10 minutes: Flow regime
t=10-20 minutes:
 Dye-injection
 Central-camera Video Recording (t=10-15 minutes)
 Acquisition with ADVs, ADVPs, WGs
 Side-camera Video Recording

Procedures for data acquisition

The beginning of the acquisition was triggered for all the instrumentation by the same signal in order to achieve synchronisation.
WGs: data from wave gauges and AAU ADVs were acquired at 40 Hz with a laboratory software produced by AAU.
ADVs: data from UB ADVs were acquired at 40 Hz, in order to maintain the same frequency adopted for the other instrumentation, with the proper SONTEK acquisition software. The start of the acquisition was chosen as “Start on Sync” and the recording mode was per “Burst”. Defining as “Samples per Burst” alternatively 7200 and 24000 bursts, it was possible to acquire continuously for the first three minutes and for the ten minutes at flow regime of each test respectively. The velocity range was imposed to be ±100 cm/s.
ADVPs: data from ADVP probes were acquired using a calibrated configuration which is reported below. The aim of this configuration was to acquire continuously from all the 6 working probes, being back to the first one in a reasonable time interval. Each measured profile was composed of 64 emissions with a pulse repetition frequency of 189 mm so that the time elapsed for measuring each profile was 22.9 ms. The multiplexer switched from one probe to the following one after measuring a single profile and thus for six probes the time interval after which the first one acquired again was 138 ms. The resolution was not assumed as a particularly relevant parameter and was therefore fixed around 0.9 cm. In order to be suitable to all tested conditions, the velocity range was ±1.4 m/s.

```
Signal Processing SA : DOP1000  :5.23.3
--------------------

Recorded data type : Velocity profile
Pulse repetition frequency....... :  189mm   256us
First channel at ................ : 11.1mm  15.0us
Resolution ...................... :  7.4mm  10.0us
Sensitivity ..................... :low
Number of emission / profile .... :   64,  21.3 ms
Emission power .................. :high
         frequency .............. :        1.0 MHz
         burst length ........... :      04 cycles
Unit ............................ :US axis
Sound speed ..................... :  1480 m/s
Doppler angle ................... :     25 degrees
Memory size ..................... :  8450,  180.5s
  Record from channel ........... :   0,   auto
  Record to channel ............. :   0,   auto
  Skip .......................... :    0p,     0ms
Maximum velocity ................ :           mm/s
  Velocity offset ............... :        0  mm/s
```

Tab. 5.1 Example of procedure for ADVP data acquisition.

6. CD file contents

ADV and ADVP output files were saved using names that correspond to the following criterion: 2 character for the instrument type (AP for ADVP files, AV for UB ADV files) + 3 characters for the test number according to the table in paragraph 3 + 1 character for identifying the part of the test (A for the first three minutes, B for the ten minutes acquisition at flow regime). For instance:

- AP001A is the output file containing ADVP measurements for the first three minutes of Test 1;
- AV088B is the output file containing ADV measurements for the minutes 10-20 of Test 88.

ADVP files were processed to be converted from binary into ASCII so that the extension of converted files is “.dat”.
ADV files contain data of both probes, the down-looking and side-looking. For each test, there are 5 different file extensions depending on the content: “.vel” contains velocities, “.snr” contains signal variance, “.cor” contains signal correlations, “.amp” contains signal amplitude, “.ctl” contains the acquiring configuration.

WG output files were saved using names that correspond to the following criterion: 2 character for the instrument type (GA) + 2 characters for the test number according to the table in paragraph 3 + 1 character for identifying the part of the test (A for the first five minutes, B for the ten minutes acquisition at flow regime). For instance:

- GA01A is the output file containing wave gauges + AAU ADV measurements for the first five minutes of Test 1.

WG files consist of several columns, each of which corresponding to a WG or an ADV labelled as in the layout sketches reported at the end of paragraph 4. The correspondence is shown in the table reported below.

Test 1-44			
Col. file	Wave gauges name	Unit in files	Elevation system
1	WG1	cm	by hand
2	WG2	cm	by hand
3	WG3	cm	p
4	WG4	cm	p
5	WG5	cm	p
6	WG6	cm	p
7	WG7	cm	p
8	WG8	cm	by hand
9	WG9	cm	p
10	WG10	cm	p
11	WG11	cm	p
12	WG12	cm	by hand
13	WG13	cm	p (over structure)
14	WG14	cm	p (over structure)
15	WG15	cm	p
16	WG16	cm	p
17	WG17	cm	p
18	WG18	cm	by hand
19	WG19	cm	p
20	WG20	cm	p
21	WG21	cm	p
22	ADV2DVX	cm/s	ultra sonic
23	ADV2DVY	cm/s	ultra sonic
24	ADV1DVX	cm/s	ultra sonic

Test 45-88			
Col. file	Wave gauges name	Unit in files	Elevation system
1	WG1	cm	p
2	WG2	cm	p
3	WG3	cm	p
4	WG4	cm	p
5	WG5	cm	p
6	WG6	cm	p
7	WG7	cm	p
8	WG8	cm	p
9	WG9	cm	p
10	WG10	cm	p
11	WG11	cm	p
12	WG12	cm	p
13	WG13	cm	p (over structure)
14	WG14	cm	p (over structure)
15	WG15	cm	p
16	WG16	cm	p
17	WG17	cm	p
18	ADV1DVX	cm/s	ultra sonic
19	ADV2DVX	cm/s	ultra sonic
20	ADV2DVY	cm/s	ultra sonic

p: Air pressure

Tab. 6.1 Association type-number of wave gauges adopted in the tests.

7. Video recordings

Video recordings of all tests from central and side camera are located at the University of Bologna, person to contact if interested in: Barbara Zanuttigh (Barbara.Zanuttigh@mail.ing.unibo.it). Please specify the test number and if you would like to receive central or/and side camera acquisition.

8. Results

Drifter/Dye tracking

Flow field was analysed using tracking of drifters for regular waves and of dye clouds for irregular waves (layout 1 in Fig. 8.1). Images were captured from central camera's videos, in order to examine rip currents at the gap, and were then acquired as background of CAD drawings. The positions of drifters or the location of the dye cloud centre were digitalised at time steps that allow to follow the changes in flow patterns (see Fig.s 8.2, 8.3: time step increase with decreasing target wave height). Images were then rectified with a procedure prepared for such aim in the Matlab environment and elaborated to obtain mean velocities at the gap centre and at the breakwater roundhead, to be compared with velocities measured with ADVs.

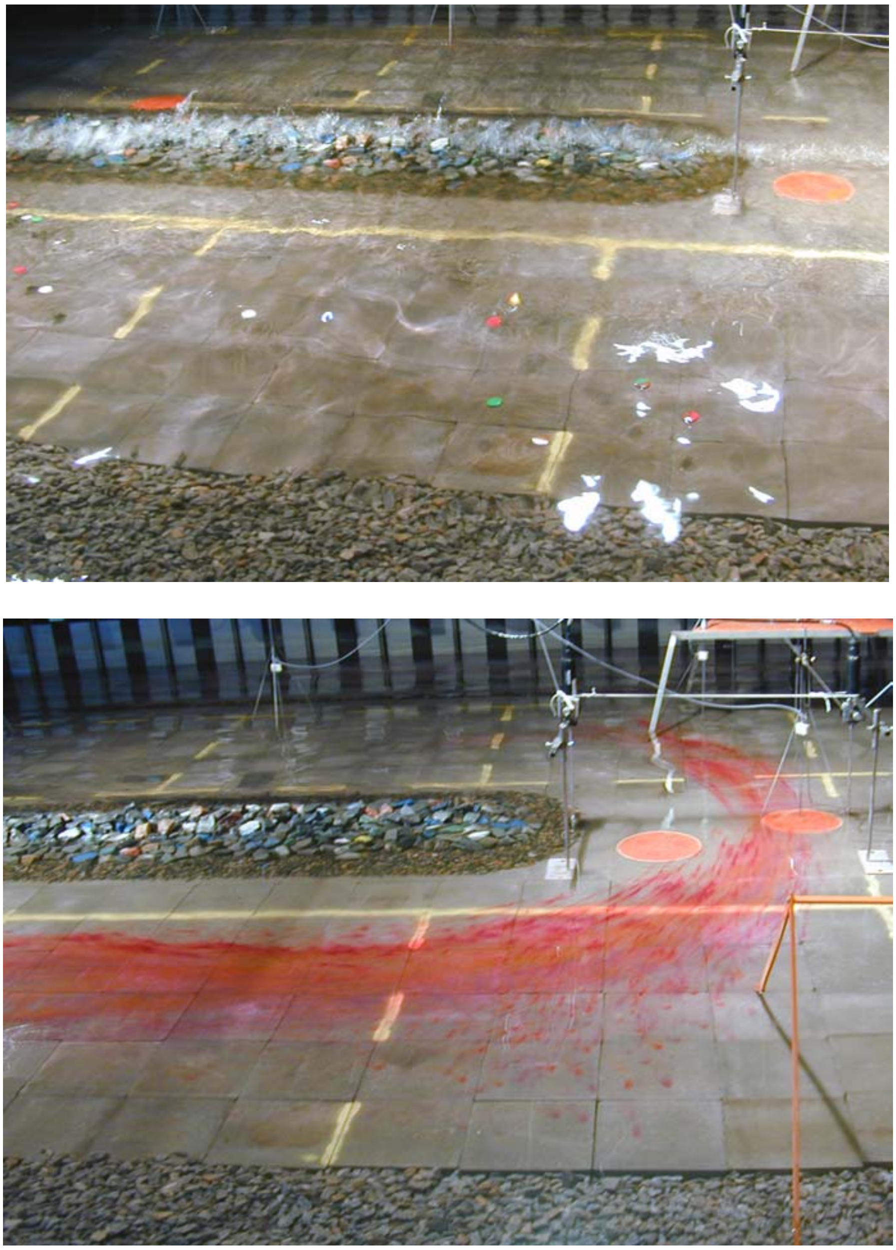

Fig. 8.1 Analysis of flow field by tracking drifters (up) for regular waves and dye injection (down) for irregular waves; images captured during tests on layout 1, narrow berm.

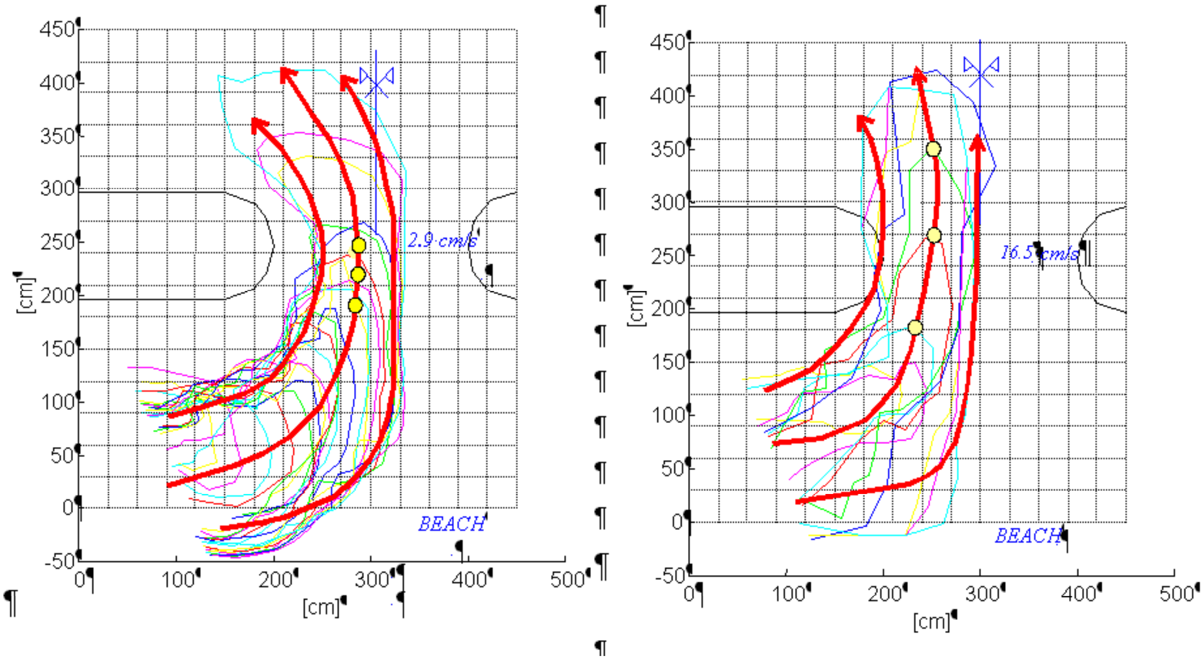

Fig. 8.2 Flow patterns obtained by image analysis for Test 18 (left), and Test 22 (right), view from the beach (co-ordinates in cm, model scale). The contour lines of the dye cloud are traced every 5 seconds for Test 18, every 10 seconds for Test 22. The mean velocity at the gap centre results 16.5 cm/s in Test 18 (measured 16.20 cm/s), 2.9 cm/s for Test 22 (measured 2.57 cm/s).

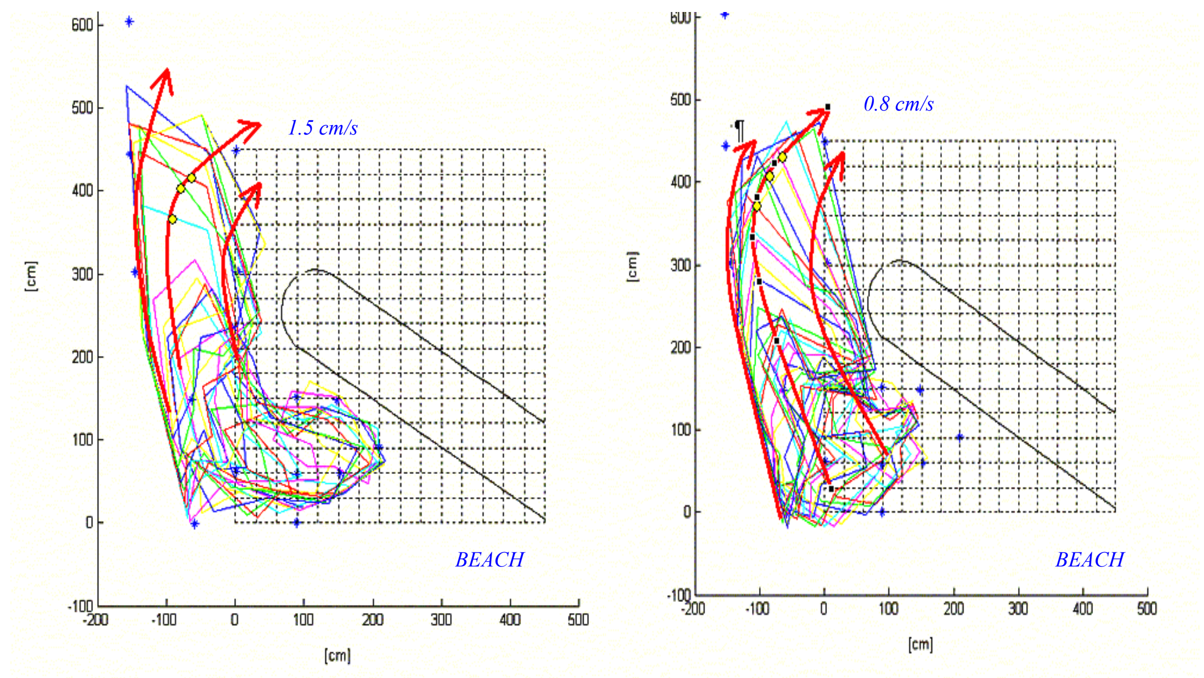

Fig. 8.3 Flow patterns obtained by image analysis for Test 56 (left), and Test 84 (right), view from the beach (co-ordinates in cm, model scale). The contour lines of the dye cloud are traced every 5 seconds for Test 56, every 10 seconds for Test 84. The mean velocity at the gap centre results 1.5 cm/s in Test 56 (measured 1.54 cm/s), 0.5 cm/s for Test 84 (measured 0.75 cm/s).

Wave reflection analysis

Reflection analysis domain adopted the method based on the linear theory that is presented for an arbitrary number of WGs by Zelt, J. A. & J. E. Skjelbreia (1992).Spectra for incident and reflected wave were determined in front (WGs 9-11 for layout 1, WGs 1-3 for layout 2) and behind (WGs 19-21 for layout 1, WGs 15-17 for layout 2) the structure and in front of the beach (WGs 15-17 for layout 1). Some typical results are presented for Test 34 (layout 1, submerged wide berm) and Test 46 (layout 2, freeboard zero narrow berm) in Fig.s 8.4-8.6 and 8.8-8.9 respectively, together with the comparison among the surface elevation obtained by the data and from the analysis (Fig.s 8.7 and 8.10).
Spectra are cut at frequency equal to 4.0 Hz, which resulted a resonance frequency for the instrumentation.

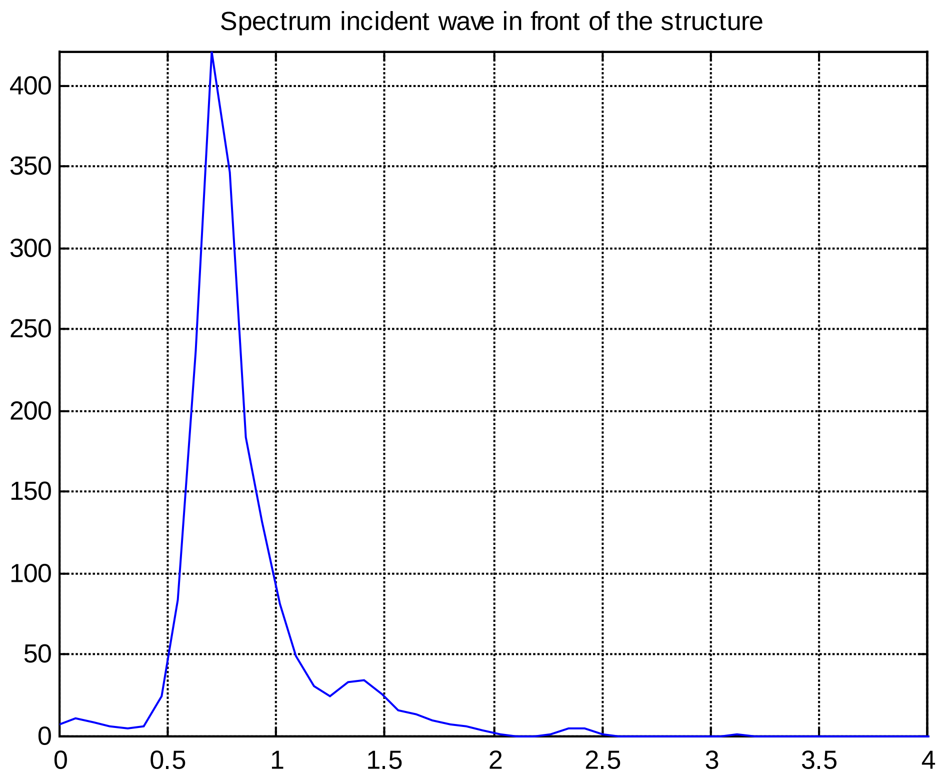

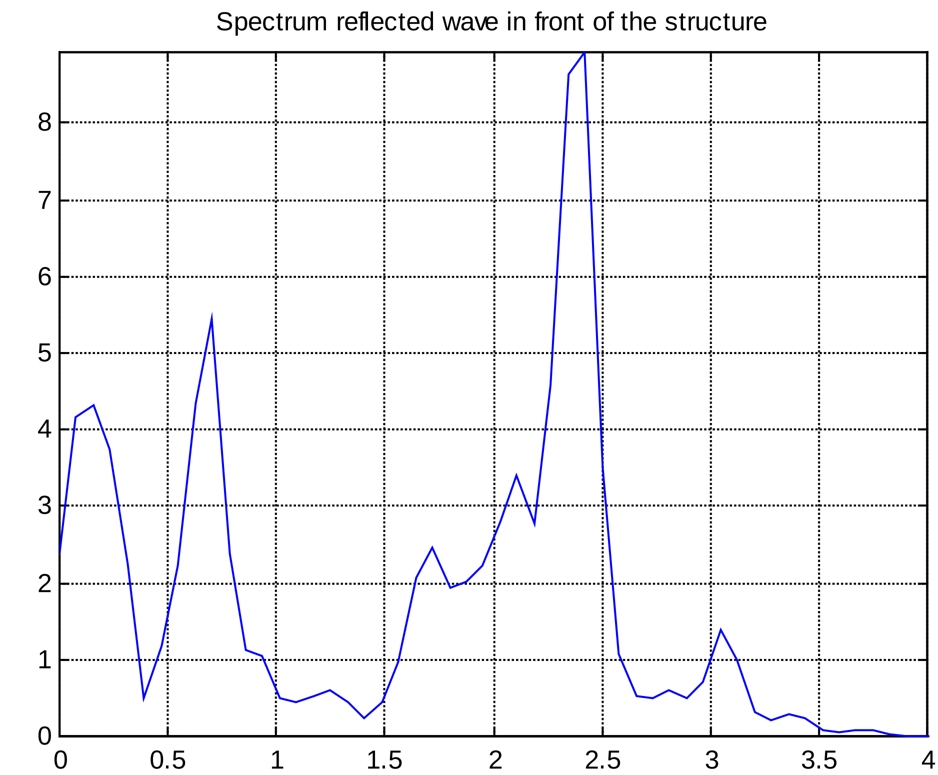

Fig. 8.4 Test 34, wave spectrum at WG 9-11, in front of the structure.

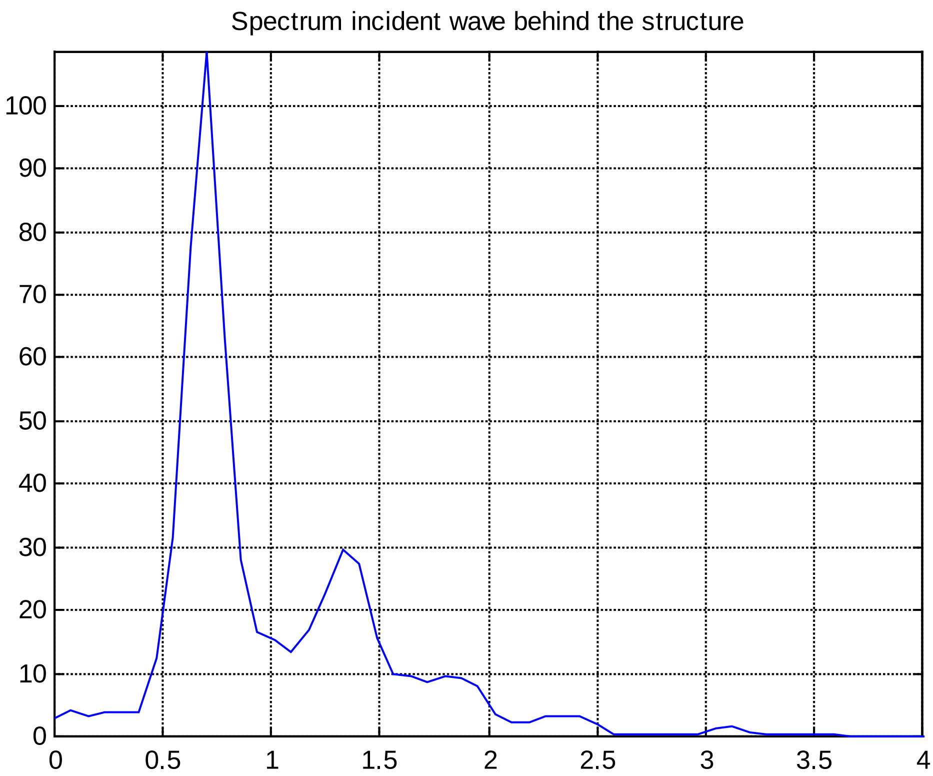

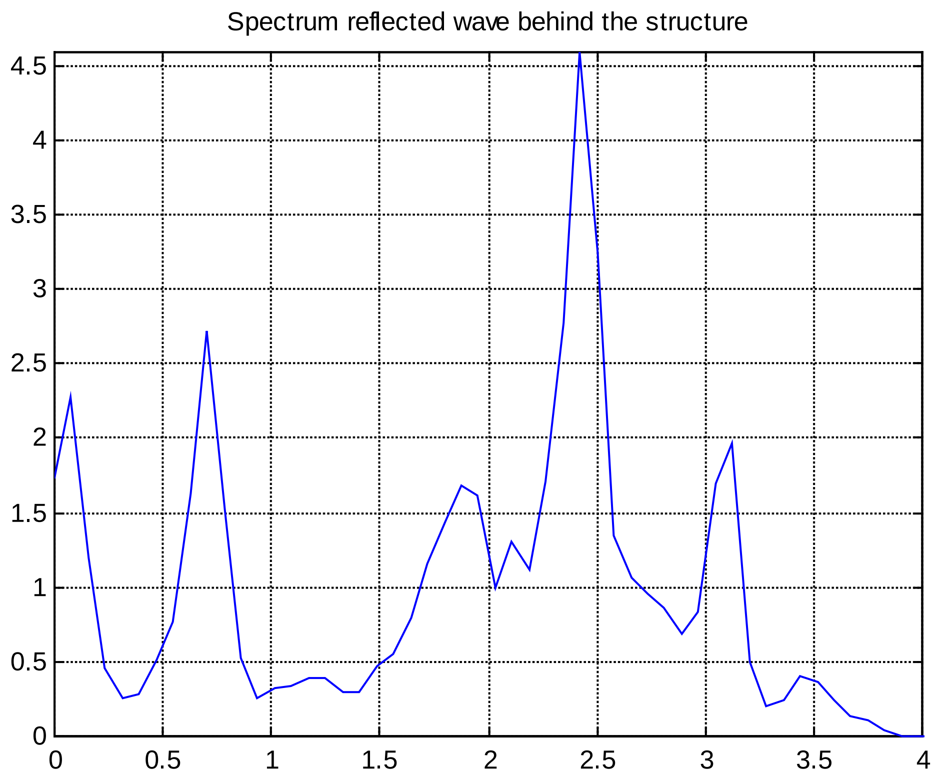

Fig. 8.5 Test 34, wave spectrum at WG 19-21, behind the structure.

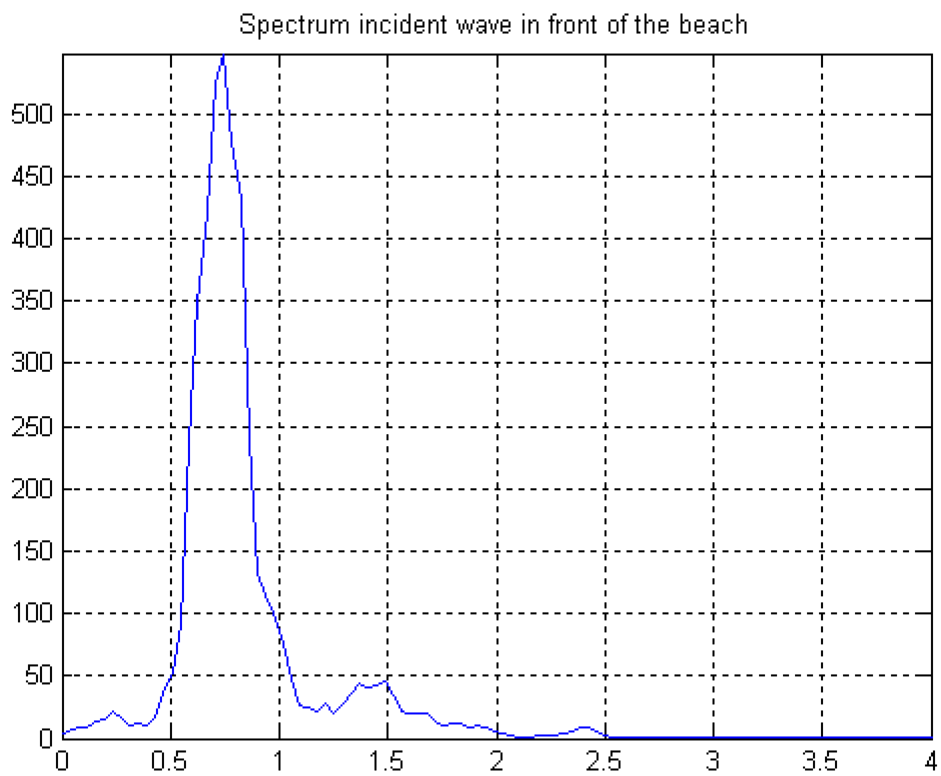

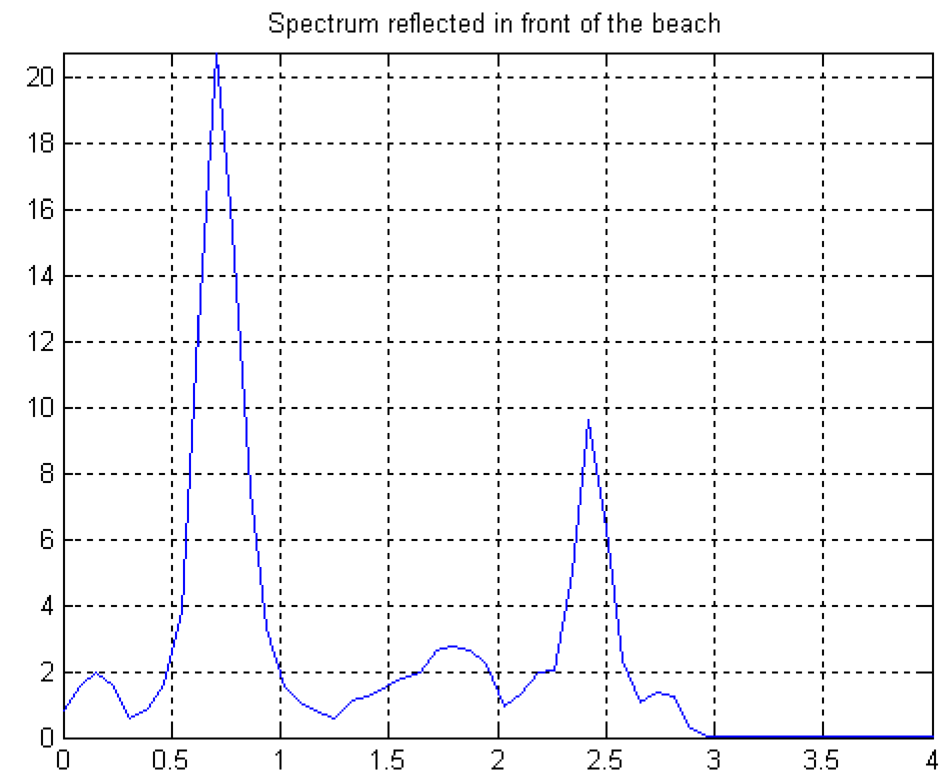

Fig. 8.6 Test 34, wave spectrum at WG 15-17, in front of the beach.

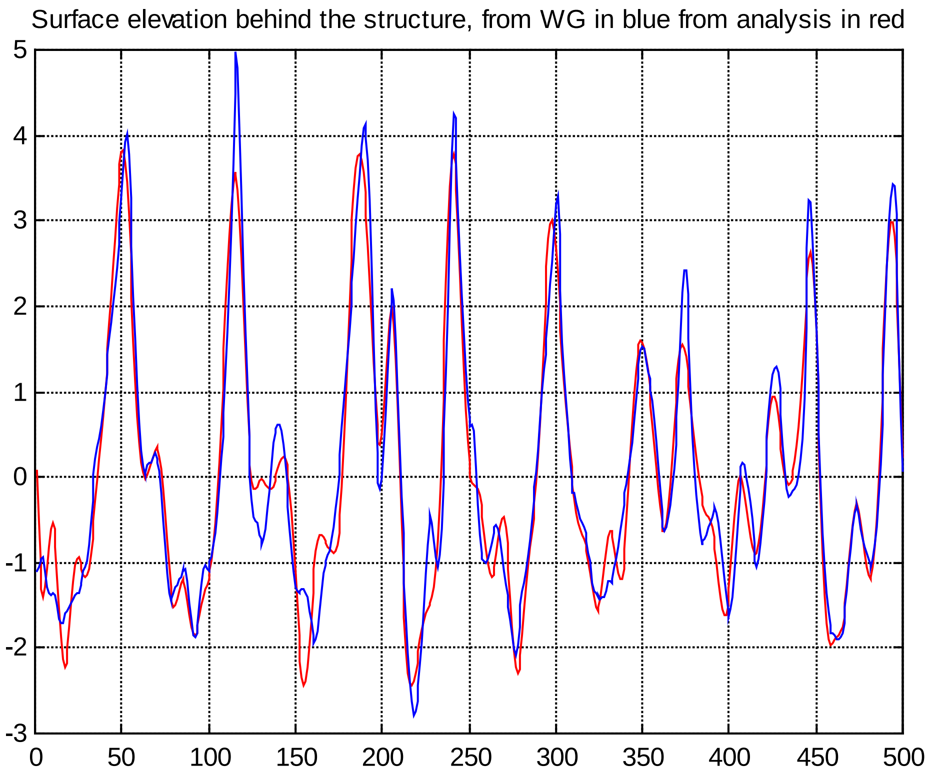

Fig. 8.7 Test 34, comparison of incident wave height obtained by experimental data (in blue) and theoretical analysis (in red), in front (up) and behind (down) the structure.

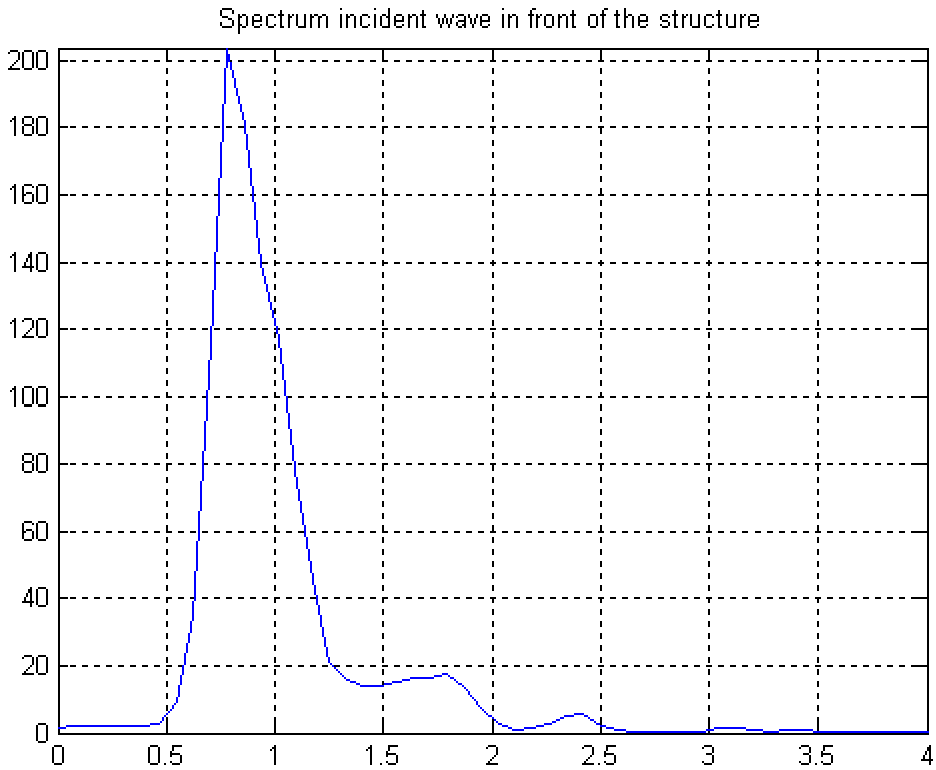

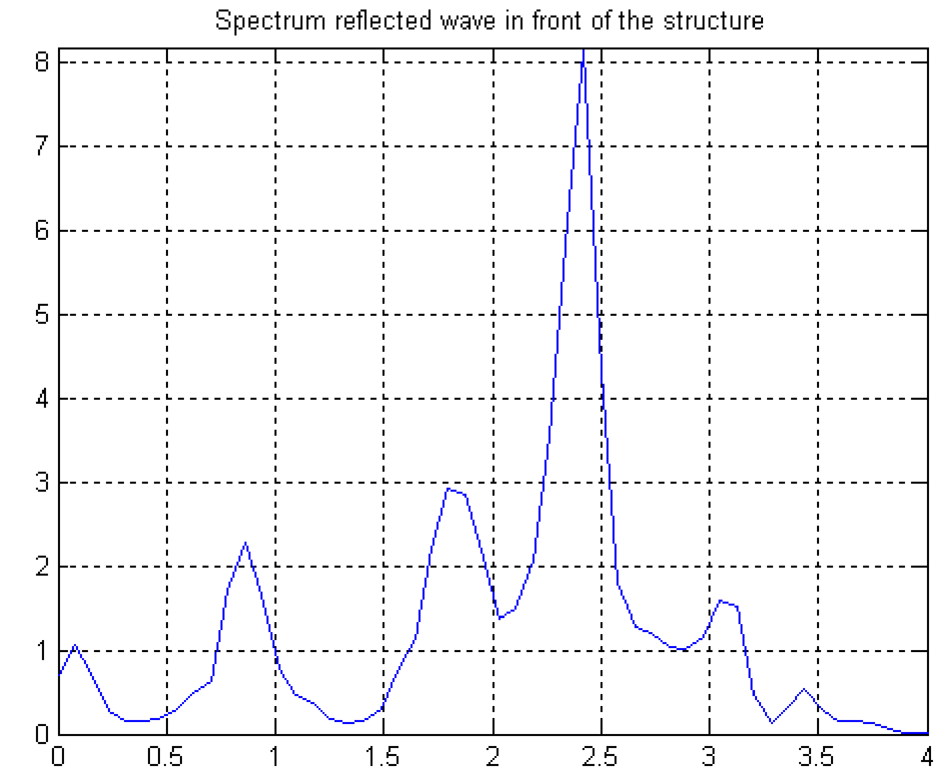

Fig. 8.8 Test 46, wave spectrum at WG 9-11, in front of the structure.

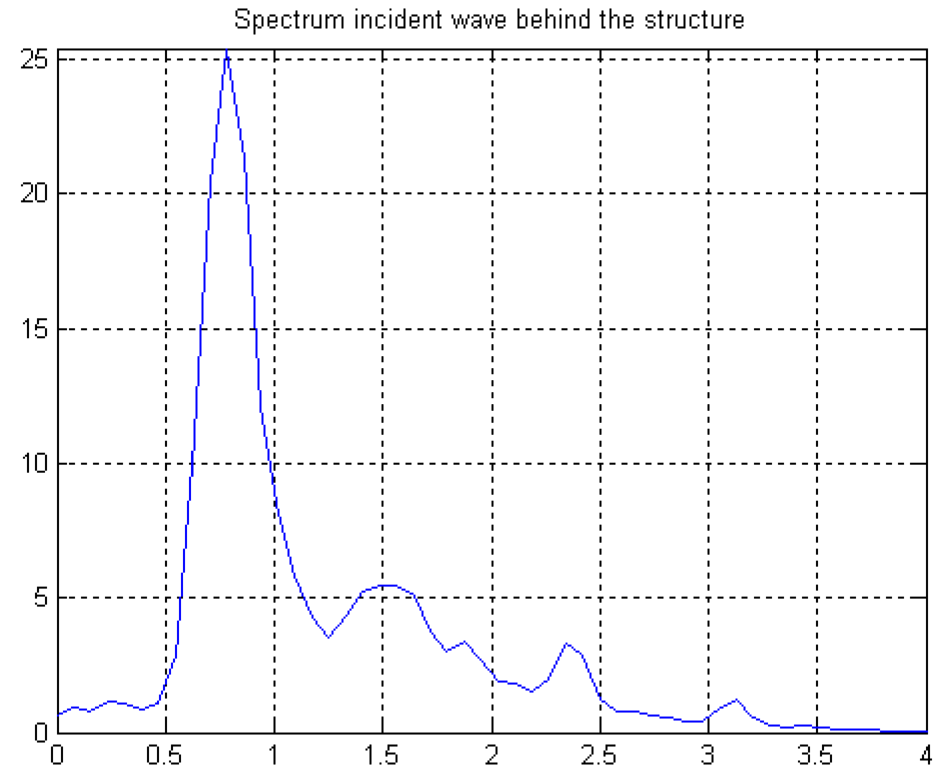

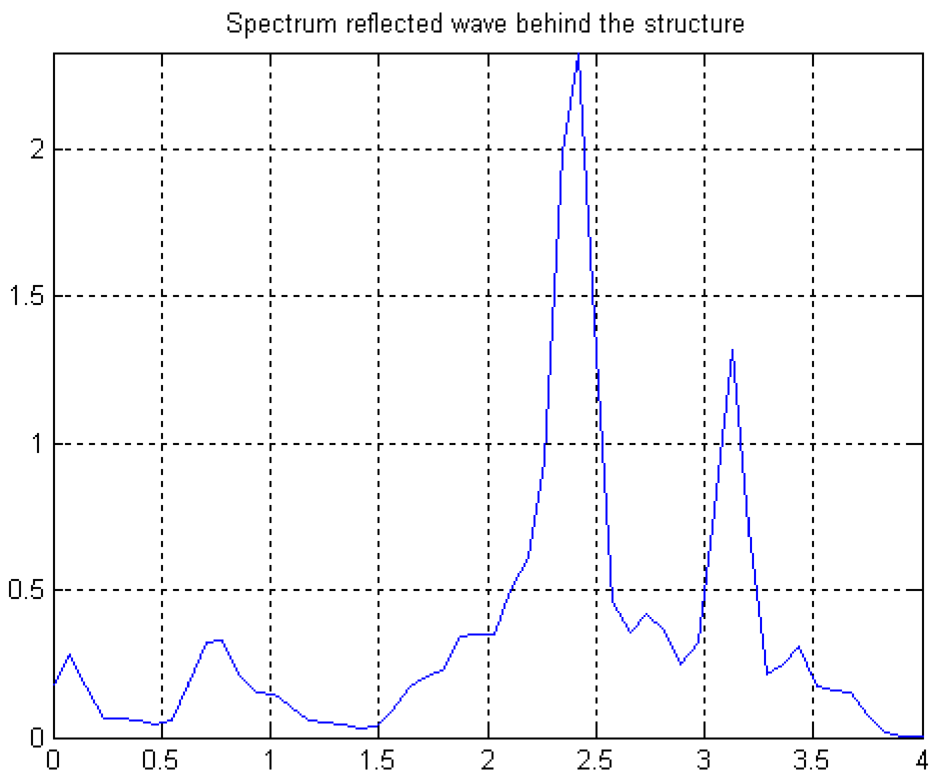

Fig. 8.9 Test 46, wave spectrum at WG 15-17, behind the structure.

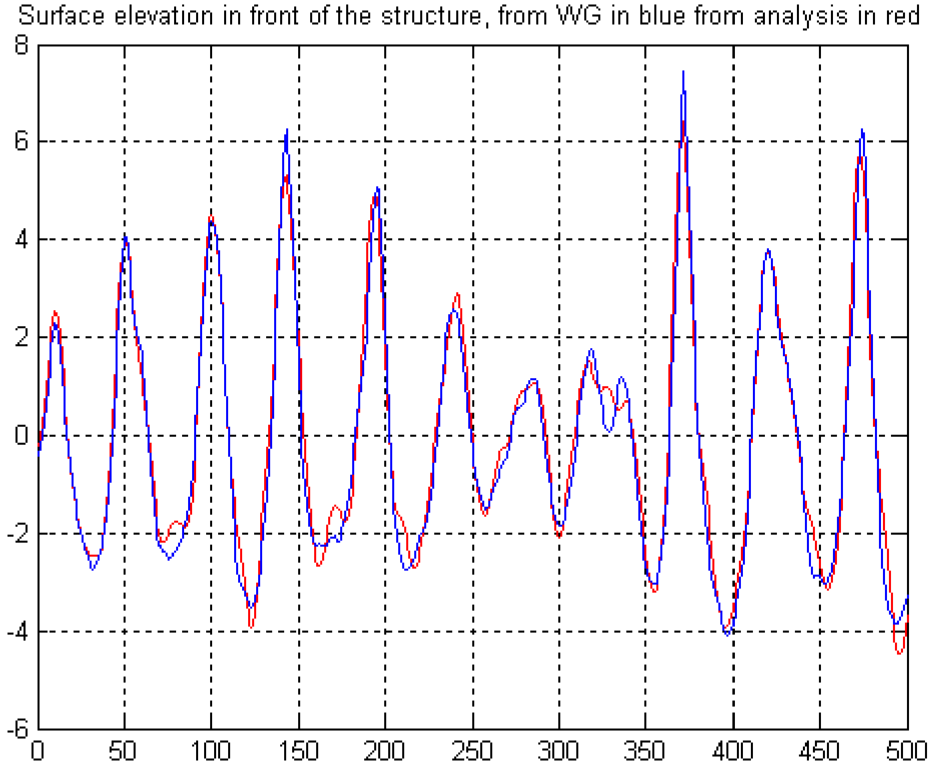

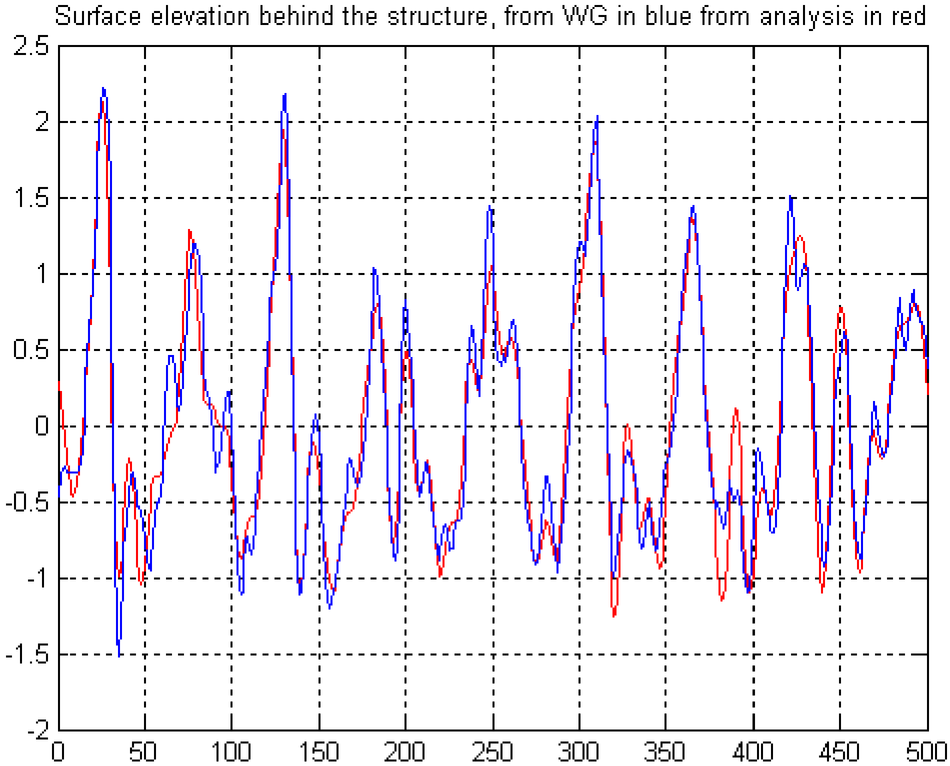

Fig. 8.10 Test 46, comparison of incident wave height obtained by experimental data (in blue) and theoretical analysis (in red), in front (up) and behind (down) the structure.

The following two pages contain results for layout 1 and 2, Tab. 8.1 and 8.2 respectively.
Table legend:
Units in CGS system
Tp is the target peak period
Hs is the target significative wave height
Hm0i is determined by 4*sqrt(M0) for irregular waves, 2.8*sqrt(M0) for regular waves.
Etai, Etar are evaluated following linear wave theory in the absence of currents.
stdEtai, stdEtar are the standard deviation of Etai, Etar evaluated following linear wave theory in the absence of currents.
Tsi is the significative wave period T1/3 of incident waves.
Tsi is the significative wave period T1/3 of reflected waves.
Hsi, Hsr are the incident, reflected significative wave height H1/3 determined with a time-domain analysis performed on incident, reflected wave signal Etai, Etar.
Kr is the reflection coefficient and is evaluated as the ratio Hsr/Hsi determined on all the frequencies.

Reflection due to the structure can be analysed for layout 1 only, in which three aligned gauges (WGs 9-11) in front of the structure were placed.
Reflection depends on freeboard adimensionalised by incident wave height, on mean berm width adimensionalised by wave length at structure toe and on slope berm width adimensionalised by wave length at structure toe, as it can be seen in Fig. s 8.11, 8.12 and 8.13 respectively. In each of this figure, fluctuations are evident, proving that none of these variables can be neglected in representing reflection due to the structure; the representation of the experimental results through a regression function of these three quantities is still in progress.

				WG 9-11							WG19-21							WG 15-17						
Test	Tp	Hs	Hm0i	stdEtai	stdEtar	Tsi	Hsi	Tsr	Hsr	Kr	stdEtai	stdEtar	Tsi	Hsi	Tsr	Hsr	Kr	stdEtai	stdEtar	Tsi	Hsi	Tsr	Hsr	Kr
1	1.70	9.00	8.78	2.19	0.75	1.52	9.38	1.15	2.88	34.04	1.22	0.36	1.54	5.15	0.64	1.22	29.68	2.28	0.46	1.48	8.46	0.83	1.86	20.40
2	1.20	9.00	7.74	1.94	0.56	1.13	7.76	0.88	2.33	29.18	0.91	0.24	1.13	3.58	0.49	0.95	26.77	1.97	0.48	1.18	7.62	0.69	1.93	24.26
3	1.13	4.00	4.45	1.11	0.27	1.11	4.47	1.22	1.10	24.48	0.50	0.12	1.10	1.95	0.50	0.46	23.69	1.23	0.26	1.09	4.95	0.88	1.10	21.57
4	0.80	4.00	2.86	0.71	0.16	0.82	2.89	0.79	0.66	22.74	0.28	0.08	0.83	1.12	0.46	0.33	29.79	0.75	0.17	0.80	2.98	0.74	0.71	22.79
5	1.56	7.60	8.34	2.98	0.71	1.56	10.13	0.50	2.24	24.00	1.60	0.47	1.56	5.48	0.54	1.68	29.44	3.03	0.48	1.56	9.53	0.65	1.69	15.91
6	1.10	7.60	7.50	2.68	0.59	1.10	8.19	1.10	2.61	22.12	1.09	0.26	1.09	3.98	0.48	1.04	24.26	2.14	0.62	1.11	7.74	0.50	2.25	29.18
7	1.04	3.40	3.50	1.25	0.23	1.04	3.55	1.03	0.74	18.46	0.65	0.09	0.75	2.32	0.47	0.35	14.09	1.68	0.38	1.04	4.90	1.03	1.23	22.44
8	0.74	3.40	3.09	1.10	0.25	0.72	3.42	0.50	0.97	22.42	0.48	0.12	0.74	1.72	0.37	0.45	25.80	1.43	0.34	0.74	4.12	0.64	1.15	23.59
9	1.70	9.00	9.16	2.29	0.76	1.50	9.68	1.04	2.96	33.32	1.20	0.32	1.50	4.99	0.53	1.27	26.69	2.41	0.52	1.50	8.88	0.89	2.02	21.58
10	1.20	9.00	8.00	2.00	0.61	1.14	7.82	1.01	2.51	30.48	1.00	0.28	1.16	3.83	0.46	1.13	28.29	2.18	0.58	1.15	8.24	0.62	2.32	26.73
11	1.57	7.65	7.61	1.90	0.72	1.42	8.12	1.01	2.79	37.80	0.68	0.20	1.25	2.72	0.61	0.79	29.89	1.85	0.41	1.38	6.98	0.83	1.62	21.92
12	1.11	7.65	6.61	1.65	0.52	1.08	6.68	0.89	2.18	31.66	0.42	0.12	1.07	1.65	0.58	0.47	28.44	1.68	0.41	1.09	6.49	0.67	1.71	24.57
13	1.04	3.40	3.47	0.87	0.23	1.06	3.45	1.10	0.91	26.23	0.22	0.05	1.12	0.85	0.89	0.20	23.58	0.83	0.17	1.01	3.35	0.97	0.71	20.74
14	0.74	3.40	1.97	0.49	0.12	0.79	2.01	0.81	0.47	23.79	0.11	0.02	0.85	0.44	0.76	0.10	21.80	0.46	0.09	0.77	1.85	0.76	0.37	19.56
15	1.44	6.46	6.38	2.28	0.81	1.44	7.66	1.13	3.16	35.55	1.07	0.29	1.01	3.30	0.42	1.07	26.85	2.32	0.32	1.44	7.22	1.08	1.14	13.79
16	1.02	6.46	6.25	2.23	0.32	1.02	6.54	0.49	1.14	14.43	0.58	0.11	0.91	2.09	0.52	0.40	18.29	2.71	0.63	1.02	8.32	0.70	1.90	23.19
17	1.97	12.15	12.74	3.18	0.95	1.74	13.72	1.43	3.87	29.77	2.01	0.54	1.78	8.00	0.86	1.99	26.88	3.14	0.73	1.73	12.09	1.32	2.87	23.15
18	1.40	12.15	11.41	2.85	0.71	1.31	11.29	0.95	2.96	24.99	1.95	0.45	1.33	7.41	0.62	1.76	22.94	2.81	0.63	1.34	10.72	0.97	2.46	22.39
19	1.81	10.26	10.33	3.69	1.08	1.81	11.75	1.80	4.15	29.28	2.63	0.70	1.81	9.12	0.98	2.61	26.73	4.44	0.75	1.81	13.33	1.81	2.95	16.85
20	1.28	10.26	10.10	3.61	0.89	1.28	10.64	0.49	2.83	24.63	2.37	0.73	1.28	7.71	0.58	2.77	30.98	3.31	0.96	1.29	11.11	0.63	3.79	29.09
21	1.32	5.40	5.96	1.49	0.26	1.25	5.80	1.39	1.05	17.14	1.20	0.19	1.27	4.85	0.56	0.76	15.56	1.61	0.34	1.26	6.43	1.18	1.40	21.41
22	0.93	5.40	14.42	1.19	0.15	0.94	4.82	0.67	0.63	12.92	0.90	0.14	0.92	3.59	0.48	0.57	15.76	1.10	0.27	0.93	4.37	0.88	1.12	24.40
23	1.70	9.00	8.78	2.19	0.65	1.53	9.48	0.84	2.63	29.68	0.70	0.21	1.40	2.82	0.79	0.80	30.54	2.15	0.48	1.47	8.06	1.05	1.91	22.21
24	1.20	9.00	7.89	1.97	0.52	1.13	7.97	0.75	2.21	26.50	0.43	0.15	1.00	1.79	0.57	0.58	34.23	1.99	0.48	1.14	7.57	0.81	1.95	24.06
25	1.13	4.00	4.23	1.06	0.18	1.11	4.30	1.00	0.73	17.26	0.18	0.07	1.19	0.72	0.83	0.26	36.91	1.01	0.21	1.11	4.00	1.06	0.88	20.98
26	0.80	4.00	2.69	0.67	0.10	0.85	2.74	0.69	0.41	15.47	0.08	0.04	0.95	0.34	0.74	0.14	41.72	0.65	0.15	0.79	2.61	0.79	0.62	22.71
27	1.56	7.60	8.04	2.87	0.61	1.56	9.64	0.49	2.23	21.41	0.87	0.25	1.54	3.25	0.44	0.97	28.66	3.04	0.69	1.56	9.86	1.54	2.29	22.70
28	1.10	7.60	7.21	2.58	0.58	1.10	7.87	1.09	2.61	22.58	0.48	0.17	0.84	1.57	0.39	0.67	35.95	2.66	0.60	1.10	8.78	0.55	2.08	22.52
29	1.04	3.40	3.84	1.37	0.20	1.03	4.23	0.58	0.78	14.80	0.15	0.08	0.75	0.56	1.03	0.30	55.16	1.67	0.35	1.04	4.64	1.04	1.03	20.77
30	0.74	3.40	2.86	1.02	0.26	0.70	3.26	0.48	1.02	25.17	0.08	0.03	0.72	0.24	0.61	0.11	35.45	1.25	0.28	0.73	3.59	0.74	0.77	22.66
31	1.70	9.00	9.45	2.36	0.76	1.49	10.16	0.80	2.98	32.01	0.69	0.20	1.42	2.87	0.65	0.77	29.27	2.30	0.54	1.45	8.62	1.03	2.12	23.52
32	1.20	9.00	7.89	1.97	0.56	1.12	7.90	0.85	2.37	28.47	0.40	0.14	1.16	1.65	0.55	0.54	35.21	2.14	0.57	1.17	8.17	0.70	2.28	26.56
33	1.97	12.15	12.88	3.22	0.88	1.77	14.04	1.29	3.70	27.23	1.66	0.55	1.79	6.58	0.86	2.00	33.31	3.04	0.73	1.75	11.55	1.48	2.83	23.98
34	1.40	12.15	10.61	2.65	0.58	1.28	10.67	0.76	2.46	21.90	1.48	0.43	1.40	5.80	0.62	1.65	29.12	2.93	0.72	1.33	11.02	0.97	2.74	24.75
35	1.32	5.40	5.84	1.46	0.20	1.24	5.67	1.13	0.80	14.03	1.05	0.22	1.26	4.10	0.51	0.88	20.83	1.62	0.40	1.24	6.32	1.15	1.61	24.74
36	0.93	5.40	4.43	1.11	0.14	0.95	4.40	0.68	0.58	13.00	0.81	0.14	0.86	3.16	0.49	0.57	17.66	1.07	0.28	0.92	4.32	0.86	1.18	26.48
37	1.81	10.26	7.85	2.80	0.56	0.81	8.22	0.41	1.80	19.94	1.29	0.42	0.81	4.27	0.41	1.61	32.15	2.79	1.35	0.81	9.38	0.48	5.27	48.35
38	1.28	10.26	10.31	3.68	0.88	1.28	10.71	0.44	2.67	23.87	1.58	0.70	1.28	5.32	0.47	2.57	44.13	3.32	0.81	1.29	11.58	0.78	3.34	24.44
39	1.57	7.65	7.52	1.88	0.63	1.39	7.97	0.90	2.59	33.64	0.30	0.12	1.63	1.20	1.45	0.49	41.58	1.92	0.42	1.36	7.21	1.00	1.72	21.92
40	1.11	7.65	6.67	1.67	0.47	1.06	6.63	0.80	1.93	27.97	0.18	0.08	1.35	0.67	1.16	0.32	46.46	1.62	0.39	1.09	6.33	0.72	1.63	24.11
41	1.44	6.46	6.18	2.21	0.73	1.44	7.17	1.31	2.98	32.98	0.40	0.12	1.44	1.39	1.16	0.47	30.73	2.51	0.42	1.44	8.02	1.09	1.48	16.87
42	1.02	6.46	6.20	2.21	0.33	1.02	6.39	0.65	1.02	14.86	0.26	0.12	1.02	0.81	1.02	0.41	44.76	2.70	0.65	1.02	9.04	0.57	1.97	24.03
43	1.04	3.40	3.25	0.81	0.18	1.03	3.34	1.12	0.73	22.19	0.11	0.05	1.16	0.43	1.17	0.19	41.18	0.81	0.17	1.02	3.25	0.99	0.71	21.03
44	0.74	3.40	1.95	0.49	0.10	0.80	1.98	0.78	0.40	20.55	0.06	0.03	0.88	0.23	0.85	0.11	45.77	0.46	0.10	0.75	1.85	0.76	0.39	20.66

Tab. 8.1 Wave reflection analysis, layout 1.

				WG 1-3						WG 15-17					
Test	Tp	Hs	Hm0i	stdEtai	stdEtaip	stdEtar	stdEtarp	Krt	Krp	stdEtai	stdEtaip	stdEtar	stdEtarp	Krt	Krp
45	1,70	9,00	10,16	2,54	2,15	0,65	0,25	25,78	11,57	1,11	0,79	0,37	0,10	33,64	13,06
46	1,20	9,00	8,57	2,14	1,95	0,58	0,20	27,22	10,33	0,83	0,65	0,29	0,08	34,92	12,22
47	1,13	4,00	4,77	1,19	1,13	0,28	0,11	23,81	9,63	0,44	0,37	0,14	0,05	31,24	14,35
48	0,80	4,00	2,92	0,73	0,72	0,12	0,07	17,08	9,99	0,27	0,23	0,08	0,03	31,95	14,18
49	1,56	7,60	10,11	3,61	3,06	0,78	0,16	21,63	5,23	1,05	0,72	0,44	0,07	41,50	10,11
50	1,10	7,60	7,86	2,81	2,61	0,55	0,15	19,63	5,86	0,86	0,67	0,32	0,06	37,22	9,33
51	1,04	3,40	3,96	1,42	1,39	0,22	0,06	15,69	4,35	0,29	0,25	0,15	0,06	51,36	22,69
52	0,74	3,40	3,71	1,33	1,28	0,51	0,37	38,26	28,76	0,32	0,30	0,09	0,06	27,11	20,74
53	1,70	9,00	10,50	2,62	2,16	0,85	0,24	32,25	11,09	0,89	0,60	0,31	0,09	34,42	14,88
54	1,20	9,00	8,63	2,16	1,94	0,61	0,16	28,25	8,06	0,61	0,46	0,21	0,07	35,13	15,11
55	1,57	7,65	8,94	2,24	1,88	0,68	0,22	30,52	11,80	0,69	0,46	0,34	0,09	48,91	18,58
56	1,11	7,65	7,28	1,82	1,66	0,51	0,19	27,84	11,20	0,44	0,35	0,16	0,07	37,68	21,43
57	1,04	3,40	3,77	0,94	0,90	0,23	0,10	24,69	10,64	0,22	0,21	0,08	0,05	33,83	22,84
58	0,74	3,40	2,02	0,51	0,50	0,09	0,07	17,89	13,51	0,12	0,11	0,04	0,03	33,08	22,50
59	1,44	6,46	8,16	2,91	2,52	0,87	0,02	29,77	9,29	0,85	0,59	0,24	0,04	28,60	6,72
60	1,02	6,46	6,61	2,36	2,25	0,33	0,05	13,90	2,36	0,44	0,36	0,14	0,06	31,03	17,05
61	1,97	12,15	13,93	3,48	2,92	0,94	0,28	27,01	9,48	1,81	1,24	0,79	0,13	43,35	10,79
62	1,40	12,15	12,10	3,02	2,69	0,87	0,27	28,64	9,89	1,52	1,16	0,57	0,12	37,44	9,63
63	1,81	10,26	12,99	4,64	4,09	0,90	0,30	19,32	7,26	1,86	1,48	0,86	0,12	46,07	8,25
64	1,28	10,26	11,74	4,19	3,75	1,43	0,26	34,06	6,81	1,60	1,20	1,02	0,10	63,62	8,54
65	1,32	5,40	6,66	1,67	1,56	0,31	0,14	18,90	8,84	0,94	0,74	0,25	0,06	26,83	8,35
66	0,93	5,40	4,70	1,18	1,14	0,22	0,09	18,76	8,12	0,64	0,52	0,18	0,05	28,79	9,58
67	1,70	9,00	10,07	2,52	2,12	0,78	0,27	30,95	12,85	0,64	0,46	0,22	0,10	34,58	20,59
68	1,20	9,00	8,68	2,17	1,97	0,60	0,19	27,82	9,88	0,47	0,39	0,16	0,08	33,57	21,11
69	1,13	4,00	4,52	1,13	1,08	0,20	0,09	17,31	8,69	0,27	0,25	0,09	0,05	30,99	21,50
70	0,80	4,00	2,77	0,69	0,68	0,11	0,06	16,04	9,10	0,14	0,14	0,04	0,03	30,85	21,17
71	1,56	7,60	9,88	3,53	3,06	0,79	0,46	22,41	15,09	0,82	0,68	0,37	0,21	42,55	32,35
72	1,10	7,60	8,11	2,90	2,76	0,52	0,28	18,00	10,29	0,50	0,33	0,18	0,09	37,06	25,52
73	1,04	3,40	4,06	1,45	1,43	0,20	0,06	13,61	3,90	0,33	0,32	0,11	0,10	32,86	32,34
74	0,74	3,40	3,34	1,19	1,17	0,43	0,34	35,90	29,36	0,13	0,12	0,05	0,02	39,76	17,11
75	1,70	9,00	10,60	2,65	2,23	0,74	0,30	28,03	13,59	0,65	0,51	0,22	0,10	34,34	19,09
76	1,20	9,00	8,89	2,22	2,03	0,54	0,17	24,20	8,42	0,49	0,41	0,18	0,09	35,53	22,32
77	1,97	12,15	14,50	3,63	3,03	1,12	0,29	31,00	9,54	1,74	1,12	0,93	0,14	53,37	12,85
78	1,40	12,15	12,13	3,03	2,74	0,72	0,22	23,69	8,07	1,48	1,11	0,59	0,13	39,93	12,18
79	1,32	5,40	6,89	1,72	1,64	0,28	0,11	16,51	6,99	1,08	0,87	0,31	0,08	28,66	9,27
80	0,93	5,40	4,75	1,19	1,15	0,22	0,09	18,13	7,56	0,85	0,73	0,24	0,07	28,07	9,80
81	1,81	10,26	11,39	4,07	3,62	0,71	0,15	17,47	4,16	1,99	1,46	0,83	0,17	41,78	11,32
82	1,28	10,26	11,31	4,04	3,82	0,84	0,21	20,85	5,46	1,58	1,32	0,83	0,10	52,72	7,45
83	1,57	7,65	8,59	2,15		0,65		30,28	14,26	0,52	0,40	0,21	0,10	39,52	24,57
84	1,11	7,65	7,43	1,86	1,70	0,50	0,18	27,03	10,34	0,39	0,32	0,15	0,09	39,20	28,08
85	1,44	6,46	7,62	2,72	2,36	0,81	0,13	29,92	5,43	0,71	0,64	0,20	0,14	27,95	21,91
86	1,02	6,46	6,21	2,22	2,07	0,45	0,13	20,18	6,11	0,30	0,19	0,17	0,07	58,63	37,75
87	1,04	3,40	3,61	0,90	0,87	0,15	0,09	17,09	10,50	0,22	0,21	0,08	0,06	35,62	27,38
88	0,74	3,40	2,03	0,51	0,50	0,09	0,06	17,69	12,54	0,10	0,10	0,04	0,03	37,63	30,21

Tab. 8.2 Wave reflection analysis, layout 2.

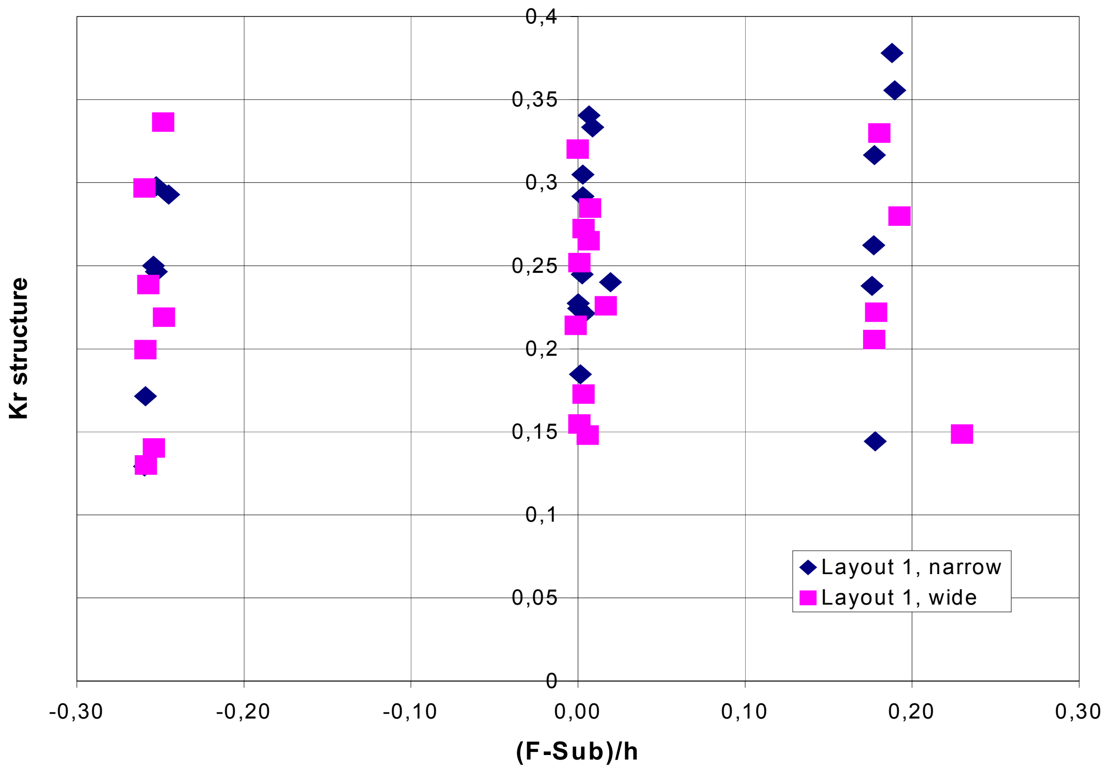

Fig. 8.11 Reflection coefficient Kr due to the structure, versus freeboard F minus setup at the barrier Sub adimensionalised by water depth at the structure.

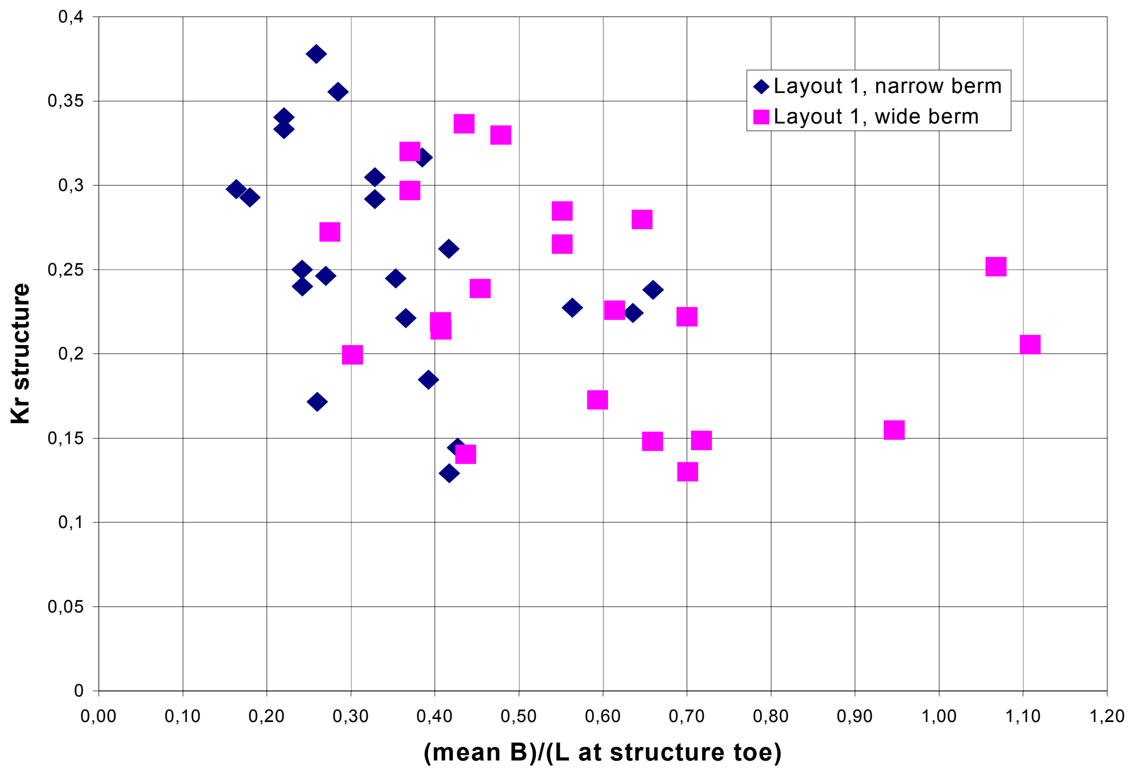

Fig. 8.12 Reflection coefficient Kr due to the structure, versus mean berm width B over wave length at structure toe L.

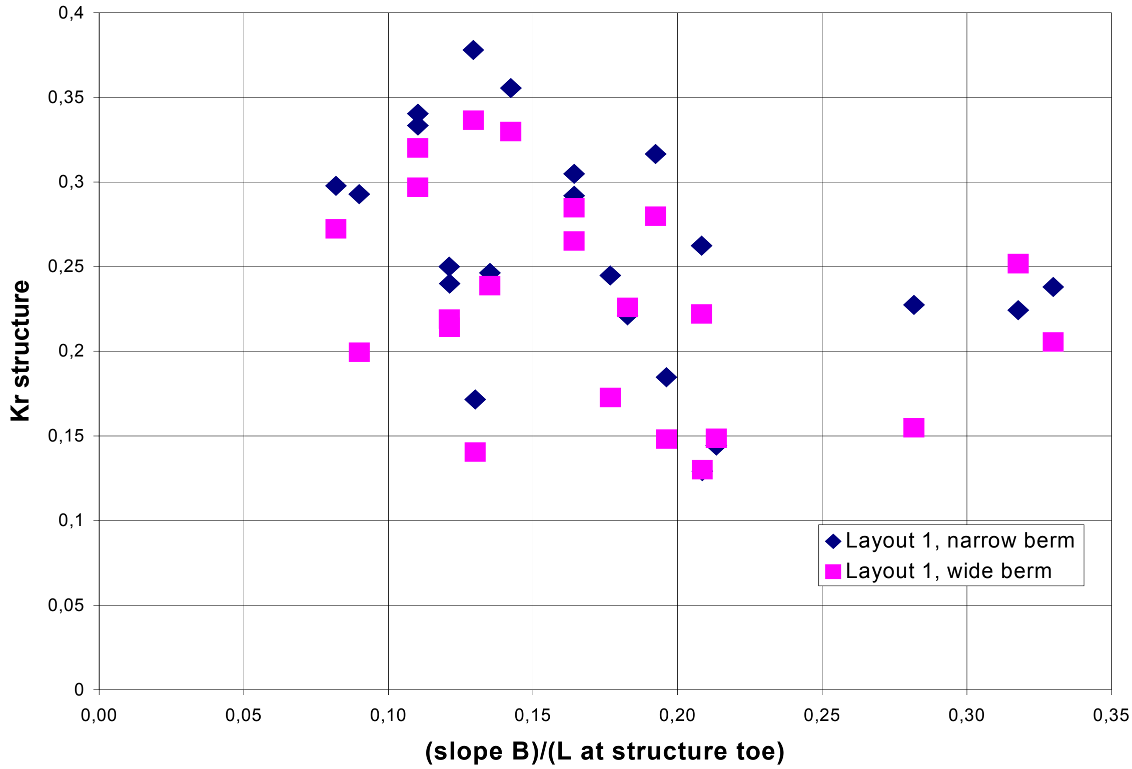

Fig. 8.13 Reflection coefficient Kr due to the structure, versus width B of the berm slope over wave length at structure toe L.

Wave directional analysis

After checking (on the Net) free available softwares in Matlab environment, we chose the DIWASP, developed by D. Johnson, Centre for Water Res. Univ. of Western Australia, Perth, is the best available free toolbox for estimation of directional wave spectra from field data (http://www.cwr.uwa.edu.au/~johnson/diwasp/diwasp.html). Five methods are implemented: DFTM (Direct Fourier Transfer Method), EMLM (extended Maximum Likelyhood Method), IMLM (Iterative Maximum Likelyhood Method), EMEP, BDM.
The following commonly used methods are compared in this note:

- EMLM is an extension of MLM to velocities, surface slopes and pressure. Due to the formulation of the equations, where the spectrum is a reciprocal of a quadratic function, peaks values, being the minimum of the denominator, are sensitive to truncation errors.
- IMLM considers an iterative procedure aiming at obtaining from the computed spectrum the same cross-spectra functions of the raw data.
- MEP: the spreading function is considered as a pdf and derived according to Jaynes' principle (a statistical consolidated method). Similarly to MLM, it can be applied only to three quantity measurement.
- EMEP: it is an extension of the previous one to multi-quantity measurement. The minimisation procedure is similar to MEP, but with a different spreading function.
- BDM: Despite of the name, no a-priori assumption of the directional spreading is made. The a-priori condition is the smoothness of the spreading function, with a smoothness weight parameter to be calibrated.

Four different methods (EMEP, EMLM, IMLM, BDM) were adopted and the directional analysis was carried out on:
5 elevation signals from Wave Gauges (WGs) in front of the wave maker for layout 1;
3 wave components, 2 velocities obtained by a 3D Acoustic Doppler Velocimeter (ADV) and 1 elevation signal, at the gap centre for both layout 1 and 2.
For layout 2, no analysis was carried out on the 5 gauges in front of the wave maker because some of them can be affected by the refraction at the breakwater roundhead.

Tab. 8.3 below reports the results of this analysis (mean values over all tests for layout 1), excluding BDM, which gives unrealistic results especially at the gap because of the low number of signals, and Regular wave tests, for which only IMLM produces reasonable results. Spreading is compared to the target value; reflection is compared to the values obtained by applying linear wave theory on three collinear WGs in front of the structure and of the beach (Zelt & Skjelbreia, 1992). Accounting for refraction at the roundheads that can affect reflection at the wave maker and for high rip currents at the gap, K_R at the wave maker may not exceed the value in front of the structure, whereas K_R at the gap centre may result in the range between the lower value in front of the beach and the higher in front of the structure.
The table shows that no general best method exists. IMLM seems to be the best for the 5 WGs array since it causes the lowest increase in spreading and reflection; in fact, all methods behave worse for 2D spectra than for 3D ones. EMEP results to be the best method for the 3 wave components at the same location, showing similar performance for 2D and 3D spectra.

Layout 1						
Jonswap 3D						
Method	Si [°]	Sr [°]	K_R [%]	Si [°]	Sr [°]	K_R [%]
TARGET	22.7°					
	5 elevation signals, WGs 3-7, at wave-maker			3 wave components, ADV III and WG 12, at gap centre		
EMEP Nfft=256, Ndir=180	74.2 ± 14.4	68.6 ± 19.7	68.4	35.3 ± 7.6	96.8 ± 4.0	29.7
EMLM Nfft=256, Ndir=180	59.5 ± 3.2	87.1 ± 4.7	39.3	65.7 ± 8.6	96.2 ± 1.5	29.7
IMLM Nfft=256, Ndir=180, It=10	52.0 ± 3.4	77.4 ± 7.6	30.1	51.7 ± 12.0	100.1 ± 24	52.7
	3 elevation signals, WGs 9-11, in front of the structure			3 elevation signals, WGs 15-17, in front of the beach		
3 Collinear WGs	-	-	24.3	-	-	22.7
Jonswap 2D (=regular in direction)						
Method	Si [°]	Sr [°]	K_R [%]	Si [°]	Sr [°]	K_R [%]
TARGET	0°					
	5 elevation signals, WGs 3-7, at wave-maker			3 wave components, ADV III and WG 12, at gap centre		
EMEP Nfft=256, Ndir=180	71.6 ± 20.3	94.6 ± 4.5	64.7	22.9 ± 1.3	48.6 ± 5.2	29.7
EMLM Nfft=256, Ndir=180	61.1 ± 8.1	84.4 ± 5.8	54.2	47.8 ± 0.9	74.0 ± 3.7	29.7
IMLM Nfft=256, Ndir=180, It=10	50.4 ± 9.8	77.5 ± 9.9	45.7	30.1 ± 1.0	57.4 ± 4.8	43.4
	3 elevation signals, WGs 9-11, in front of the structure			3 elevation signals, WGs 15-17, in front of the beach		
3 Collinear WGs	-	-	31.1	-	-	24.6

Tab. 8.3 Wave directional analysis, layout 1 ; mean values of incident and reflected spreading (Si, Sr) and reflection coefficient (K_R) in front of the wave maker and at the gap.

The result quality depends on a number of parameters: noise to signal ratio in the data, frequency resolution (or Nfft), directional resolution, tested method, number of iteration (IMLM only). Figure 8.14 below show a directional analysis in the gap: a wave gauge close to a 3-D ADV is present, so that a 4 wave information is available. Nevertheless, since the vertical velocity signal is rather noiseful (the bottom turbulence becomes important related to the low signal), the analysis gives better results if the information from the vertical velocity is disregarded (in fact, the table just presented contains results obtained with three wave components only). On the contrary, when signals are equally affected by noise, independent information contributes rather well to reduce uncertainties.

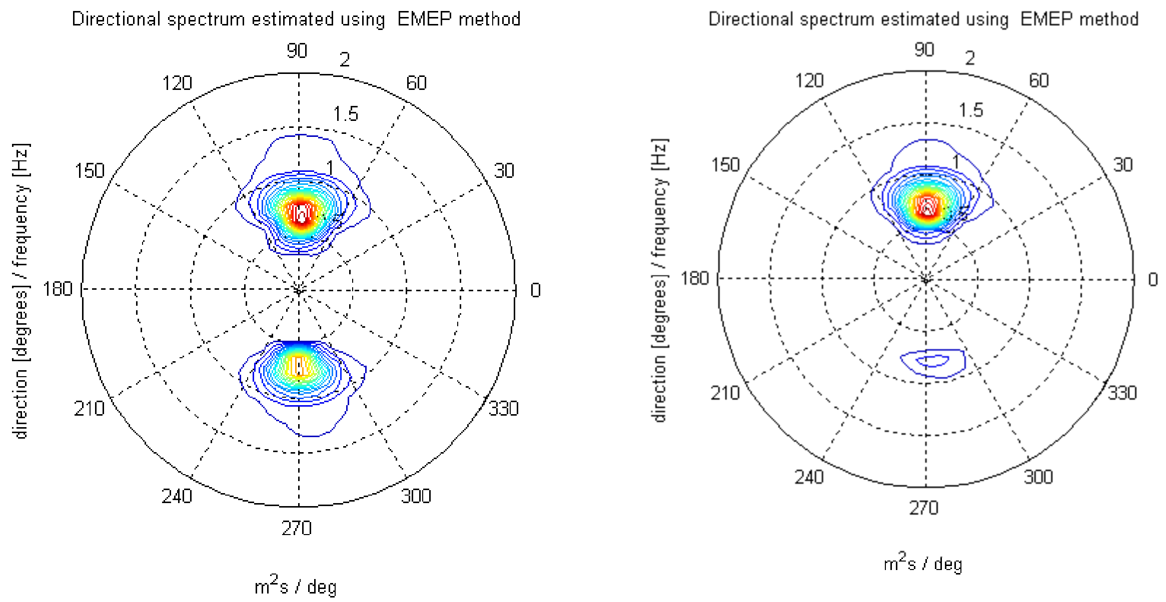

Fig. 8.14 Wave directional analysis at the gap. At the left hand-side, 4 wave components, Hsi =8.6 cm, Hsr = 7.3 cm; S_I= 44°; S_R=45°, EMEP; unrealistic wave reflection is obtained.
At the right hand-side, 3 wave components, H_{si} =10.6 cm, H_{sr}=3.7 cm; S_I= 40°, S_R=63°; the vertical velocity is abandoned and a realistic spectrum is found.

The following two pages contain results for layout 1 and 2 respectively.
Table legend:
Units in CGS system
Thetai is the incident wave direction;
Thetar is the reflected wave direction;
si is the incident wave spreading index;
sr is the reflected wave spreading index;
Hi is the estimated incident wave height;
Hr is the estimated reflected wave height;
Kr is the reflection coefficient.

	EMEP, Nfft=256, Dir=180. GAP							IMLM, Nfft=256, Dir=180, It=10. GAP							EMLM, Nfft=256, Dir=180. GAP						
Test	thetai	thetar	si	sr	Hi	Hr	Kr	thetai	thetar	si	sr	Hi	Hr	Kr	thetai	thetar	si	sr	Hi	Hr	Kr
1	88.01	-269.62	37.05	58.55	7.79	2.36	30.30	86.51	-266.25	46.80	84.32	7.62	3.00	39.32	86.63	-266.04	61.43	92.19	7.35	3.61	30.30
2	85.64	-268.67	34.37	44.93	6.82	3.62	53.05	81.38	-268.23	53.71	79.31	6.81	3.62	53.16	82.35	-266.61	67.25	88.02	6.57	4.03	53.05
3	88.70	-100.90	34.53	89.57	4.79	1.06	22.14	80.19	-97.49	70.23	78.73	3.72	3.02	81.36	82.70	-94.48	79.75	86.29	3.65	3.11	22.14
4	87.66	-99.62	47.82	85.93	2.88	0.92	31.92	83.40	-97.78	71.66	79.87	2.30	1.88	81.81	85.74	-94.54	79.79	86.16	2.26	1.93	31.92
5	86.52	-262.19	26.65	98.36	10.23	1.31	12.83	86.15	-92.67	32.21	61.33	9.57	4.05	42.35	86.62	-91.20	51.30	78.65	9.10	4.86	12.83
6	86.59	-247.54	20.80	104.29	11.48	0.57	5.00	85.55	-91.93	27.14	47.62	10.60	4.89	46.16	85.93	-90.64	46.59	68.63	10.01	5.72	5.00
7	87.22	-93.20	13.57	17.84	5.74	3.86	67.27	85.37	-96.02	20.76	30.34	5.90	3.77	63.89	85.73	-95.48	37.83	49.46	5.61	4.06	67.27
8	85.66	-100.39	18.94	22.48	4.48	2.13	47.50	79.43	-100.96	26.51	31.97	3.93	3.10	78.89	80.67	-99.26	49.36	56.44	3.80	3.19	47.50
9	87.14	-96.72	22.50	49.27	8.09	2.08	25.74	86.46	-94.60	29.57	61.37	7.89	3.04	38.51	86.91	-93.03	46.81	76.51	7.46	3.80	25.74
10	87.56	-96.11	24.17	54.95	7.71	2.07	26.91	86.18	-94.43	31.66	55.23	7.20	3.43	47.66	86.73	-93.02	49.16	72.13	6.81	3.99	26.91
11	86.99	-266.92	34.53	52.17	6.27	1.87	29.80	85.55	-265.73	44.24	79.54	6.11	2.47	40.36	85.71	-265.06	59.89	89.20	5.89	2.95	29.80
12	87.27	-267.95	28.18	36.15	5.99	2.65	44.32	85.95	-265.96	39.87	66.34	5.90	2.92	49.54	86.08	-265.31	58.41	81.18	5.67	3.33	44.32
13	86.70	-255.86	29.47	84.29	3.32	0.48	14.57	83.98	-93.94	42.28	69.90	2.97	1.50	50.59	84.92	-91.49	60.12	83.54	2.85	1.71	14.57
14	88.08	-268.67	40.91	59.25	1.72	0.78	45.06	85.90	-269.68	63.27	74.28	1.49	1.15	77.23	87.02	-268.26	73.73	82.20	1.46	1.19	45.06
15	88.23	-268.57	20.65	61.40	6.74	1.39	20.60	86.83	-94.24	29.56	57.15	6.47	2.61	40.39	87.46	-92.76	48.37	75.90	6.14	3.13	20.60
16	86.78	-94.03	17.01	15.09	9.05	4.53	50.09	85.55	-96.63	25.66	44.17	9.29	4.45	47.93	86.16	-95.54	40.40	59.30	8.72	5.15	50.09
17	87.22	-257.97	38.30	81.40	11.71	2.17	18.55	85.72	-259.25	52.28	90.68	11.07	4.22	38.12	85.64	-261.81	64.88	96.17	10.69	5.13	18.55
18	87.72	-259.52	40.84	63.08	10.66	3.73	35.05	84.21	-257.44	54.65	88.18	10.39	4.42	42.56	84.26	-259.98	66.73	94.11	10.03	5.19	35.05
19	85.93	-102.75	21.02	97.25	11.13	1.42	12.79	85.81	-95.66	20.71	51.08	15.03	4.74	31.53	86.10	-93.75	34.50	64.01	14.17	6.49	12.79
20	87.30	-266.88	27.85	88.78	6.35	0.71	11.10	85.86	-267.68	39.63	77.81	5.96	2.27	38.09	86.06	-267.21	57.65	89.85	5.73	2.80	11.10
21	87.30	-106.59	25.39	101.11	17.76	2.07	11.65	85.94	-92.26	30.06	59.75	16.79	6.60	39.33	86.22	-90.99	48.59	77.11	15.89	8.18	11.65
22	87.76	-90.36	30.00	48.85	4.39	1.17	26.63	86.09	-268.89	42.05	69.13	4.05	2.08	51.31	86.43	-267.87	59.88	82.94	3.90	2.36	26.63
23	85.64	-267.24	32.24	58.18	7.36	1.74	23.65	84.67	-90.81	41.44	78.30	7.01	2.70	38.53	85.25	-268.91	58.20	89.35	6.75	3.28	23.65
24	86.94	-268.88	29.86	39.11	7.11	2.64	37.07	85.81	-268.26	40.60	71.43	6.97	3.07	44.06	86.12	-267.25	58.54	84.97	6.70	3.61	37.07
25	86.34	-93.62	27.27	42.30	3.71	1.22	32.79	84.49	-91.35	41.59	71.16	3.52	1.68	47.58	85.10	-269.65	59.70	84.98	3.39	1.94	32.79
26	86.54	-93.14	44.21	83.16	2.54	0.77	30.09	81.96	-96.69	67.13	78.48	2.08	1.60	76.55	84.21	-93.33	76.66	85.59	2.04	1.66	30.09
27	85.97	-268.01	20.80	47.86	11.01	2.21	20.09	84.98	-95.03	26.64	47.55	10.07	4.84	48.09	85.55	-93.63	46.51	68.93	9.52	5.63	20.09
28	87.82	-110.03	15.42	100.11	11.69	0.61	5.18	85.90	-93.63	24.38	35.92	10.25	6.02	58.70	86.32	-92.85	43.65	57.96	9.69	6.58	5.18
29	89.19	-267.47	13.35	103.85	6.42	0.48	7.55	88.40	-92.99	19.54	32.30	5.69	3.09	54.39	88.56	-92.76	34.18	49.28	5.37	3.49	7.55
30	86.16	-103.93	19.67	79.69	4.40	0.50	11.30	80.39	-99.69	27.04	35.19	3.60	2.62	72.96	81.54	-97.83	49.76	59.60	3.47	2.75	11.30
31	85.66	-93.25	23.69	47.87	7.61	2.29	30.06	85.21	-94.13	29.68	61.24	7.43	2.89	38.82	85.69	-92.41	47.62	77.68	7.05	3.56	30.06
32	87.00	-94.13	21.28	42.39	7.03	2.53	35.97	85.77	-94.14	29.70	51.60	6.75	3.27	48.48	86.27	-92.77	47.62	69.68	6.37	3.77	35.97
33	86.58	-264.22	39.20	80.29	11.93	2.81	23.53	84.79	-266.00	53.00	92.98	11.41	4.23	37.09	85.24	-266.12	65.18	97.37	11.02	5.15	23.53
34	87.60	-263.86	37.26	97.02	11.00	1.57	14.27	87.25	-269.77	45.82	87.21	10.44	3.77	36.14	87.53	-268.98	60.69	94.07	10.06	4.69	14.27
35	87.94	-95.31	27.65	62.94	6.22	1.43	22.98	84.78	-91.33	49.36	76.21	5.58	2.93	52.56	85.43	-269.99	64.89	87.26	5.38	3.29	22.98
36	87.96	-93.92	36.59	80.98	4.34	1.05	24.13	82.46	-96.42	64.21	77.06	3.55	2.62	73.67	84.31	-93.68	75.29	85.58	3.47	2.73	24.13
37	83.78	-96.90	22.53	21.72	10.05	4.68	46.57	81.29	-96.97	28.95	44.72	9.65	5.66	58.58	82.13	-95.19	49.04	65.24	9.18	6.22	46.57
38	-89.45	-264.98	32.46	60.19	12.66	4.57	36.08	-88.62	-268.56	38.56	69.49	12.49	5.52	44.19	-88.65	-268.66	55.71	82.22	11.90	6.42	36.08
39	85.84	-90.83	28.45	50.60	6.32	1.56	24.74	84.59	-91.25	38.13	71.87	6.00	2.41	40.10	85.17	-269.24	56.47	85.88	5.78	2.90	24.74
40	88.16	-101.88	29.46	97.50	6.07	0.68	11.27	84.30	-269.02	48.16	73.73	5.44	2.79	51.34	84.91	-267.50	63.66	84.92	5.23	3.14	11.27
41	87.56	-96.77	18.08	36.04	8.92	1.87	20.98	85.34	-96.57	26.80	51.01	8.33	3.38	40.61	86.01	-94.82	46.32	72.44	7.87	4.13	20.98
42	85.86	-92.24	17.06	21.42	7.38	2.43	32.93	82.76	-98.52	26.64	40.30	6.81	3.96	58.16	83.51	-96.88	41.20	54.95	6.43	4.35	32.93
43	88.46	-96.59	33.01	87.40	3.12	0.65	20.68	82.97	-94.67	63.50	76.94	2.54	1.83	72.23	84.58	-92.40	74.77	85.52	2.48	1.92	20.68
44	89.69	-96.77	59.84	61.34	1.44	1.21	84.13	88.05	-94.92	76.40	81.34	1.41	1.24	87.71	89.62	-92.75	82.44	86.21	1.39	1.26	84.13

Tab. 8.4 Wave directional analysis, layout 1 , at the gap, with EMEP, EMLM and IMLM methods.

	EMEP, Nfft=256, Dir=180. WAVEMAKER							IMLM, Nfft=256, Dir=180, It=10. WAVEMAKER							EMLM, Nfft=256, Dir=180. WAVEMAKER						
Test	thetai	thetar	si	sr	Hi	Hr	Kr	thetai	thetar	si	sr	Hi	Hr	Kr	thetai	thetar	si	sr	Hi	Hr	Kr
1	86.92	-269.31	61.87	95.48	8.42	3.48	41.32	89.87	-265.80	60.83	96.44	8.56	2.58	30.19	89.87	-267.96	67.41	95.43	8.35	3.21	38.44
2	84.94	-269.94	55.74	94.13	7.07	2.27	32.16	87.15	-267.17	55.60	97.91	7.05	2.21	31.30	87.30	-268.58	62.49	95.27	6.85	2.65	38.69
3	84.13	-91.18	49.95	96.84	4.51	0.99	21.93	89.41	-269.28	54.60	95.95	4.43	1.15	25.89	89.26	-269.67	60.92	92.91	4.30	1.54	35.75
4	86.56	-262.82	55.74	100.10	2.73	0.78	28.43	-88.41	-267.90	52.05	97.87	2.62	1.10	42.06	-88.82	-269.29	59.55	93.81	2.50	1.33	53.08
5	87.09	-269.48	56.63	103.03	12.24	4.10	33.47	84.54	-93.07	64.46	103.76	12.36	3.90	31.56	85.13	-91.90	70.55	98.30	12.01	4.85	40.36
6	89.42	-91.25	89.62	99.69	8.82	6.88	77.99	-88.76	-90.62	51.43	94.90	10.92	3.03	27.73	-88.58	-91.40	58.98	93.78	10.58	3.87	36.55
7	86.85	-265.72	66.25	106.24	5.51	1.62	29.46	85.11	-90.84	53.58	101.49	5.62	1.19	21.12	85.63	-90.40	59.53	94.73	5.45	1.79	32.89
8	58.56	-255.00	90.67	102.97	3.66	2.87	78.44	-86.18	-266.54	56.40	92.17	3.97	2.42	60.99	-87.12	-267.70	63.99	91.30	3.81	2.67	70.06
9	88.11	-97.82	57.42	87.82	7.92	3.91	49.35	85.08	-267.07	61.11	66.94	7.35	4.53	61.62	85.44	-267.55	70.30	78.18	7.18	4.82	67.12
10	-89.64	-90.99	54.65	96.41	7.40	2.43	32.83	84.18	-268.96	56.37	73.53	6.78	3.52	51.87	84.48	-269.02	65.31	81.38	6.54	3.94	60.14
11	79.09	-96.87	55.29	82.60	7.07	3.51	49.64	84.78	-266.51	55.35	98.41	7.43	2.22	29.84	85.13	-268.02	63.00	96.15	7.23	2.78	38.42
12	82.46	-100.60	62.59	97.10	5.85	3.02	51.61	84.55	-269.31	49.55	101.16	6.29	1.90	30.16	84.59	-268.78	56.68	96.34	6.10	2.31	37.93
13	85.83	-91.03	88.70	97.55	2.43	2.12	87.28	85.00	-269.47	47.87	99.31	3.11	0.84	27.19	85.25	-269.44	55.41	93.89	3.00	1.15	38.30
14	81.29	-105.86	59.88	102.59	1.68	0.77	46.15	85.63	-259.87	50.43	103.19	1.66	0.77	46.14	86.23	-265.32	59.56	98.26	1.58	0.92	57.96
15	79.01	-254.27	58.34	100.52	8.63	2.75	31.88	76.88	-104.19	59.96	107.46	8.55	3.23	37.73	78.61	-99.62	67.13	101.59	8.29	3.71	44.80
16	76.76	-254.12	97.20	97.73	6.27	6.07	96.77	83.27	-94.51	54.80	93.49	8.34	3.02	36.22	84.04	-92.03	61.81	91.09	7.98	3.71	46.53
17	83.53	-90.98	83.97	97.69	9.06	8.02	88.58	80.28	-254.93	54.83	100.48	11.54	3.13	27.11	80.47	-258.51	62.77	97.47	11.28	4.03	35.76
18	87.30	-90.94	93.05	97.56	7.36	7.37	100.05	82.78	-259.51	51.28	99.68	10.07	2.54	25.27	82.81	-262.24	59.29	96.88	9.84	3.27	33.20
19	80.24	-269.64	64.47	98.31	11.53	6.84	59.33	80.69	-91.58	49.69	105.24	12.80	3.27	25.52	81.51	-91.01	58.50	101.45	12.55	4.06	32.34
20	79.66	-91.13	48.65	97.31	5.38	2.40	44.71	82.28	-264.72	51.64	106.29	5.59	1.14	20.40	82.55	-266.68	58.91	98.98	5.47	1.62	29.65
21	85.37	-90.53	87.38	98.19	12.73	11.44	89.87	85.13	-90.25	52.90	101.14	16.63	4.06	24.40	85.75	-90.73	60.17	99.12	16.30	4.97	30.51
22	83.96	-91.08	77.72	97.62	3.37	2.51	74.28	82.77	-264.54	49.11	104.30	4.03	1.08	26.75	82.85	-266.71	56.22	96.75	3.91	1.45	37.01
23	80.49	-90.21	76.99	97.43	7.11	5.56	78.27	83.69	-267.84	55.99	97.70	8.30	2.42	29.14	84.33	-269.14	63.49	96.12	8.10	3.04	37.50
24	79.71	-97.31	66.28	100.42	6.52	3.79	58.22	82.22	-266.55	51.99	100.89	7.27	2.04	28.01	82.63	-267.33	59.05	96.87	7.08	2.48	35.05
25	88.97	-90.68	96.60	97.75	2.73	2.73	99.89	84.04	-269.36	49.96	102.59	3.77	0.89	23.71	84.20	-269.05	57.19	96.38	3.66	1.22	33.41
26	83.22	-96.61	74.37	98.55	2.07	1.49	71.85	83.85	-264.10	47.63	102.62	2.36	0.97	41.06	84.17	-267.42	56.33	96.56	2.26	1.19	52.66
27	84.84	-90.72	91.79	98.62	9.07	7.59	83.65	81.18	-268.80	58.86	104.86	11.37	3.27	28.74	82.43	-90.25	65.88	99.31	11.10	4.07	36.64
28	-84.34	-98.87	92.27	99.41	7.43	6.03	81.19	84.06	-98.28	52.91	89.07	9.07	3.31	36.45	84.95	-96.71	61.67	90.26	8.72	4.04	46.35
29	86.63	-268.09	95.42	100.47	4.21	3.66	86.84	89.81	-264.45	56.50	88.56	5.42	1.32	24.34	-89.24	-267.72	62.31	90.08	5.25	1.88	35.90
30	88.74	-269.73	98.99	97.35	3.10	3.10	99.98	84.19	-98.98	57.23	95.85	3.67	2.41	65.66	85.74	-96.64	65.38	94.01	3.54	2.59	73.13
31	80.61	-91.74	75.84	96.89	7.12	5.48	76.96	78.96	-266.86	42.80	79.52	8.22	3.07	37.43	79.90	-267.82	55.32	86.67	7.89	3.77	47.78
32	89.99	-90.78	98.64	97.18	5.01	4.99	99.59	79.78	-264.15	41.51	90.22	6.81	2.16	31.71	80.57	-263.10	53.37	91.41	6.54	2.75	41.98
33	83.18	-90.76	82.95	97.61	8.83	7.86	89.02	82.09	-254.69	56.56	99.36	11.19	3.14	28.07	82.11	-258.46	64.13	97.07	10.94	4.02	36.72
34	87.16	-90.84	92.31	97.60	7.66	7.55	98.52	79.79	-256.74	50.57	99.22	10.39	2.72	26.19	79.76	-259.97	58.28	96.78	10.16	3.36	33.09
35	88.00	-90.94	94.54	97.58	4.13	4.11	99.52	81.13	-261.32	51.58	102.24	5.68	1.17	20.61	81.08	-263.17	58.67	97.32	5.56	1.65	29.72
36	85.01	-92.97	81.58	98.81	3.42	2.64	77.29	82.03	-266.44	48.62	104.51	4.18	1.11	26.45	82.29	-267.95	55.89	96.89	4.05	1.49	36.74
37	87.50	-267.63	98.64	98.19	8.02	7.87	98.06	81.65	-91.71	61.52	80.02	9.29	6.30	67.84	83.68	-92.10	68.22	82.66	8.95	6.77	75.65
38	85.38	-91.40	87.40	98.52	12.51	11.25	89.87	81.33	-92.33	54.36	104.22	16.23	4.41	27.16	82.03	-90.52	61.92	100.70	15.86	5.30	33.43
39	79.21	-91.13	57.24	86.98	6.96	3.08	44.32	83.53	-266.50	54.75	98.99	7.19	2.12	29.52	84.00	-268.21	62.43	96.45	7.01	2.65	37.82
40	80.40	-97.59	71.14	98.76	4.93	3.25	66.01	83.69	-91.48	49.38	99.28	5.71	1.75	30.68	84.20	-91.14	56.77	94.88	5.53	2.15	38.80
41	76.15	-91.07	85.18	100.88	7.19	4.81	66.87	74.04	-94.96	59.61	100.51	8.26	3.41	41.32	76.35	-94.74	66.69	98.11	8.04	3.76	46.79
42	78.85	-259.03	73.93	71.41	6.25	6.21	99.31	88.36	-94.58	57.22	88.33	8.55	2.62	30.71	89.55	-94.63	63.22	88.84	8.20	3.40	41.48
43	86.28	-90.84	88.58	97.54	2.36	2.08	88.14	82.40	-269.94	46.31	97.93	3.04	0.83	27.26	82.80	-269.13	53.90	92.78	2.93	1.12	38.01
44	81.76	-265.04	67.10	96.36	1.63	0.98	60.38	84.19	-90.40	49.36	103.15	1.72	0.79	45.87	84.79	-91.03	58.76	97.76	1.64	0.95	57.73

Tab. 8.5 Wave directional analysis, layout 1 , in front of the wave maker, with EMEP, EMLM and IMLM methods.

	EMEP		Nfft=256, Dir=180 GAP					IMLM		Nfft=256, Dir=180, It=10 - GAP					EMLM		Nfft=256, Dir=180 - GAP				
Test	thetai	thetar	si	sr	Hi	Hr	Kr	thetai	thetar	si	sr	Hi	Hr	Kr	thetai	thetar	si	sr	Hi	Hr	Kr
45	82.11	-262.53	44.05	105.00	7.03	1.13	16.07	82.21	-96.11	72.08	94.42	6.23	3.51	56.34	83.69	-93.10	78.79	96.83	6.04	3.08	51.04
46	84.19	-107.98	40.29	84.19	6.69	0.95	14.20	78.02	-98.62	66.30	87.57	5.79	3.44	59.41	80.29	-94.54	75.58	92.67	5.60	3.74	66.79
47	87.51	-90.43	36.09	107.60	3.97	0.05	1.36	84.18	-95.69	66.82	88.47	3.41	2.04	59.82	85.37	-93.50	75.85	93.05	3.31	2.22	67.07
48	-88.77	-269.09	51.65	105.71	2.59	0.05	2.01	-86.83	-264.53	77.37	89.56	2.10	1.55	73.81	-87.90	-266.74	82.62	91.96	2.05	1.62	79.02
49	-88.79	-267.49	37.73	102.60	7.80	1.78	22.82	-87.63	-91.02	55.44	74.64	6.72	4.27	63.54	-87.87	-91.12	68.70	84.21	6.51	4.59	70.51
50	85.42	-269.96	21.70	102.88	10.42	0.65	6.24	82.74	-97.58	25.76	34.69	8.78	5.91	67.31	83.18	-97.07	42.94	53.69	8.35	6.26	74.97
51	85.43	-98.68	44.88	104.53	5.85	0.70	11.97	77.94	-105.11	44.81	49.66	4.43	3.80	85.78	80.59	-101.99	65.01	69.53	4.37	3.88	88.79
52	-89.58	-269.59	50.97	97.92	4.45	2.15	48.31	88.05	-91.50	28.75	35.15	3.93	3.02	76.84	88.20	-91.33	49.99	57.86	3.80	3.13	82.37
53	82.92	-103.76	43.18	105.96	6.38	1.17	18.34	82.13	-98.19	66.33	88.75	5.66	3.24	57.24	83.74	-94.77	75.10	93.31	5.48	3.52	64.23
54	84.16	-93.77	37.71	102.92	6.42	0.98	15.26	80.47	-102.00	60.35	81.72	5.58	3.28	58.78	82.51	-97.65	71.81	-97.65	5.40	3.57	66.11
55	83.92	-261.42	42.03	92.68	5.87	1.27	21.64	81.50	-95.99	72.29	89.81	5.09	3.19	62.67	83.28	-93.24	79.22	93.25	4.94	3.41	69.03
56	83.16	-94.86	36.98	104.64	5.75	0.07	1.25	79.48	-98.71	64.19	84.60	4.93	3.04	61.66	81.52	-94.98	74.29	90.44	4.77	3.28	68.76
57	87.46	-93.17	32.96	106.05	3.23	0.04	1.30	86.91	-268.34	67.58	86.58	2.72	1.74	63.97	87.18	-268.64	76.38	91.37	2.64	1.86	70.45
58	-89.35	-95.24	51.52	107.72	1.75	0.35	20.00	-88.04	-268.54	82.14	93.47	1.41	1.06	75.18	-88.65	-269.45	85.20	93.51	1.38	1.11	80.43
59	89.62	-100.65	36.57	105.89	7.23	0.89	12.31	83.98	-99.38	52.34	61.94	5.76	4.47	77.60	85.53	-97.23	67.81	75.74	5.64	4.63	82.09
60	85.09	-245.26	23.39	100.29	9.51	0.52	5.47	76.76	-103.41	24.28	35.02	8.16	5.11	62.62	77.46	-102.16	37.63	48.99	7.75	5.54	71.48
61	78.82	-267.18	45.63	105.24	9.50	1.34	14.11	78.35	-93.93	68.01	95.32	8.60	4.53	52.67	80.22	-91.05	76.11	97.45	8.31	5.00	60.17
62	80.05	-263.25	43.81	103.51	8.90	1.51	16.97	77.23	-92.09	68.28	93.02	7.95	4.40	55.35	79.19	-269.67	79.57	95.84	7.69	4.84	62.94
63	83.37	-269.23	69.78	99.10	7.66	4.98	65.01	76.72	-92.95	64.99	86.15	7.22	4.78	66.20	78.61	-90.67	74.45	90.93	7.01	5.05	72.04
64	81.37	-262.86	43.86	105.51	11.13	2.18	19.59	75.41	-99.29	49.31	64.96	9.22	6.29	68.22	77.56	-95.88	65.83	78.86	8.94	6.70	74.94
65	84.22	34.90	-250.98	104.37	5.46	0.64	11.72	79.24	-103.74	64.86	91.04	4.88	2.51	51.43	81.52	-97.85	74.41	95.99	4.71	2.81	59.66
66	88.46	44.20	-98.50	105.70	3.92	0.81	20.66	86.31	-96.64	72.20	88.00	3.25	2.23	68.62	87.34	-94.65	79.48	91.76	3.16	2.36	74.68
67	84.23	-92.48	41.15	102.96	7.01	1.19	16.98	81.61	-97.44	67.94	89.31	6.18	3.60	58.25	83.27	-94.25	76.31	93.65	5.99	3.90	65.11
68	85.07	-261.63	35.95	104.38	6.65	0.85	12.78	81.55	-99.59	65.36	86.81	5.78	3.39	58.65	83.36	-95.86	74.89	92.22	5.59	3.69	66.01
69	89.48	-92.33	30.24	104.32	3.89	0.49	12.60	87.69	-94.63	62.53	84.93	3.36	1.99	59.23	88.28	-93.34	73.14	91.04	3.25	2.16	66.46
70	-89.13	-92.99	43.52	104.28	2.48	0.50	20.16	-89.95	-92.11	71.31	86.41	2.04	1.44	70.59	-89.86	-91.86	78.47	90.06	1.99	1.51	75.88
71	87.72	-104.41	29.37	94.53	9.18	1.59	17.32	87.31	-92.97	42.69	59.67	7.87	5.04	64.04	87.64	-91.94	60.80	75.20	7.61	5.41	71.09
72	75.48	-110.91	36.63	108.36	8.65	0.66	7.63	73.63	-107.23	34.81	42.25	6.81	5.34	78.41	76.29	-103.54	58.82	66.56	6.65	5.54	83.31
73	-89.92	-91.01	97.93	97.81	4.13	4.16	100.73	-87.14	-267.51	23.78	37.07	5.13	2.95	57.50	-87.27	-267.91	40.33	55.73	4.85	3.26	67.22
74	-89.86	-91.20	95.09	97.85	3.31	3.15	95.17	88.58	-91.70	30.66	38.19	3.66	2.76	75.41	88.78	-91.59	51.65	60.42	3.54	2.87	81.07
75	88.50	-268.50	32.71	103.46	7.36	1.18	16.03	86.85	-100.11	56.20	78.47	6.49	3.78	58.24	87.93	-97.31	68.93	87.39	6.28	4.10	65.29
76	85.94	-98.91	30.30	104.03	7.01	0.87	12.41	81.13	-102.52	53.04	76.14	6.15	3.48	56.59	83.02	-98.40	67.34	86.67	5.94	3.83	64.48
77	81.91	-262.11	42.96	104.20	9.42	1.62	17.20	81.00	-95.86	69.32	93.78	8.42	4.62	54.87	82.67	-92.92	77.13	96.71	8.15	5.06	62.09
78	80.94	-265.99	40.04	104.27	9.53	1.42	14.90	78.18	-97.11	66.88	89.69	8.26	4.91	59.44	80.28	-93.45	76.21	94.07	8.00	5.32	66.50
79	88.06	-269.14	27.49	105.57	5.94	0.70	11.78	85.21	-97.36	56.43	82.13	5.20	2.89	55.58	86.21	-94.83	69.34	90.28	5.03	3.19	63.42
80	89.14	-99.40	38.30	105.57	4.30	0.74	17.21	87.51	-92.74	67.12	85.31	3.61	2.37	65.65	88.05	-91.97	76.07	90.31	3.50	2.52	72.00
81	80.56	-268.56	37.97	87.37	13.78	2.47	17.92	76.65	-101.89	45.17	56.92	11.26	8.34	74.07	78.86	-98.74	63.91	74.26	10.97	8.73	79.58
82	82.82	-98.49	33.51	106.64	15.07	1.39	9.22	76.15	-102.35	35.99	-102.34	12.32	8.79	71.35	77.93	-99.65	57.47	68.46	11.92	9.27	77.77
83	89.17	-98.70	35.60	102.89	5.91	0.87	14.72	87.95	-93.61	69.87	89.11	5.15	3.12	60.58	88.48	-92.60	77.41	92.94	5.00	3.35	67.00
84	88.34	-104.44	32.27	105.71	5.89	0.85	14.43	83.94	-95.19	67.34	83.44	4.92	3.31	67.28	85.20	-93.31	76.44	89.15	4.78	3.51	73.43
85	89.39	-90.53	25.99	60.06	7.93	2.82	35.56	86.33	-94.05	45.98	53.77	6.39	5.18	81.06	87.08	-93.25	64.29	70.81	6.27	5.34	85.17
86	-89.32	-91.14	85.59	97.81	6.04	6.02	99.67	-87.29	-268.24	30.67	38.86	6.89	4.99	72.42	-87.51	-268.79	49.27	58.30	6.60	5.20	78.79
87	-89.17	-98.04	34.38	102.67	3.10	0.44	14.19	-87.35	-269.23	73.61	92.72	2.63	1.64	62.36	-87.90	-90.25	80.04	94.97	2.55	1.77	69.41
88	-88.15	-94.77	48.61	103.92	1.85	0.42	22.70	-85.62	-268.44	80.56	92.89	1.51	1.11	73.51	-86.68	-269.73	84.21	93.36	1.47	1.16	78.91

Tab. 8.6 Wave directional analysis, layout 2 , at the gap, with EMEP, EMLM and IMLM methods.

Wave transmission

Wave transmission was derived by the ratio of incident wave heights in front and behind the structure obtained by the reflection analysis that has been reported in the previous section.
Figure 8.15 shows experimental transmission coefficients K_t decreasing with increasing F/H_{si} ratio. K_t values for LCS (F/H_{si} around zero) are compared to prediction by van der Meer formula (1990): values are generally in good agreement for narrow berm, whereas are overestimated about 20% for wide berm. The highest scatter is clearly around $F \approx 0$, for which the parameter F/H_{si} seems not suitable to estimate K_t because in such case the influence of H_{si} is lost. Following the results of Ruol & Faedo (2002), a similar analysis was repeated adopting the parameter $(F\text{-}R)/H_{si}$ proposed by Davies & Kriebel (1992), where R is the potential wave run-up, withour obtaining significant improvement.
Berm crest width has a relevant effect on transmission; van der Meer formula (1992) accounts for the relative crest width B/D_{n50} and other variables

$$K_t = \left(0.031\frac{H_{si}}{D_{n50}} - 0.24\right)\frac{F}{D_{n50}} - 5.42 s_m + 0.032\frac{H_{si}}{D_{n50}} - 0.0017\left(\frac{B}{D_{n50}}\right)^{1.84} + 0.51 \qquad 1$$

where *sop* is fictitious incident wave steepness given by

$$sop = \frac{2\pi H_{si}}{g T_p^2}$$

Van der Meer formula (1992) provides good results, as it is proven by the comparison presented in Fig. 8.16 among experimental coefficients K_{te} and computed values K_{tc}.
Typical discrepancies among experimental and van der Meer (1992) results are within ± 0.2; this might be related to wave diffraction from the gap mouth. This interpretation is actually not supported by the fact that deviation is roughly proportional to K_t rather than constant and by the fact that transmission obtained by Zelt & Skjelbreia method tend to cancel oblique waves coming from the gap that do not satisfy the expected phase lag.
The analysis of changes in wave spectra due to transmission over the structure has been performed following Van der Meer et al. (2000); results for irregular tests are reported in Tab.s 8.7 and 8.8 for layout 1 and 2 respectively.
After transmission, peak period remains more or less constant: the transmitted frequency peak fpt is in average 0.95 the incident one (standard deviation 0.04).
Fig.s 8.17, 8.18 and 8.19 show the peak frequency ratio fpt/fpi as a function of transmission coefficient Kt, incident wave peak frequency fpi and wave steepness sop respectively; the ratio appears almost constant varying all these parameters.
Following Van der Meer et al. (2000), the transmitted spectrum drops to zero at a frequency close to 4 (instead of 3.5) fpi and about the 30% (instead of 40%) of the total transmitted energy is present at the higher frequencies of the spectrum between 1.5 and 3.5 fpi. From Tab. 8.7 and 8.8, the transmitted energy shifted at higher frequencies is in average around the 30% of the total transmitted energy, with high scatters from the mean value.
Fig. 8.20 presents the transmitted energy between 1.5 and 3.5 fpi versus the transmission coefficient Kt. The percentage of shifted energy increases with increasing transmission till Kt reaches values close to 0.4, then it tends to assume an almost constant value around the 40% (in agreement with Van der Meer et al., 2000) and finally decreases for Kt higher than 0.6.

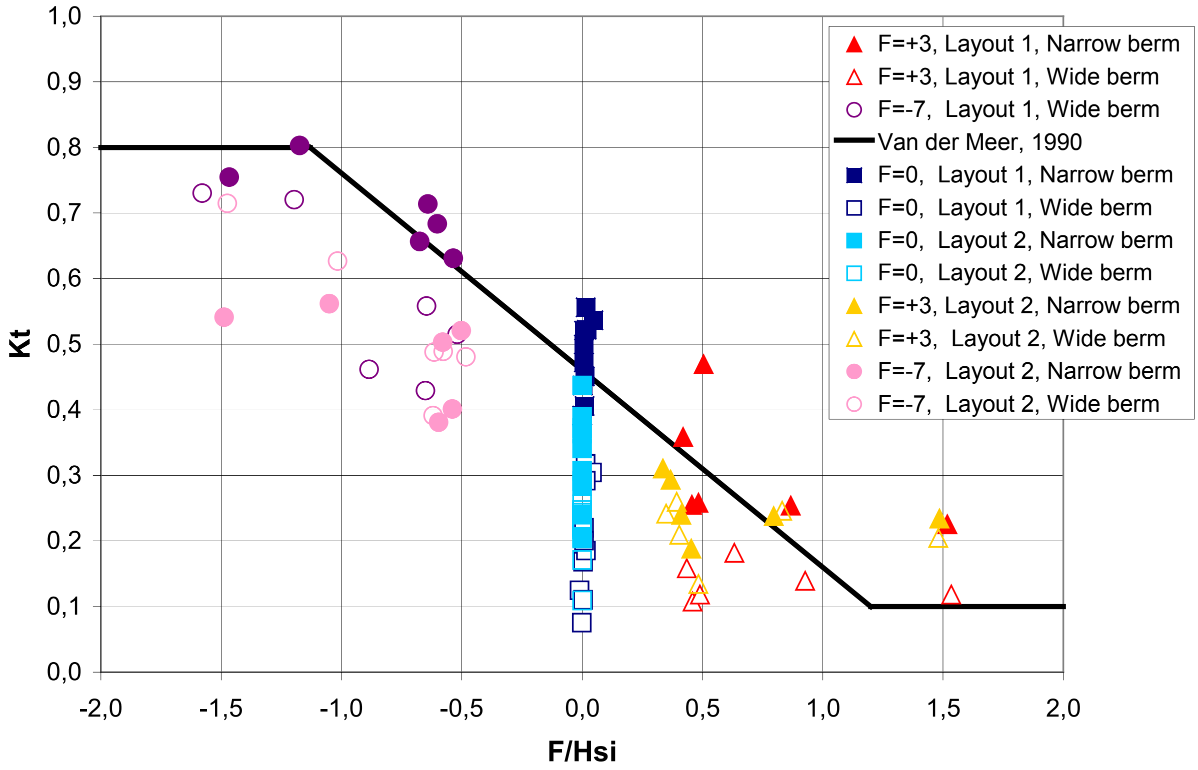

Fig. 8.15 Wave transmission coefficient Kt versus the freeboard F to incident wave height Hsi ratio. Up, narrow berm tests; down, wide berm tests.

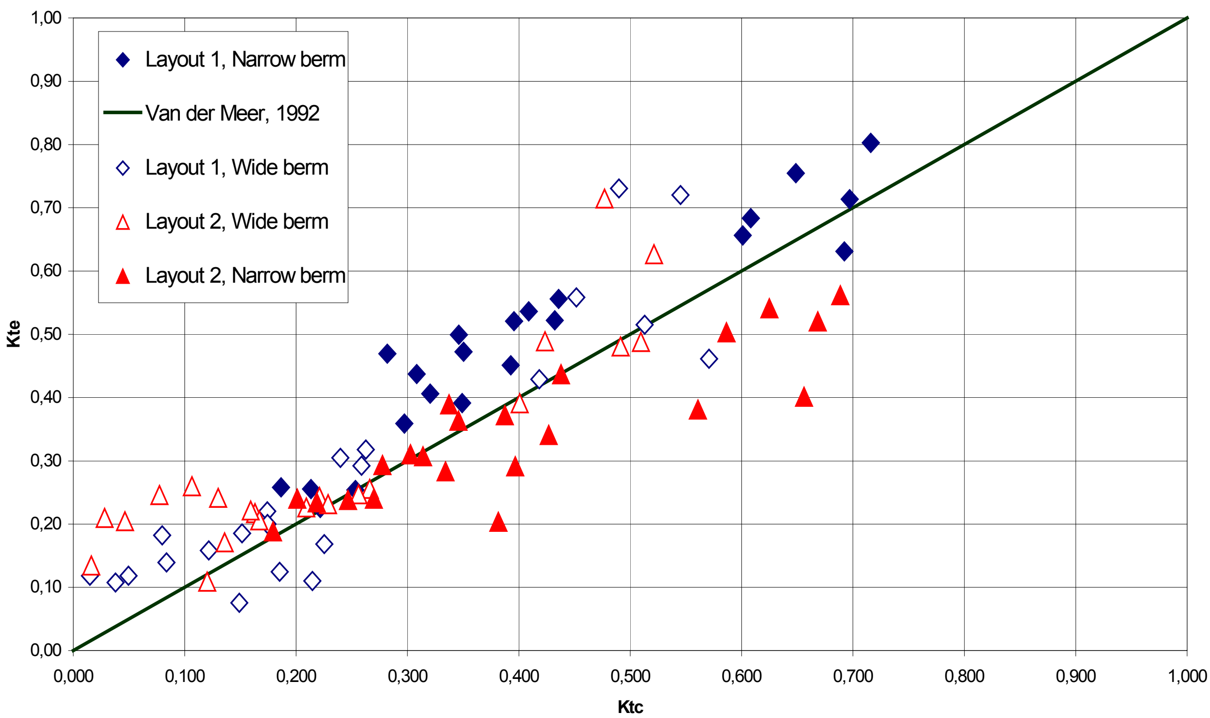

Fig. 8.16 Experimental wave transmission coefficient Kte versus wave transmission coefficient Ktc computed using (1).

Test	2/3 D	F	Hs	Hsi	fp	sop	Kt	fpi	Ei 1,5fpi	Ei3,5fpi	Eifimax	Ei total	fpt	Et 1,5fpi	Et 3,5fpi	Et fimax	Et ftmax	Et total	ft max	fpt/fpi	ftmax/fpi
1	J3D	0	9,00	8,78	0,59	0,02	0,56	0,62	948,50	1230,70	1244,70	1250,80	0,58	205,90	355,37	364,26	368,72	368,72	3,83	0,95	6,21
2	J3D	0	9,00	7,74	0,83	0,03	0,47	0,85	847,84	968,08	972,48	972,61	0,81	161,02	215,07	217,74	217,89	217,89	3,83	0,95	4,49
3	J3D	0	4,00	4,45	0,88	0,02	0,45	0,86	308,31	331,97	332,17	332,32	0,83	475,82	61,79	62,30	62,58	62,58	3,83	0,97	4,46
4	J3D	0	4,00	2,86	1,25	0,03	0,39	1,18	125,42	132,19	132,11	132,19	1,15	16,62	20,44	20,31	20,44	20,44	3,83	0,97	3,25
9	J2D	0	9,00	9,16	0,59	0,02	0,52	0,63	1009,20	1304,70	1318,50	1325,30	0,61	216,38	360,03	367,01	372,01	372,03	3,75	0,96	5,92
10	J2D	0	9,00	8,00	0,83	0,04	0,50	0,85	864,25	993,84	998,57	998,73	0,80	166,62	256,35	259,60	259,77	259,78	3,83	0,93	4,49
11	J3D	3	7,65	7,61	0,64	0,02	0,36	0,62	657,54	887,86	907,64	907,85	0,60	61,75	111,70	123,50	123,55	123,50	3,83	0,97	6,20
12	J3D	3	7,65	6,61	0,90	0,03	0,26	0,89	600,80	697,81	699,75	699,81	0,82	33,86	47,20	47,48	47,49	47,49	3,83	0,92	4,29
13	J3D	3	3,40	3,47	0,96	0,02	0,25	0,96	177,11	187,57	187,56	187,61	0,89	12,63	13,64	13,64	13,65	13,65	3,52	0,93	3,68
14	J3D	3	3,40	1,97	1,35	0,02	0,23	1,23	60,92	63,27	63,25	63,27	1,17	2,97	3,08	3,08	3,07	3,08	3,83	0,95	3,12
17	J3D	-7	12,15	12,74	0,51	0,02	0,63	0,53	2110,00	2684,30	2695,00	2720,60	0,54	632,10	1005,20	1019,40	1035,50	1035,50	3,75	1,02	7,14
18	J3D	-7	12,15	11,41	0,72	0,04	0,68	0,72	1944,30	2226,30	2210,70	2232,60	0,71	762,38	973,70	964,40	981,11	981,29	3,59	0,98	4,99
21	J3D	-7	5,40	5,96	0,76	0,02	0,80	0,76	510,23	542,74	542,68	543,40	0,73	282,21	347,63	347,36	349,97	350,13	3,36	0,97	4,45
22	J3D	-7	5,40	4,78	1,07	0,04	0,75	1,01	320,84	334,48	334,40	334,59	1,03	177,24	221,91	221,83	221,96	221,99	3,67	1,02	3,63
23	J3D	0	9,00	8,78	0,59	0,02	0,32	0,63	890,80	1142,70	1156,60	1162,80	0,57	67,85	115,41	122,78	125,66	125,66	3,83	0,91	6,07
24	J3D	0	9,00	7,89	0,83	0,04	0,22	0,81	923,30	1076,70	1076,60	1081,70	0,78	30,44	47,27	47,04	50,15	50,15	3,91	0,96	4,79
25	J3D	0	4,00	4,23	0,88	0,02	0,17	0,90	271,57	286,89	286,49	287,04	0,79	6,93	8,17	7,99	8,24	8,24	3,83	0,88	4,27
26	J3D	0	4,00	2,69	1,25	0,03	0,12	1,18	102,85	106,83	106,81	106,83	1,08	1,76	1,87	1,87	1,87	1,87	3,75	0,92	3,18
31	J2D	0	9,00	9,45	0,59	0,02	0,29	0,60	982,00	1324,20	1343,20	1351,60	0,59	65,82	112,21	117,58	120,50	120,50	3,83	0,97	6,34
32	J2D	0	9,00	7,89	0,83	0,04	0,20	0,84	796,58	929,79	929,47	934,57	0,70	25,98	38,06	37,86	39,78	39,78	3,91	0,84	4,68
33	J3D	-7	12,15	12,88	0,51	0,02	0,52	0,53	2081,20	2673,60	2684,90	2707,60	0,53	424,58	672,26	685,35	702,56	702,59	3,75	1,01	7,13
34	J3D	-7	12,15	10,61	0,72	0,03	0,56	0,73	1598,90	1822,80	1822,90	1827,10	0,69	386,90	573,96	574,17	581,41	581,43	3,75	0,95	5,17
35	J3D	-7	5,40	5,84	0,76	0,02	0,72	0,77	515,32	544,21	544,17	544,81	0,74	179,16	286,95	286,73	291,29	291,30	3,75	0,96	4,87
36	J3D	-7	5,40	4,43	1,07	0,03	0,73	1,04	294,29	305,92	305,91	305,98	1,02	112,39	165,45	165,43	165,50	165,50	3,83	0,98	3,69
39	J3D	3	7,65	7,52	0,64	0,02	0,16	0,67	659,06	867,13	873,79	880,04	0,61	19,03	22,80	23,19	23,42	23,42	3,67	0,92	5,51
40	J3D	3	7,65	6,67	0,90	0,03	0,11	0,90	656,11	753,11	755,08	755,15	0,80	7,69	8,42	8,43	8,43	8,43	3,36	0,89	3,75
43	J3D	3	3,40	3,25	0,96	0,02	0,14	0,97	153,51	161,01	160,99	161,03	0,87	3,22	3,38	3,38	3,37	3,38	2,66	0,90	2,74
44	J3D	3	3,40	1,95	1,35	0,02	0,12	1,29	61,00	62,79	62,76	62,79	1,16	0,82	0,85	0,85	0,85	0,85	3,83	0,90	2,96

yellow colour marks tests for which 3,5fpi is higher than 4Hz

cyan colour marks tests for which ftmax is significative (not too close to the "cut" frequency = 4 Hz)

Tab. 8.7 Analysis of wave transmitted spectra, irregular tests, layout 1.

Test	2/3 D	F	Hs	Hsi	fp	sop	Kt	fpi	Ei 1,5fpi	Ei3,5fpi	Eifimax	Ei total	fpt	Et 1,5fpi	Et 3,5fpi	Et fimax	Et ftmax	Et total	ft max	fpt/fpi	ftmax/fpi
45	J3D	0	9,00	10,16	0,59	0,02	0,44	0,64	1302,10	1657,90	1673,40	1683,00	0,62	189,68	300,07	307,40	313,15	313,15	3,83	0,97	5,99
46	J3D	0	9,00	8,57	0,83	0,04	0,39	0,84	964,10	1115,50	1122,30	1122,40	0,78	120,98	176,82	180,66	180,76	180,76	3,83	0,93	4,55
47	J3D	0	4,00	4,77	0,88	0,02	0,37	0,89	346,91	371,18	370,79	371,37	0,85	36,22	48,19	47,01	48,97	48,97	3,91	0,95	4,37
48	J3D	0	4,00	2,92	1,25	0,03	0,36	1,21	140,99	146,35	146,30	146,35	1,15	13,83	17,60	17,31	17,60	17,60	3,91	0,95	3,22
53	J2D	0	9,00	10,50	0,59	0,02	0,34	0,62	1324,00	1770,70	1794,80	1810,60	0,60	112,19	187,69	195,03	199,85	199,85	3,83	0,96	6,17
54	J2D	0	9,00	8,63	0,83	0,04	0,28	0,83	1063,90	1262,50	1272,20	1272,20	0,81	64,34	92,07	94,93	95,01	95,01	3,91	0,97	4,69
55	J3D	3	7,65	8,94	0,64	0,02	0,31	0,69	957,00	1238,00	1255,10	1255,10	0,65	64,82	100,94	105,85	105,86	105,86	3,91	0,94	5,65
56	J3D	3	7,65	7,28	0,90	0,04	0,24	0,86	732,06	860,63	866,46	866,51	0,85	33,10	45,40	46,25	46,29	46,29	3,83	0,99	4,44
57	J3D	3	3,40	3,77	0,96	0,02	0,24	0,98	209,43	220,94	220,52	220,97	0,95	11,61	12,50	12,46	12,50	12,51	3,28	0,97	3,36
58	J3D	3	3,40	2,02	1,35	0,02	0,23	1,35	67,83	69,34	69,32	69,34	1,21	3,48	3,55	3,55	3,55	3,55	3,36	0,89	2,49
61	J3D	-7	12,15	13,93	0,51	0,02	0,52	0,55	2196,70	2804,90	2812,40	2845,30	0,54	454,18	738,28	744,66	763,60	763,63	3,75	0,98	6,86
62	J3D	-7	12,15	12,10	0,72	0,04	0,50	0,74	1882,10	2215,20	2215,50	2226,80	0,71	365,04	539,91	540,23	547,97	548,00	3,75	0,96	5,04
65	J3D	-7	5,40	6,66	0,76	0,02	0,56	0,76	630,79	691,13	691,11	692,26	0,76	142,02	218,90	223,74	223,74	223,74	3,83	1,00	5,02
66	J3D	-7	5,40	4,70	1,07	0,03	0,54	1,11	326,95	339,42	339,20	339,42	1,07	67,95	101,01	99,98	101,01	101,01	3,91	0,96	3,52
67	J3D	0	9,00	10,07	0,59	0,02	0,26	0,65	1116,80	1475,00	1490,10	1497,90	0,61	63,34	98,05	102,77	105,17	105,17	3,91	0,94	5,99
68	J3D	0	9,00	8,68	0,83	0,04	0,22	0,88	1036,00	1188,00	1192,30	1192,40	0,77	45,40	59,01	59,61	59,63	59,63	3,83	0,87	4,35
69	J3D	0	4,00	4,52	0,88	0,02	0,24	0,91	294,15	313,04	312,75	313,14	0,85	16,80	18,72	18,59	18,73	18,74	3,28	0,94	3,61
70	J3D	0	4,00	2,77	1,25	0,03	0,21	1,23	122,69	126,31	126,24	126,31	1,16	4,80	5,03	5,02	5,02	5,03	3,28	0,94	2,66
75	J2D	0	9,00	10,60	0,59	0,02	0,25	0,62	1339,50	1753,10	1773,40	1785,00	0,59	76,09	100,84	105,39	108,44	108,44	3,83	0,95	6,14
76	J2D	0	9,00	8,89	0,83	0,04	0,22	0,84	1076,20	1245,10	1252,50	1252,60	0,75	50,62	62,26	62,89	60,91	62,91	3,75	0,89	4,46
77	J3D	-7	12,15	14,50	0,51	0,02	0,48	0,53	2371,20	2989,30	3002,90	3027,40	0,54	367,61	593,96	607,27	625,24	625,24	3,83	1,03	7,25
78	J3D	-7	12,15	12,13	0,72	0,04	0,49	0,76	2142,80	2436,40	2436,00	2445,10	0,70	367,17	541,00	540,60	549,12	549,14	3,75	0,91	4,92
79	J3D	-7	5,40	6,89	0,76	0,03	0,63	0,78	669,34	715,09	715,10	716,11	0,78	202,41	288,89	288,92	293,33	293,34	3,75	0,99	4,81
80	J3D	-7	5,40	4,75	1,07	0,04	0,71	1,13	331,69	344,33	344,29	344,33	1,08	150,35	192,67	192,56	192,67	192,67	3,83	0,95	3,38
83	J3D	3	7,65	8,59	0,64	0,02	0,24	0,67	857,90	1125,80	1147,30	1147,30	0,62	47,94	64,72	66,56	66,54	66,57	3,44	0,92	5,12
84	J3D	3	7,65	7,43	0,90	0,04	0,21	0,93	784,78	900,91	903,43	903,45	0,86	28,71	37,56	37,61	37,60	37,61	3,67	0,92	3,93
87	J3D	3	3,40	3,61	0,96	0,02	0,25	0,98	210,41	222,08	222,04	222,12	0,87	10,22	11,13	11,13	11,13	11,13	3,28	0,89	3,35
88	J3D	3	3,40	2,03	1,35	0,02	0,20	1,29	65,06	66,99	66,97	66,99	1,20	2,67	2,75	2,75	2,75	2,75	3,28	0,93	2,54

yellow colour marks tests for which 3,5fpi is higher than 4Hz

cyan colour marks tests for which ftmax is significative (not too close to the "cut" frequency = 4 Hz)

Tab. 8.8 Analysis of wave transmitted spectra, irregular tests, layout 2.

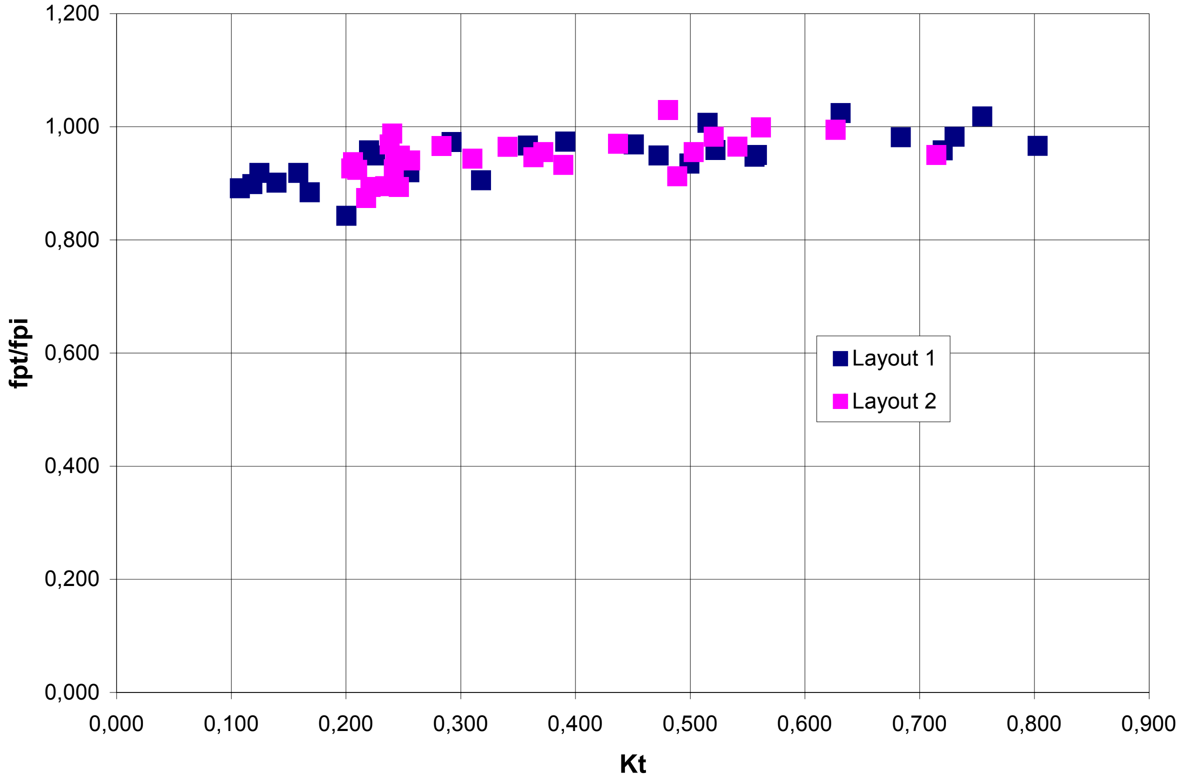

Fig. 8.17 Transmitted fpt over incident fpi peak frequency versus transmission coefficient Kt.

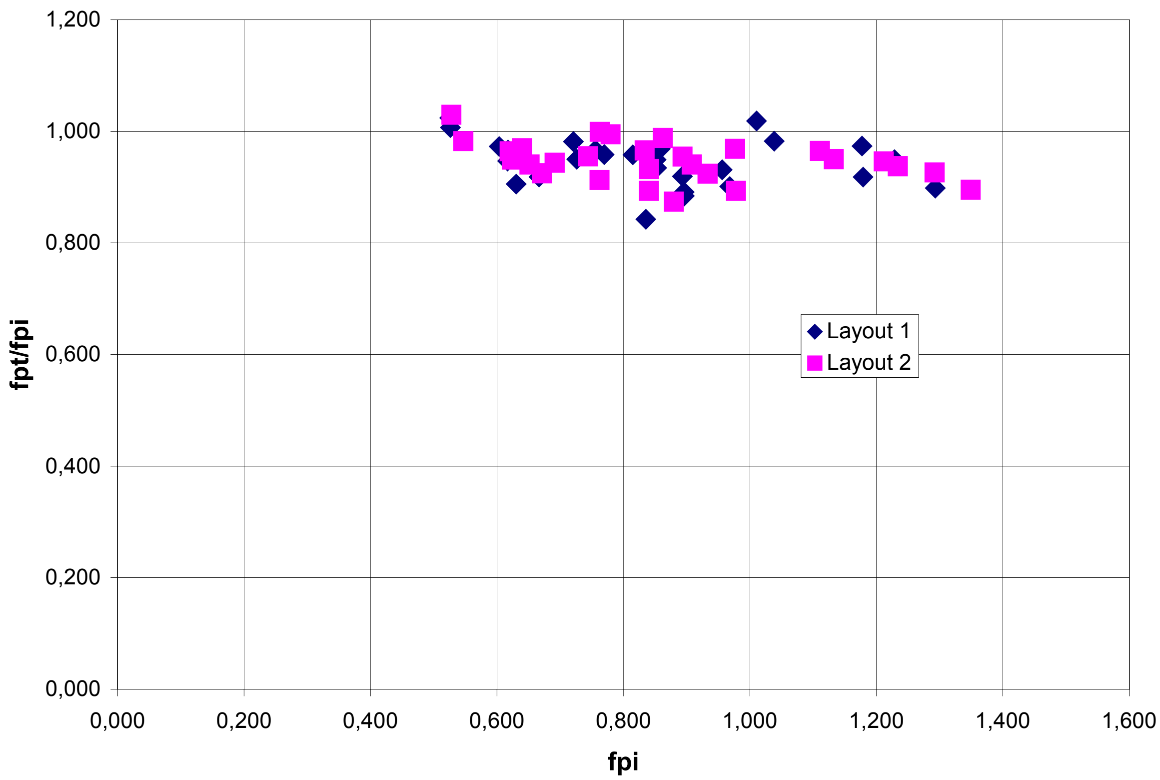

Fig. 8.18 Transmitted fpt over incident fpi peak frequency versus incident peak frequency fpi.

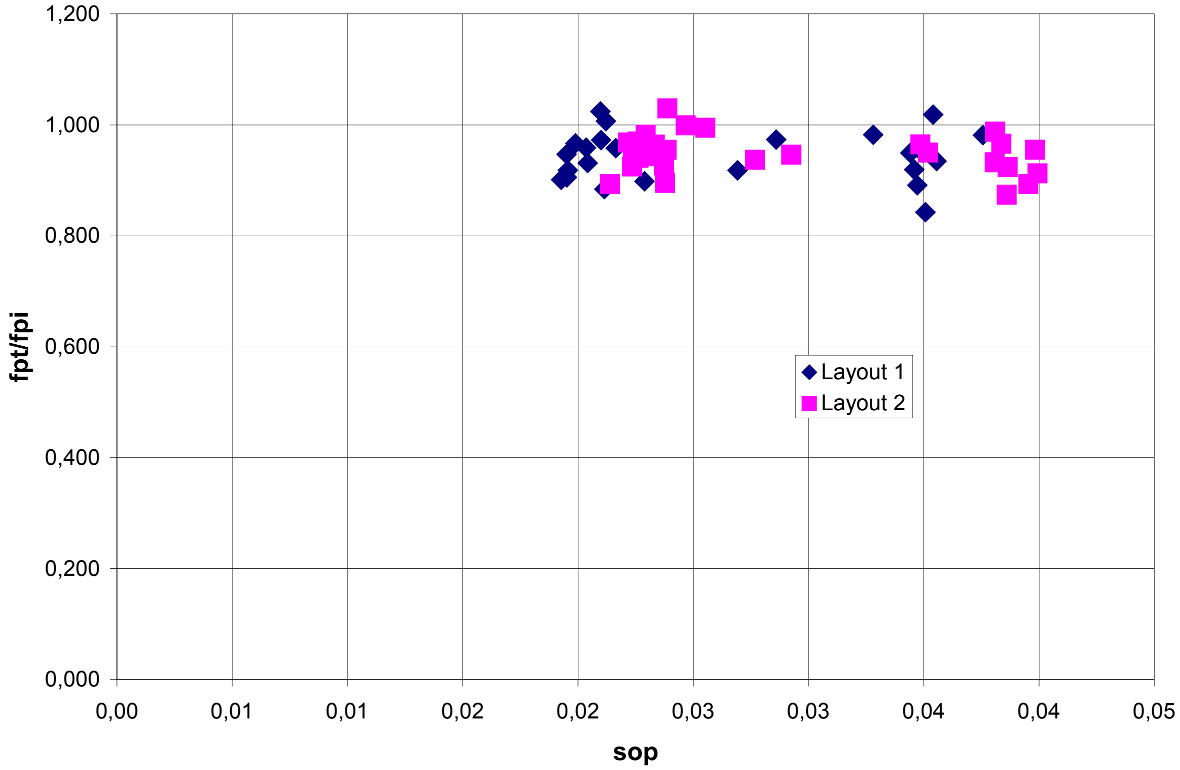

Fig. 8.19 Transmitted fpt over incident fpi peak frequency versus incident wave steepness sop.

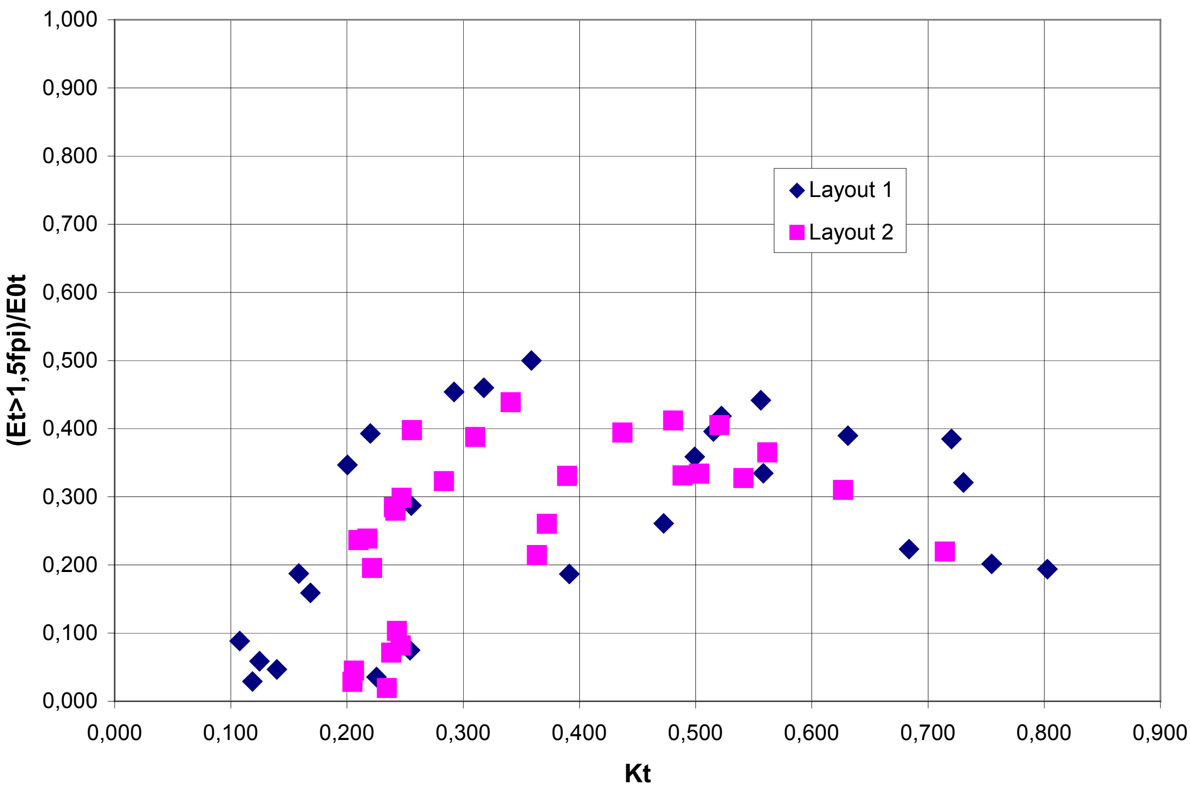

Fig. 8.20 Transmitted fpt over incident fpi peak frequency versus incident peak frequency fpi.

Overtopping and fluxes analysis

This analysis,which has been performed for layout 1only, is aimed to provide an estimation of:

- mean flux overtopping the structure;
- mean filtration flux through the structure;
- mean rip flux through the gap.

These objectives are achieved using data obtained by the following measuring devices:

- 2 wave gauges over the structure (WGs 13, 14);
- 3 wave gauges seaward of the structure (WGs 9, 10, 11);
- 1 wave gauge at the gap centre (WG 12);
- 3 wave gauges leeward of the structure (WGs 19, 20, 21);
- 1 ADV at the gap centre (ADV III).

Fig. 8.21 shows elevation signals measured at WG 13 and 14, when almost all waves produce overtopping (21a for emergent and 21c for submerged structure) and a case when overtopping is rare and weak and most volume percolates in the mound (8.21b).

Fluxes are evaluated in sections perpendicular to the structure (i.e. flux per unit width of the structure); q [$m^3/s/m$] is defined as

$$q = \left\langle \int_{-h}^{\eta} u_x \cdot dz \right\rangle \tag{2}$$

where η is the instantaneous free surface elevation, h is the local water depth, u_x is the shoreward horizontal velocity, z is the vertical co-ordinate and < > is the long term average operator. The quantity evaluated in Eq. 2 must be calculated in different ways, depending whether submerged areas or barrier sections are considered.

When regime conditions are reached, due to mass conservation equation, fluxes must satisfy the relation

$$\left(q_{ovt} - q_{fil}\right) L_{bar} = q_{gap} L_{gap} \tag{3}$$

where L_{bar} and L_{gap} are the barrier and gap lengths (10,1 and 2,4 m respectively), q_{ovt}, q_{fil} and q_{gap} are discharges per unit width overtopping the barrier, returning offshore by filtration and through the gap.

Returning flux through the gap

For the evaluation of q through the gap, u_x, measured at mean water depth, is assumed to be representative of the mean velocity over z. Hence, Eq. 2 gives

$$q_{gap} = \langle u_x \rangle \cdot h + \left\langle \tilde{u}_x\big|_{z=0} \cdot \eta \right\rangle = \langle u_x \rangle \cdot h + \left(\langle \eta_i^2 \rangle - \langle \eta_r^2 \rangle \right) \cdot \left(\frac{\omega}{tanh(kh)} \right) \tag{4}$$

where $\langle \eta_i^2 \rangle$ is incident surface elevation variance, $\langle \eta_r^2 \rangle$ is reflected surface elevation variance and

$$\tilde{u}_x\big|_{z=0} = \frac{\omega \cdot \eta}{tanh(kh)} \tag{5}$$

a)

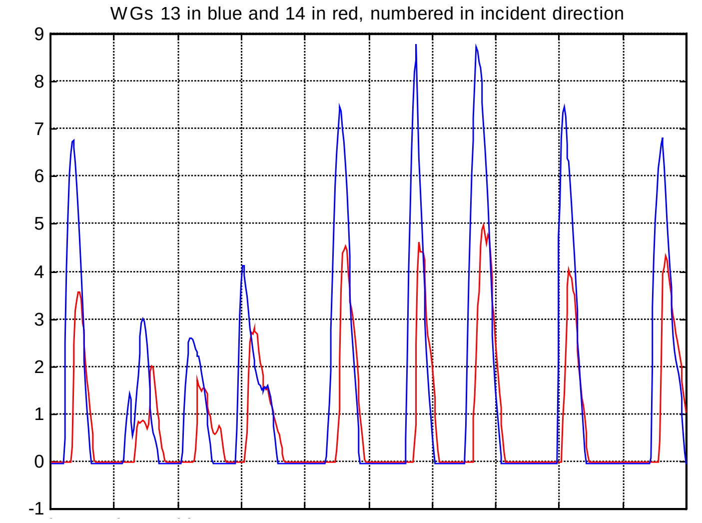

b)

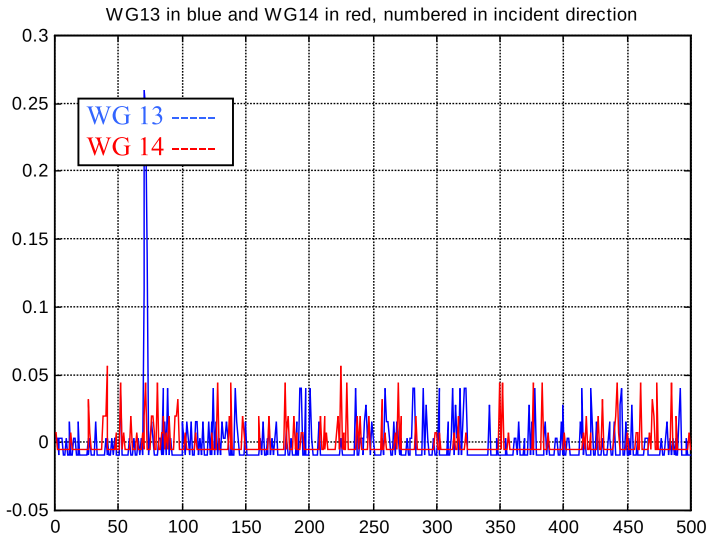

c)

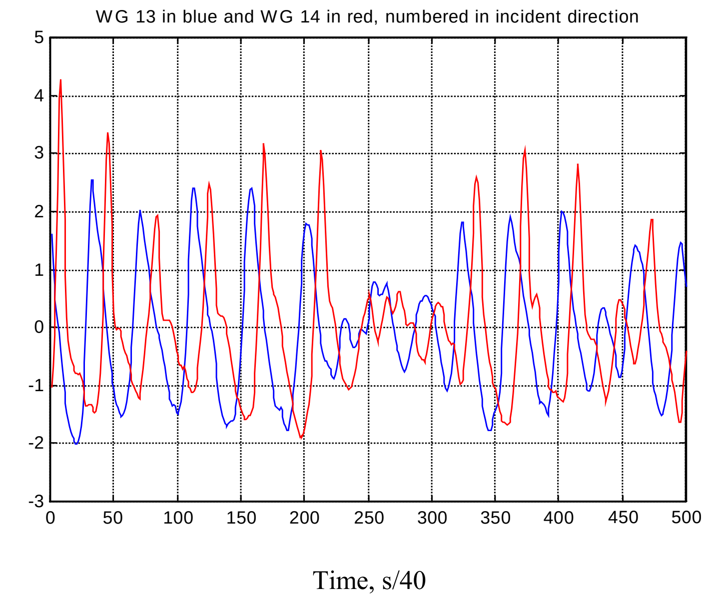

Fig. 8.21 Typical elevations in cm measured at WGs 13, 14: a) emergent or freeboard zero structure with relevant overtopping; b) emergent structure with minor overtopping ; c) submerged structure.

Terms in Eq. 4 are evaluated as follows: $\langle u_x \rangle$ is the mean velocity value measured at ADV III; h is the mean water depth measured at WG 12; $\langle \eta_i^2 \rangle$ and $\langle \eta_r^2 \rangle$ are the mean variances of incident and reflected surface elevation obtained by applying the method by Zelt and Skjelbreia (1992) to WGs 9-11 and 19-21 respectively.

Overtopping flux

The overtopping event is schematised as a simple progressive wave that travels with celerity c and is characterised by a profile η (x-ct).
From mass balance, the following relation is derived

$$\frac{\partial \eta}{\partial t}+\frac{\partial q}{\partial x}=\frac{\partial}{\partial x}\left(q-c\cdot\eta\right)=\frac{\partial}{\partial t}\left(q-c\cdot\eta\right)=0 \qquad 6$$

Assuming $\eta = 0$ at barrier crest level, since flux is zero when the crest is dry ($\eta = 0 \Rightarrow q = 0$), instantaneous q, single wave average $[q]$ and test average q_{ovt} can be obtained

$$q = c\cdot\eta \qquad 7$$

$$[q]=c\cdot[\eta] \qquad 8$$

$$q_{ovt} = \{[q]\} \qquad 9$$

where { } denotes the average over all waves identified in each test.
Celerity is calculated from the delay between forward front passage at WGs 13 and 14. Since a relation among crest celerity and volume is likely to occur (see Fig. 8.22b), Eq. 8 is evaluated wave-by-wave and then average values are computed.
As crest volume decreases along overtopping due to percolation in the rubble mound (Fig. 8.22c), the average value derived from the two WGs is used in Eq. 8.

When the barrier is submerged an offshore back flux, caused by wave set-up behind the barrier, takes place during troughs. The assumption for integrating Eq. 6 thus may change to $\eta = \eta_{trough} \Rightarrow q = -q_{crit}$.
As critical flow is provided by

$$q_{crit} = \eta_{trough}\cdot\sqrt{g\cdot\eta_{trough}/\beta} \qquad 10$$

where β is the momentum coefficient assumed to be 4/3 (constant shear), imposing this initial value at wave trough Eq. 6 gives

$$\langle q\rangle + q_{crit} = c\cdot\left(\langle\eta\rangle - \eta_{trough}\right) \qquad 11$$

and q_{ovt} over the barrier can be estimated by averaging among waves the mean wave overtopping discharge

$$[q]\cong c\cdot\left([\eta]-\eta_{trough}\right)-\left(\eta_{trough}\cdot\sqrt{g\cdot\eta_{trough}/\beta}\right) \qquad 12$$

Filtration flux through the structure

Filtration through the structure was evaluated on the basis of Debski & Loveless (1997) results.
The Forchheimer equation, as described by van Gent (1993), may be used to predict the flow quantity through a rock structure for a given hydraulic gradient or head difference per unit length I

$$I = \frac{Xu}{D_{n50}{}^2} + \frac{Yu|u|}{D_{n50}} \tag{13}$$

where X, Y are constants depending on porosity and u is bulk velocity through the porous medium.

Since in prototype and in our model the linear term at the second member is negligible, the mean hydraulic gradient can be evaluated as

$$\langle I \rangle = \frac{Y}{D_{n50}} \left\langle (u + \tilde{u})^2 \right\rangle \tag{14}$$

The mean hydraulic gradient $\langle I \rangle$ can be expressed as setup S_u over mean submerged berm width b; in our tests assumes maximum values 1/40 and 1/80 for narrow and wide berm respectively. Considering wave conditions that contain a significant number of breaking waves, wave piezometric slope is an order of magnitude higher than mean piezometric slope and Eq. 14 can be rewritten as

$$\frac{S_u}{b} = \frac{Y \langle u \rangle \langle |\tilde{u}| \rangle}{D_{n50}}$$

from which mean velocity $\langle u \rangle$ can be derived

$$\langle u \rangle = Y \frac{S_u}{b} \frac{D_{n50}}{\langle |\tilde{u}| \rangle} \tag{15}$$

As wave piezometric slope is preserved in the model and mean velocity is very small compared to wave velocity, the scale factor λ for wave velocity $\tilde{u}$ is equal to the square root of the scale factor for grain size and the scale rule for mean filtration velocity $\langle u \rangle$ is given by

$$\lambda_{\langle u \rangle} = \frac{\lambda_{S_u}}{\lambda_B} \lambda_{D_{n50}}^{1/2} \tag{16}$$

Using Eq. 16 to re-scale filtration velocity measured by Debski & Loveless (1997), $\langle u \rangle$ is computed as

$$\langle u \rangle = \langle u_L \rangle \frac{S_u}{S_{uL}} \frac{B_L}{B} \left(\frac{D_{n50}}{D_{n50L}} \right)^{0.5} \tag{17}$$

where quantities with subscript L denote data derived from Debski & Loveless'work for the most similar structure. Finally filtration discharge per unit width q_{fil} is obtained by integrating over the structure height h_s

$$q_{fil} = \langle u \rangle h_s \tag{18}$$

In Debski & Loveless (1997), a unique relation u-S_u was obtained for zero-freeboard and submerged structures, whereas for emergent structures at least incident wave height and crest elevation affect filtration velocity and no unique relation u-S_u was proposed. As a consequence, filtration discharge has not been evaluated for emergent structures.

Results

Tables 8.9 and 8.10 present test parameters for the wave attacks, wave setup, transmission coefficients and main results derived from the fluxes analysis described in the previous section, for layout 1 and 2 respectively.

Description of wave attacks includes wave spectrum W_s, freeboard F, incident wave height H_{si}, peak period T_p.

Setup S_u is calculated as the difference bewteen inshore setup (i.e. mean elevation leeward,

WGs 9-11) and offshore setup (i.e mean elevation seaward, WGs 19-21).
Transmission coefficients K_t were computed as the ratio between leeward and seaward incident wave heights. Leeward and seaward H_{si} were evaluated applying the method by Zelt & Skjelbreia (1992) to WGs 19-21 and WGs 9-11 respectively. Reflection of the structure and of the beach varied in the range 20÷30% and reflected waves do not show a dominant effect on processes.
Results of fluxes analysis are discharges per unit width q_{ovt}, q_{gap} and q_{fil}.

Front celerity increases with increasing water depth at crest and overtopping volume (Fig. 8.22a, b), proving the necessity of a wave-by-wave analysis of measured data. The correlation among crest celerity and elevation is similar to that characterising solitary waves ($c = \sqrt{gh_{crest}}$), augmented by 30 cm/s in average for the case shown in Fig. 8.22a.

Relations among overtopped volumes show an almost linear 1:1 behaviour but volume at WG 14 is always smaller than volume at WG 13, proving the water loss for percolation in the rubble mound (Fig. 8.22c).
Because of surf beat and consequent periodic flux at a intermediate time scale, crest celerities and volumes result highly variable for irregular waves and slightly variable as wave height for actual regular waves (Fig. 8.23), proving the reliability of the method.

The hypotheses on which the analysis is based are: progressive wave (i.e. absence of return waves from the beach) and critical condition at trough. The first is always approximately valid, the second is valid only when H_{si} is approximately higher than 1.4 times the submergence, see Tab. 8.7. This condition represents the limit of application of the method we are proposing. In case of deeply submerged structures, the stream arriving at the barrier assumes a strong relevance: in fact, overtopping along the barrier is not uniformly distributed and overtopping discharge is generally overestimated because measurement points (WGs 13, 14) fall near the stream axis.

This procedure gives better results for layout 1 (Tab 8.9) than for layout 2 (Tab 8.10). Thi is due to the higher complexity of representing the overtopping ophenomenon in this layout.
First of all, the breakwater is oblique and it is not possible an accurate estimate of the wave obliquity on the structure (from video analysis the wave travelling on the breakwater maintains substantially the direction perpendicular to the beach) and so of wave celerity. Moreover, the return flux through the gap is more difficult, so that in case of submerged structure the most flux returns over the barrier and the critical condition at wave trough cannot apply (the procedure gives in all cases a negative overtopping discharge). Finally, the gauges are placed at an higher distance along the perpendicular to the beach between each other, so that in several cases the overtopping volume for emergent structure can be estimated at WG 13 only. Both for freeboard zero and emergent structure the overtopping discharge results thus underestimated because of the missing representation of the volume lost for percolation through the structure itself.

Despite of integrating errors due to the few measurement points available along the barrier and at the gap, mass balance is satisfied at least for layout 1, within ±20%; Fig. 8.24 and 8.25 show q_{ovt} versus the sum of q_{gap} and q_{fil} (i.e., the returnign flow) for zero-freeboard structure, for layout 1 and 2 respectively.

For both F=0 and F=+3, return fluxes have a fixed path through the gap, see the common q_{gap}-S_u relation in Fig. 8.26 for layout 1; less clear, for the reasons already told before, are the return paths for layout 2, Fig. 8.27 . In case of submerged barrier, other return paths to the sea seem to be present (Fig. 8.26), which are caused for instance by small berm inhomogeneity; the area feeding the gap becomes thus smaller, producing lower setup for constant gap discharge (shorter return paths).

Overtopping discharge q_{ovt} increases almost linearly with increasing wave intensity (Fig.s 8.28 and 8.29), measured by the product $H_{rmsi}T_p$; the rate is approximately 14 cm/s^2, see Fig. 8.28.
Freeboard and berm width affect the minimum wave intensity necessary for positive overtopping discharge; q_{ovt} is zero for

Berm width	F=0	F=+3
Narrow	$H_{rmsi}T_p$<1	$H_{rmsi}T_p$<5
Wide	$H_{rmsi}T_p$<2	$H_{rmsi}T_p$<6

Overtopping discharge is not affected by wave directionality but is influenced by wave sepctrum type, see for instance Table 8.9. In fact, comparing tests charcterised by similar H_{si} and T_p on regular and irregular waves (Test 5 and 1, Test 6 and 2, Test 8 and 4, Tests 16 and 12, Tests 20 and 18, Tests 27 and 23, Tests 29 and 25, Tests 38 and 34, Tests 41 and 39 respectively) and with 2D and 3D spectra (Tests 9 and 1, Tests 10 and 2, Tests and 31 ans 23, Tests 32 and 24 respectively), q_{ovt} results higher for regular than for irregular waves, whereas does not significantly vary from 2D to 3D irregular wave tests.

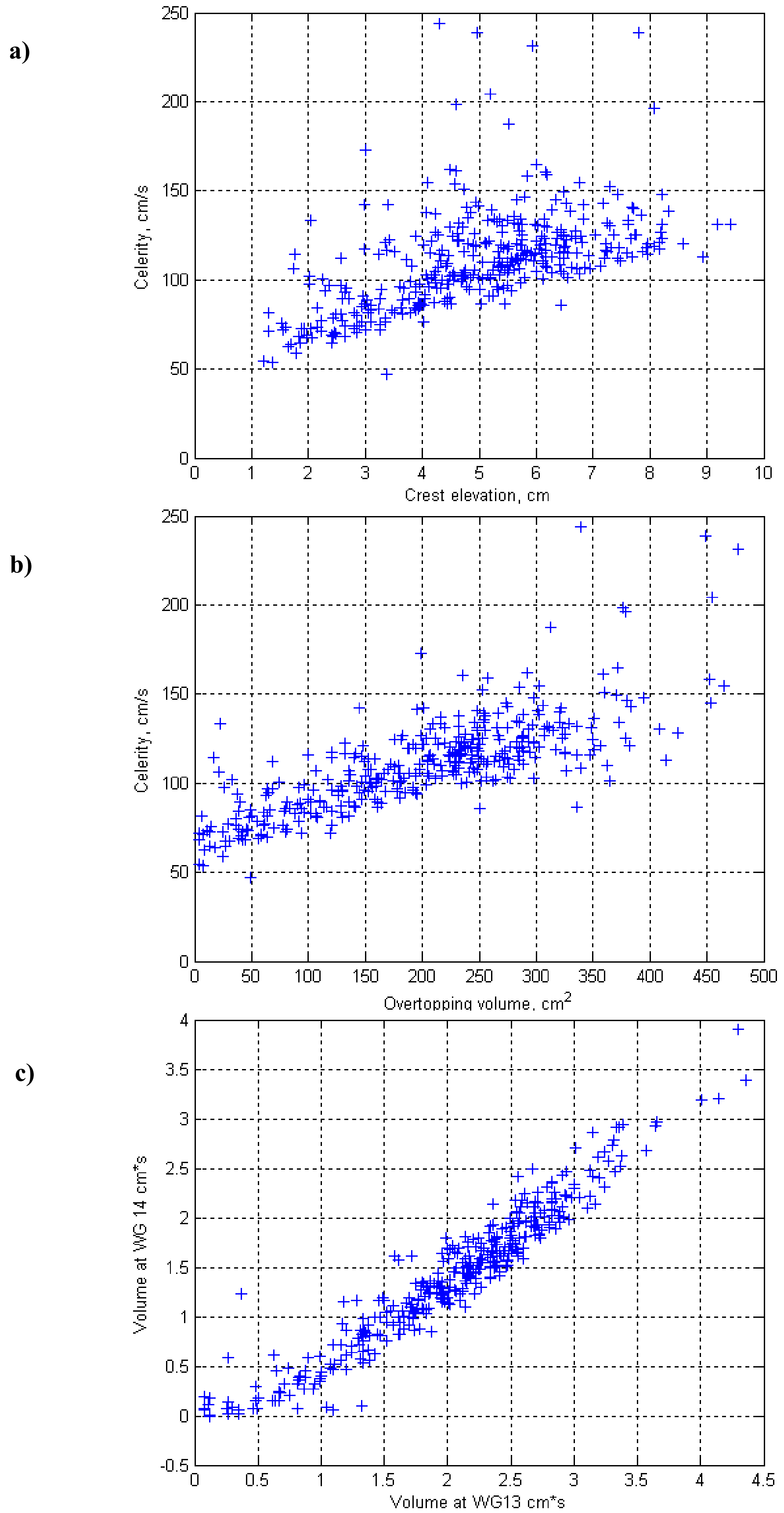

Fig. 8.22 Some results of the overtopping fluxes evaluation procedure; Test 1, J3D, narrow berm, *F*=0: a) front celerity versus crest elevation; b) front celerity versus crest volume; c) relation among overtopping “volumes” (time integrated surface elevation) at WG 13 and 14.

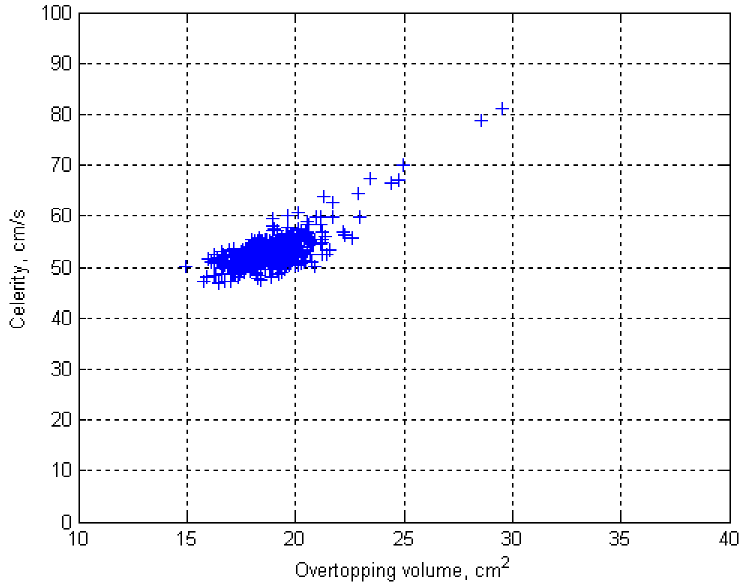

Fig. 8.23 Front celerity versus overtopping volume for regular waves.
Test 28, wide berm, F=0.

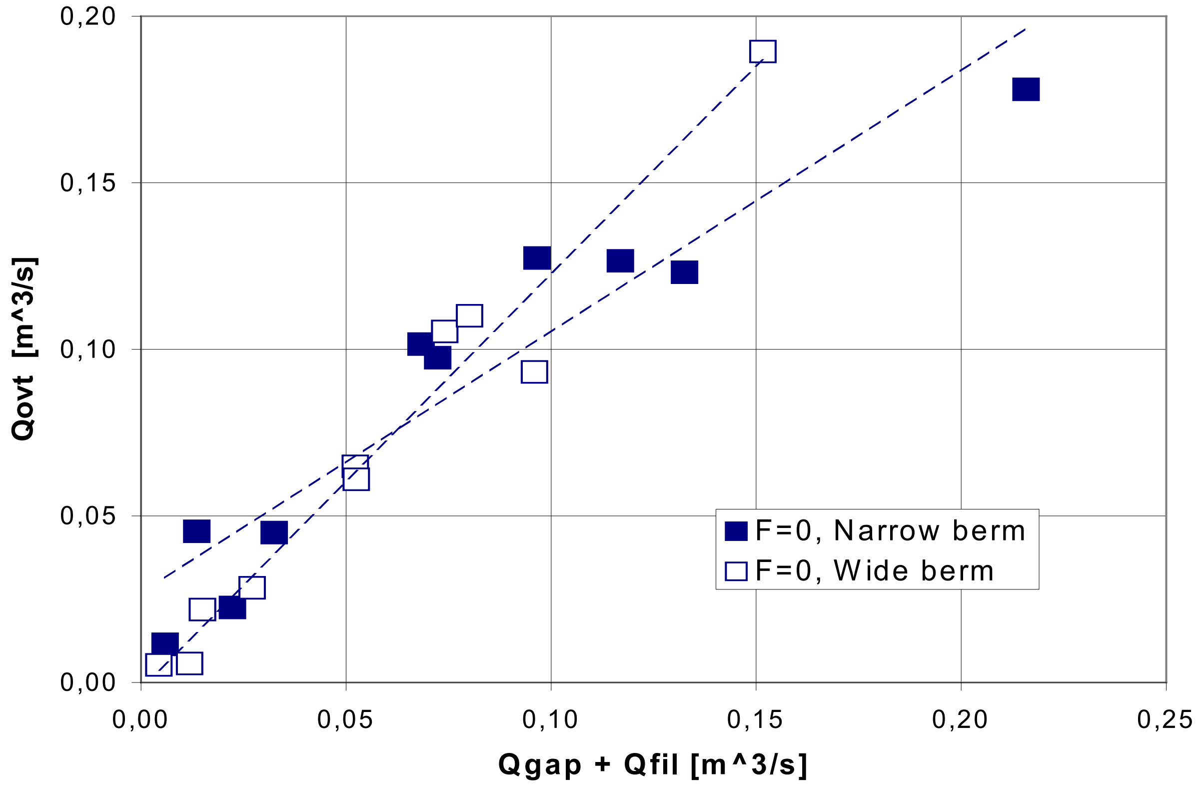

Fig. 8.24 Integrated overtopping discharge Q_{ovt} versus integrated discharge at the gap Q_{gap} plus integrated filtration discharge through the barriers Q_{fil}, freeboard zero, layout 1.

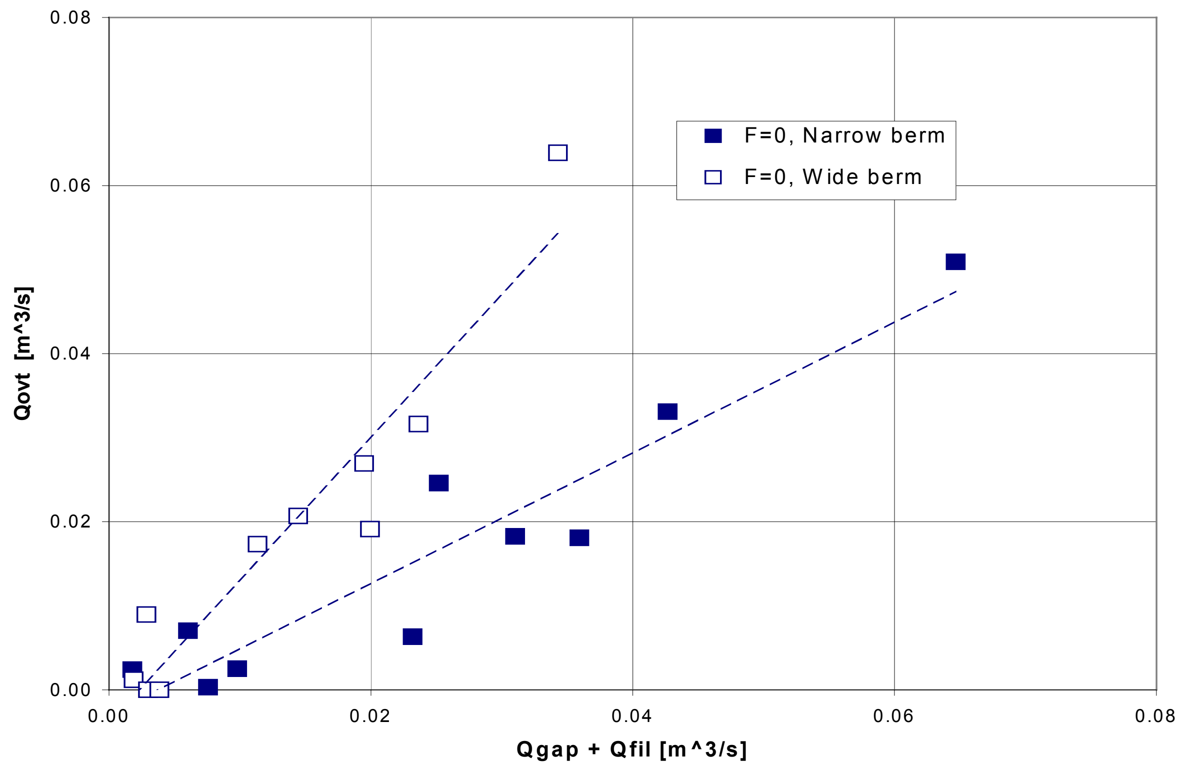

Fig. 8.25 Integrated overtopping discharge Q_{ovt} versus integrated discharge at the gap Q_{gap} plus integrated filtration discharge through the barriers Q_{fil}, freeboard zero, layout 1.

Tab. 8.9. Test conditions and results for Layout 1: F is freeboard; H_{si} is incident wave height; T_p is wave peak period; S_u is mean setup; S_{ub} is mean setup at the barrier; c is median crest celerity; vol13 and vol14 are the median 'volumes' at WGs 13 and 14; q_{ovt}, q_{gap} and q_{fil} are overtopping, return at the gap and filtration discharges per unit width; the error is given by the difference between q_{gap} and (q_{ovt} - q_{fil}) over the maximum of the two values.

Ntest	R/i	F	Hsi	Tp	Su	Sub	%ovt	c	vol13	vol14	qovt	qgap	qfil	(qovt-qfil) int	qgap int	Error
1	I	0	8.78	1.70	0.306	-0.131	0.79	107.37	90.18	55.72	126.16	294.28	25.69	101476.72	70627.50	0.30
2	I	0	7.74	1.20	0.180	-0.058	0.73	93.13	65.35	33.81	100.59	220.89	15.13	86315.71	53014.45	0.39
3	I	0	4.45	1.13	0.017	-0.051	0.73	87.35	29.59	15.14	44.95	50.71	1.42	43957.93	12169.34	0.72
4	I	0	2.86	0.80	0.000	-0.002	0.64	64.25	10.30	2.03	11.34	24.52	-0.03	11487.64	5884.00	0.49
5	R	0	8.34	1.56	0.995	-0.389	0.70	138.94	92.58	65.34	176.27	547.70	83.59	93616.09	131447.05	-0.29
6	R	0	7.50	1.10	0.265	-0.074	0.70	112.02	59.33	35.67	121.96	404.09	22.25	100703.87	96981.23	0.04
7	R	0	3.50	1.04	0.068	-0.029	0.70	79.93	33.21	13.16	44.58	111.25	5.74	39230.42	26699.13	0.32
8	R	0	3.09	0.74	0.053	-0.009	0.70	71.25	16.52	2.00	22.30	74.35	4.41	18069.20	17845.19	0.01
9	I	0	9.16	1.70	0.446	-0.175	0.78	114.78	80.99	52.55	125.30	329.47	37.45	88723.96	79071.63	0.11
10	I	0	8.00	1.20	0.182	-0.058	0.75	103.30	53.54	32.50	96.56	236.98	15.32	82054.93	56875.91	0.31
11	I	3	7.61	1.57	0.037	-0.195	0.67	117.40	19.65	8.47	25.46	152.67		25716.82	36641.72	-0.30
12	I	3	6.61	1.11	0.073	-0.017	0.79	105.16	15.81	4.53	20.70	115.90		20907.00	27816.13	-0.25
13	I	3	3.47	1.04	0.020	-0.009	0.10	80.00	9.00	0.00	1.13	31.12		1146.08	7469.00	-0.85
14	I	3	1.97	0.74	0.025	0.009	0.00	50.00	1.00	0.00	0.00	13.36		0.00	3206.12	-1.00
15	R	3	6.38	1.44	0.532	-0.223	0.71	115.08	22.20	7.72	30.20	175.87		30506.55	42208.05	-0.28
16	R	3	6.25	1.02	0.099	-0.023	0.98	91.68	15.20	3.25	43.41	213.77		43839.96	51305.77	-0.15
17	I	-7	12.74	1.97	0.466	-0.180	0.83	112.91	417.36	262.31	550.18	662.46	39.11	516180.30	158990.20	0.69
18	I	-7	11.41	1.40	0.324	-0.139	0.74	108.27	483.28	352.44	221.22	499.69	27.24	195919.50	119926.17	0.39
19	R	-7	10.33	1.81	0.778	-0.385	0.69	115.23	437.32	279.57	628.49	789.75	65.35	568777.97	189540.46	0.67
20	R	-7	10.10	1.28	0.560	-0.184	0.72	92.98	357.84	207.56	724.79	766.58	47.07	684502.35	183978.15	0.73
21	I	-7	5.96	1.32	0.042	-0.008	0.70	96.69	314.21	201.03	-13.79	144.63	3.52	-17484.51	34710.92	
22	I	-7	4.78	0.93	0.027	0.006	0.65	97.06	237.27	147.80	-262.91	78.98	2.22	-267783.22	18954.34	
23	I	0	8.78	1.70	0.229	-0.128	0.76	122.56	67.35	38.92	104.34	268.15	9.63	95662.45	64356.83	0.33
24	I	0	7.89	1.20	0.126	-0.068	0.72	97.35	42.86	18.23	64.22	195.45	5.28	59529.91	46907.40	0.21
25	I	0	4.23	1.13	0.030	-0.016	0.71	72.70	22.34	4.28	21.67	57.05	1.28	20593.60	13691.17	0.34
26	I	0	2.69	0.80	0.003	0.028	0.52	36.87	11.90	0.20	5.18	17.78	0.11	5119.99	4268.38	0.17
27	R	0	8.04	1.56	0.821	-0.334	0.73	159.99	83.66	56.77	187.55	486.98	34.46	154623.63	116874.46	0.24
28	R	0	7.21	1.10	0.317	-0.117	0.75	124.41	41.59	19.55	92.30	343.93	13.32	79777.88	82542.91	-0.03
29	R	0	3.84	1.04	0.058	-0.017	0.73	86.14	24.78	1.31	28.11	102.54	2.44	25931.35	24609.91	0.05
30	R	0	2.86	0.74	0.008	0.004	0.40	60.00	18.00	0.00	7.83	47.86	0.34	7561.27	11487.45	-0.34
31	I	0	9.45	1.70	0.379	-0.147	0.75	127.71	69.39	38.67	108.98	266.94	15.90	94012.01	64065.62	0.32
32	I	0	7.89	1.20	0.172	-0.067	0.72	99.10	48.55	24.71	60.36	188.50	7.21	53682.91	45239.58	0.16
33	I	-7	12.88	1.97	0.571	-0.310	0.82	118.37	285.78	222.43	243.15	728.04	23.98	221359.58	174728.62	0.21
34	I	-7	10.61	1.40	0.349	-0.145	0.69	108.34	233.28	175.00	117.79	544.98	14.66	104156.15	130795.07	-0.20
35	I	-7	5.84	1.32	0.044	-0.015	0.75	52.72	202.94	162.55	-251.98	157.25	1.85	-256375.07	37740.46	
36	I	-7	4.43	0.93	0.010	-0.009	0.71	49.72	144.03	107.65	-340.50	63.78	0.42	-344328.59	15306.12	
37	R	-7	7.85	1.81	0.137	-0.054	1.00	59.12	117.65	70.56	-140.49	403.21	5.74	-147688.36	96770.73	
38	R	-7	10.31	1.28	0.965	-0.298	0.70	105.51	220.28	165.08	259.24	866.07	40.54	220886.80	207856.26	0.06
39	I	3	7.52	1.57	0.157	-0.271	0.95	103.41	10.99	1.06	26.10	122.15		26365.65	29315.27	-0.10
40	I	3	6.67	1.11	0.081	-0.066	0.18	56.66	6.14	0.05	1.05	87.29		1060.50	20950.11	-0.95
41	R	3	6.18	1.44	0.244	-0.909	1.00	105.72	10.36	0.33	38.58	193.92		38964.08	46541.43	-0.16
42	R	3	6.20	1.02	0.072	-0.034	0.20	48.27	2.59	0.07	0.88	114.67		889.35	27521.14	-0.97
43	I	3	3.25	1.04	0.003	-0.013	0.10	25.00	1.10	0.00	0.10	23.40		97.81	5615.24	-0.98
44	I	3	1.95	0.74	-0.006	0.002	0.10	15.00	0.50	0.00	0.03	48.59		26.68	11662.65	-1.00

Tab. 8.10. Test conditions and results for Layout 2: F is freeboard; H_{si} is incident wave height; T_p is wave peak period; S_u is mean setup; S_{ub} is mean setup at the barrier; c is median crest celerity; vol13 and vol14 are the median 'volumes' at WGs 13 and 14; q_{ovt}, q_{gap} and q_{fil} are overtopping, return at the gap and filtration discharges per unit width; the error is given by the difference between q_{gap} and (q_{ovt} - q_{fil}) over the maximum of the two values.

Ntest	R/i	F	Hsi	Tp	Su	Sub	%ovt-1	nw	c	vol13	vol14	qovt	qgap	qfil	(qovt-qfil) int	qgap int	Error
45	I	0	10.16	1.70	0.31	0.10	1.10	379.00	125.99	46.61	21.38	68.92	132.43	22.66	34235.66	33108.73	0.03
46	I	0	8.57	1.20	0.12	-0.04	1.03	491.00	114.29	30.77	11.02	51.22	87.53	8.71	31455.33	21881.86	0.30
47	I	0	4.77	1.13	0.03	-0.03	0.92	458.00	91.99	13.30	2.33	14.63	21.02	2.04	9315.49	5255.25	0.44
48	I	0	2.92	0.80	-0.01	-0.01	0.80	542.00	76.35	5.17	0.01	4.99	6.32	0.56	3281.46	1579.79	0.52
49	R	0	10.11	1.56	0.79	-0.41	1.00	382.00	159.32	56.18	27.25	106.07	153.99	57.74	35765.98	38497.86	-0.07
50	R	0	7.86	1.10	0.08	-0.05	1.00	543.00	111.92	24.73	5.15	38.01	117.36	5.96	23715.82	29339.38	-0.19
51	R	0	3.96	1.04	0.04	-0.09	1.00	572.00	87.09	5.03	-0.02	5.24	35.69	2.56	1981.50	8923.49	-0.78
52	R	0	3.71	0.74	-0.02	-0.08	1.00	192.00	93.90	0.39	0.01	0.63	29.03	1.23	-443.63	7257.79	-1.06
53	I	0	10.50	1.70	0.31	-0.16	1.01	350.00	125.88	29.27	11.03	37.68	105.13	22.28	11399.77	26283.41	-0.57
54	I	0	8.63	1.20	0.10	-0.09	0.84	402.00	109.77	11.08	2.57	13.18	81.90	7.38	4285.12	20474.16	-0.79
55	I	3	8.94	1.57	0.45	0.01	0.56	187.00	115.23	9.20	0.65	5.09	70.81		3763.27	17702.03	-0.79
56	I	3	7.28	1.11	0.06	-0.05	0.17	48.00	106.77	3.45	0.02	0.71	35.82		527.03	8955.30	-0.94
57	I	3	3.77	1.04	0.00	-0.03	1.10	100.00	90.56	0.06	0.00	0.06	14.80		47.21	3698.91	-0.99
58	I	3	2.02	0.74	-0.02	0.00	0.71	218.00	90.83	0.06	0.00	0.07	3.61		3.40	903.43	-1.00
59	R	3	8.16	1.44	0.46	-0.13	1.00	414.00	124.71	34.33	8.60	46.48	76.82		34398.31	19203.99	0.44
60	R	3	6.61	1.02	0.00	-0.01	1.00	400.00	80.92	1.82	0.01	1.82	51.57		1345.02	12891.76	-0.90
61	I	-7	13.93	1.97	0.27	-0.47							306.87	19.81	-14662.58	76717.79	-1.19
62	I	-7	12.10	1.40	0.26	-0.34							287.89	18.65	-13802.70	71973.28	-1.19
63	R	-7	12.99	1.81	1.06	-0.53							379.93	76.75	-56793.82	94982.36	-1.60
64	R	-7	11.74	1.28	0.43	-0.19	negative overtopping discharge						510.19	31.13	-23035.98	127548.58	-1.18
65	I	-7	6.66	1.32	0.08	-0.26							79.70	5.47	-4046.76	19925.21	-1.20
66	I	-7	4.70	0.93	0.03	-0.58							28.74	2.40	-1777.33	7185.31	-1.25
67	I	0	10.07	1.70	0.11	0.13	1.08	273.00	110.50	60.07	14.53	65.89	90.17	4.17	45677.24	22542.18	0.51
68	I	0	8.68	1.20	0.06	-0.01	1.04	277.00	95.62	37.70	3.91	43.06	55.82	2.19	30242.76	13954.66	0.54
69	I	0	4.52	1.13	0.00	0.01	0.98	44.00	83.20	20.22	0.16	18.67	11.56	0.17	13685.93	2891.08	0.79
70	I	0	2.77	0.80	0.05	-0.27	0.65	24.00	162.73	1.40	0.08	2.46	4.35	1.76	518.22	1087.74	-0.52
71	R	0	9.88	1.56	0.50	-0.31	0.99	382.00	156.99	80.56	25.24	133.09	106.48	18.21	85011.50	26619.16	0.69
72	R	0	8.11	1.10	0.08	-0.03	1.00	540.00	97.89	35.67	0.14	39.83	77.29	2.88	27345.15	19322.41	0.29
73	R	0	4.06	1.04	-0.04	-0.02	non zero volume only at WG13						15.60	-1.60	1187.48	3900.33	-0.70
74	R	0	3.34	0.74	-0.01	-0.03	non zero volume only at WG13						16.63	-0.30	221.33	4156.59	-0.95
75	I	0	10.60	1.70	0.16	-0.07	1.02	311.00	110.43	55.72	11.47	56.08	69.35	5.94	37106.63	17337.08	0.53
76	I	0	8.89	1.20	0.03	-0.02	0.99	219.00	90.55	36.67	1.66	36.07	45.24	1.01	25943.73	11308.92	0.56
77	I	-7	14.50	1.97	0.29	-0.38							293.19	10.56	-7815.58	73297.87	-1.11
78	I	-7	12.13	1.40	0.25	-0.03							200.14	9.13	-6756.20	50035.27	-1.14
79	I	-7	6.89	1.32	0.03	0.01							47.59	1.20	-886.82	11897.17	-1.07
80	I	-7	4.75	0.93	0.01	0.01	negative overtopping discharge						21.36	0.28	-206.53	5339.71	-1.04
81	R	-7	11.39	1.81	0.95	-0.38							289.85	34.60	-25607.26	72462.46	-1.35
82	R	-7	11.31	1.28	0.54	-0.11							346.07	19.77	-14630.84	86517.27	-1.17
83	I	3	8.59	1.57	0.12	-0.01	non zero volume only at WG13						49.23		0.00	12306.78	-1.00
84	I	3	7.43	1.11	0.06	-0.01	2.05	477.00	145.44	0.26	0.02	0.95	28.93		704.78	7232.75	-0.90
85	R	3	7.62	1.44	0.43	-0.14	non zero volume only at WG13						49.43		0.00	12356.66	-1.00
86	R	3	6.21	1.02	0.10	0.00	1.80	433.00	187.96	0.06	0.00	0.21	49.67		152.66	12416.99	-0.99
87	I	3	3.61	1.04	0.00	0.01	no overtopping						10.82		0.00	2704.80	-1.00
88	I	3	2.03	0.74	0.01	0.02	no overtopping						2.59		0.00	647.29	-1.00

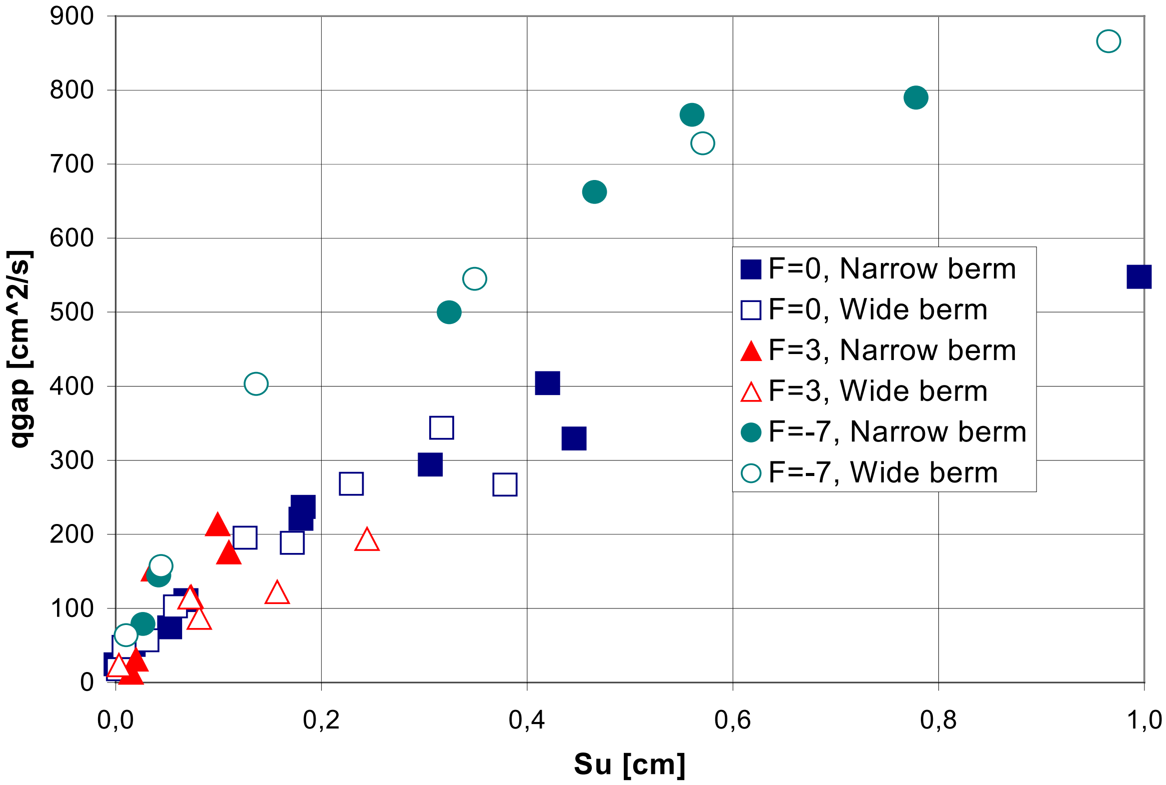

Fig. 8.26 Discharge at the gap per unit width q_{gap} versus setup S_u, freeboard zero and emergent structures, layout 1.

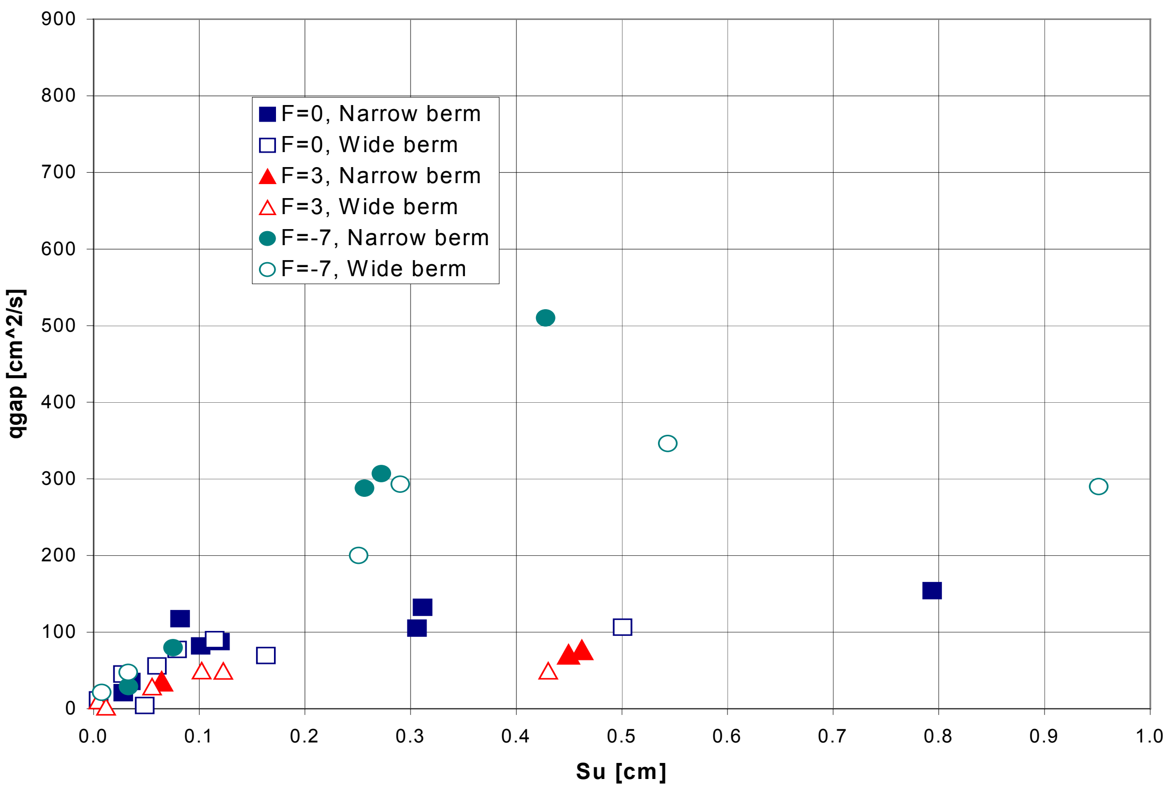

Fig. 8.27 Discharge at the gap per unit width q_{gap} versus setup S_u, freeboard zero and emergent structures, layout 2.

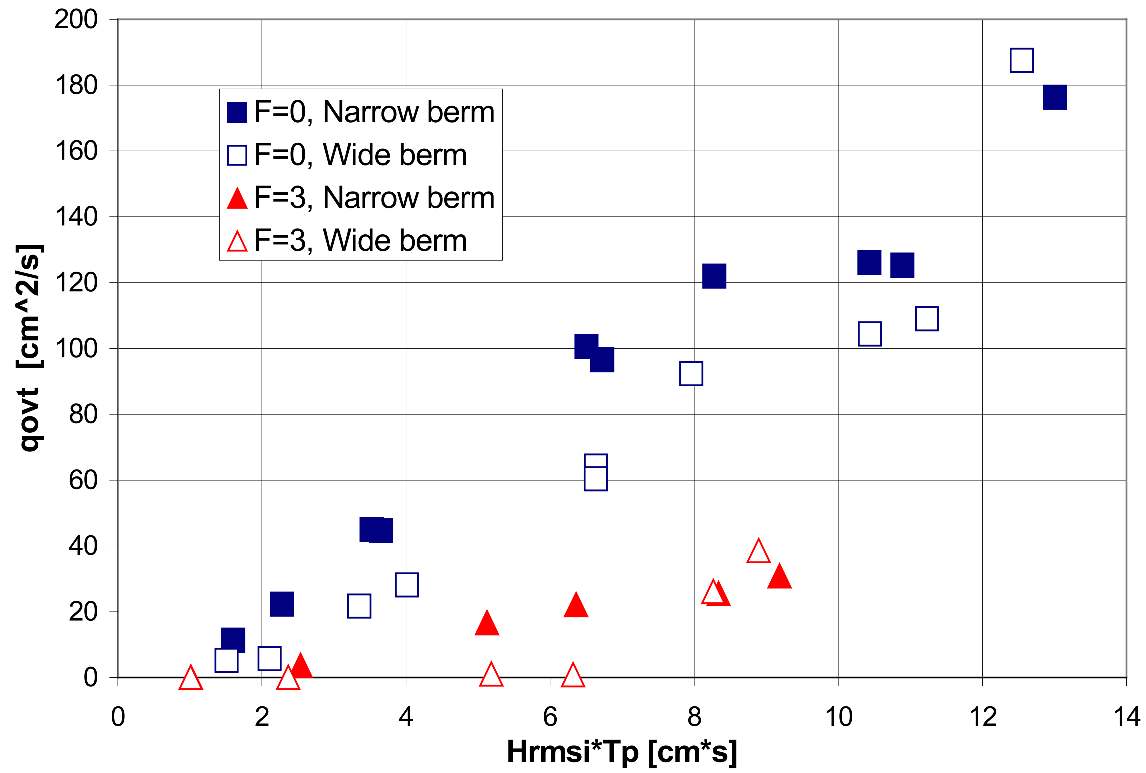

Fig. 8.28 Overtopping discharge per unit width qovt versus the product incident wave height Hrmsi per peak period Tp, freeboard zero and emergent structures, layout 1.

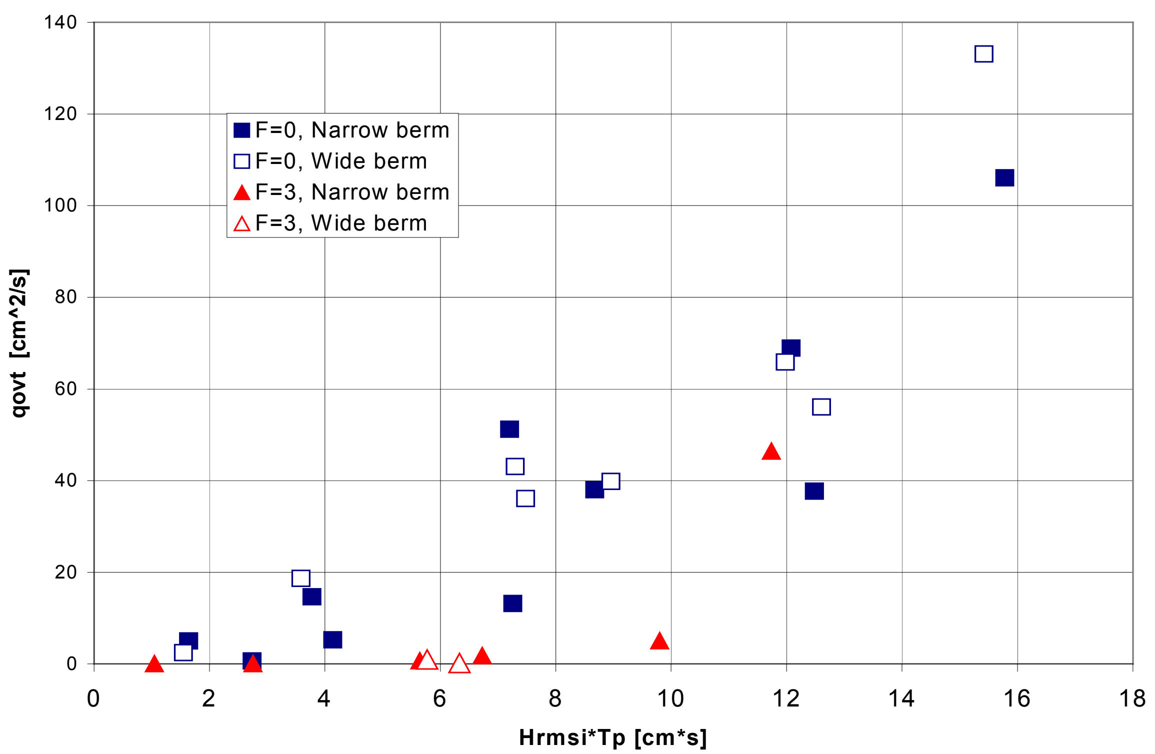

Fig. 8.29 Overtopping discharge per unit width qovt versus the product incident wave height Hrmsi per peak period Tp, freeboard zero and emergent structures, layout 2.

9. Conclusions

Wave reflection

Reflection in front of the structure and of the beach varies in the same range: 20-40%; structure and beach are in fact both made of quarry stones of similar size, Dn50=5.0 and 4.5 cm respectively.

Reflection due to the structure depends on freeboard adimensionalised by incident wave height, on mean berm width and on slope berm width adimensionalised by wave length at structure toe; the representation of the experimental results through a regression function of these three quantities is still in progress.

Wave directional analysis (DIWASP)

BDM should be used only when the number *N* of available wave signals exceeds three; the analysis "directional resolution" should not be higher than $2\pi/N(N\text{-}1)$. EMEP is applicable to three and multi-quantity measurements and seems to give the best results.

IMLM can recognise regular waves and very peaked spectra, whereas the others fail to converge; low number of iterations are suggested.

Directional analysis was applied to laboratory data in case of 5 or 3 wave signals. Mean direction is in general correctly evaluated (within a 5° resolution). Spreading is much more uncertain:

- BDM should be used only when the number *N* of available wave signals exceeds three. Bad results were indeed obtained when applied to a single location gauge. The requested directional resolution should be not higher than $N(N\text{-}1)$. Results deteriorate when number of direction exceeds a certain number, of the order of N^2.
- EMEP is applicable to three and multi-quantity measurements. When dealing with our laboratory data it presents a high level of noise in the spectrum, computing less pronounced directional peaks and higher spreadings than BDM. When this uniformly distributed noise is cancelled, the method is substantially equivalent to BDM.
- IMLM resembles the others only after cancelling the uniformly distributed noise, which is particularly high. Even in this case it seems to overestimate reflected waves. This method can recognize regular waves and very peaked spectra, whereas the others fail to converge. Low number of iterations are suggested: 20÷30 iterations are too many and the directional spectrum shows many peaks (also function of the number of independent wave gauges).

All methods (except BDM) evaluate a relevant energy uniformly distributed over directions. Such energy changes with the method and is most probably due to noise in the cross-correlation signals. Identification of this noise is quite easy (being the minimum of the spreading function) and the rescaled spreading function seems more accurate.

The uniformly distributed noise, when not identified, induces a relevant apparent reflection and the directional analysis overestimated reflection coefficient. The collinear wave gauge method by Zelt & Skjelbreia (1992) for longcrested waves gives better results. Of course when the reflected wave has more spreading than the incident one, the three wave gauge methods underestimates reflection.

Frequency resolution *df* should be consistent with an error in the spectral densities not higher than 1/4 of the true spectrum (i.e. 16 statistical degrees of freedom are needed); anyway *df* should be at least 0.25 f_p in order to have an accurate frequency description. In conclusion $df \approx 0.1\div0.2\ f_p$ is suggested. Directional information is difficult to obtain far from the frequency peak, out of the range $0.75\div1.5\ f_p$. Channels with high noise to signal ratio (like for instance vertical velocity close to the bottom) can reduce rather than increase the overall accuracy.

Longcrested waves are seldom correctly recognized, since the hypothesis at the base of the interpretation models (especially BDM) tend to force a smooth spectrum. The outcome in these cases is either a flat spectrum or something virtually indistinguishable from a broad spectrum. Only IMLM succeeds in recognizing the regular cases (longcrested with regular or irregular frequency).

Wave transmission

Experimental transmission coefficients are in good agreement with van der Meer formula (1992) accounting for berm width; typical discrepancies among experimental and van der Meer (1992) results are within ± 0.2.

The analysis of changes in wave spectra due to transmission over the structure has been performed following Van der Meer et al. (2000). After transmission, peak period remains more or less constant: the transmitted frequency peak is in average 0.95 the incident one (standard deviation 0.04). The peak frequency ratio fpt/fpi is almost constant with varying transmission coefficient Kt, incident wave peak frequency fpi and fictitious incident wave sop.

The transmitted spectrum drops to zero at a frequency close to 4 fpi and about the 30% of the total transmitted energy is present at the higher frequencies of the spectrum between 1.5 and 3.5 fpi. The percentage of shifted energy increases with increasing transmission till Kt reaches values close to 0.4, then it tends to assume an almost constant value around the 40% (in agreement with Van der Meer et al., 2000) and finally decreases for Kt higher than 0.6.

Wave overtopping

A method for evaluating wave overtopping over low-crested structures from wave gauge records is presented and verified through experimental data collected from 3D wave basin tests. This method can be applied to moderately submerged or emergent structures ($-F<0.7H_{si}$) and gives better results for the symmetrical than for the oblique layout.

Filtration discharge was reconstructed re-scaling data measured by Loveless & Debski (1997) for zero freeboard and submerged structures and results for LCS are at least an order of magnitude lower than overtopping discharge.

Our flux measurements and estimates satisfy mass balance within ±20%. Major discrepancies can be found for cases of no relevant overtopping over emergent structures, for which it is hard to reconstruct the inshore discharge percolating and filtrating through the structure, and for deeply submerged structures, over which a high return flow occurs. Validation of results is in progress.

The analysis of fluxes shows that the most relevant process parameters are setup, incident wave height and period and berm width.

Overtopping discharge increases with incident wave intensity and causes a proportional setup. Both wave overtopping and transmission decrease with increasing berm width, as a fraction of the overtopping volume is lost by percolation through the structure.

10. Acknowledgements

The personnel directly involved in 3D hydrodynamic tests are listed in the following table.

Name and title	Working period at AAU	Institution
Alberto Lamberti, Professor	July 24th – July 28th	UB
Barbara Zanuttigh, PhD	July 24th – August 8th	UB
Morten Kramer, PhD Student	July 1st – August 30th	AAU
Matteo Tirindelli, PhD Student	August 6th – August 30th	UB

Marcello Di Risio, PhD Student	July 22nd – August 6th	UR3
Massimo Guerrero, Engineer	August 19th – August 24th	UB
Erika Vivi, Undergraduate Student	August 1st – August 30th	UB

Several people from Aalborg University helped the DELOS group during tests, in particular: Dr. Peter Frigaard, Jørgen Sørensen, Niels Drustrup, Kurt Sørensen and Jens Ildal are gratefully acknowledged.
Authors acknowledge also the strong effort and the good work by Matteo Tirindelli, Massimo Guerrero and Erika Vivi from the University of Bologna and by Marcello di Risio from the 3rd University of Rome.

11. References

Battjes, J. P. & Jannsen, F. M., 1978: "Energy loss and set-up due to breaking of random waves", *Proc. Coastal Engineering*, Hamburg, ASCE, 569-587.

Borthwick, A., Foote, Y. & A. Ridehalgh, 1997: "Measurements at a cusped beach in the UKCRF", *Coastal Dynamics '97*, ASCE, 953-963.

Chapman, B., Ilic, S., Simmonds, D. & A. Chadwick, 2000: "Physical model evaluation of the hydrodynamic produced around a detached breakwater scheme", *Coastal Structures '99*, Losada ed., Balkema, 803-812.

Davies, B. L. & Kriebel, D. L. 1992: "Model testing on wave transmission past low-crested breakwaters", Proc. Of the 25th ICCE, Orlando, ASCE, 2418-2427.

Debski, D. & Loveless, J. 1997: "The design and performance of submerged breakwaters", Report for Ministry of Agriculture Fisheries and Food, University of Bristol.

Diskin M.H., Asce A.M., Vajda M.L. & Amir I.: 1970: ""Piling-up Behind Low and Submerged Permeable Breakwaters". *J. of Waterways & Harbours Division*, ASCE 05 / 1970.

Drei E. & Lamberti A. 1999: "Wave Pumping Effect of a Submerged Barrier". *Proceedings Coastal Structures '99*, 667-673.

Dronen, N., Karunarathna, H., Fredsoe, J., Sumer, M. B. & R. Deigaard, 1997: "Scour at the round head of a rubble mound breakwater", *Coastal Engineering*, 29, 231-262.

Fredsoe, J. & M. Sumer 1997: "Scour at the round head of a rubble mound breakwater", *Coastal Engineering*, 29, 231-262.

Gourley, G., 1974: "Wave set-up and wave generated currents in the lee of a breakwater or a headland", *Proc. Coastal Engineering '74*, 1976-1995.

Hamm, L. 1992: "Directional wave propagation over a rip channel: an experiment", *Proc. Coastal Engineering*, Venice 1992, 31, ASCE ed., 226-239.

Ilic, S., Chapman, B., Chadwick, A. J., Pan, S., O'Connor, B. A. & N. J. MacDonald, 2000: "Laboratory measurements of flow around a detached breakwater scheme", *Coastal Structures '99*, Losada ed., Balkema, 813-855.

Kajima, R. 1969: "Estimation of incident wave spectrum in the sea area influencedby reflection". *Coastal Engineering in Japan*, JSCE, 12, 9-16.

Kobayashi N. & Wurjanto A. 1989: "Wave Transmission over Submerged Breakwaters". *J. of waterway, Port, Coastal and Ocean Engineering*, 115, N.5, 662-680.

Losada I.J., Dalrymple R.A. & Losada, M.A. 1998: "Wave Induced Mean Flows in Vertical Rubble Mound Structures". *Coastal Engineering*, 35, 251-282

Loveless, J., Debski, D. & MacLeod, A.B. 1998: "Sea Level Set-up behind Detached Breakwaters". Proc. ICCE '98, Copenhagen, Denmark.

Mitsuyasu, H. et al., 1975: "Observation of the directional spectrum of ocean waves using a cloverleaf buoy". *J. of Physics. oceanography*, 5, n. 4, 750-760.

Mory, M. & L. Hamm 1997: "Wave set-up and currents around a detached breakwater", *Coastal Engineering*, 31, 77-96.

Ruol P. & Faedo A. 2002: “Physical Model Study on Low-Crested Structures under Breaking Wave Conditions” *Proceedings MEDCOAST* Workshops on Beaches of the Mediterranean and Black Sea: Dynamics, Regeneration, Ecology & Management, E. Ozhan (Editor), 24-27 October 2002, Turkey.

Sutherland, J., Whitehouse, R. J. S. & B. Chapman, 2000: “Scour and deposition around a detached rubble-mound breakwater”, *Coastal Structures ‘99*, Losada ed., Balkema, 897-904.

Tirindelli M., Drei E., Lamberti A. & Aminti P. 2001: “Experimental Analysis of the Hydrodynamic Effects of a Submerged Barrier” *Proceedings MEDCOAST 2001*, Hammamet

van der Meer, J. W., 1990: “Data on wave transmission due to overtopping”, Delft Hydraulics Report H986, Delft Hydraulics, Marknesse, The Netherlands.

van der Meer, J. W., 1992: “Conceptual design of rubble mound breakwaters”, ICCE 1992, Proc. Of the short course on Design and reliability of coastal structures, Venice, 1-3 October 1992.

van Gent, M. R. A., 1993: “Stationary and oscillatory flow through coarse porous media”, Communications on Hydraulic and Geotechnical Engineering, Report N. 93-9, Delft University of Technology 1993.

Van der Meer, et. al. (2000) Spectral Changes due to Wave Transmission and Effects of Bimodal Wave Spectra on Overtopping. INFRAM publication number 6.

Vidal, C., Losada, M. A., Medina, R., Mansard, E. P. D. & G. Gomez-Pina, 1992: “An universal analysis for the stability of both low-crested and submerged breakwaters”, *Proc. Coastal Engineering ‘92*, ASCE, 1679-1692.

Zelt, J. A., Skjelbreia, J. E. 1992: “Estimating incident and reflected wave field using an arbitrary number of wave gauges”. *Proc. ICCE 1992*, I, 777-789.

Papers prepared on the results of the 3D hydrodynamic tests in Aalborg:

Lamberti, A., Zanuttigh, B. & M. Tirindelli, 2003. “3D Hydrodynamic tests with low-crested structures: analysis of overtopping and velocity fields”, presented at *ISOPE 2003*, Honolulu, May 2003.

Lamberti, A., Zanuttigh, B. and M. Kramer, 2003. “Wave and current flow around low-crested coastal defence structures”, to be presented at *Coastal Structure*, Portland, Oregon, August 2003.

Lamberti, A., Zanuttigh, B. & M. Tirindelli, 2003. Evaluation of overtopping processes on low-crested structures, to be presented at *MEDCOAST 2003*, Ravenna, October 2003.

Martinelli, L., Zanuttigh, B. & A. Lamberti, 2003. “Comparison of directional wave analysis methods on laboratory data”, to be presented at *IAHR 2003*, Thessaloniki, August 2003.

Zanuttigh, B., Guerrero, M. & Lamberti, A. 2003. “3D experimental analysis and numerical simulations of hydrodynamics around low-crested structures”, to be presented at *IAHR 2003*, Thessaloniki, August 2003.

Zanuttigh, B., Lamberti, A & M. Guerrero, 2003. “3D hydrodynamics around low-crested structures: experimental results and numerical simulations”, to be presented at *MEDCOAST 2003*, Ravenna, October 2003.

EU Fifth Framework Programme 1998-2002
Energy, Environment and Sustainable Development

Environmental Design of Low Crested Coastal Defence Structures

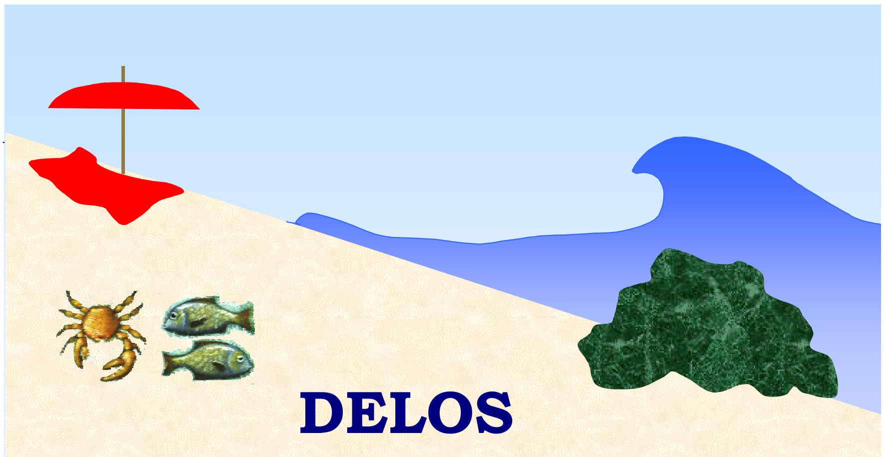

Wave basin transmission tests

Internal Report

Date of preparation: 15.06.2003 **Contract EVK3-CT-2000-00041**

ABSTRACT

The EU-funded project DELOS aims to promote effective and environmentally compatible design of low crested structures to defend European shores against coastal erosion. As one of its objectives, oblique wave transmission at low-crested structures has been studied in this research. It presents results of physical model tests and data analysis of three-dimensional wave transmission at rubble and smooth structures.

Based on physical model tests in flumes, where the sections were subjected to direct long crested wave attack, transmission formulas have been derived for both rubble and smooth structures by many researchers. But, in some cases, wave attack is oblique to the alignment of the structure instead of perpendicular. Until now little has been known about short-crested oblique wave transmission. Physical model tests with wave attack angles varying from 0° to 60° to the normal were carried out in the present research in order to investigate the mechanics of three-dimensional wave transmission. The tests were performed at the short-crested wave basin of Aalborg University, Denmark, in August 2002.

The research focused on four parts: 1) Validation of existing formulae; 2) Derivation of modified formulae for 2-D and 3-D wave transmission at smooth structures; 3) Oblique wave main direction change after transmission; 4) Wave spectral change. The Bayesian Directional Spectrum Estimation Method (BDM) was used to analyse the short-crested wave data sets. Oblique wave transmissions at low-crested structures were characterised in this report and the following conclusions were reached.

It was found that the wave direction is not a dominant parameter for rubble structures in the DELOS tests, because of its slight influences on transmission coefficient. However, transmission at smooth structures is significantly affected by the incident wave angle.

The transmission formula proposed by Daemen (1991) was reviewed to investigate the agreement with new data sets. This study confirmed that it is a good expression for rubble structures with a narrow crest width.

Based on more available data sets on smooth structures, the two-dimensional wave transmission formula presented by De Jong (1996) was modified in this research. We found, as earlier by Infram (2000), that the crest width does not play a role in wave transmission at smooth structures. Moreover, a new formula was proposed for oblique wave transmission at smooth structures.

The wave main direction will decrease after transmission. The relations between incident and transmitted wave direction were given as a function of incident wave angle.

For rubble and smooth structures the peak frequency of the transmitted spectrum is similar to that of the incident spectrum. The phenomenon that more energy shifts to the higher frequency range was also observed in the research.

CONTENTS

LIST OF TABLES

LIST OF FIGURES

NOTATION

m_o	zeroth moment of wave energy density spectrum	[-]
H_i	Incident wave height based on spectrum $4\sqrt{m_0}$	[m]
H_t	Transmitted wave height based on spectrum $4\sqrt{m_0}$	[m]
H_r	Reflected wave height based on spectrum $4\sqrt{m_0}$	[m]
T_p	Peak period	[s]
f_p	Peak frequency	[1/s]
f_{max}	Max. frequency	[1/s]
h	Water depth at structure	[m]
h_c	Crest height	[m]
B_c	Crest width	[m]
D_{n50}	Nominal diameter of rock size	[m]
ρ	Mass density of rock	[kg/m^3]
R_c	Crest Freeboard	[m]
s_{op}	Fictitious wave steepness	[-]
ξ	Surf similarity or breaker parameter, based on T_P	[-]
β_i	Angle of incident wave attack	[Degree]
β_t	Transmitted wave angle	[Degree]

1. INTRODUCTION

Oblique wave transmission at low-crested structures has been studied in this research. It presents results of physical model test and data analysis of three-dimensional wave transmission at rubble and smooth structures. This research is one of the objectives within EU-funded project, DELOS.

1.1 Background

DELOS (Environmental Design of Low Crested Coastal Defence Structures, Contract N°: EUK-CT-2000-00041, Website: www.delos.unibo.it), aims to promote effective and environmentally compatible design of low crested structure to defend European shores against coastal erosion, and to preserve the littoral environment and coast economic development. To achieve this aim, engineers from different research fields, such as coastal defence system, coastal oceanography, marine ecology, economics and politics, are engaged in the project. 18 partners from 7 European countries participate in the project for various objectives.

Waves, approaching a coastline under an oblique angle, cause a transport of sediment in long shore direction. The breaking waves produce a current parallel to the coastline, which transport sediment along the coast. Differences in long shore transport along the coast cause erosion and sedimentation.

Low-crested structures are typically built in shallow water as detached breakwaters for coastal protection purposes. This is because of their capability of feeding protected areas with suitable amount of water as well as their minimal visual intrusion. Low-crest structures affect the beach by altering the lee side wave climate. Waves approaching the beach are either reflected by the structures or overtop and pass through the structures. The wave energy in lee side will be less than on the open area.

Sediment transport evaluation at lee side of structures needs reliable estimations of transmitted wave height. Therefore functional design of low crested structure requires an accurate prediction of wave transmission in the protected areas. Also from construction cost point of view, since the volume of material used in the structure is proportional to the square of it's height, the crest level should be designed as low as possible. All of them are the main reasons that the continued attentions have been devoted to the study on transmission at low-crested structures.

Two types of low-crested structures, rubble and smooth structures, have been used for coastal protections worldwide. Rubble structures refer to conventional rubble mound breakwaters. Smooth structures are asphalt grouted breakwaters and groins as built in Dutch coastline, where the rock supplies for construction of the rubble mound breakwaters are limited.

1.2 Objectives of the study

Low-crested structures are usually parallel to the shoreline with in some cases wave attack almost perpendicular to the structure. However, actual wave fields are directional. The principal wave direction is dependent on the prevailing wind direction and underling topography. Various oblique angles can occur all time. Groin systems or breakwaters for harbours, where structures are not parallel to shore line are other examples in which oblique wave attack occurs.

Many physical model tests were performed in flumes where the test sections were subject to direct long crested wave attacks. Based on these two-dimensional (2-D) test data sets, some transmission formulae were derived. Two well-known formulae describing wave transmission over rubble mound breakwater were derived by Van der Meer (1990b) and Daemen (1991). De Jong (1996) proposed one transmission formula for smooth (impermeable) structures.

But, if in some cases as mentioned above wave attack is oblique to the alignment of structure instead of perpendicular, what could the influences of incident wave directions then be? In addition, due to energy spreading, the directions of short-crested waves could be different from the wave main direction; some can be perpendicular to the structure. Can the short-crested wave transmission be larger than the two-dimensional wave attack? The influence of such parameters as wave directionality and directional spreading, which are often representative of real sea conditions, cannot be examined in wave flumes. Inaccurate results can be produced if the 2-D formulae are used for the estimation of transmission coefficient in a three-dimensional (3-D) wave field. Only 3-D investigation in a short-crested basin can give the answers to these questions.

The objectives of the research are to answer the following specific questions:

- How can we describe oblique wave transmission?
- What is the influence of short-crested waves compared to long-crested waves?
- Does the wave direction change after transmission?
- Is the wave spectral change similar to the perpendicular wave attack?

1.3 Methodology

Physical model tests with various wave attack angles were carried out in order to investigate the mechanics of three-dimensional wave transmission. The tests of the present research were performed at the short-crested wave basin of Aalborg University, Denmark, in August 2002. Two structures were tested; a rubble structure and a smooth plywood structure. A total of 84 tests with wave attack angles varying from 0° to 60° to the normal were performed to identify the effect of different hydrodynamic conditions for each type of structure.

In the tests, the target irregular 3-D waves were generated using the parameterised Jonswap spectrum and spreading function of cosine distribution with spreading parameter s=50.

A package for directional wave analysis (PADIWA) and WAVELAB program provided by Department of Civil Engineering of Aalborg University were used to process the test data sets in this research. Bayesian Directional Spectrum Estimation Method (BDM) in the PADIWA package was adopted to estimate directional wave spectrum. The program presents the incident significant and reflection wave height based on spectrum $4\sqrt{m_0}$, peak frequency, wave direction, and energy density distributions both for seaside and leeside. WAVELAB program was used to process the data sets of individual gauge.

Data analysis focuses on validation of previous transmission formulae, influence of wave directions, wave direction change and the comparison between short-crested waves and long-crested wave transmission.

To derive a formula for oblique wave transmission, an existing or modified formula for perpendicular wave transmission has to be developed first based on all present data sets. And then the formula for oblique wave transmission can be achieved by analysis on the wave direction influence from the DELOS data set.

BDM program gives the peak frequency and the energy distribution along frequency and direction. By comparing incident wave peak frequency with transmitted wave frequency, their relation can be found. In the research the range of high frequency is defined as from $1.5f_p$ to maximum frequency f_{max}. To analyse the energy shift, the percentage of the total transmitted energy at the higher frequencies was calculated for each test. The influence of various wave parameters on energy redistribution, such as freeboard, wave steepness and transmission coefficient, can be identified.

The rest of this report is further divided into the following seven parts. In Chapter 2, two-dimensional wave transmission study is reviewed. Three-dimensional wave transmission test set-ups are described in Chapter 3. Chapter 4 details data processing of BDM program. Analysis of data is presented in Chapter 5. Chapter 6 demonstrates derivation of formula for oblique wave transmission at smooth structures. The spectral change due to wave transmission is investigated in Chapter 7. Finally, the Chapter 8 gives the conclusions and recommendations.

2. REVIEW ON 2-D WAVE TRANSMISSION

2.1 Governing parameters

Wave transmission is the phenomena that wave energy will overtop and pass through the permeable breakwater. At the structure incident energy with wave height H_i is partly reflected as reflected wave height H_r. Some remaining energy will be transmitted to the lee side, causing a transmitted wave height H_t. The transmission coefficient K_t is expressed by the ratio between transmitted height H_t and incident wave height H_i:

$$K_t = \frac{H_t}{H_i} = \sqrt{\frac{m_{o,t}}{m_{o,i}}}$$

$m_{o,i}$ is zeroth moment of incident wave energy density spectrum. $m_{o,t}$ is zeroth moment of transmitted wave energy density spectrum

The incident wave height and transmitted wave height are measured in front of and behind the structure respectively, eliminating the effects of reflection. The most important parameters with respect to wave transmission are summarised below. A definition sketch is given in Figure 2.1.

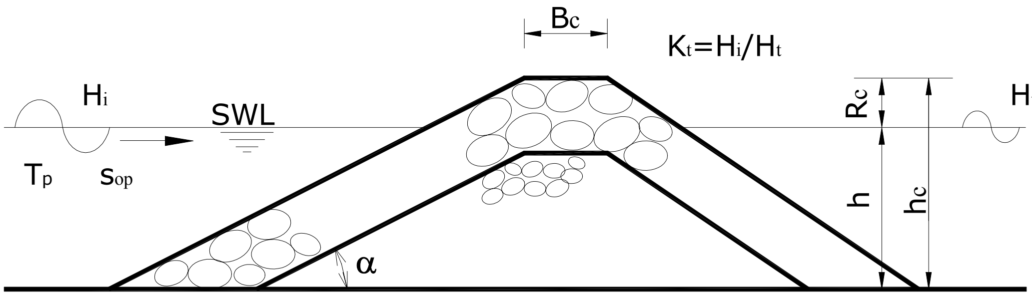

Figure 2.1 Governing parameters related to wave transmission

Hydraulic parameters: Incident wave height H_i and transmitted wave height H_t

In this research the wave height H_i and H_t were based on spectrum $4\sqrt{m_0}$. m_o is zeroth moment of wave energy density spectrum

Peak period T_P

Water depth at structure h

Geometrical parameters: Crest height h_c

Crest width B_c

Angle of structure seaward slope α

Nominal diameter of rock size D_{n50}

Other governing parameters can be derived or calculated from those listed above:

Fictitious wave steepness: $s_{op} = \dfrac{2\pi H_i}{gT_p^2}$

Crest Freeboard : $R_c = h_c - h$

The overview of each parameter influence will be given in the following section.

2.2 Influences of parameters

To get a better insight in wave transmission, a brief discussion will focus on its phenomena and mechanism concluded in previous studies. First the phenomena of wave run-up and overtopping are defined, and then the influences of specific parameters are discussed both for rubble and smooth structures here.

Wave run-up and overtopping

Wave run-up is the phenomenon that when a wave approaches a slope face, a wave tongue runs up the slope. The tongue reaches a maximum elevation above still water level, which is called run-up level. If the crest of the structure is lower than the run-up level, the wave tongue will pass over the crest. Run-up can only occur when the freeboard of the structure is positive.
Overtopping is the phenomenon of masses of water passing over the crest of the structure. When the run-up is smaller than the freeboard, wave can not overtop the structure, therefore, no overtopping occurs. If the run-up exceeds the crest level, there will be overtopping. If the structure is submerged, all waves will overtop the structure.

Freeboard

The crest freeboard R_c is defined as the distance between the still water level and crest level of the structures. For smooth structures (impermeable), wave run-up determines the degree of overtopping and thus the wave transmission. The transmission through the structure is zero. Wave transmission will not occur providing there is no overtopping. A decreasing crest freeboard leads to larger run-up and overtopping. Therefore, the transmission coefficient K_t will increase.
For rubble structures, although the transmission is also affected by the wave transmission through structure body, freeboard plays an important role in wave overtopping. Higher freeboard gives a lower transmission coefficient.
When the structure is submerged and the crest is far below the water level, the influence of freeboard will disappear. Nevertheless, for low-crested structures, the crest freeboard R_c is one of the most important parameters both for rubble mound and smooth structures. It is very clear that the lower the freeboard, the higher the wave transmission.
Two methods, which make the freeboard R_c dimensionless for rubble structures, were proposed in literatures. One is R_c/D_{n50} (Daemen 1991); the freeboard is divided by nominal stone diameter. The other is R_c/H_i (Van der Meer 1990, De Jong 1996); the freeboard is divided by incident wave height. For smooth structures, the relative freeboard of R_c/H_i was adopted to derive the transmission formula, because they do not have a presenting nominal diameter D_{n50}.. It should

be pointed out that the way of R_c/H_I has its disadvantage. All influence of the wave height will be lost when R_c becomes zero.

Wave height

According to Daemen (1991), at rubble mound structures, an increasing wave height will lead to a decreasing transmission coefficient for low crested breakwater which are non-overtopped. A lager wave height will lead to more energy dissipation inside the breakwater and therefore a lower K_t .

For a low-crested smooth and rubble structure that is overtopped, an increasing wave height will cause a higher run-up level, which means more overtopping and a higher transmitted wave height.

When the structure is submerged, overtopping always exists. The influence of wave height is different from the structures with lower water level. At submerged structures a higher wave height will lead to a lower K_t . A bigger wave will be more affected by the crest than a smaller wave. However, when the crest height is far below the still water level, the crest will loose its influence and every wave can pass unhindered. Consequently, the wave height will hardly affect the wave transmission coefficient.

Wave period

The wave period is brought into account by using the fictitious wave steepness $s_{op} = \dfrac{2\pi H_i}{gT_p^2}$. A longer wave period means lower wave steepness. For rubble structures without overtopping, wave with longer period can propagate easier through the structure body and gave a larger transmission. For rubble and smooth structures that are overtopped, lower wave steepness will increase the run-up level, therefore larger transmission coefficient is expected.

For submerged structures, Van de Meer (1990) found that longer waves could pass unhindered, while shorter waves are influenced by the breakwaters. However, Powell & Allsop (1985) gave the opposite conclusion: a higher wave period leads to a decreasing K_t. The parameter $R_p^* = \dfrac{R_c}{H_{mo}}\sqrt{\dfrac{S_{op}}{2\pi}}$ was used to investigate the influence. Van der Meer (1990) concluded that this is not a good parameter to describe wave transmission. The influence of wave period will be also investigated in present research, see Chapter 5.

Crest width

Previous studies indicated that the influence of the crest width is obvious, a wider crest will reduce the wave transmission. Daemen (1991) summarised the influence of crest width for submerged structures: An increasing crest width will force the wave to break and therefore more energy is dissipated on the crest, therefore a lower transmission coefficient. In addition, he also pointed out small crest width has no influence on wave transmission at all. However, De Jong (1996) found this was not true in his investigation, and concluded that even small relative crest width, B/H_i does show influence on wave transmission. The significant influences of crest widths were put into his formulae, for both rubble and smooth structures.

Slope

For structures with positive freeboard, the slope angle has some influence on the wave run-up and therefore wave transmission. On the gentler slope more energy will be dissipated and less transmission occurs. According to Daemen (1991) the slope angle has only influence on very smooth slopes. For submerged structures he concluded that slope no influence is present because the slope mainly affects the wave run-up. However, using surf similarity parameter $\xi = \frac{\tan\alpha}{\sqrt{S_{op}}}$, De Jong (1996) introduced the slope influence into his formulae. Surf similarity parameter ξ describing wave-breaking type on the slope presented some influence on transmission.

Roughness

Physically, the rougher the slope and crest, more energy will be dissipated on the structures and the lower the transmission will be. For submerged structures the influence of slope roughness becomes small. The roughness on the crest will play a role on the transmission together with crest width.

For smooth structures the roughness on the structure surface comes close to zero, no roughness could effect the wave transmission. Question should be given to transmission formula proposed by De Jong (1996) for smooth structures. In this formula significant influence of relative crest width was present.

2.3 Existing wave transmission formulae

Van der Meer (1990)

Extensive investigations on 2-D wave transmission have been carried out. Based on these 2-D tests, transmission formulae were derived. Van der Meer (1990) proposed a formula for wave transmission in his report "Data on wave transmission due to overtopping" which was given by:

$$K_t = 0.80 \qquad \text{for } -2.0 < \frac{R_c}{H_i} < -1.13$$

$$K_t = 0.46 - 0.3\frac{R_c}{H_i} \qquad \text{for } -1.13 < \frac{R_c}{H_i} < -1.2$$

$$K_t = 0.10 \qquad \text{for} \quad 1.2 < \frac{R_c}{H_i} < 2.0 \tag{2.1}$$

Daemen (1991)

The analysis on data sets of wave transmission described in Van der Meer(1990) led to a practical formula in Daemen(1991). The following formula for wave transmission at conventional breakwaters was proposed:

$$K_t = a\frac{R_c}{D_{50}} + b \tag{2.2}$$

$$a = 0.031\frac{H_i}{D_{n50}} - 0.24$$

$$b = -5.42 s_{op} + 0.0323\frac{H_i}{D_{n50}} + 0.51 - 0.0017\left(\frac{B_c}{D_{n50}}\right)^{1.84}$$

The tests of Daemen consisted of data on low-crested as well as submerged breakwaters. Most tests were performed on a breakwater covered by an armour layer with a D_{n50} of 0.040m. A few tests were performed with D_{n50} of 0.061m. The test concentrated on three parameters: relative crest height $\frac{R_c}{D_{50}}$, relative wave height $\frac{H_i}{D_{50}}$, and fictitious wave steepness $s_{op} = \frac{2\pi H_i}{gT_p^2}$. To make R_c and H_i dimensionless, the nominal diameter D_{n50} was introduced. Comparing with the method using the parameter of $\frac{R_c}{H_i}$, it has some advantages. The influence of each parameter of R_c and H_i can be studied individually. Also the influence of wave height is not lost when R_c becomes zero. Boundaries were set at K_{tmax}=0.75 and K_{tmin}=0.075, while the validity of the formulas was limited for $1<H_s/D_{n50}<6$ and $0.01<s_{op}<0.05$.

De Jong (1996) for rubble structures

De Jong (1996) proposed another transmission formula for rubble structures, described by:

$$K_t = -0.4\frac{R_c}{H_i} + \left[\frac{B}{H_i}\right]^{-0.31} * (1 - e^{-0.5\xi}) * 0.64 \tag{2.3}$$

The formula was derived based on available data on rubble mound breakwaters and breakwater with an armour layer of Tetrapods. An extensive investigation on the influences of crest width and surf similarity parameter $\xi = \frac{\tan\alpha}{\sqrt{S_{op}}}$ was carried out in his research.

Queen's (1998)

Physical model test studies were performed at the Queen's University Coastal Engineering Research Laboratory in Kingston, Canada, to assess the performance of the submerged rubble mound breakwaters under a wide range of design conditions. The testing program involved 13 submerged breakwater geometries tested under 5 different water levels with a number of incident wave characteristics. In total, approximately 800 tests were carried out with Jonswap wave spectrum. A design equation for transmission at submerged breakwaters was proposed as:

$$K_t = 1 - (e^{0.65(\frac{R_c}{H_i}) - 1.09(\frac{Hi}{B})} - 0.047(\frac{BR_c}{LD_{n50}}) + 0.067(\frac{R_c H_i}{BD_{n50}})) \qquad (2.4)$$

The formula is only valid for submerged breakwaters. It was recommended that caution be used when applying the equation outside of the following variable ranges.

$$-7.08 \le \frac{BR_c}{LD_{n50}} \le 0$$

$$-2.14 \le \frac{R_c H_i}{BD_{n50}} \le 0$$

De Jong (1996) for smooth structures

The transmission formula for impermeable structure was derived by De Jong (1996), which was

$$K_t = -0.4\frac{R_c}{H_i} + \left[\frac{B}{H_i}\right]^{-0.31} * (1 - e^{-0.5\xi}) * 0.80\,, \qquad (2.5)$$

The formula was derived based on available data sets for breakwater with an impermeable armour layer. These data sets included Delft Hydraulics (H2014), Daemrich and Kahle (Daka) Impermeable and Seeling (Bw1). The maximum value 0.80 and the minimum value 0.075 of predicted K_t were chosen. This formula is similar to equation 2.3 for rubble structure proposed by De Jong (1996). The constant coefficient of 0.80 in the second term for smooth structures was found in stead of 0.64 for rubble structures as presented in equation 2.3.

2.4 Wave spectral changes due to transmission

Goda (1985), Tanimoto et al.(1987), Raichlen et al.(1992) and Van der Meer (1990) all concluded that the mean period reduces to 0.4-1.0 of the incident mean period. This means transmission generates more waves. Furthermore, Raichlen et al.(1992) and Lee (1994) presented some examples of the transmitted wave spectrum. Both of their examples indicate the peak of transmitted spectrum is similar to that of the incident spectrum. In addition, much more energy will shift to the range of higher frequencies.

Based on the analysis of the tests performed in the flume of Delft Hydraulics, Van der Meer et al. (2000) detailed the wave spectrum changes. Some of the conclusions were as follows:

- The peak period remains more or less constant
- For $K_t > 0.15$ about 40% of the total transmitted energy is present at the higher frequencies of the spectrum, more specifically between $1.5f_p$ and $3.5f_p$.

3. 3-D WAVE TRANSMISSION TEST

3.1 General set-up

The three-dimensional wave transmission tests were carried out in the short-crested wave basin (9.0m×12.5m×0.9m) at Aalborg University, Denmark. Two structures were tested; a rubble structure and a smooth plywood structure. Analysis on influence of oblique wave attack was carried out to investigate the mechanics of three-dimensional wave transmission at these two kinds of structure.

Wave spectrum

Directional spectrum S (f,θ) is the fundamental property of ocean wave. It describes the distribution of the wave energy in both the spatial and frequency domains, and is expressed as a product of the unidirectional wave spectrum $S_\eta(f)$ and a spreading function $D(\theta, f)$, that is $S_\eta(f,\theta) = S_\eta(f)\cdot D(\theta, f)$.

$S_\eta(f)$ is the one-side frequency spectrum which is determined from the free surface elevation. D(θ,f) is the spreading function that characterises the distribution of wave energy in wave propagation directions from 0 to 2π. Even though the wave energy can be distributed in different direction, the total energy in wave field should remain constant. It is defined by $\int_0^{2\pi} D(\theta, f)d\theta = 1$. In the tests, the target irregular 3-D waves were generated using the parameterised Jonswap spectrum and spreading function of cosine distribution with spreading parameter s.

Parameterised Jonswap spectrum function:

$$S_\eta(f) = \frac{1.4}{\gamma}\frac{5}{16}H_s^2 f_p^4 f^{-5}\gamma^\alpha \exp\left[-\frac{5}{4}\left(\frac{f_p}{f}\right)^4\right] \tag{3.1}$$

$$\alpha = \exp\left[-\frac{(f-f_p)^2}{2\sigma_f^2 f_p^2}\right]$$

where: $\alpha_f = 0.10 \qquad f \le f_p$

$\alpha_f = 0.50 \qquad f > f_p$

$\gamma = 3.3$

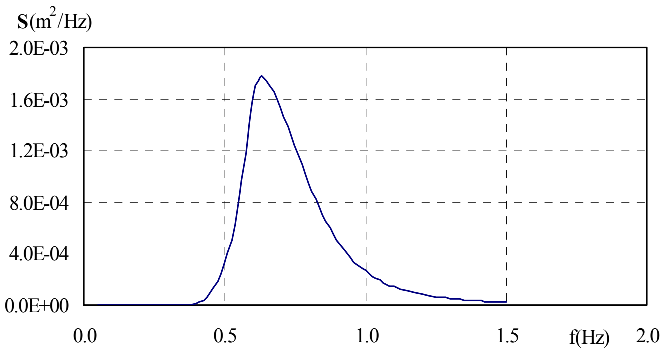

Figure 3.1 Jonswap spectrum

Several semi-empirical proposals to the formulation of D(θ,f) have been reported and most suggest to be independent of the frequency. The Cosine-power or $\cos^{2s}$ spreading function is as following:

$$D(\theta, f) = \frac{2^{2s-1}}{\pi}\frac{\Gamma^2(s+1)}{\Gamma(2s+1)}\cos^{2s}\left[\frac{\theta-\theta_0}{2}\right] \tag{3.2}$$

where: θ = wave propagation angle θ_0 =main wave propagation direction

Γ=Gamma function

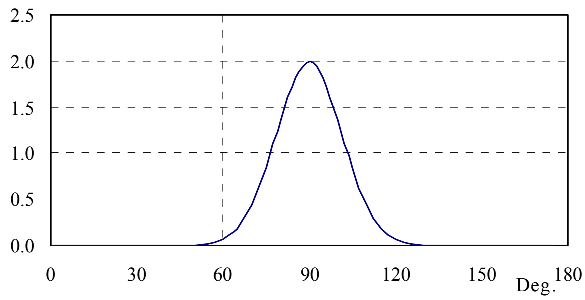

Figure 3.2 Spreading with s=50

Goda (1985) relates the relative water depth (h/L_0) and deepwater steepness to shallow water steepness. In average the relative water depth in the teat is 0.10. In this case the following parameters should be used:

Deep water steepness 0.02: s_{max}=60 (long wave, small spreading)

Deep water steepness 0.04: s_{max}=30 (short waves, moderate spreading)

In the laboratory a constant value of s=50 was used in 3-D wave generation. An example of parameterised Jonswap spectrum and spreading with s=50 are demonstrated in Figure 3.1 and 3.2

Wave depth and steepness

In total, 84 tests were performed to identify the effect of different hydrodynamic conditions for each type of structure. Being research mode, here was no actual reference to particular prototype condition. The test program was designed to explore the effect of the principal parameters. It consisted of different water levels, mainly around the crest level of the structure. Wave steepness values were either 0.02 or 0.04. Various heights from 0.07m to 0.17m, including non-broken waves and broken depth limited condition were adopted. The ratio of wave height to water depth was from 0.3 to 0.57 at rubble structures and 0.26 to 0.49 at smooth structures.

Wave direction

Oblique waves in the range 60°-110° were generated (90°=normal incidence) from wave generator. Three model layouts were tested, namely 0°, 30° and 50°. For the layout with 0°, only normal incident wave attack was tested. For the layouts with 30° and 50°, wave directions with 30°, 40°, 50°, 60° and 70° were performed by changing generating waves under an angle of 10 degrees.

Test record

A five-gauge array was used to measure the directional wave spectra. Two systems were positioned in front and rear of the structure respectively. Reflection from the rear wall of the basin was minimised using 1:5 rubble beach. A sampling rate of 30 H_z was used throughout the experiments. The record length of each test was about 15 minutes. The digital video of about three minuets and digital photos were taken for each test.

3.2 Layouts and Cross-sections

Figures 3.3 and 3.4 show examples of the layouts for rubble structure (30°) and smooth structure (50°) in pictures.

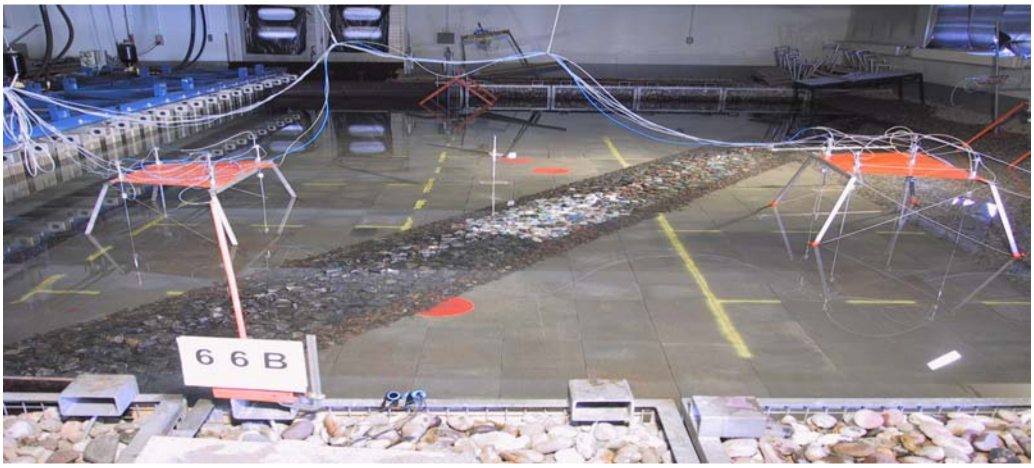

Figure 3.3 The layout of rubble structure (30°) in picture

Figure 3.4 The layout of smooth structure (50°) in picture

The structures were located at a plateau 0.16m above the deepwater seabed. The water level in deep water was varied from 0.36m to 0.51m, which gives water depth from 0.20m to 0.30m at rubble structures and from 0.25m to 0.35m at smooth structures. It is shown in the following sketch.

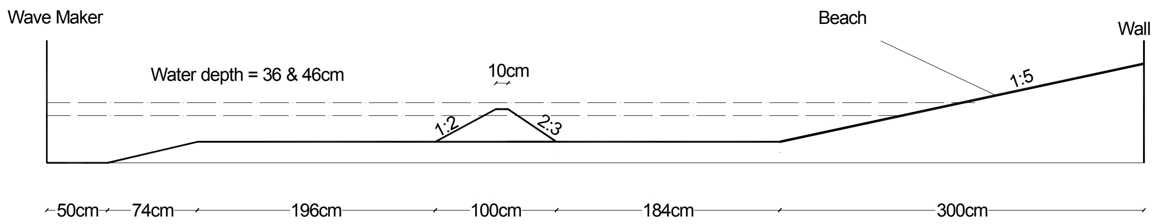

Figure 3.5 Bottom topography and location of rubble structures in transmission tests

Rubble structure

Three types of quarry rock were used in the cross-section, called type A, B and C. Approximate sizes were: $D_{n50,\,A}$=4.7cm, $D_{n50,\,B}$=3.1cm, and $D_{n50,\,C}$=1.6cm.
Height of rubble structure: 25 cm
Width at sea bed: 100 cm
Crest width: 10 cm
Slope: seaside 1:2, lee side: 2:3
For the cross section, see Figure B-1 in Appendix B. The layouts with 0º, 30º and 50º are shown in Figure B-2, B-3 and B-4 in Appendix B. A concrete block wall was constructed for layout with 0º in the basin. Only the area behind the right structure was used.

Smooth structure

The plywood structure was made from 4 sections with each 2.5m long giving a total length of 10m.
Height of smooth structure: 30 cm
Width at sea bed: 170 cm
Crest width: 20 cm
Slope: seaside 1:3, lee side: 1:2
Figure B-5 in Appendix B shows the cross section of smooth structure. The layouts with 0º, 30º and 50º are presented in Figure B-6, B-7 and B-7. Five-gauge system in layout with 0º was rotated and oblique waves were generated to achieve perpendicular wave attack.

3.3 Stone size and grading of armour layer

Three types of available stone were mixed to one grading and after the tests sorted out again. These stones were kept in boxes, here numbered as boxes 1, 2 and 3. In some layouts another stone type was used, here called box 4. The stone grading and shape of all the boxes were measured by taking 75 stones from each box. The weight and three dimensions, L, B and H, were measured of each stone. From the measurements a grading curve (actually a weight curve) was constructed, and for the mixed boxes 1-3 a grading curve was composed from the separate boxes, knowing the volume used for mixing for each of the boxes. The grading curves are given in Figure 3.6.

In the figure 15%, 50% an 85% lines have been given. A grading can be represented by a straight line on a log-linear plot as in Figure 3.6.

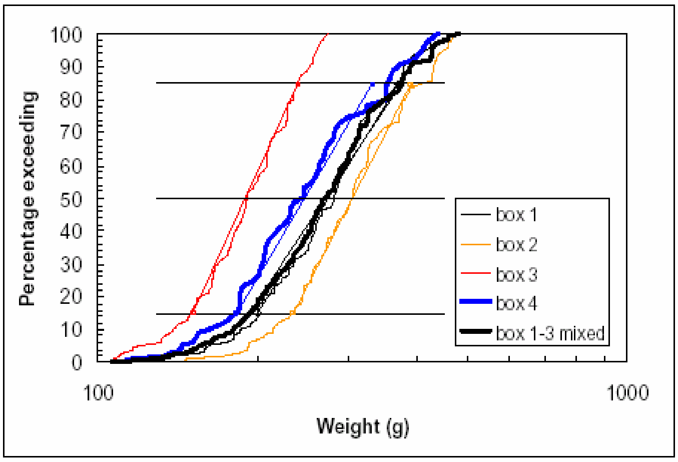

Figure 3.6 Stone gradings of boxes 1-4 and mixed grading of boxes 1-3

The grading should be more or less straight between 15% and 85% lines. These lines have been fitted through the actual curve, giving the W_{50} and grading D_{n85}/D_{n15}.

From the dimensions of each stone, the ratio largest/smallest dimension L/H was calculated. The percentage of stones (in number, not in weight) exceeding this ratio has been given in Figure 3.7. A ratio of 1.0 means a cube or sphere. The larger the ratio the more elongated the stones are. The shape can be described by two values: the percentages for exceeding 2L/H and 3L/H. Another parameter that gives an idea about the shape of the stones is the blockiness coefficient, which is defined as the volume of the stone divided by its cubical dimensions: $B_k = V/(L \times B \times H)$

The mass density of all the stones was 2650 kg/m^3. With the measured weight the volume can be calculated. The blockiness coefficient for each stone was calculated, together with the average blockiness coefficient. The blockiness coefficient normally ranges between 0.4 and 0.7. The low value means elongated, flaky stones, the upper value cubical stones.

Table 3.1 gives summary results from Figures 1 and 2. The mixed boxes 1-3 can be characterised by an average weight of W_{50} = 270 g and a grading of D_{n85}/D_{n15} = 1.25, which is a fairly narrow grading. The shape of the stones in boxes 1-3 varied a lot. Box 2 had stones where

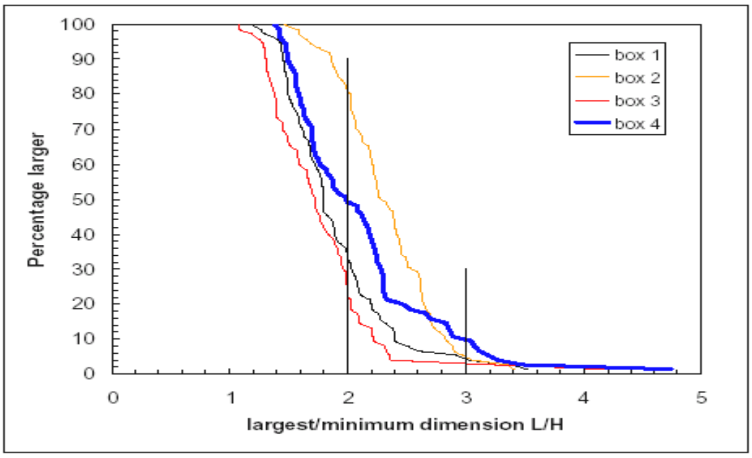

Figure 3.7. Shape of the stones

Grading	Box1	Box2	Box 3	Box 4	Box 1-3 Mixed
W_{15} (%)	200	234	152	183	194
W_{85} (%)	370	390	239	330	375
W_{85}/W_{15}	1.85	1.67	1.57	1.8	1.93
D_{n85}/D_{n15}	1.23	1.19	1.16	1.22	1.25
W_{50} (g)	272	302	191	246	270
W_{50} curve(g)	280	303	191	244	269
Shape					
> 2L/H (%)	35	81	25	49	+/-50
> 2L/H (%)	4	4	3	9	+/-4
Blockiness	0.42	0.41	0.43	0.43	0.42

Table 3.1 Summary of grading and shape of stones

81% had a dimension L/H larger than 2. For box 4 this was only 25%. An estimation for the mixed boxes 1-3 is that 50% of the stones had a dimension larger than 2L/H and only 4% larger than 3L/H. Box 4 had an average weight of W_{50} = 246 g and a grading of D_{n85}/D_{n15} = 1.22. This is only a little lighter than the mixed boxes 1-3 and the same grading. The shape was also similar. In all cases the blockiness coefficient was around 0.42, describing the elongated and flaky shape of the stones. So, the nominal diameter of rock size can be calculated

$$D_{n50} = \sqrt[3]{\frac{W_{50}}{\rho}} = 0.047m$$

4.0 DATA PROCESSING

4.1 BDM method

A package for directional wave analysis, PADIWA, was provided by Department of Civil Engineering, Aalborg University, and was used in this research. In the package, the Bayesian Directional Spectrum Estimation Method (BDM) was adopted to estimate directional wave spectrum. A brief introduction of BDM method is given here.

A convenient way to describe a three-dimensional sea state in the frequency domain is to determine the corresponding directional wave spectrum. This assumes that it is possible to describe directional irregular waves as a sum of regular waves each travelling with one frequency and in one direction.

An analysis based on surface elevation yields the following relation between measurement at position n and m and the corresponding directional wave spectrum.

$$\frac{S^*_{\eta_n\eta_m}(f)}{S_{\eta\eta}(f)} = \int_0^{2\pi} D(f,\theta)\exp(ik(d,f)r_{nm}\cos(\theta-\beta_{nm}))d\theta$$

Where

$S_{\eta\eta}(f)$ is the autospectrum (wave energy spectrum)

$S_{\eta_n\eta_m}(f)$ is the cross-spectrum between η_n and η_m

* Denotes the complex conjugate

$D(f,\theta)$ is the directional spreading function, $S(f) = D(f,\theta)S(f)$

$k(d,f)$ is wave number

d is depth of water

f is frequency

r_{nm} is the distance from position n to m

β_{nm} is the angle from position n to m

θ is the direction of travel

i is the imaginary unit ($=\sqrt{-1}$)

So it is possible to estimate the directional wave spectrum based on recorded time series of some wave properties, e.g. surface elevation, sub surface pressure or particle velocities. However, a transformation to surface elevations is required, if the above equation is to be used.

An analytic solution to above equation has not been achieved, giving rise to various fitting methods. The Bayesian Directional Spectrum Estimation Method, BDM, has been proposed for this purpose.

As opposed to other methods, by avoiding a-priori assumptions regarding e.g. the shape of the directional spreading functions, the BDM method is relatively unrestricted. It does, however, assume the directional spreading function to be smooth. This advantage especially arises when analysing field measurements, where no target conditions exist.

The BDM method is used for analysis of directional wave spectrum. Subsequently it can be used to estimate the reflection from structure exposed to short crested wave. Having estimated the complete directional wave spectrum it is possible to extract information on the incident and reflection wave respectively. Therefore it is also possible to assess the reflection performance of the structure causing the reflection.

4.2 Input of program

The present software package of PADIWA contain programs for cross-spectral analysis of time series, estimation of directional wave spectrum using BDM and presentation of results, To run the program, required input information, such as filing, geometry, sampling rate etc., must be stored in a set-up file. The main information defined in the calculation process is introduced here.

Layout of data file: Lines in header are 2400, number of gauges is 5.
Number of columns to skip is 5. Columns 1, 2, 3, 4 and 5 are for see side calculation and columns 6, 7, 8, 9 and 10 are for lee side calculation.

Spectral analysis: 1024 (2^{10}) FFT elements, 20 % of tapering, 20 % of overlapping

Acquisition: 40 sampling rate in H_z
Calibration coefficients 0.01, that will result the dimension in meter.

Physical condition: Depth of water in meter

Position of gauges:

No. of Gauge	Coordinate X	Coordinate Y
1	0.00	0.00
2	-0.18	0.56
3	0.30	0.40
4	0.59	0.00
5	0.77	0.56

The number of discrete directions in the directional spreading functions is typically in the range from 36 to 72, corresponding to $\Delta\theta$ from 10° to 5°. In this research the directional spreading functions were discretized into 72 intervals causing a directional resolution of $\Delta\theta$=5°. The frequency bandwidth was 0.039 H_z.

For the orientation of gauges the system 1 was used which means that the incident waves are in range [0°: 180°]. This will form the basis for estimating reflection coefficients. Waves propagating between 180° and 360° are reflected waves.

4.3 Processed Results

The program presented the incident significant wave height and reflected wave height based on based on spectrum $4\sqrt{m_0}$, wave main directions and energy density distributions. Finally, the program drew four graphs showing results as a function of frequency: 1) spectral density of incident and reflected waves; 2) main direction and directional spreading of incident waves; 3) reflection coefficients; 4) main direction and directional spreading of reflected waves. The results were shown in the frequency domain.

To examine the processed results from the program, the measured incident wave spectra and parameterised Jonswap target spectra are plotted in Figure 4.1. It indicates that the total energy and the shape of wave spectrums are close to each other. The decreased energy is evident in the transmitted spectrum after wave transmission. The processed results are summarised in Table A-1 and A-2 for rubble structures, and Table A-3 and A-4 for smooth structures, see Appendix A.

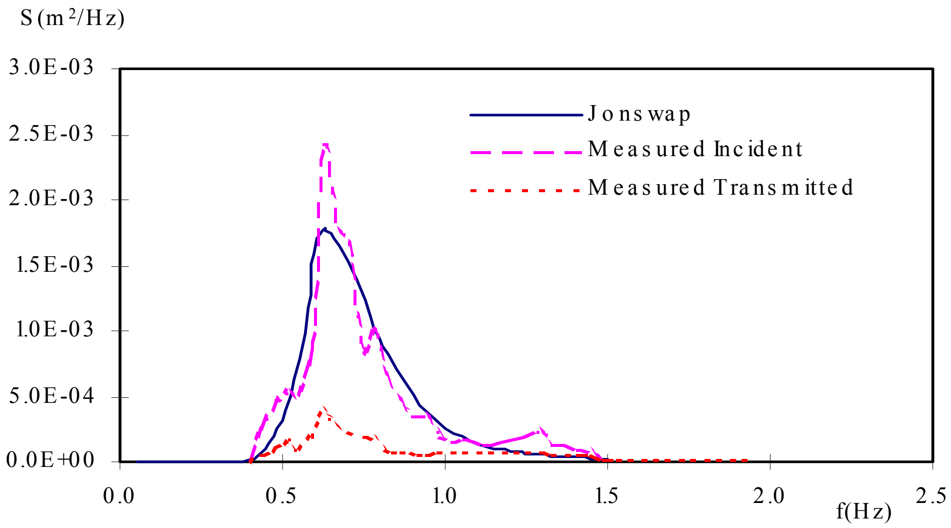

Figure 4.1 Comparison of wave spectra

Analysis on individual gauge was also carried out using the WAVELAB program provided by Department of Civil Engineering, Aalborg University. A 10-gauge data set was calculated for time series analysis of surface elevation in each test. Tables A-8 and A-9 in Appendix present the results of the WAVELAB calculations. It can be found that wave heights and wave periods calculated by the BDM and WAVELAB are similar. However, generally the wave heights from individual gauge analysis are a little higher than those from the BDM program. This could be caused by the wave reflection. As mentioned above BDM program can extract information on the incident and reflection wave respectively. While on the contrary the individual gauge analysis gives the totally energy comprising incident and reflection wave, therefore bigger wave heights are expected.

5.0 ANALYSIS OF DATA

5.1 Overview

The relations between transmission coefficient K_t and relative freeboard R_c / H_i for rubble and smooth structures are shown in Figures 5.1 and 5.2. They give the first impression of the measured transmission coefficients. The data set at the smooth structures are much more scattered than rubble structures. The different influences of wave direction on two types of the structures can already be perceived from them. The data of smooth structures are more scattered than rubble structure. The incident wave directions demonstrate more influence on transmission at the smooth structures than the rubble structures. Furthermore, all present data together with other available data for rubble structures are potted in Figure C-1 and C-2. They are generally in agreement with previous tests. All available data including DELOS data for perpendicular wave attack at smooth structures are redrawn in Figure C-3. It can be found that the present data are in higher positions. A more detailed analysis and explanation will be given in Chapter 6.

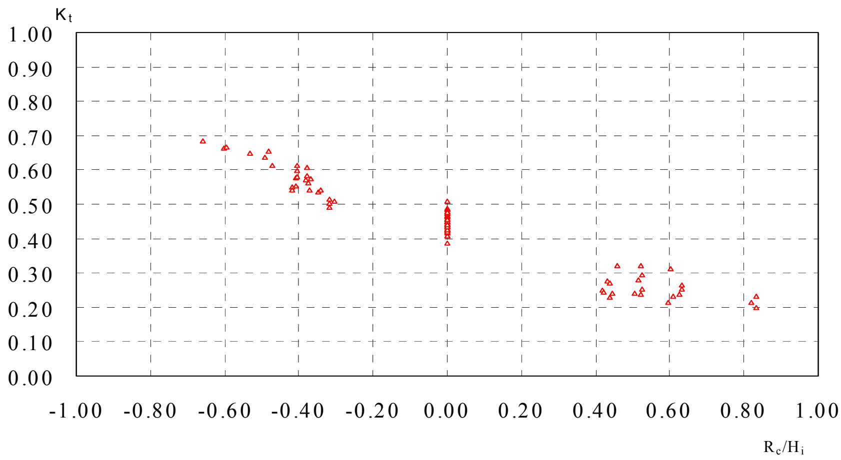

Figure 5.1 K_t—R_c/H_i at rubble structures

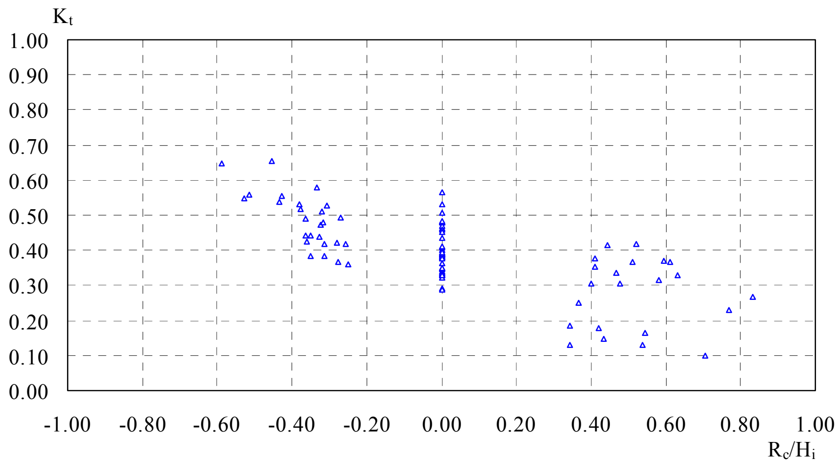

Figure 5.2 K_t—R_c/H_i at smooth structures

5.2 Influences of short-crested wave transmission parameters

To obtain a good understanding of the short crested wave behaviour, the transmission coefficients were analysed with respect to the various incident waves and structure characteristics. The influences of dominant wave parameters and comparison with previous 2-D wave transmission studies were investigated by grouping the data sets and plotting some simple graphical trend analysis of the data.

Freeboard

Figures 5.1 and 5.2 demonstrate that the crest freeboard R_c has a strong influence on the wave transmission. It is an important parameter both for rubble mound and smooth structures. Changes in R_c affect the amount of wave energy that can pass over or through the structures. In all analysed cases, it is clear enough the lower the freeboard the higher the wave transmission. The transmission coefficient at lower-crested structures is very sensitive to the freeboard.

Wave height

The data were sorted into groups of wave incident angle, freeboard and wave steepness. The general trend of wave height influence can be found in Figures C-4, C-5 and C-6 for rubble structures and Figures C-7, C-8 and C-9 for smooth structures.

The measured relative freeboard R_c/H_i is in the range from -0.65 to 0.83 for rubble structures and -0.59 to 0.83 for smooth structures. The different influences of wave heights can be identified corresponding to various water levels.

When structures are submerged, higher wave heights will lead to a lower K_t. Bigger waves will be more affected by crest levels than smaller ones. When the water levels are lower than the crest levels, higher wave heights will lead to larger transmission coefficients. Increasing wave heights will cause more overtopping and therefore more wave transmission. The influences of wave heights seem not significant around R_c=0.0, especially for smooth structures. Physically it is possible. A dividing point should exist to convert the negative into positive influences and vice versa.

Wave Steepness

Wave steepness plays a same role as described in previous 2-D tests. It can be seen that smaller steepness gives a larger transmission in Figures C-4 — C-9. Waves with longer period can propagate easier through the rubble structure body. At the same time waves with longer period will increase the run-up levels at rubble and smooth structures, so larger transmission coefficients are expected.

Incident wave direction

It should be pointed out that the wave direction perpendicular to structure is defined as 90° in the physical model tests. But it has been changed to 0° instead of 90° in the following data analysis as indicated in Figure 5.5. So this will lead to target wave angles should be expressed in 0°, 20°, 30°, 40°, 50° and 60° corresponding to 90°, 70°, 60°, 50°, 40° and 30° in the physical model tests.

Rubble structure

When the wave attack is oblique to the alignments of the structure instead of perpendicular, what will then be the influence of incident directions?
The relation between transmission coefficients and incident angles for rubble structures can be discovered in Figure C-10. It indicates that the transmission is slightly influenced by incident direction. Furthermore, transmission of waves with a smaller steepness is less affected by incident direction than that with larger steepness. Especially when the structures are submerged, incident wave angle hardly has influence on long wave transmission. Physically, when wave attack is oblique to the structures instead of perpendicular, the distance they travel will be longer and more energy will be dissipated, therefore less transmission. Longer wave can pass the structure unhindered, while shorter wave is influenced by structure. It can be concluded that the transmission of shorter wave is more sensitive to the wave direction. However, the average decrease of over the range from 0° to 70° is only about 10% for wave with smaller steepness. The influence of wave direction with bigger steepness is even less.
For rubble structure, the transmission is dominated both by overtopping and the transmission through the structure body. The transmission mechanics at rubble structures is more complicated than smooth structures. Generally speaking, for the rubble structure the influence of incident wave direction on wave transmission is small. The structure slope set in the physical model tests is 1:2 at the seaside. But when the slope of rubble structure is gentler than 1:2, for example 1:3 or 1:4, then the influence of wave direction maybe become significant? In addition, wave transmission passing through rubble structures probably is less influenced by the incident wave angle when the crest width is relatively small, because the travel distance could not increase a lot as wave angle become bigger. Probably this is the case as a narrow crest width of 0.10 m was adopted in the tests. More physical tests with wider crest and gentler slope are needed to make these arguments convincing.

Smooth structure

Figure C-11 shows the relation between transmission coefficients and incident directions for smooth structures. It shows that incident wave angles strongly affect the transmission.

Physically, smooth structures are impermeable, there is no transmission through the structure. The transmission is purely influenced by run-up and overtopping. Bigger incident wave angle leads to longer distance or gentler slope, therefore less run-up and smaller transmission. An expression of wave direction influence is derived in Chapter 6.

The influence of the wave angle could be dependent on the slope of structure. For smooth structures, a gentle slope of 1:3 was set in this research. When the slope becomes steep, for instance 1:1.5 or 1:2, the wave does not break on the slope in some cases, the influence of incident wave angle could become weak.

5.3 Comparison between short-crested and long-crest wave transmission

Due to the energy spreading, the direction of a single wave could be different from the main wave direction; some can be perpendicular to the structures. Can the transmission of short-crested waves be larger than that of short-crested waves especially for larger incident angles? Three-dimensional tests in a short-crested basin were carried out to investigate the influence. For each type of structure with a freeboard of zero, 10 long-crested wave tests with grouped set-ups were performed. To analyse the influence, the short-crested (3-D) and long-crested (2-D) wave data under similar conditions are plotted as a function of incident wave directions in Figures 5.3 and 5.4.

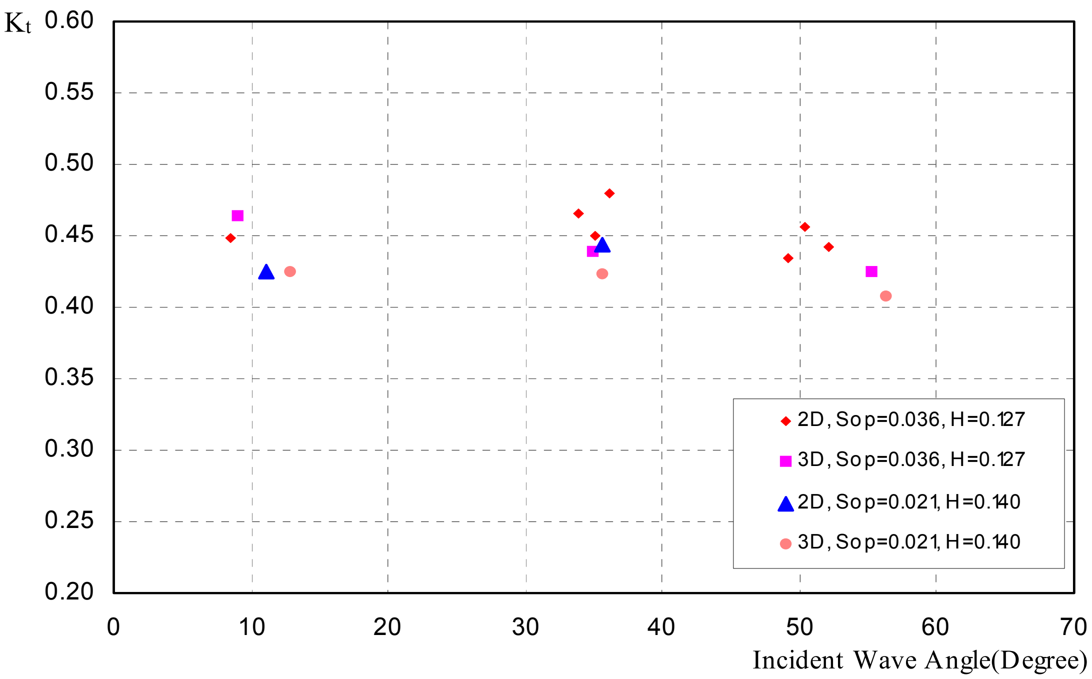

Figure 5.3 Comparison between short-crested and long-crested wave transmission at rubble structures

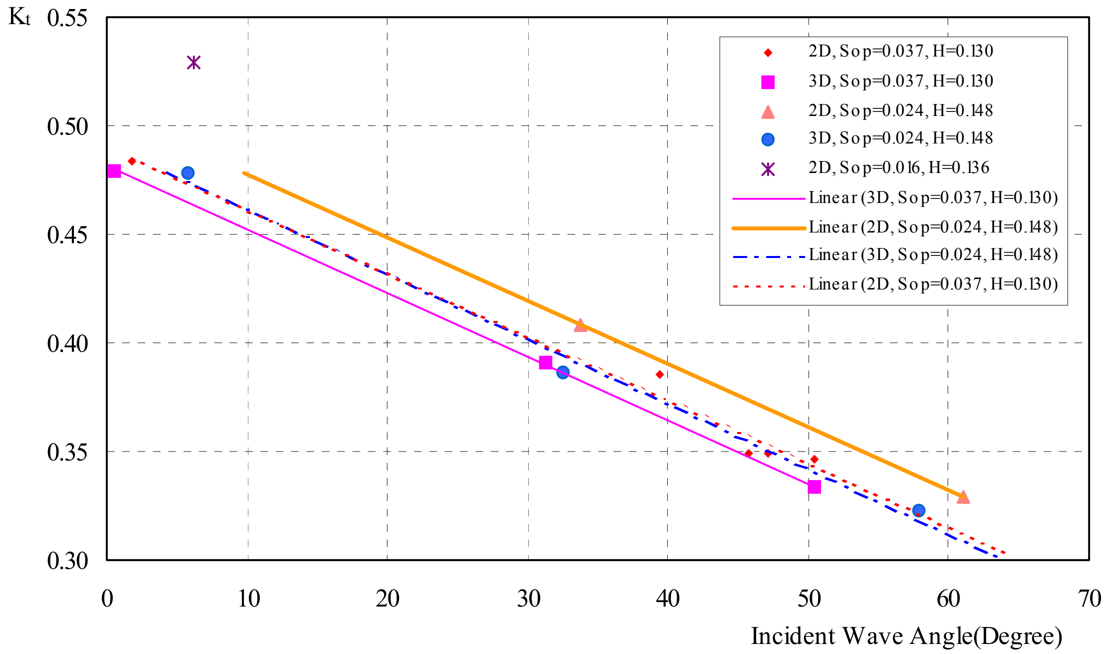

Figure 5.4 Comparison between short-crested and long-crested wave transmission at smooth structures

It can be identified that the short-crested wave transmission is marginally smaller than the long-crested wave transmission both for rubble and smooth structures. Rubble structures do not present any clear influence of wave parameters. For smooth structures, regular influence trends seem clearer. The gaps of transmission coefficient between 2-D wave and 3-D wave do not vary with incident wave directions but wave steepness, the larger wave steepness the smaller difference. However, the 3-D wave transmission coefficients are about 3% smaller than 2-D wave both for rubble and smooth structures. From engineering point of view, it is slight.

Physically, although some waves can be perpendicular to the structures in 3-D wave field, it also should be aware that there are some waves will attack structures with more oblique angles. That could balance the increasing perpendicular wave energy partly and make no substantial difference present.

5.4 Validation of existing transmission formulae

Rubble structure

Based on 2-D tests, some transmission formulae have been derived. For conventional breakwaters, a practical formula was presented in Daemen (1991), see equation (2.2). De Jong (1996) also proposed one transmission formula (2.3) for rubble structure in his master thesis.

An extensive investigation on submerged breakwaters was carried out in Queen's University and an improved design equation (2.4) was proposed for submerged breakwaters only.

The influence of short crested wave parameters has been analysed in section 4.3. It was concluded that the influence of each dominant parameter has the same trend in 2-D and 3-D wave fields. Moreover, the wave direction hardly plays a role on wave transmission at rubble structure, so the wave direction influence can be ignored and all DELOS data can be used when existing formulas are validated.

Firstly, the equation developed by Queen's University was used. The relation between measured (DELOS data) and calculated K_t (Queen's) is present in Figure C-12. Clearly, they can not fit well. It is not surprising because their study only focussed on the submerged structures and DELOS data are not completely in the recommended boundaries.

$$-7.08 \le \frac{BR_c}{LD_{n50}} \le 0, \quad -2.14 \le \frac{R_c H_i}{BD_{n50}} \le 0$$

The boundaries in DELOS tests were calculated to investigate the application range for present research. They were found in the following ranges:

$$-0.06 \le \frac{BR_c}{LD_{n50}} \le 0.06, \quad -1.49 \le \frac{R_c H_i}{BD_{n50}} \le 1.49.$$

The DELOS data at the structures with positive freeboard are not in Queen's boundaries. The data within the boundaries $-0.06 \le \frac{BR_c}{LD_{n50}} \le 0$ and $-1.49 \le \frac{R_c H_i}{BD_{n50}} \le 0$ ARE located in Queen's recommended ranges, but they still can not fit very well. Probably the influence of crest width derived by Queen's University is not true for the structures with narrow crest.

Secondly, the transmission formula (2.3) derived by De Jong (1996) was used. Figure C-13 in Appendix C shows the relation between measured (DELOS data) and calculated K_t (De Jong). Although the agreement is much better, the calculated for submerged conditions results are still higher than the measured.

Finally, the transmission expression proposed by Daemen (1991) was used. From Figure C-14, it can be found that results agree well and all data are better than those calculated by Queen's equation and De Jong's formula although the scatter does still exist. A further study on this formula, however, indicates that it can not fit the data of Queen's University as shown in Figure C-15. Only the data with narrow crest width are close to coefficients by Queen's University. Others are much higher than the measured.

In conclusion, none of the existing formulae of wave transmission at rubber structures are sufficient for application over a wide range of incident wave characteristics and structure geometries. A more extensive investigation is necessary, especially to describe the influence of the crest width.

Comparatively speaking, the transmission formula proposed by Daemen (1991) could be regarded as a best expression in term of the agreement to oblique wave transmission as performed in present research.

Smooth structure

Based on data sets of Delft Hydraulics (H2014), Daemrich and Kahle (Daka Imp.) and Seeling (Bw1), De Jong (1996) derived transmission a formula for impermeable structures, see equation (2.5). This formula is similar to equation 2.3 for rubble structures proposed by him. More extensive researches have been carried out since then and therefore more data became available to evaluate the formula.

A physical model test investigation was performed in a wave flume of Delft Hydraulics and the results were analysed by Infram. Totally five different structures were tested: smooth (asphalt) with various crest widths, smooth covered with rock and a very wide caisson. All slopes were 1:4, both seaward and landward of the crest. In total 18 test results of smooth (asphalt) structures are given in the Table A-6.

Data are also selected from the present DELOS tests. 20 tests of perpendicular wave attack were performed with different water levels, wave heights and peak frequencies. Although most of these data come from 3-D wave transmission tests, the difference between 2-D and 3-D wave transmission is slight as concluded in section 5.3. That makes it possible to adopt these data in the validation process.

All data of waves perpendicular at smooth structures are summarised in Tables A-5, A-6 and A-7. The cross sections used in the tests are illustrated in Figures B-9, B-10 and B-11. Figure C-16 in Appendix C shows the relation between measured and calculated transmission coefficient K_t (De Jong). Obviously the formula does not fit the data sets of Infram and DELOS for lower values of transmission coefficient. It requires that a new formula must be developed first before the influence of wave direction is investigated. A detailed study on wave transmission at smooth structures is presented in Chapter 6.

5.5 Change of wave main direction after transmission

Rubble structure

The wave spectrum is significantly modified due to wave breaking. The modifications cover not only wave energy but also wave direction. The definition of wave direction used in the present research is sketched in Figure 5.5.

Figure C-17 presents the relation between incident and transmitted wave direction at rubble structures. To investigate the influences of some dominant parameters, the data are sorted out and plotted in the figure. It can be seen that the wave direction will change after transmission. The influences of freeboard and wave steepness are not evident in the figure. The transmitted wave direction is chiefly affected by incident wave angle. Statistical study found that the incident and transmitted wave directions have a linear relation and the scatter is normal, as confirmed by the correlation coefficient R^2=0.94. The mathematical expression can be obtained:

$$\beta_t = 0.8\beta_i + 2.9$$

Where β_t is transmitted wave angle in degree:

β_i is incident wave angle in degree

However, this expression will give a constant value of β_t=2.9 degrees for transmitted wave direction when the incident wave is perpendicular to the structures β_i=0°. Physically it is not correct. No reasons can explain that perpendicular waves will change their main directions after transmitted. This could be caused by measurement error and should be discarded. Therefore, the final equation will become:

$$\beta_t = 0.8\beta_i$$

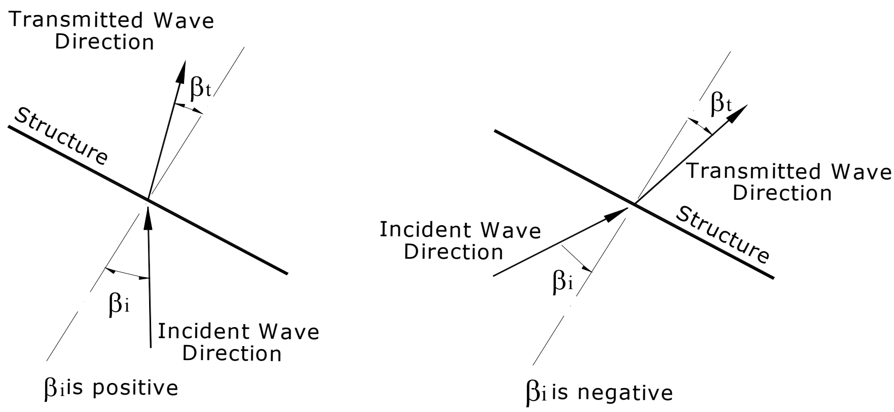

Figure 5.5 Sketch of incident and transmitted wave directions

Smooth structure

To study the wave direction change after transmission at smooth structures, the relation between incident and transmitted wave directions is shown in Figure C-18 using grouped data sets. In addition, the net direction changes vs. incident wave angles are drawn in Figure C-19. One clear trend is presented in the figures. When the incident wave angles are larger than 50 degrees, the transmitted wave angles will not change with incident wave directions and become constant.

The test data are scattered around the line of “Transmitted Angle =0.9*Incident Angle” in the angle range from 0° to 50°. The wave parameters, such as freeboard and wave steepness, could contribute the scatter. However, the influence for one single parameter is not evident in the figures. To estimate the transmitted wave direction at smooth structures, the relation is approximately described by the following expression:

$$\beta_t = 0.9\beta_i \quad \text{if } \beta_t < 50°$$

$$\beta_t = 45° \quad \text{if } \beta_t \geq 50°$$

Due to the physical limit, the above relation can only be applied to the situation that the relative freeboard R_c/H_i is larger than -1.0. When $R_c/H_i \leq -1.0$, the influence of the structures will loose its influence and every wave can pass unhindered. Therefore, the wave directions will hardly change. The transmitted wave directions equal to the incident wave directions, $\beta_t = \beta_i$.

6. OBLIQUE WAVE TRANSMISSION FORMULA FOR SMOOTH STRUCTURES

6.1 Analysis on the existing formula

To derive a formula for oblique wave transmission at smooth structures, first a modified formula for perpendicular wave transmission has to be developed based on the present data sets. And then the formula for oblique wave transmission can be achieved by analysis on the wave direction influence from the DELOS data set.

The conclusion was reached that the transmission formula derived by De Jong (1996) can not describe the data sets of Infram and DELOS accurately enough, and a more detailed investigation is necessary. To modify an equation for perpendicular wave transmission at smooth structures, the approach described by De Jong will be reviewed and the cause that could produce inaccurate outcomes maybe can be found.

De Jong analysed the data in a similar way as was originally done by Van der Meer and Daemen for rubble structures. The equation is related to the relative freeboard and expressed by

$$K_t = a\frac{R_c}{H_i} + b$$

in which: **a** determines the slope of the line, and appears to be independent of any of the parameter considered.

b is the value of K_t when $\frac{R_c}{H_i} = 0.0$

De Jong used two parameters, relative crest width $\frac{B}{H_i}$ and surf similarity parameter ξ to describe the coefficient **b**. All available data with $\frac{R_c}{H_i} = 0.0$ were taken and investigated on the influence of relative crest width, relative wave height and fictitious wave steepness or surf similarity parameter. After having determined the influences of above each parameter, all data with other values of $\frac{R_c}{H_i}$ will be taken into account. With the found formula for **b,** the influence of any parameter on the slope angle **a** will be determined.

The relation between the relative crest width $\frac{B}{H_i}$ and wave transmission coefficient was studied by analysis on general influence trend of relative crest width $\frac{B}{H_i}$. De Jong assumed that the influence of the crest width is the same order of magnitude $\left[\frac{B}{H_i}\right]^{-0.31}$ for impermeable as for rubble mound breakwaters. He also pointed out that there is a lot of scatter, for which no reasonable explanation could be found. In addition, it was also assumed that the slope of line, **a**, has the same value as has been derived for rubble structure, namely –0.40.

However, analysis on the present available data does not support these two assumptions. There is no doubt that a large influence of crest width is present at rubble structures. But for smooth structures the influence is different. Van der Meer et al. (Infram, 2000) found that the width of crest hardly plays a role at smooth structures.

The present analysis on data sets of Infram, DELOS and H2014 also show that there is very little difference among the smooth structures with various crest widths. This phenomenon can be explained by the way of wave breaking and the smooth surface as already pointed out by Van der Meer et al. (Infram, 2000). Waves will break over the gentle slope and the up-rushing wave tongue jumps over the smooth crest. In this process the width of the crest plays hardly a role as the surface is smooth without friction or permeability to disperse the wave energy. Therefore, the influence of $\frac{B}{H}$ should be ignored instead of $\left[\frac{B}{H_i}\right]^{-0.31}$. It gives a reasonable explanation why there is a lot of scatter in De Jong's studies.

But, the influence of $\left[\frac{B}{H_i}\right]^{-0.31}$ is obvious in the Daemrich and Kahle (Daka Imp.) data sets. In present research, the same general influence trend of $1-e^{-0.5\xi}$ for surf similarity parameter was found as De Jong's. Further study indicates that influence of relative crest width is related to the surf similarity parameter ξ. For different values of ξ, waves break in a completely different way. When ξ, is smaller than the value around 3, the plunging breaker type occurs on the slope. The transition between breaking and non-breaking lies around ξ =2.5-3. The waves with ξ=3 to 5 can be identified as surging type. Therefore, when $\xi \geq 3$, waves do not break on the slope. But they could be forced to break on the crest. On the wider crest, the more energy will be dissipated. Moreover if a wave can not jump over a smooth crest, the part of energy will be lost on it. The influence of $\frac{B}{H}$ is significant for $\xi \geq 3$ as shown by the Daemrich and Kahle (Daka Imp.). So different expressions should be given according to the value of the surf similarity parameter.

Regarding the other assumption about the slope of the line a=-0.40, a closer look indicates it is not completely exact for either the previous or current data sets.

6.2 Derivation of modified formula for perpendicular wave attack

As long as the weaknesses in the previous formula were found, the further study will focus on them and derive a more precise formula based on the data sets of Delft Hydraulics (H2014), Daemrich and Kahle (Daka Imp.), Seeling (Bw1), Infram and DELOS. The same procedure as described in De Jong (1996) will be followed to derive a modified formula for wave transmission at smooth structures. This process and outcome are summarised as followings:

- Find the influence expression of $\frac{B}{H_i}$ when $\frac{R_c}{H_i}=0.0$. The trend is $\left[\frac{B}{H_i}\right]^{-0.31}$ only for Daemrich and Kahle (Daka Imp.) data set when $\xi \geq 3$, see Figure 6.1. Other data sets indicate that influence of $\frac{B}{H_i}$ is not evident. To ignore the influence of relative crest width, it was assumed the influence is $\left[\frac{B}{H_i}\right]^{0}=1.0$ for $\xi<3$.

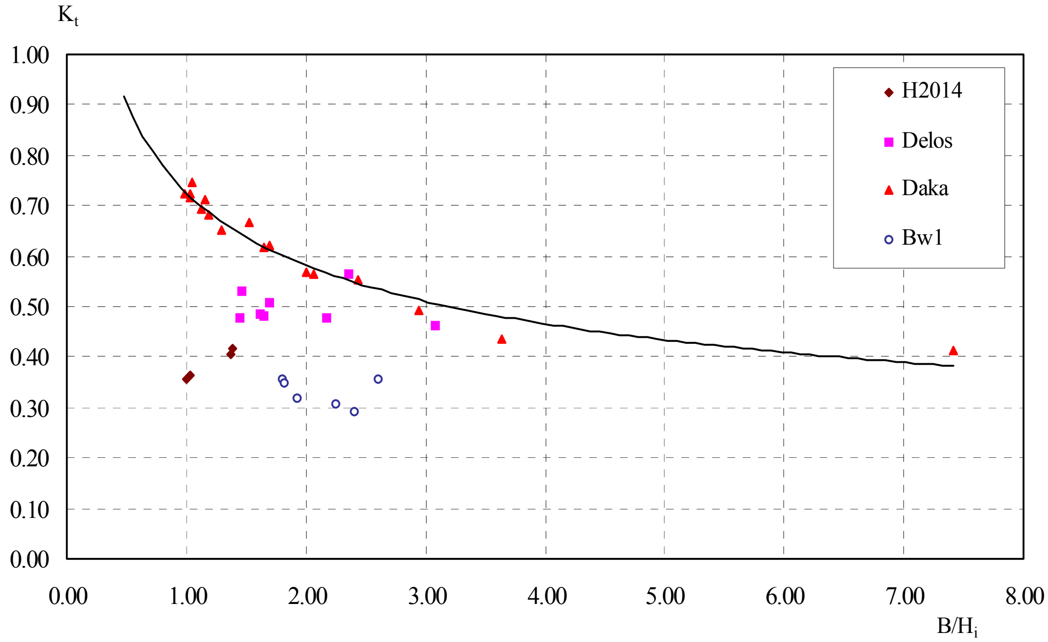

Figure 6.1 Relation between K_t and B/H_i for R_c=0.0 at smooth structures

- Use data sets with $\frac{R_c}{H_i}=0.0$, find the influence of ξ after the different influence expressions of relative crest width are taken into account, $\left[\frac{B}{H_i}\right]^{-0.31}$ or $\left[\frac{B}{H_i}\right]^{0}$. The general influence trend of surf similarity parameter can be found as $1-e^{-0.5\xi}$, see Figure 6.2.

- Then the formula can be assumed as $K_t=a\frac{R_c}{H_i}+\left[\frac{B}{H_i}\right]^{-0.31}*(1-e^{-0.5\xi})*c$ for $\xi \geq 3$ or $K_t=a\frac{R_c}{H_i}+(1-e^{-0.5\xi})*c$ for $\xi<3$. Use data sets with $\frac{R_c}{H_i}=0.0$ to find

$c = \dfrac{K_t}{\left[\dfrac{B}{H_i}\right]^{-0.31}(1-e^{-0.5\xi})}$ or $c = \dfrac{K_t}{1-e^{-0.5\xi}}$. Use all data sets with $\dfrac{R_c}{H_i} = 0.0$, the average value of c is found as 0.75.

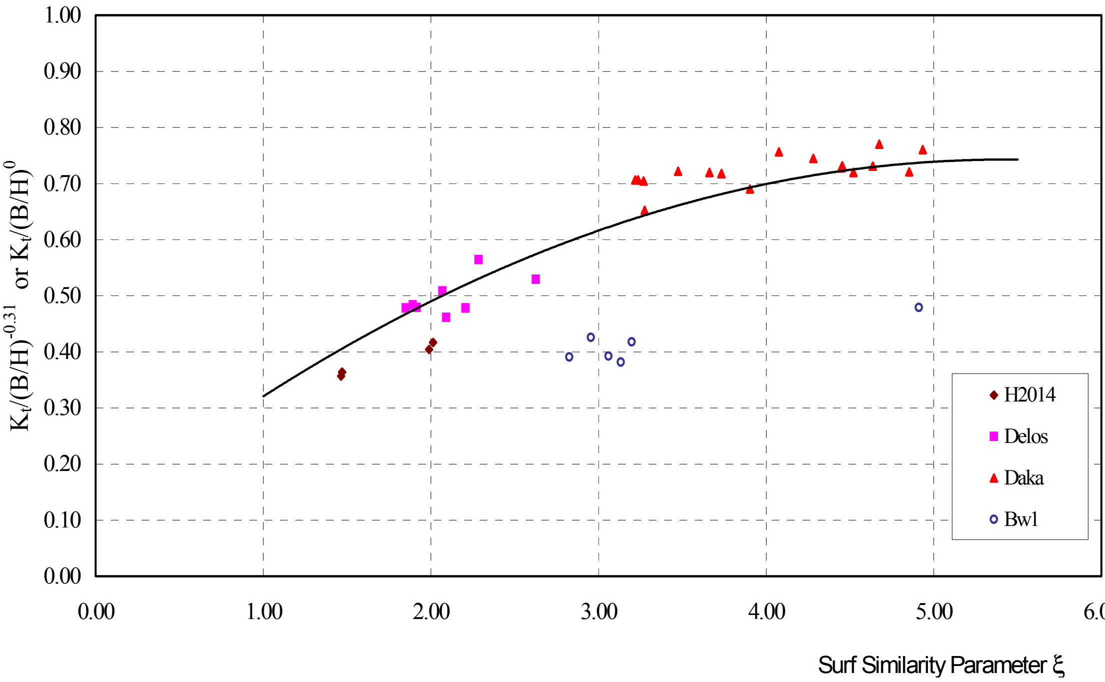

Figure 6.2 Relation between $K_t/(B/H)^{-0.31}$ and surf similarity parameter ξ at smooth structures

- Take into account all data sets, the coefficient **a** is derived by equation $a\dfrac{R_c}{H_i} = K_t - \left[\dfrac{B}{H_i}\right]^{-0.31} * (1-e^{-0.5\xi}) * 0.75$ and $a\dfrac{R_c}{H_i} = K_t - (1-e^{-0.5\xi}) * 0.75$. The average value of a is calculated as -0.30.
- With the found coefficients and general influence trends for each term, the final formulas are expressed by equations 6.1 and 6.2. The boundaries are limited within the ranges of test set-ups.

$$K_t = -0.30\frac{R_c}{H_i} + 0.75(1-e^{-0.5\xi}) \qquad (6.1)$$

Tested boundaries: $1.0 < \xi < 3.0$, $1.0 < \dfrac{B}{H_i} < 8.6$

$$K_t = -0.30\frac{R_c}{H_i} + 0.75\left[\frac{B}{H_i}\right]^{-0.31} * (1-e^{-0.5\xi}) \qquad (6.2)$$

Boundaries: $3.0 \le \xi < 8.2$, $1.0 < \dfrac{B}{H_i} < 8.3$

The fit of formula for predicted and measured transmission coefficients is shown in Figure D-1. The proposed formulas fit the test data well, resulting in a fair statistical fit R^2=0.91.

To obtain the confidence levels of the formulae, the standard deviation of difference between measured and calculated wave transmission should be explored. The method adopted by De Jong (1996) was used to derive the standard deviation. It is assumed that the scatter around the line $K_{t\text{-measured}} = K_{t\text{-calculated}}$ can be described by Standard Normal Distribution. Two lines of constant difference between the measured and the calculated transmission coefficients are plotted in steps of ±0.10. Using a two-sided truncated Normal distribution function with mean μ=0 and deviation σ=1, see Figure 6.3, the standard deviations foe each boundary can be calculated. The percentage of points within theses boundaries are counted and the probability can be obtained by:

$$P(-b<x<b)=\text{Percentage within boundary}$$

The value of b can be found from the table of Standard Normal Distribution. With this value of b the standard deviation σ for the specific boundary, e.g. 0.01, is calculated using the following equation:

$$\sigma(boundary = 0.01) = \frac{0.01}{b_i}$$

The calculation results of standard deviation for the wave transmission formulas are summarised in Table 6.1.

The data sets of Seeling (bw1) was discarded because they are not in accordance with general trend. The average of standard deviation is 0.056 without Seeling (bw1). If the data sets of Seeling (bw1) are taken into account, a higher standard deviation value of 0.69 is expected.

With the standard deviation of 0.056 one can obtain the confidence levels of the formulas. For the 90% confidence level the value of 1.64 for b is found. The 90% confidence intervals become $K_t \pm 1.64\sigma = K_t \pm 0.092$. The Figure D-1 gives the 90% confidence intervals.

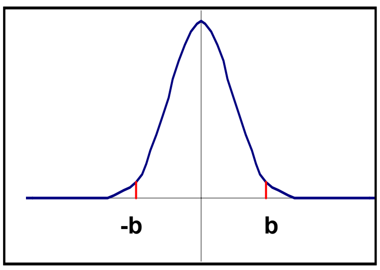

Figure 6.3 Normal distribution N(0,1)

Standard Deviation

Boundary Width	% within Boundary	b	St.Dev. σ
0.01	0.123	0.155	0.065
0.02	0.235	0.305	0.066
0.03	0.432	0.570	0.053
0.04	0.556	0.765	0.052
0.05	0.642	0.920	0.054
0.06	0.728	1.100	0.055
0.07	0.778	1.220	0.057
0.08	0.877	1.540	0.052
0.09	0.938	1.870	0.048
0.10	0.951	1.970	0.051
0.11	0.963	2.080	0.053
0.12	0.963	2.080	0.058
0.13	0.963	2.080	0.063
0.14	0.988	2.500	0.056
	Average		**0.056**

Table 6.1 Standard deviation for 2-D transmission formula at smooth structures

6.3 Derivation of formula for oblique wave transmission

Formula for oblique wave transmission was derived by analysis on the wave direction influence presented in the DELOS data set. The measured range of surf similarity parameters was $1.47 < \xi < 2.63$. The relative crest width $\frac{B}{H_i}$ was located in the range of $1.00 < \frac{B}{H_i} < 3.33$, with B=0.20m. Therefore, the equation 6.1 can be taken as a basic formula and the influence of wave direction will be put into it.

The Figures 6.4 shows the relation between $\frac{K_t}{-0.30\frac{R}{H_i}+0.75(1-e^{-0.5\xi})}$ and incident wave angle β.

Through trial and error, the relation was found as $(\cos\beta)^{2/3}$. So the finalised formula was developed:

$$K_t = [-0.30\frac{R_c}{H_i} + 0.75(1-e^{-0.5\xi})](\cos\beta)^{2/3} \qquad (6.3)$$

The proposed formula results a relatively fair statistical fit to 3-D test data, R^2=0.84. The comparison between measured and calculated transmission coefficients is presented in Figure D-2.

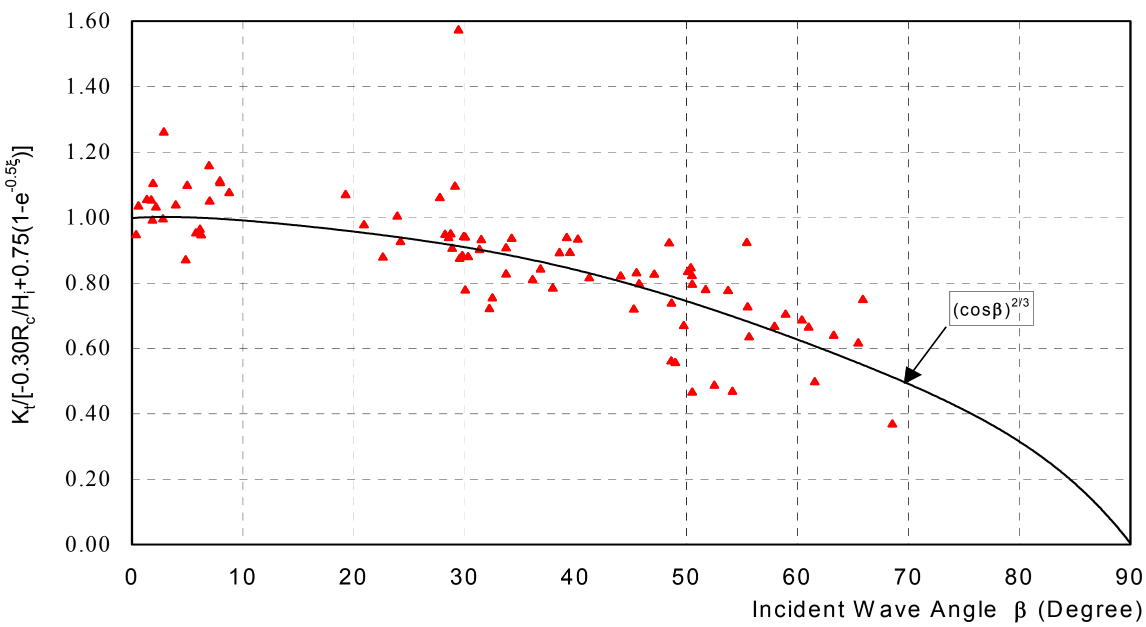

Figure 6.4 Relation between $\frac{K_t}{-0.30\frac{R}{H_i}+0.75(1-e^{-0.5\xi})}$ and incident wave angle β

Physically when the perpendicular waves attack the structure, β=0°, the transmission coefficients should have maximum values. This is well defined by the expression $(\cos\beta)^{2/3}$. If the angles increase, the influences of relative freeboard and the second term with surf similarity parameter ξ will be both modified by $(\cos\beta)^{2/3}$. The slope of the line becomes flatter and the second term decreases as well. Finally the coefficient will drop to zero when the β=90°.

A bigger incident wave angle leads to longer travelling distance or gentler slope, therefore less run-up level and smaller transmission. At the same time, more energy of short-crested wave will not approach and pass the structures as increasing incident wave angle. That is to say less incident wave energy can attack the structures and consequently transmission will decrease.

The magnitude of the direction influence is given by the function of $(\cos\beta)^{2/3}$. The reduction, in percentage, of the transmission coefficient is 10%, 20% and 50% corresponding to the incident wave angle β=30°, 45°, 70°. Significant effect of wave direction is present when the incident wave angle is bigger than 30°.

Some studies show that wave transmission still exists when the wave directions are between 90° and 120° in 3-D wave field. This seems not agreeable to the above expression. However, this could require more data sets to find the influence of incident wave direction nearly parallel to the structure, especially at the range of 70° and 120°. On the other hand, from the engineering point of view, waves nearly parallel to the structures are less of concern. Therefore, the above expression can be accepted when the direction boundary is set in the range between 0° and 70° as performed in DELOS tests. The applicable ranges for oblique wave transmission are summarised as following:

$$1.0 < \xi < 3.0, \quad 1.0 \le \frac{B}{H_i} \le 4.0, \quad 0^\circ \le \beta \le 70^\circ$$

The calculation results of standard deviation for oblique wave transmission formula are summarised in Table 6.2. The average of standard deviation is 0.052. With the standard deviation of 0.052 the confidence levels of the formula can be obtained. For the 90% confidence level the value of 1.64 for b is expected. The 90% confidence intervals become $K_t \pm 1.64\sigma = K_t \pm 0.09$. The Figure D-2 indicates the 90% confidence intervals.

Standard Deviation

Boundary Width	% within Boundary	b	St.Dev. σ
0.01	0.133	0.172	0.058
0.02	0.255	0.325	0.062
0.03	0.473	0.633	0.047
0.04	0.582	0.810	0.049
0.05	0.673	0.980	0.051
0.06	0.770	1.200	0.050
0.07	0.824	1.355	0.052
0.08	0.897	1.630	0.049
0.09	0.939	1.875	0.048
0.10	0.958	2.130	0.047
0.11	0.970	2.160	0.051
0.12	0.970	2.160	0.056
0.13	0.976	2.250	0.058
0.14	0.988	2.510	0.056
0.15	0.994	2.750	0.055
Average			**0.052**

Table 6.2 Standard deviation for 3-D transmission formula at smooth structures

7. SPECTRAL CHANGE DUE TO WAVE TRANSMISSION

7.1 Peak frequency

After transmission over low-crested structures, wave energy is dispersed and wave height decreases. The wave transmission coefficient is not the only important parameter that needs to be studied. Transmitted wave period and spectral shape sometimes may have influence on the lee side structure design, for instance, wave run-up on the a dike behind a low-crested structures depends largely on the transmitted wave period.

Van der Meer et al. (2000) found that the peak period remains more or less constant after transmission. For $K_t > 0.15$ about 40% of the total transmitted energy is present at the higher frequencies of the spectrum between $1.5f_p$ and $3.5f_p$. The investigation was carried out in present research to validate the conclusions for DELOS data.

The directional wave spectrum analysis was carried out using the BDM program. It gives the peak frequency and the energy distribution along frequency and direction. The percentage of total energy in the higher frequency range can also be calculated. These results are summarised in Tables A-10—A14. Figure 7.1 gives an example of incident and transmitted wave spectra at rubble structures.

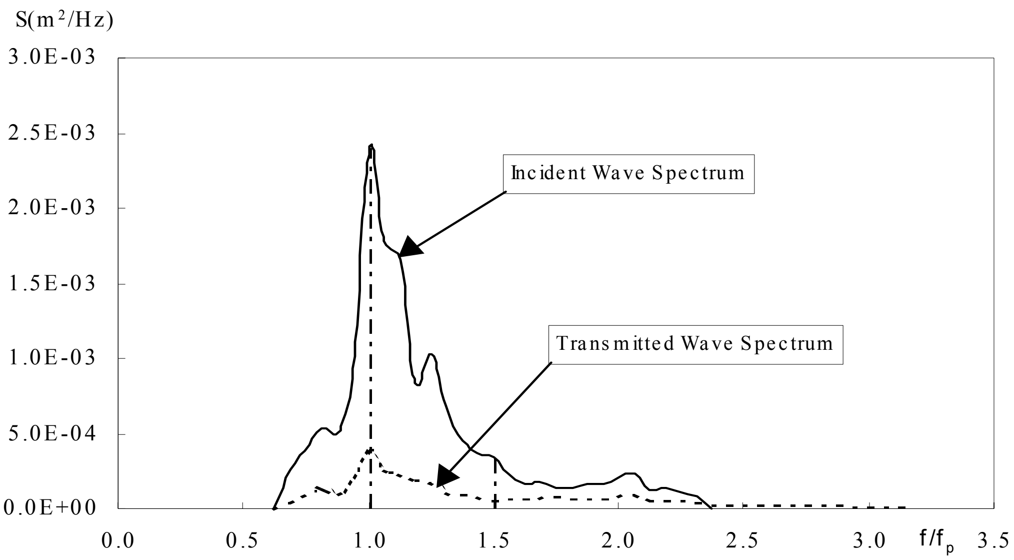

Figure 7.1 Incident and transmitted wave spectra

Figures E-1—E6 show the peak frequency ratio f_{pt}/f_{pi} as a function of incident wave peak frequency, transmission coefficient K_t and wave steepness for rubble and smooth structures. The influences of parameter f_{pi} , s_{op} and K_t are not evident. The ratios fluctuate around 1.0. Generally speaking, the peak frequency of transmitted wave is more or less same as that of the incident wave.

7.2 Energy distribution

The incident wave energy will be redistributed and is broadened with a shift of energy to higher frequencies after transmission. Figure 7.1 gives an example of energy shift of rubble structure test 1. To analyse the change, the range of high frequency is defined as from $1.5f_p$ to maximum frequency f_{max}. Therefore the percentage of the total transmitted energy at the higher frequencies can be quantified. The maximum frequency f_{max} was obtained by finding the point at which the energy sharply drops to zero.

The influence of various parameters on the ratio of f_{max}/f_p and percentage of total energy at high frequency range were analysed. These parameters are incident wave angle β_i, relative freeboard R_c / H_i, wave steepness s_{op} and transmission coefficient K_t.

Wave direction has no direct influence on the ratio of f_{max}/f_p and energy shift at rubble structures and smooth structures. This can be seen in Figures E-7, E-8, E-9 and E-10. Some of the other parameters do show influence tendencies at rubble structures and smooth structures. Detailed discussions are given to each type of structure.

Rubble structure

The ratio of f_{max}/f_p is found in the range from 2.1 to 4.3 instead of a nearly constant value. Its average value is 3.2. It is close to the value of 3.5 found by Van der Meer et al. (2000).

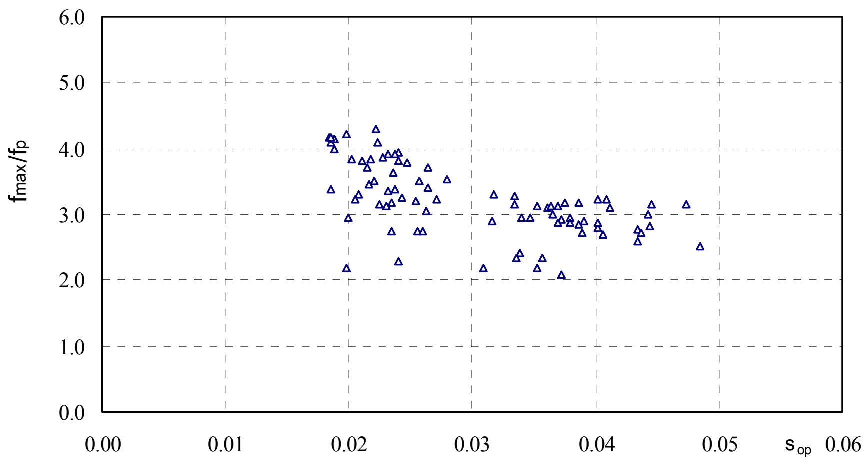

Figure 7.2 Relation between f_{max}/f_p and s_{op} for rubble structures

Wave steepness s_{op} shows a consistent influence, the smaller the steepness the larger the ratio. The relation between f_{max}/f_p and relative freeboard R_c/H_i the ratio will decrease indicates when water levels are far away from crests as indicated in Figures E-11. The obvious influence related to transmission coefficient is not observed. The percentage of the total transmitted energy at the high frequency is found in range of 20% to 51%. The average value is 34%. The influence of wave steepness is clear, the larger the s_{op}, the smaller the percentage. These can be observed in Figure E-13.

Smooth structure

The ratio of f_{max}/f_p is present in range from 2.9 to 5.6 and its average value is 3.8 for smooth structures. The positive freeboard has a little higher ratio of f_{max}/f_p. In addition, it will increase when water level is close to crest, see Figure E-12. Figure 7.3 presents a relatively good linear relation between transmission coefficient and f_{max}/f_p. An expression was found to estimate f_{max}/f_p as a function of the transmission coefficient K_t

$$\frac{f_{\max}}{f_p} = -3.43K_t + 5.20 \quad \text{If } 0.10 \le K_t \le 0.65 \qquad (6.1)$$

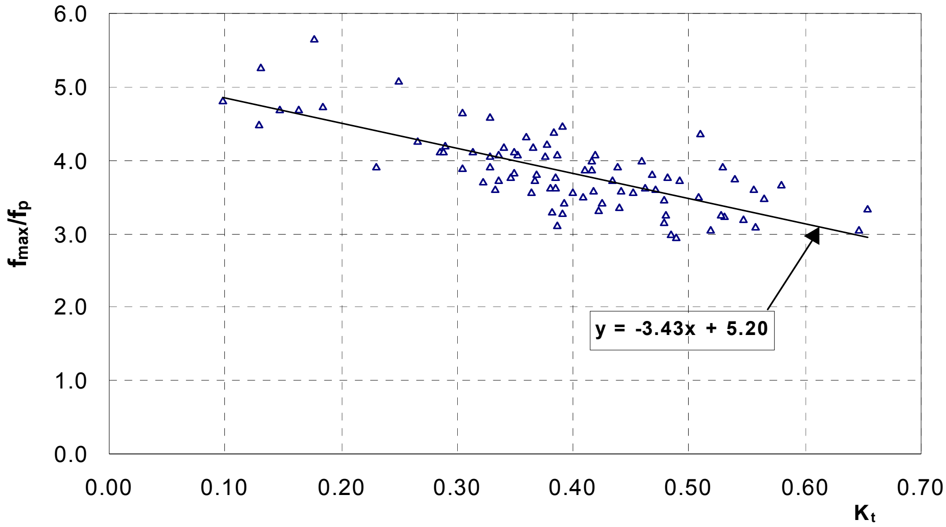

Figure 7.3 Relation between f_{max}/f_p and K_t for smooth structures

A larger transmission coefficient gives a smaller ratio of f_{max}/f_p, therefore a smaller f_{max}. This means the relative narrow distribution is produced for the wave transmission with a bigger coefficient.

The percentage of the total transmitted energy at the high frequency is most located in range of 30% to 60%. The average value is 42%. It is also close to the value of 40% proposed by Van der Meer et al. (2000).

The influence of transmission coefficient on the wave energy shift is clearly shown in the Figure E-14. It can be seen that the percentages trend to a constant value of 40% when the transmission coefficients are bigger than 0.3. The percentages will decrease as increasing coefficients between 0.10 and 0.30.

8. CONCLUSIONS AND RECOMMENDATIONS

8.1 Conclusions

Based on three-dimensional wave transmission tests, oblique wave transmissions at rubble and smooth structures were studied within DELOS project. A number of conclusions have been reached as follows:

- The freeboard, wave height and steepness have a similar behaviour as presented by previous research for 2-D wave attack. They are still dominant parameters for short-crested wave transmission.
- Wave transmission at rubble structures is slightly influenced by incident wave angle. However, wave direction strongly affects the transmission over smooth structures.
- There is hardly any diffidence between short-crested and long crested wave transmission coefficients. If any, the short-crested waves give a 3% smaller transmission coefficient than the long-crested waves.
- The transmission formula proposed by Daemen (1991) fits well with oblique wave transmission at rubble structures. Due to the slight influence of wave direction, without any modification, this formula can be used to predict the oblique wave transmission at rubble structures with a narrow crest width.
- Based on more available data sets, the two-dimensional wave transmission formula presented by De Jong (1996) was modified. By distinguishing the surf similarity parameter ξ, different expressions are given as follows:

  $$K_t = -0.30\frac{R_c}{H_i} + 0.75(1 - e^{-0.5\xi}),\ \xi < 3$$

  $$K_t = -0.30\frac{R_c}{H_i} + 0.75\left[\frac{B}{H_i}\right]^{-0.31} * (1 - e^{-0.5\xi}),\ \xi \geq 3$$

- Oblique wave transmission over smooth structures was derived as

  $$K_t = (-0.30\frac{R_c}{H_i} + 0.75(1 - e^{-0.5\xi}))(\cos\beta)^{2/3},\ \xi < 3$$

- The wave main direction will decrease after transmission at rubble and smooth structures. The transmitted wave direction β_t is dominated by incident wave angle β_I. Wave direction change at rubble structures can be expressed by

  $$\beta_t = 0.8\beta_i$$

  The relation between incident and transmitted wave direction for smooth structures can be approximately described by:

  $$\beta_t = 0.9\beta_i \quad \text{if } \beta_t < 50°$$

  $$\beta_t = 45° \quad \text{if } \beta_t \geq 50°$$

- For both rubble and smooth structures, the peak frequency of transmitted spectrum is similar to that of the incident spectrum.
- The average ratios of f_{max}/f_p are 3.2 and 3.8 for rubble and smooth structures respectively. They are close to the value of 3.5 found by Van der Meer et al. (2000)
- For the smooth structures the following expression was proposed to estimate f_{max}/f_p as a function of the transmission coefficient K_t

$$\frac{f_{max}}{f_p} = -3.43K_t + 5.20 \quad \text{If } 0.10 \le K_t \le 0.65$$

  For rubble structures, the ratio of f_{max}/f_p is in range from 2.1 to 4.3. There seems to be a smaller effect of s_{op}. A smaller steepness gives a larger ratio.
- The average percentages of the total transmitted energy at the higher frequencies are 34% and 42% for rubble and smooth structures respectively.

8.1 Recommendations

- The formulae proposed by Daemen (1991), De Jong (1996) and Queen's (1998) were used to validate the transmission equations for rubble structures in the research. It was found that none of the existing formulae of wave transmission at rubble structures are sufficient for application over a wide range of incident wave characteristics and structure geometries. A more extensive investigation is necessary, especially to describe the influence of the narrow crest width.
- The modified transmission formula at smooth structures was given by distinguishing the surf similarity parameter $\xi < 3$ and $\xi \ge 3$. It should be noticed that the data set of Daemrich and Kahle (Daka) is only available test for $\xi \ge 3$ and demonstrates the influence of crest width. The wave transmission for the case $\xi \ge 3$ needs a more detailed study. It is recommended that the transmission formula for $\xi \ge 3$ be used with caution.
- It was concluded that incident wave angles slightly influence wave transmission at rubble structures and strongly affect wave transmission at smooth structures in this research. The conclusions were drawn based on the present test set-ups with fixed slope and crest width. More physical tests with various crest width and slope are needed to confirm the conclusions.

REFERENCE

Ahrens, J.P. (1987) Characteristics of Reef Breakwaters, Technical report CERC-87-17, Waterways Experiment Station, US Army Corps of Engineers.

Madrigal, B.G. (1999) Loads on Caisson Breakwaters in Multidirectional Random Non-Breaking Seas COPEDEC V Vol. 2, pp.1314-1326.

Davies, B.L. and Kriebel, D.L (1992) Model testing of wave transmission past low-crested breakwaters, Proc. 23rd ICCE, Asce, Venice, Italy, PP. 1115-1127.

Daemen, I.F.R. (1991) Wave Transmission at Low-crested Structures, Master Thesis, Delft University of Technology, Delft and Delft Hydraulics.

De Jon, R.J (1996) Wave Transmission at Low-crested Structures, Master Thesis, Delft University of Technology, Delft Hydraulics

Zyserman, J.A. et al. (1998) On The Design of Shore-parallel Breakwaters. Coastal Engineering (1998), Vol. 2, pp.1693-1705.

De Waal, J.P. and Van der Meer J.W. (1992) Wave run-up and overtopping at coastal structures, Proc. 23rd ICCE, Venice, Italy, pp. 1758-1771.

Kamphuis, W.J. (1998) Long Wave in Flume Experiments, Coastal Engineering (1998), Vol. 2, pp.1154-1167.

Daemrich, K.F. and Mathias, H.J. (1999) Overtopping at Vertical Walls with Oblique Wave Approach. COPEDEC V Vol. 2, pp.1294-1301

Kawasaki, K. and Iwata, K. (1998) Numerical Analysis of Wave Breaking Due to Submerged Breakwater in There-dimensional Wave Field. Coastal Engineering (1998), Vol. 1, pp.853-866.

Loveless, J. and Debski, D. (1997) The Design and Performance of Submerged Breakwaters, Ministry of Agriculture Fisheries and Food, contract CSA 2606, Department of Civil Engineering, University of Bristol.

Mitsuyasu, H. et. al. (1975) Observations of the Directional Spectrum of Ocean Waves using a Cloverleaf Buoy, Journal of Physical Oceanography, Vol. I, pp. 750-760.

Nicholas, C.K et al. (1994) Modern Functional Design of Groin Systems. Coastal Engineering (1994), Vol. 2, pp.1327-1342.

Allsop N.W.H., DURAND N. & Hurdle D.P. (1998) Influence of Steep Seabed Slopes on Breaking Waves structure Design. Coastal Engineering (1998), Vol. 1, pp. 906-919.

Seabrook, S. R. and Hall, K.R. (1998) Wave Transmission at Submerged Rubble mound Breakwaters. Coastal Engineering (1998), Vol. 2, pp. 2000-2013.

Hiraishi, T. and Maruyama, H. (1998) Directional Wave Overtopping Estimation Model and Experimental Verification. Coastal Engineering (1998), Vol. 2, pp.2249-2268.

Van der Meer, J.W. (1990) Data on Wave Transmission Due to Overtopping. Delft Hydraulics.

Van der Meer, J.W. (1991) Stability and transmission at low-crested structure. Technical report, Delft Hydraulics, Publication number 453.

Van der Meer, J.W. and Pilarczyk, K.W. (1990) Stability of Low-crested and Reef Breakwaters, Proc. 22nd International Conference on Coastal Engineering, Vol. 2, pp. 1375-1388, Delft, The Netherlands.

Van der Meer, J.W., Tutuarima, W.H. and Burger, G. (1996). Influence of Rock Shape and Grading on Stability of Low-Crested Structures, Proc. 25th International Conference on Coastal Engineering, chapter 152, pp 1957-1970, Orlando, Florida.

Van der Meer, et. al. (2000) Spectral Changes due to Wave Transmission and Effects of Bi-modal Wave Spectra on Overtopping. INFRAM publication number 6.

Kittitanasuan, W. and Goda, Y. (1994), Analysis of Non-linear Coefficients of Reflection and Transmission of Wave Propagating over a Rectangular Step. Coastal Engineering (1994), Vol. 2, pp.1241-1254.

APPENDIX A

Tables of the various data sets

Table A-1 Tests on Rubble Structure (Test 1-42)

Test set-up												Seaside						Lee side				K_t	β_t	β_i
Test no.	Layout	R_c [m]	h [m]	Wave type	s_{op}	Hs [m]	T_p [s]	L [m]	Dir. [°]	Spread S	H/h	H_i	f_p	s_{op}	Dir. (Hi) [°]	Ref. (Hr) [°]	(%)	H_t	Dir. (Ht) [°]	Ref. (Hr) [°]	(%)	H_t/H_i	[°]	[°]
1	0	0.00	0.25	3D	0.02	0.08	1.60	4.0	90	50	0.32	0.094	0.625	0.024	101	262	24	0.046	96	291	21	**0.49**	**-11.3**	**-5.5**
2	0	0.00	0.25	3D	0.02	0.11	1.88	5.5	90	50	0.44	0.120	0.547	0.023	101	259	29	0.054	93	268	28	**0.45**	**-10.6**	**-2.5**
3	0	0.00	0.25	3D	0.02	0.14	2.12	7.0	90	50	0.56	0.132	0.469	0.019	103	256	37	0.056	91	269	31	**0.42**	**-12.9**	**-1.2**
4	0	0.00	0.25	3D	0.04	0.08	1.13	2.0	90	50	0.32	0.063	0.82	0.027	96	242	6	0.032	99	269	17	**0.51**	**-6.4**	**-8.6**
5	0	0.00	0.25	3D	0.04	0.11	1.33	2.8	90	50	0.44	0.095	0.703	0.030	93	275	20	0.046	93	274	21	**0.48**	**-3.3**	**-3.3**
6	0	0.00	0.25	3D	0.04	0.14	1.50	3.5	90	50	0.56	0.112	0.664	0.032	99	267	24	0.052	100	265	23	**0.46**	**-9.0**	**-10.2**
7	0	0.00	0.25	2D	0.02	0.14	2.12	7.0	90	-	0.56	0.134	0.469	0.019	101	259	38	0.057	87	274	27	**0.43**	**-11.1**	**3.5**
8	0	0.00	0.25	2D	0.04	0.14	1.50	3.5	90	-	0.56	0.127	0.625	0.032	99	265	28	0.057	96	265	25	**0.45**	**-8.6**	**-5.7**
9	0	0.05	0.20	3D	0.02	0.07	1.50	3.5	90	50	0.35	0.083	0.625	0.021	98	267	24	0.026	92	282	15	**0.31**	**-8.1**	**-2.4**
10	0	0.05	0.20	3D	0.02	0.09	1.70	4.5	90	50	0.45	0.096	0.625	0.024	99	264	29	0.031	94	270	18	**0.32**	**-8.6**	**-3.9**
11	0	0.05	0.20	3D	0.02	0.11	1.88	5.5	90	50	0.55	0.109	0.586	0.024	104	257	38	0.035	95	272	20	**0.32**	**-13.9**	**-5.4**
12	0	0.05	0.20	3D	0.04	0.07	1.06	1.8	90	50	0.35	0.060	0.938	0.034	97	256	13	0.014	92	271	14	**0.23**	**-7.0**	**-2.0**
13	0	0.05	0.20	3D	0.04	0.09	1.20	2.3	90	50	0.45	0.079	0.938	0.045	99	260	21	0.021	94	277	16	**0.27**	**-8.6**	**-3.8**
14	0	0.05	0.20	3D	0.04	0.11	1.33	2.8	90	50	0.55	0.095	0.742	0.034	98	263	29	0.028	96	316	24	**0.29**	**-8.0**	**-6.3**
15	0	-0.05	0.30	3D	0.02	0.09	1.70	4.5	90	50	0.30	0.094	0.625	0.024	100	261	27	0.061	96	267	14	**0.65**	**-10.4**	**-6.5**
16	0	-0.05	0.30	3D	0.02	0.13	2.04	6.5	90	50	0.43	0.131	0.508	0.022	103	258	30	0.075	92	260	25	**0.57**	**-12.7**	**-2.1**
17	0	-0.05	0.30	3D	0.02	0.17	2.33	8.5	90	50	0.57	0.157	0.469	0.022	101	258	26	0.081	90	263	30	**0.52**	**-10.6**	**0.0**
18	0	-0.05	0.30	3D	0.04	0.09	1.20	2.3	90	50	0.30	0.076	0.703	0.024	97	218	4	0.052	87	267	10	**0.68**	**-6.9**	**2.8**
19	0	-0.05	0.30	3D	0.04	0.13	1.44	3.3	90	50	0.43	0.106	0.703	0.034	99	266	16	0.065	90	268	15	**0.61**	**-8.7**	**0.4**
20	0	-0.05	0.30	3D	0.04	0.17	1.65	4.3	90	50	0.57	0.144	0.664	0.041	100	260	28	0.077	96	263	24	**0.53**	**-10.2**	**-6.4**
21	30	0.00	0.25	3D	0.02	0.08	1.60	4.0	90	50	0.32	0.095	0.625	0.024	82	271	23	0.042	91	261	11	**0.44**	**37.9**	**29.1**
22	30	0.00	0.25	3D	0.02	0.11	1.88	5.5	90	50	0.44	0.127	0.586	0.028	82	274	28	0.053	92	248	11	**0.42**	**37.9**	**27.9**
23	30	0.00	0.25	3D	0.02	0.11	1.88	5.5	80	50	0.44	0.129	0.547	0.025	75	278	25	0.050	84	229	18	**0.39**	**45.4**	**35.7**
24	30	0.00	0.25	3D	0.02	0.11	1.88	5.5	100	50	0.44	0.120	0.586	0.026	88	275	32	0.054	94	265	16	**0.45**	**32.1**	**26.2**
25	30	0.00	0.25	3D	0.02	0.14	2.12	7.0	90	50	0.56	0.144	0.508	0.024	84	273	28	0.061	99	261	21	**0.42**	**35.6**	**21.1**
26	30	0.00	0.25	3D	0.04	0.08	1.13	2.0	90	50	0.32	0.072	0.898	0.037	88	225	5	0.034	91	273	20	**0.47**	**31.9**	**28.6**
27	30	0.00	0.25	3D	0.04	0.11	1.33	2.8	90	50	0.44	0.103	0.820	0.044	85	273	19	0.048	93	257	18	**0.47**	**34.6**	**26.8**
28	30	0.00	0.25	3D	0.04	0.11	1.33	2.8	80	50	0.44	0.110	0.820	0.047	79	279	21	0.045	92	260	16	**0.41**	**41.3**	**27.6**
29	30	0.00	0.25	3D	0.04	0.11	1.33	2.8	100	50	0.44	0.103	0.781	0.040	89	280	19	0.050	95	290	17	**0.49**	**31.3**	**25.1**
30	30	0.00	0.25	3D	0.04	0.14	1.50	3.5	90	50	0.56	0.130	0.703	0.041	85	276	24	0.057	91	254	17	**0.44**	**34.9**	**28.9**
31	30	0.00	0.25	2D	0.02	0.14	2.12	7.0	90	-	0.56	0.144	0.469	0.020	84	274	25	0.064	90	261	22	**0.44**	**35.6**	**30.1**
32	30	0.00	0.25	2D	0.04	0.14	1.50	3.5	90	-	0.56	0.131	0.664	0.037	85	273	24	0.059	88	239	20	**0.45**	**35.0**	**32.2**
33	30	0.00	0.25	2D	0.04	0.14	1.50	3.5	80	-	0.56	0.123	0.664	0.035	84	267	20	0.059	91	239	20	**0.48**	**36.2**	**28.8**
34	30	0.00	0.25	2D	0.04	0.14	1.50	3.5	100	-	0.56	0.133	0.664	0.038	86	272	20	0.062	93	266	17	**0.47**	**33.9**	**27.3**
35	30	0.05	0.20	3D	0.02	0.07	1.50	3.5	90	50	0.35	0.080	0.625	0.020	82	286	27	0.019	97	256	15	**0.24**	**37.9**	**22.8**
36	30	0.05	0.20	3D	0.02	0.09	1.70	4.5	90	50	0.45	0.096	0.586	0.021	79	289	30	0.023	95	236	18	**0.24**	**40.6**	**24.7**
37	30	0.05	0.20	3D	0.02	0.11	1.88	5.5	90	50	0.55	0.120	0.508	0.020	80	282	34	0.030	97	254	16	**0.25**	**39.7**	**23.3**
38	30	0.05	0.20	3D	0.02	0.11	1.88	5.5	80	50	0.55	0.114	0.508	0.019	73	286	34	0.026	90	233	17	**0.23**	**46.8**	**30.3**
39	30	0.05	0.20	3D	0.02	0.11	1.88	5.5	100	50	0.55	0.116	0.547	0.022	85	279	34	0.032	100	259	16	**0.28**	**35.2**	**20.1**
40	30	0.05	0.20	3D	0.04	0.07	1.06	1.8	90	50	0.35	0.060	0.898	0.031	92	257	22	0.012	94	261	12	**0.20**	**28.3**	**25.6**
41	30	0.05	0.20	3D	0.04	0.09	1.20	2.3	90	50	0.45	0.084	0.820	0.036	90	274	21	0.018	94	258	15	**0.21**	**29.9**	**25.7**
42	30	0.05	0.20	3D	0.04	0.11	1.33	2.8	90	50	0.55	0.099	0.781	0.039	83	292	26	0.024	98	244	15	**0.24**	**36.5**	**21.7**

Table A-2 Tests on Rubble Structure (Test 42-84)

Test set-up												Seaside						Lee side				K_t	β_t	β_i
Test	Layout	R_c	h	Wave	s_{op}	Hs	T_p	L	Dir.	Spread	H/h	H_i	f_p	S_{op}	Dir. (Hi)	Ref. (Hr)		H_t	Dir. (Ht)	Ref. (Hr)		H_t/H_i	[°]	[°]
no.		[m]	[m]	type		[m]	[s]	[m]	[°]	S					[°]	[°]	(%)		[°]	[°]	(%)			
43	30	-0.05	0.30	3D	0.02	0.09	1.70	4.5	90	50	0.30	0.102	0.625	0.026	82	264	20	0.065	89	266	6	**0.64**	**37.8**	**31.4**
44	30	-0.05	0.30	3D	0.02	0.13	2.04	6.5	90	50	0.43	0.136	0.508	0.022	86	268	21	0.078	91	262	19	**0.57**	**34.4**	**28.8**
45	30	-0.05	0.30	3D	0.02	0.13	2.04	6.5	80	50	0.43	0.135	0.508	0.022	77	268	19	0.073	86	256	22	**0.54**	**42.9**	**34.5**
46	30	-0.05	0.30	3D	0.02	0.13	2.04	6.5	100	50	0.43	0.132	0.469	0.019	94	265	24	0.080	99	273	19	**0.61**	**25.9**	**21.4**
47	30	-0.05	0.30	3D	0.02	0.17	2.33	8.5	90	50	0.57	0.165	0.469	0.023	87	271	19	0.084	89	269	27	**0.51**	**33.1**	**31.1**
48	30	-0.05	0.30	3D	0.04	0.09	1.20	2.3	90	50	0.30	0.083	0.820	0.036	90	284	4	0.055	92	283	14	**0.66**	**30.0**	**28.1**
49	30	-0.05	0.30	3D	0.04	0.13	1.44	3.3	90	50	0.43	0.123	0.703	0.039	84	268	18	0.068	90	245	22	**0.55**	**36.2**	**29.9**
50	30	-0.05	0.30	3D	0.04	0.13	1.44	3.3	80	50	0.43	0.120	0.703	0.038	76	277	19	0.066	88	252	14	**0.55**	**43.5**	**32.3**
51	30	-0.05	0.30	3D	0.04	0.13	1.44	3.3	100	50	0.43	0.124	0.781	0.048	94	268	20	0.074	102	281	12	**0.60**	**25.8**	**17.5**
52	30	-0.05	0.30	3D	0.04	0.17	1.65	4.3	90	50	0.57	0.146	0.625	0.037	86	268	30	0.079	93	262	17	**0.54**	**34.3**	**26.6**
53	50	0.00	0.25	3D	0.02	0.08	1.60	4.0	90	50	0.32	0.093	0.664	0.026	84	284	5	0.044	89	267	20	**0.47**	**55.9**	**50.8**
54	50	0.00	0.25	3D	0.02	0.11	1.88	5.5	90	50	0.44	0.120	0.586	0.026	84	266	9	0.053	89	267	30	**0.44**	**56.1**	**50.9**
55	50	0.00	0.25	3D	0.02	0.11	1.88	5.5	80	50	0.44	0.117	0.586	0.026	73	306	8	0.050	84	269	26	**0.43**	**66.8**	**56.2**
56	50	0.00	0.25	3D	0.02	0.11	1.88	5.5	100	50	0.44	0.123	0.547	0.024	89	267	20	0.057	96	264	28	**0.46**	**51.3**	**43.6**
57	50	0.00	0.25	3D	0.02	0.14	2.12	7.0	90	50	0.56	0.140	0.508	0.023	84	268	11	0.057	88	269	35	**0.41**	**56.3**	**52.0**
58	50	0.00	0.25	3D	0.04	0.08	1.13	2.0	90	50	0.32	0.072	0.859	0.034	85	294	1	0.033	102	281	19	**0.46**	**54.7**	**38.1**
59	50	0.00	0.25	3D	0.04	0.11	1.33	2.8	90	50	0.44	0.103	0.781	0.040	93	271	16	0.047	96	283	19	**0.46**	**47.1**	**43.9**
60	50	0.00	0.25	3D	0.04	0.11	1.33	2.8	80	50	0.44	0.100	0.781	0.039	81	252	20	0.042	87	276	16	**0.42**	**58.6**	**53.2**
61	50	0.00	0.25	3D	0.04	0.11	1.33	2.8	100	50	0.44	0.099	0.781	0.039	88	271	17	0.047	103	275	24	**0.47**	**52.1**	**37.1**
62	50	0.00	0.25	3D	0.04	0.14	1.50	3.5	90	50	0.56	0.127	0.703	0.040	85	274	17	0.054	91	267	28	**0.43**	**55.2**	**49.1**
63	50	0.00	0.25	2D	0.02	0.14	2.12	7.0	90	-	0.56	0.131	0.469	0.018	57	312	6	0.057	85	274	34	**0.44**	**83.5**	**55.1**
64	50	0.00	0.25	2D	0.04	0.14	1.50	3.5	90	-	0.56	0.131	0.664	0.037	91	269	14	0.057	89	272	30	**0.44**	**49.2**	**50.9**
65	50	0.00	0.25	2D	0.04	0.14	1.50	3.5	80	-	0.56	0.129	0.664	0.036	88	271	13	0.057	90	270	30	**0.44**	**52.1**	**49.7**
66	50	0.00	0.25	2D	0.04	0.14	1.50	3.5	100	-	0.56	0.125	0.664	0.035	90	271	14	0.057	89	271	29	**0.46**	**50.4**	**51.0**
67	50	0.05	0.20	3D	0.02	0.07	1.50	3.5	90	50	0.35	0.079	0.625	0.020	85	280	13	0.020	92	270	14	**0.25**	**54.8**	**47.7**
68	50	0.05	0.20	3D	0.02	0.09	1.70	4.5	90	50	0.45	0.097	0.625	0.024	82	278	12	0.027	93	268	29	**0.28**	**57.5**	**46.6**
69	50	0.05	0.20	3D	0.02	0.11	1.88	5.5	90	50	0.55	0.119	0.547	0.023	82	275	17	0.029	88	272	29	**0.24**	**58.2**	**52.3**
70	50	0.05	0.20	3D	0.02	0.11	1.88	5.5	80	50	0.55	0.112	0.547	0.021	75	299	15	0.027	83	273	27	**0.24**	**64.8**	**57.4**
71	50	0.05	0.20	3D	0.02	0.11	1.88	5.5	100	50	0.55	0.114	0.508	0.019	88	270	20	0.031	98	267	31	**0.27**	**51.7**	**41.5**
72	50	0.05	0.20	3D	0.04	0.07	1.06	1.8	90	50	0.35	0.061	0.977	0.037	91	306	15	0.013	95	280	17	**0.21**	**49.1**	**44.6**
73	50	0.05	0.20	3D	0.04	0.09	1.20	2.3	90	50	0.45	0.082	0.820	0.035	93	274	21	0.019	93	265	21	**0.23**	**47.3**	**46.7**
74	50	0.05	0.20	3D	0.04	0.11	1.33	2.8	90	50	0.55	0.095	0.820	0.041	88	275	22	0.024	95	266	21	**0.25**	**52.3**	**45.4**
75	50	-0.05	0.30	3D	0.02	0.09	1.70	4.5	90	50	0.30	0.104	0.625	0.026	87	280	2	0.068	91	266	14	**0.65**	**53.1**	**48.8**
76	50	-0.05	0.30	3D	0.02	0.13	2.04	6.5	90	50	0.43	0.124	0.508	0.021	86	268	21	0.076	94	262	23	**0.61**	**53.6**	**45.7**
77	50	-0.05	0.30	3D	0.02	0.13	2.04	6.5	80	50	0.43	0.133	0.547	0.026	78	289	4	0.075	89	264	23	**0.56**	**61.7**	**51.1**
78	50	-0.05	0.30	3D	0.02	0.13	2.04	6.5	100	50	0.43	0.132	0.508	0.022	93	265	19	0.077	98	264	29	**0.58**	**46.5**	**41.7**
79	50	-0.05	0.30	3D	0.02	0.17	2.33	8.5	90	50	0.57	0.157	0.430	0.019	87	258	11	0.077	90	267	30	**0.49**	**53.0**	**49.9**
80	50	-0.05	0.30	3D	0.04	0.09	1.20	2.3	90	50	0.30	0.084	0.898	0.043	90	289	4	0.056	103	306	10	**0.67**	**50.5**	**36.9**
81	50	-0.05	0.30	3D	0.04	0.13	1.44	3.3	90	50	0.43	0.123	0.742	0.043	86	269	16	0.071	99	279	18	**0.58**	**54.4**	**41.3**
82	50	-0.05	0.30	3D	0.04	0.13	1.44	3.3	80	50	0.43	0.120	0.703	0.038	76	260	20	0.065	88	261	23	**0.54**	**63.5**	**52.3**
83	50	-0.05	0.30	3D	0.04	0.13	1.44	3.3	100	50	0.43	0.124	0.742	0.044	96	251	14	0.072	102	270	19	**0.58**	**44.0**	**38.1**
84	50	-0.05	0.30	3D	0.04	0.17	1.65	4.3	90	50	0.57	0.157	0.664	0.044	87	265	14	0.079	91	268	27	**0.50**	**53.4**	**49.2**

Table A-3 Tests on Smooth Structure (Test 1-42)

Test set-up												Seaside						Lee side				K_t	β_t	β_i
Test no.	Layout	R_c [m]	h [m]	Wave type	s_{op}	Hs [m]	T_p [s]	L [m]	Dir. [°]	Spread S	H/h	H_i	f_p	S_{op}	Dir. (Hi) [°]	Ref. (Hr) [°]	Ref. (Hr) (%)	H_t	Dir. (Ht) [°]	Ref. (Hr) [°]	Ref. (Hr) (%)	H_t/H_i	[°]	[°]
1s	0	0.00	0.3	3D	0.02	0.08	1.60	4.0	120	50	0.27	0.085	0.625	0.021	88	274	26	0.048	82	299	22	**0.56**	**1.9**	**8.3**
2s	0	0.00	0.3	3D	0.02	0.11	1.88	5.5	120	50	0.37	0.118	0.586	0.026	83	281	27	0.060	83	296	30	**0.51**	**7.0**	**6.8**
3s	0	0.00	0.3	3D	0.02	0.14	2.12	7.0	120	50	0.47	0.138	0.508	0.023	84	282	31	0.066	82	293	35	**0.48**	**5.8**	**7.8**
4s	0	0.00	0.3	3D	0.04	0.08	1.13	2.0	120	50	0.27	0.065	0.781	0.025	90	315	10	0.030	90	307	34	**0.46**	**0.4**	**0.2**
5s	0	0.00	0.3	3D	0.04	0.11	1.33	2.8	120	50	0.37	0.092	0.742	0.032	89	275	18	0.044	88	308	26	**0.48**	**1.3**	**2.2**
6s	0	0.00	0.3	3D	0.04	0.14	1.50	3.5	120	50	0.47	0.121	0.625	0.030	91	272	26	0.058	83	299	31	**0.48**	**-0.6**	**6.7**
7s	0	0.00	0.3	2D	0.02	0.14	2.12	7.0	120	-	0.47	0.136	0.430	0.016	84	278	29	0.072	83	278	33	**0.53**	**6.1**	**7.4**
8s	0	0.00	0.3	2D	0.04	0.14	1.50	3.5	120	-	0.47	0.124	0.625	0.031	88	272	28	0.060	84	283	29	**0.48**	**1.7**	**5.7**
9s	0	0.05	0.25	3D	0.02	0.07	1.50	3.5	120	50	0.28	0.082	0.625	0.021	85	274	37	0.030	85	293	28	**0.37**	**5.0**	**4.6**
10s	0	0.05	0.25	3D	0.02	0.09	1.70	4.5	120	50	0.36	0.096	0.547	0.018	82	279	36	0.040	85	297	26	**0.42**	**7.9**	**5.4**
11s	0	0.05	0.25	3D	0.02	0.11	1.88	5.5	120	50	0.44	0.113	0.547	0.022	82	282	36	0.047	84	293	29	**0.42**	**7.9**	**5.6**
12s	0	0.05	0.25	3D	0.04	0.07	1.06	1.8	120	50	0.28	0.060	0.781	0.023	81	285	29	0.016	85	284	35	**0.27**	**8.8**	**4.9**
13s	0	0.05	0.25	3D	0.04	0.09	1.20	2.3	120	50	0.36	0.079	0.742	0.028	83	283	26	0.026	87	297	30	**0.33**	**7.0**	**3.0**
14s	0	0.05	0.25	3D	0.04	0.11	1.33	2.8	120	50	0.44	0.098	0.742	0.035	87	275	27	0.036	87	290	26	**0.37**	**2.9**	**2.8**
15s	0	-0.05	0.35	3D	0.02	0.09	1.70	4.5	120	50	0.26	0.110	0.586	0.024	86	290	26	0.072	81	301	25	**0.65**	**3.9**	**9.0**
16s	0	-0.05	0.35	3D	0.02	0.13	2.04	6.5	120	50	0.37	0.150	0.469	0.021	84	290	30	0.087	79	293	35	**0.58**	**6.2**	**10.5**
17s	0	-0.05	0.35	3D	0.02	0.17	2.33	8.5	120	50	0.49	0.185	0.469	0.026	85	279	33	0.091	82	290	33	**0.49**	**4.8**	**8.4**
18s	0	-0.05	0.35	3D	0.04	0.09	1.20	2.3	120	50	0.26	0.085	0.781	0.033	88	284	10	0.055	85	328	30	**0.65**	**2.2**	**5.3**
19s	0	-0.05	0.35	3D	0.04	0.13	1.44	3.3	120	50	0.37	0.132	0.703	0.042	87	283	18	0.070	83	309	34	**0.53**	**2.8**	**6.6**
20s	0	-0.05	0.35	3D	0.04	0.17	1.65	4.3	120	50	0.49	0.163	0.586	0.036	88	283	27	0.086	81	309	36	**0.53**	**1.8**	**8.6**
21s	30	0.00	0.30	3D	0.02	0.08	1.60	4.0	90	50	0.27	0.094	0.625	0.024	90	300	19	0.044	86	254	31	**0.47**	**30.0**	**34.2**
22s	30	0.00	0.30	3D	0.02	0.11	1.88	5.5	90	50	0.37	0.122	0.586	0.027	91	294	23	0.053	83	257	35	**0.43**	**28.9**	**36.5**
23s	30	0.00	0.30	3D	0.02	0.11	1.88	5.5	80	50	0.37	0.123	0.547	0.024	82	292	21	0.048	83	251	37	**0.39**	**37.9**	**36.7**
24s	30	0.00	0.30	3D	0.02	0.11	1.88	5.5	100	50	0.37	0.124	0.547	0.024	96	288	21	0.057	90	258	33	**0.46**	**24.2**	**30.0**
25s	30	0.00	0.30	3D	0.02	0.14	2.12	7.0	90	50	0.47	0.150	0.469	0.021	88	291	22	0.058	88	261	37	**0.39**	**32.5**	**32.1**
26s	30	0.00	0.30	3D	0.04	0.08	1.13	2.0	90	50	0.27	0.079	0.859	0.037	90	314	16	0.030	90	248	30	**0.38**	**29.5**	**29.5**
27s	30	0.00	0.30	3D	0.04	0.11	1.33	2.8	90	50	0.37	0.105	0.781	0.041	91	323	13	0.042	89	259	37	**0.40**	**28.7**	**31.3**
28s	30	0.00	0.30	3D	0.04	0.11	1.33	2.8	80	50	0.37	0.107	0.742	0.038	83	295	17	0.039	86	252	40	**0.36**	**36.8**	**34.3**
29s	30	0.00	0.30	3D	0.04	0.11	1.33	2.8	100	50	0.37	0.104	0.781	0.041	101	320	22	0.047	92	258	31	**0.45**	**19.2**	**27.7**
30s	30	0.00	0.30	3D	0.04	0.14	1.50	3.5	90	50	0.47	0.133	0.664	0.038	89	303	20	0.052	86	258	37	**0.39**	**31.3**	**34.3**
31s	30	0.00	0.30	2D	0.02	0.14	2.12	7.0	90	-	0.47	0.147	0.508	0.024	86	277	20	0.060	84	268	36	**0.41**	**33.7**	**36.3**
32s	30	0.00	0.30	2D	0.04	0.14	1.50	3.5	90	-	0.47	0.140	0.703	0.044	81	281	19	0.054	81	267	36	**0.39**	**39.2**	**38.6**
33s	30	0.00	0.30	2D	0.04	0.14	1.50	3.5	80	-	0.47	0.139	0.664	0.039	81	277	19	0.053	81	266	38	**0.38**	**38.5**	**39.2**
34s	30	0.00	0.30	2D	0.04	0.14	1.50	3.5	100	-	0.47	0.135	0.664	0.038	81	280	20	0.052	81	266	36	**0.39**	**39.5**	**38.7**
35s	30	0.05	0.25	3D	0.02	0.07	1.50	3.5	90	50	0.28	0.086	0.625	0.022	86	300	42	0.027	95	230	34	**0.31**	**34.2**	**24.7**
36s	30	0.05	0.25	3D	0.02	0.09	1.70	4.5	90	50	0.36	0.107	0.586	0.024	90	292	35	0.036	94	237	35	**0.34**	**29.9**	**26.4**
37s	30	0.05	0.25	3D	0.02	0.11	1.88	5.5	90	50	0.44	0.122	0.547	0.023	91	305	34	0.043	91	239	40	**0.35**	**28.5**	**29.1**
38s	30	0.05	0.25	3D	0.02	0.11	1.88	5.5	80	50	0.44	0.125	0.547	0.024	84	294	35	0.038	93	232	38	**0.30**	**36.1**	**27.4**
39s	30	0.05	0.25	3D	0.02	0.11	1.88	5.5	100	50	0.44	0.122	0.547	0.023	96	290	32	0.046	97	252	35	**0.38**	**23.9**	**22.6**
40s	30	0.05	0.25	3D	0.04	0.07	1.06	1.8	90	50	0.28	0.065	0.898	0.034	92	292	40	0.015	103	247	35	**0.23**	**27.8**	**16.9**
41s	30	0.05	0.25	3D	0.04	0.09	1.20	2.3	90	50	0.36	0.084	0.898	0.043	91	308	37	0.024	99	237	38	**0.37**	**29.4**	**20.5**
42s	30	0.05	0.25	3D	0.04	0.11	1.33	2.8	90	50	0.44	0.105	0.781	0.041	91	308	35	0.032	96	232	36	**0.30**	**29.1**	**24.2**

Table A-4 **Tests on Smooth Structure (Test 43-84)**

Test set-up												Seaside						Lee side				K_t	β_t	β_i
Test no.	Layout	R_c [m]	h [m]	Wave type	s_{op}	Hs [m]	T_p [s]	L [m]	Dir. [°]	Spread S	H/h	H_i	f_p	S_{op}	Dir. (Hi) [°]	Ref. (Hr) [°]	(%)	H_t	Dir. (Ht) [°]	Ref. (Hr) [°]	(%)	H_t/H_i	[°]	[°]
43s	30	-0.05	0.35	3D	0.02	0.09	1.70	4.5	90	50	0.26	0.117	0.625	0.029	89	288	11	0.065	86	260	25	**0.56**	**31.5**	**34.3**
44s	30	-0.05	0.35	3D	0.02	0.13	2.04	6.5	90	50	0.37	0.155	0.469	0.022	90	277	22	0.073	86	258	31	**0.47**	**30.0**	**34.0**
45s	30	-0.05	0.35	3D	0.02	0.13	2.04	6.5	80	50	0.37	0.153	0.469	0.022	75	290	19	0.067	83	258	33	**0.44**	**45.2**	**36.6**
46s	30	-0.05	0.35	3D	0.02	0.13	2.04	6.5	100	50	0.37	0.157	0.508	0.026	97	277	17	0.080	92	267	32	**0.51**	**22.6**	**28.2**
47s	30	-0.05	0.35	3D	0.02	0.17	2.33	8.5	90	50	0.49	0.194	0.430	0.023	88	280	19	0.081	86	268	34	**0.42**	**32.2**	**34.2**
48s	30	-0.05	0.35	3D	0.04	0.09	1.20	2.3	90	50	0.26	0.097	0.781	0.038	92	327	4	0.054	94	276	23	**0.56**	**28.2**	**26.2**
49s	30	-0.05	0.35	3D	0.04	0.13	1.44	3.3	90	50	0.37	0.143	0.742	0.050	90	286	8	0.063	87	261	34	**0.44**	**29.8**	**33.1**
50s	30	-0.05	0.35	3D	0.04	0.13	1.44	3.3	80	50	0.37	0.139	0.703	0.044	79	308	13	0.059	81	265	36	**0.42**	**41.2**	**39.2**
51s	30	-0.05	0.35	3D	0.04	0.13	1.44	3.3	100	50	0.37	0.133	0.703	0.042	99	298	24	0.069	93	267	27	**0.52**	**20.9**	**26.7**
52s	30	-0.05	0.35	3D	0.04	0.17	1.65	4.3	90	50	0.49	0.178	0.664	0.050	90	282	16	0.075	84	264	35	**0.42**	**30.3**	**35.8**
53s	50	0.00	0.3	3D	0.02	0.08	1.60	4.0	90	50	0.27	0.093	0.664	0.026	88	325	11	0.035	92	268	36	**0.38**	**51.7**	**47.6**
54s	50	0.00	0.3	3D	0.02	0.11	1.88	5.5	90	50	0.37	0.131	0.547	0.025	80	296	15	0.044	91	267	35	**0.34**	**60.4**	**48.7**
55s	50	0.00	0.3	3D	0.02	0.11	1.88	5.5	80	50	0.37	0.131	0.586	0.029	75	299	14	0.038	91	264	35	**0.29**	**65.5**	**48.6**
56s	50	0.00	0.3	3D	0.02	0.11	1.88	5.5	100	50	0.37	0.122	0.547	0.023	96	293	17	0.05	94	263	36	**0.41**	**44.1**	**45.6**
57s	50	0.00	0.3	3D	0.02	0.14	2.12	7.0	90	50	0.47	0.158	0.508	0.026	82	280	22	0.051	92	266	36	**0.32**	**57.9**	**48.2**
58s	50	0.00	0.3	3D	0.04	0.08	1.13	2.0	90	50	0.27	0.073	0.859	0.035	91	341	6	0.024	91	271	50	**0.33**	**48.6**	**48.5**
59s	50	0.00	0.3	3D	0.04	0.11	1.33	2.8	90	50	0.37	0.106	0.820	0.046	90	309	22	0.036	90	273	44	**0.34**	**50.1**	**50.1**
60s	50	0.00	0.3	3D	0.04	0.11	1.33	2.8	80	50	0.37	0.104	0.820	0.045	81	329	10	0.03	93	269	47	**0.29**	**58.9**	**47.5**
61s	50	0.00	0.3	3D	0.04	0.11	1.33	2.8	100	50	0.37	0.107	0.742	0.038	106	313	10	0.042	95	276	36	**0.39**	**33.7**	**45.3**
62s	50	0.00	0.3	3D	0.04	0.14	1.50	3.5	90	50	0.47	0.132	0.703	0.042	90	318	17	0.044	93	271	40	**0.33**	**50.5**	**47.2**
63s	50	0.00	0.3	2D	0.02	0.14	2.12	7.0	90	-	0.47	0.146	0.508	0.024	79	277	20	0.048	91	265	35	**0.33**	**61.0**	**49.4**
64s	50	0.00	0.3	2D	0.04	0.14	1.50	3.5	90	-	0.47	0.127	0.742	0.045	90	278	13	0.044	93	269	39	**0.35**	**50.4**	**46.6**
65s	50	0.00	0.3	2D	0.04	0.14	1.50	3.5	80	-	0.47	0.129	0.703	0.041	93	271	14	0.045	93	268	42	**0.35**	**47.1**	**46.5**
66s	50	0.00	0.3	2D	0.04	0.14	1.50	3.5	100	-	0.47	0.129	0.664	0.036	94	272	14	0.045	96	265	40	**0.35**	**45.7**	**43.6**
67s	50	0.05	0.25	3D	0.02	0.07	1.50	3.5	90	50	0.28	0.092	0.742	0.032	91	336	29	0.015	105	258	42	**0.16**	**48.6**	**35.5**
68s	50	0.05	0.25	3D	0.02	0.09	1.70	4.5	90	50	0.36	0.119	0.547	0.023	86	323	23	0.021	99	261	45	**0.18**	**54.1**	**41.3**
69s	50	0.05	0.25	3D	0.02	0.11	1.88	5.5	90	50	0.44	0.146	0.547	0.028	78	298	24	0.027	98	263	44	**0.18**	**61.6**	**41.8**
70s	50	0.05	0.25	3D	0.02	0.11	1.88	5.5	80	50	0.44	0.146	0.586	0.032	71	300	24	0.019	99	259	46	**0.13**	**68.6**	**41.4**
71s	50	0.05	0.25	3D	0.02	0.11	1.88	5.5	100	50	0.44	0.136	0.547	0.026	90	297	25	0.034	99	264	41	**0.25**	**49.7**	**41.3**
72s	50	0.05	0.25	3D	0.04	0.07	1.06	1.8	90	50	0.28	0.071	0.977	0.043	88	316	38	0.007	111	251	35	**0.10**	**52.5**	**29.2**
73s	50	0.05	0.25	3D	0.04	0.09	1.20	2.3	90	50	0.36	0.093	0.781	0.036	90	331	36	0.012	109	254	40	**0.13**	**50.5**	**31.0**
74s	50	0.05	0.25	3D	0.04	0.11	1.33	2.8	90	50	0.44	0.115	0.82	0.050	91	337	30	0.017	103	259	46	**0.15**	**49.0**	**37.2**
75s	50	-0.05	0.35	3D	0.02	0.09	1.70	4.5	90	50	0.26	0.115	0.664	0.033	85	292	11	0.062	100	288	18	**0.54**	**55.4**	**40.5**
76s	50	-0.05	0.35	3D	0.02	0.13	2.04	6.5	90	50	0.37	0.16	0.508	0.026	85	274	18	0.067	99	255	30	**0.42**	**55.5**	**41.1**
77s	50	-0.05	0.35	3D	0.02	0.13	2.04	6.5	80	50	0.37	0.159	0.469	0.022	77	276	18	0.061	99	267	30	**0.38**	**63.3**	**41.0**
78s	50	-0.05	0.35	3D	0.02	0.13	2.04	6.5	100	50	0.37	0.158	0.508	0.026	95	272	17	0.076	94	261	30	**0.48**	**45.5**	**46.4**
79s	50	-0.05	0.35	3D	0.02	0.17	2.33	8.5	90	50	0.49	0.2	0.439	0.025	84	269	20	0.072	92	265	33	**0.36**	**55.6**	**47.8**
80s	50	-0.05	0.35	3D	0.04	0.09	1.20	2.3	90	50	0.26	0.095	0.781	0.037	92	321	5	0.052	102	289	19	**0.55**	**48.4**	**38.0**
81s	50	-0.05	0.35	3D	0.04	0.13	1.44	3.3	90	50	0.37	0.138	0.664	0.039	90	324	7	0.061	96	273	28	**0.44**	**50.5**	**44.4**
82s	50	-0.05	0.35	3D	0.04	0.13	1.44	3.3	80	50	0.37	0.143	0.703	0.045	74	299	10	0.055	93	259	31	**0.38**	**65.9**	**46.9**
83s	50	-0.05	0.35	3D	0.04	0.13	1.44	3.3	100	50	0.37	0.137	0.703	0.043	100	325	19	0.067	100	271	29	**0.49**	**40.2**	**39.8**
84s	50	-0.05	0.35	3D	0.04	0.17	1.65	4.3	90	50	0.49	0.182	0.664	0.051	86	291	18	0.067	95	266	33	**0.37**	**53.7**	**44.7**

Table A-5 All Data with Wave Perpendicular to Smooth Structure(1)

Test	Type	B	h_o	R_o	Incident			s_{op}	Transmitted	R_o/H_i	ξ	B/L0	B/H_d	H_d/h	K_t	K_{tc}
		(m)	(m)	(m)	H_{mo}(m)	T_p(s)	L_0(m)	-	H_t(m)							
1	Daka-Imp	0.20	0.70	-0.20	0.06	1.23	2.4	0.026	0.05	-3.28	3.11	0.085	3.279	0.087	**0.89**	**1.39**
2	Daka-Imp	0.20	0.70	-0.20	0.10	1.63	4.1	0.025	0.08	-1.92	3.16	0.048	1.923	0.149	**0.80**	**1.06**
3	Daka-Imp	0.20	0.50	-0.20	0.16	2.04	6.5	0.025	0.13	-1.25	3.18	0.031	1.250	0.320	**0.81**	**0.93**
4	Daka-Imp	0.20	0.50	0.00	0.10	1.63	4.1	0.024	0.06	0.00	3.22	0.048	2.000	0.200	**0.57**	**0.48**
5	Daka-Imp	0.20	0.60	-0.10	0.10	1.63	4.1	0.024	0.07	-1.01	3.24	0.048	2.020	0.165	**0.71**	**0.79**
6	Daka-Imp	0.20	0.50	0.00	0.16	2.04	6.5	0.024	0.10	0.00	3.24	0.031	1.290	0.310	**0.65**	**0.56**
7	Daka-Imp	0.20	0.60	-0.10	0.16	2.04	6.5	0.024	0.12	-0.65	3.24	0.031	1.290	0.258	**0.80**	**0.75**
8	Daka-Imp	0.20	0.50	0.00	0.10	1.63	4.1	0.023	0.06	0.00	3.27	0.048	2.062	0.194	**0.56**	**0.48**
9	Daka-Imp	0.20	0.50	0.00	0.06	1.23	2.4	0.023	0.02	0.00	3.28	0.085	3.636	0.110	**0.44**	**0.40**
10	Daka-Imp	0.20	0.50	-0.10	0.06	1.23	2.4	0.023	0.04	-1.82	3.28	0.085	3.636	0.110	**0.77**	**0.95**
11	Daka-Imp	0.20	0.60	-0.20	0.21	2.45	9.4	0.022	0.17	-0.97	3.37	0.021	0.971	0.343	**0.85**	**0.91**
12	Daka-Imp	0.20	0.50	-0.20	0.21	2.45	9.4	0.022	0.16	-0.98	3.38	0.021	0.976	0.410	**0.77**	**0.91**
13	Daka-Imp	0.20	0.60	-0.10	0.20	2.45	9.4	0.021	0.16	-0.51	3.46	0.021	1.020	0.327	**0.84**	**0.77**
14	Daka-Imp	0.20	0.50	0.00	0.19	2.45	9.4	0.021	0.14	0.00	3.47	0.021	1.031	0.388	**0.72**	**0.61**
15	Daka-Imp	0.20	0.60	-0.10	0.13	2.04	6.5	0.020	0.11	-0.76	3.51	0.031	1.515	0.220	**0.79**	**0.77**
16	Daka-Imp	0.20	0.50	-0.20	0.13	2.04	6.5	0.020	0.10	-1.55	3.55	0.031	1.550	0.258	**0.75**	**1.01**
17	Daka-Imp	0.20	0.70	-0.20	0.08	1.63	4.1	0.019	0.06	-2.56	3.64	0.048	2.564	0.111	**0.78**	**1.24**
18	Daka-Imp	0.20	0.50	0.00	0.12	2.04	6.5	0.019	0.08	0.00	3.66	0.031	1.653	0.242	**0.62**	**0.54**
19	Daka-Imp	0.20	0.50	0.00	0.17	2.45	9.4	0.018	0.11	0.00	3.73	0.021	1.190	0.336	**0.68**	**0.60**
20	Daka-Imp	0.20	0.60	-0.10	0.07	1.63	4.1	0.017	0.05	-1.41	3.82	0.048	2.817	0.118	**0.71**	**0.89**
21	Daka-Imp	0.20	0.60	-0.10	0.16	2.45	9.4	0.017	0.13	-0.63	3.83	0.021	1.250	0.267	**0.81**	**0.78**
22	Daka-Imp	0.20	0.60	-0.10	0.21	2.86	12.8	0.017	0.18	-0.47	3.88	0.016	0.943	0.353	**0.83**	**0.80**
23	Daka-Imp	0.20	0.50	0.00	0.07	1.63	4.1	0.016	0.03	0.00	3.90	0.048	2.941	0.136	**0.49**	**0.46**
24	Daka-Imp	0.20	0.60	-0.10	0.10	2.04	6.5	0.016	0.08	-0.99	4.01	0.031	1.980	0.168	**0.75**	**0.82**
25	Daka-Imp	0.20	0.60	-0.10	0.20	2.86	12.8	0.015	0.15	-0.51	4.02	0.016	1.015	0.328	**0.76**	**0.80**
26	Daka-Imp	0.20	0.50	-0.20	0.10	2.04	6.5	0.015	0.07	-2.02	4.05	0.031	2.020	0.198	**0.75**	**1.13**
27	Daka-Imp	0.20	0.50	0.00	0.19	2.86	12.8	0.015	0.14	0.00	4.08	0.016	1.042	0.384	**0.75**	**0.64**
28	Daka-Imp	0.20	0.50	0.00	0.17	2.86	12.8	0.014	0.12	0.00	4.28	0.016	1.149	0.348	**0.71**	**0.63**
29	Daka-Imp	0.20	0.50	0.00	0.08	2.04	6.5	0.013	0.05	0.00	4.45	0.031	2.439	0.164	**0.55**	**0.51**
30	Daka-Imp	0.20	0.50	0.00	0.12	2.45	9.4	0.013	0.07	0.00	4.45	0.021	1.695	0.236	**0.62**	**0.57**
31	Daka-Imp	0.20	0.60	-0.10	0.16	2.86	12.8	0.013	0.13	-0.63	4.47	0.016	1.250	0.267	**0.81**	**0.81**
32	Daka-Imp	0.20	0.60	-0.10	0.12	2.45	9.4	0.012	0.09	-0.86	4.49	0.021	1.724	0.193	**0.78**	**0.83**
33	Daka-Imp	0.20	0.60	-0.10	0.21	3.27	16.7	0.012	0.17	-0.49	4.50	0.012	0.971	0.343	**0.83**	**0.82**
34	Daka-Imp	0.20	0.70	-0.20	0.05	1.63	4.1	0.012	0.04	-3.92	4.51	0.048	3.922	0.073	**0.83**	**1.62**
35	Daka-Imp	0.20	0.50	0.00	0.20	3.27	16.7	0.012	0.15	0.00	4.52	0.012	0.980	0.408	**0.72**	**0.68**
36	Daka-Imp	0.20	0.50	0.00	0.19	3.27	16.7	0.012	0.14	0.00	4.64	0.012	1.031	0.388	**0.72**	**0.67**
37	Daka-Imp	0.20	0.50	0.00	0.03	1.23	2.4	0.011	0.01	0.00	4.67	0.085	7.407	0.054	**0.41**	**0.36**
38	Daka-Imp	0.20	0.60	-0.10	0.19	3.27	16.7	0.011	0.13	-0.53	4.71	0.012	1.064	0.313	**0.66**	**0.83**
39	Daka-Imp	0.20	0.60	-0.10	0.04	1.63	4.1	0.011	0.03	-2.27	4.85	0.048	4.545	0.073	**0.73**	**1.11**
40	Daka-Imp	0.20	0.50	0.00	0.18	3.27	16.7	0.011	0.12	0.00	4.85	0.012	1.130	0.354	**0.69**	**0.66**
41	Daka-Imp	0.20	0.70	-0.20	0.03	1.23	2.4	0.011	0.02	-8.00	4.86	0.085	8.000	0.036	**0.92**	**2.76**
42	Daka-Imp	0.20	0.50	0.00	0.13	2.86	12.8	0.010	0.09	0.00	4.93	0.016	1.527	0.262	**0.67**	**0.60**
43	Daka-Imp	0.20	0.60	-0.10	0.02	1.23	2.4	0.010	0.02	-4.17	4.96	0.085	8.333	0.040	**0.84**	**1.61**
44	Daka-Imp	0.20	0.70	-0.20	0.07	2.04	6.5	0.010	0.05	-3.08	5.00	0.031	3.077	0.093	**0.76**	**1.41**
45	Daka-Imp	0.20	0.60	-0.10	0.13	3.27	16.7	0.008	0.10	-0.78	5.71	0.012	1.563	0.213	**0.79**	**0.85**

Table A-6 All Data with Wave Perpendicular to Smooth Structure(2)

Test	Type	B (m)	h_o (m)	R_c (m)	Incident H_{mo}(m)	Incident T_p(s)	Incident L_0(m)	s_{op} -	Transmitted H_t(m)	R_c/H_i	ξ	B/L0	B/H_s	H_s/h	K_t	K_{tc}
1	Infram	2.00	5.70	1.40	1.29	5.24	4.34	0.030	0.08	1.09	1.44	0.047	1.550	0.226	**0.06**	**0.06**
2	Infram	2.00	5.70	1.10	1.46	5.70	4.61	0.029	0.26	0.75	1.47	0.039	1.370	0.256	**0.18**	**0.16**
3	Infram	2.00	5.70	0.80	1.66	5.95	4.91	0.030	0.46	0.48	1.44	0.036	1.205	0.291	**0.28**	**0.24**
4	Infram	2.00	5.70	0.50	1.83	6.37	5.38	0.029	0.61	0.27	1.47	0.032	1.093	0.321	**0.34**	**0.31**
5	Infram	2.00	5.70	0.10	2.02	6.71	5.38	0.029	0.81	0.05	1.47	0.028	0.990	0.354	**0.40**	**0.38**
11	Infram	4.50	5.70	1.40	1.34	5.29	4.31	0.031	0.07	1.04	1.43	0.103	3.358	0.235	**0.06**	**0.07**
12	Infram	4.50	5.70	1.10	1.53	5.71	4.60	0.030	0.25	0.72	1.44	0.088	2.941	0.268	**0.17**	**0.17**
13	Infram	4.50	5.70	0.80	1.72	6.06	4.88	0.030	0.44	0.47	1.44	0.079	2.616	0.302	**0.26**	**0.25**
14	Infram	4.50	5.70	0.50	1.90	6.45	5.13	0.029	0.61	0.26	1.46	0.069	2.368	0.333	**0.32**	**0.31**
14a	Infram	4.50	5.70	0.50	1.87	6.62	4.81	0.027	0.57	0.27	1.51	0.066	2.406	0.328	**0.30**	**0.32**
15	Infram	4.50	5.70	0.10	2.07	6.67	5.39	0.030	0.82	0.05	1.45	0.065	2.174	0.363	**0.40**	**0.37**
16	Infram	15.00	6.80	1.60	1.91	6.41	5.09	0.030	0.19	0.84	1.45	0.234	7.853	0.281	**0.10**	**0.14**
17	Infram	15.00	6.80	1.20	2.07	6.65	5.34	0.030	0.39	0.58	1.44	0.217	7.246	0.304	**0.19**	**0.21**
18	Infram	15.00	6.80	1.90	1.75	5.99	4.90	0.031	0.09	1.09	1.41	0.268	8.571	0.257	**0.05**	**0.05**
18a	Infram	15.00	6.80	1.90	1.75	5.99	4.87	0.031	0.10	1.09	1.41	0.268	8.571	0.257	**0.06**	**0.05**
19	Infram	15.00	6.80	0.60	2.18	6.70	5.45	0.031	0.60	0.28	1.42	0.214	6.881	0.321	**0.27**	**0.30**
20	Infram	15.00	6.80	0.60	2.02	6.35	5.25	0.032	0.51	0.30	1.40	0.238	7.426	0.297	**0.25**	**0.29**
20a	Infram	15.00	6.80	-0.20	2.01	6.33	5.24	0.032	0.66	-0.10	1.39	0.240	7.463	0.296	**0.33**	**0.41**
3101	H2014	0.20	0.62	0.08	0.19	1.84	5.28	0.037	0.05	0.41	1.49	0.038	1.031	0.313	**0.27**	**0.27**
3102	H2014	0.20	0.70	0.00	0.15	2.13	7.08	0.021	0.06	0.00	1.99	0.028	1.370	0.209	**0.40**	**0.47**
3103	H2014	0.20	0.70	0.00	0.20	1.83	5.22	0.038	0.07	0.00	1.46	0.038	1.005	0.284	**0.36**	**0.39**
3104	H2014	0.20	0.78	-0.08	0.21	1.83	5.22	0.039	0.09	-0.39	1.44	0.038	0.976	0.263	**0.44**	**0.50**
3105	H2014	0.20	0.86	-0.16	0.16	2.16	7.28	0.022	0.12	-0.99	1.92	0.027	1.242	0.187	**0.71**	**0.76**
3106	H2014	0.20	0.86	-0.16	0.21	1.80	5.05	0.041	0.13	-0.78	1.42	0.040	0.976	0.238	**0.63**	**0.62**
3141	H2014	0.20	0.78	-0.08	0.21	1.83	5.22	0.039	0.09	-0.39	1.44	0.038	0.971	0.264	**0.45**	**0.50**
3142	H2014	0.20	0.86	-0.16	0.16	2.16	7.28	0.022	0.11	-1.00	1.93	0.027	1.250	0.186	**0.71**	**0.76**
3151	H2014	0.20	0.70	0.00	0.14	2.14	7.14	0.020	0.06	0.00	2.01	0.028	1.389	0.206	**0.42**	**0.48**
3152	H2014	0.20	0.70	0.00	0.20	1.82	5.17	0.038	0.07	0.00	1.47	0.039	1.026	0.279	**0.36**	**0.39**
3153	H2014	0.20	0.78	-0.08	0.21	1.81	5.11	0.040	0.09	-0.39	1.43	0.039	0.976	0.263	**0.45**	**0.50**

Table A-7 All Data with Wave Perpendicular to Smooth Structure(3)

Test	Type	B (m)	h_o (m)	R_c (m)	Incident H_{mo}(m)	Incident T_p(s)	Incident L_0(m)	s_{op} -	Transmitted H_t(m)	R_c/H_i	ξ	B/L0	B/H_d	H_d/h	K_t	K_{tc}
1s	Delos	0.20	0.30	0.00	0.09	1.60	3.99	0.021	0.05	0.00	2.28	0.050	2.353	0.283	**0.56**	**0.51**
2s	Delos	0.20	0.30	0.00	0.12	1.71	4.54	0.026	0.06	0.00	2.07	0.044	1.695	0.393	**0.51**	**0.48**
3s	Delos	0.20	0.30	0.00	0.14	1.97	6.05	0.023	0.07	0.00	2.21	0.033	1.449	0.460	**0.48**	**0.50**
4s	Delos	0.20	0.30	0.00	0.07	1.28	2.56	0.025	0.03	0.00	2.09	0.078	3.077	0.217	**0.46**	**0.49**
5s	Delos	0.20	0.30	0.00	0.09	1.35	2.83	0.032	0.04	0.00	1.85	0.071	2.174	0.307	**0.48**	**0.45**
6s	Delos	0.20	0.30	0.00	0.12	1.60	3.99	0.030	0.06	0.00	1.91	0.050	1.653	0.403	**0.48**	**0.46**
7s	Delos	0.20	0.30	0.00	0.14	2.33	8.44	0.016	0.07	0.00	2.63	0.024	1.471	0.453	**0.53**	**0.55**
8s	Delos	0.20	0.30	0.00	0.12	1.60	3.99	0.031	0.06	0.00	1.89	0.050	1.613	0.413	**0.48**	**0.46**
9s	Delos	0.20	0.25	0.05	0.08	1.60	3.99	0.021	0.03	0.61	2.33	0.050	2.439	0.328	**0.37**	**0.33**
10s	Delos	0.20	0.25	0.05	0.10	1.83	5.21	0.018	0.04	0.52	2.46	0.038	2.083	0.384	**0.42**	**0.37**
11s	Delos	0.20	0.25	0.05	0.11	1.83	5.21	0.022	0.05	0.44	2.26	0.038	1.770	0.452	**0.42**	**0.38**
12s	Delos	0.20	0.25	0.05	0.06	1.28	2.56	0.023	0.02	0.83	2.18	0.078	3.333	0.240	**0.27**	**0.25**
13s	Delos	0.20	0.25	0.05	0.08	1.35	2.83	0.028	0.03	0.63	2.00	0.071	2.532	0.316	**0.33**	**0.28**
14s	Delos	0.20	0.25	0.05	0.10	1.35	2.83	0.035	0.04	0.51	1.79	0.071	2.041	0.392	**0.37**	**0.29**
15s	Delos	0.20	0.35	-0.05	0.11	1.71	4.54	0.024	0.07	-0.45	2.14	0.044	1.818	0.314	**0.65**	**0.63**
16s	Delos	0.20	0.35	-0.05	0.15	2.13	7.09	0.021	0.09	-0.33	2.29	0.028	1.333	0.429	**0.58**	**0.61**
17s	Delos	0.20	0.35	-0.05	0.19	2.13	7.09	0.026	0.09	-0.27	2.06	0.028	1.081	0.529	**0.49**	**0.56**
18s	Delos	0.20	0.35	-0.05	0.09	1.28	2.56	0.033	0.06	-0.59	1.83	0.078	2.353	0.243	**0.65**	**0.63**
19s	Delos	0.20	0.35	-0.05	0.13	1.42	3.16	0.042	0.07	-0.38	1.63	0.063	1.515	0.377	**0.53**	**0.53**
20s	Delos	0.20	0.35	-0.05	0.16	1.71	4.54	0.036	0.09	-0.31	1.76	0.044	1.227	0.466	**0.53**	**0.53**
1	bw1	0.30	0.75	0.00	0.16	1.34	2.80	0.056	0.05	0.00	2.82	0.107	1.923	0.208	**0.32**	**0.46**
2	bw1	0.30	0.60	0.15	0.17	1.46	3.33	0.052	0.03	0.85	2.93	0.090	1.744	0.287	**0.15**	**0.23**
3	bw1	0.30	0.75	0.00	0.17	1.45	3.28	0.051	0.06	0.00	2.95	0.091	1.796	0.223	**0.36**	**0.48**
4	bw1	0.30	0.75	0.00	0.13	1.34	2.80	0.047	0.04	0.00	3.06	0.107	2.256	0.177	**0.31**	**0.46**
5	bw1	0.30	0.75	0.00	0.13	1.33	2.76	0.045	0.04	0.00	3.13	0.109	2.400	0.167	**0.29**	**0.45**
6	bw1	0.30	0.75	0.00	0.17	1.56	3.80	0.043	0.06	0.00	3.20	0.079	1.818	0.220	**0.35**	**0.50**
7	bw1	0.30	0.60	0.15	0.17	1.62	4.09	0.041	0.03	0.87	3.28	0.073	1.775	0.282	**0.18**	**0.25**
8	bw1	0.30	0.60	0.15	0.16	1.60	3.99	0.040	0.02	0.93	3.35	0.075	1.899	0.263	**0.10**	**0.22**
9	bw1	0.30	0.60	0.15	0.16	2.02	6.37	0.024	0.03	0.95	4.27	0.047	1.935	0.258	**0.16**	**0.25**
10	bw1	0.30	0.60	0.15	0.13	2.05	6.56	0.020	0.01	1.15	4.77	0.046	2.344	0.213	**0.07**	**0.18**
11	bw1	0.30	0.75	0.00	0.12	2.00	6.24	0.018	0.04	0.00	4.91	0.048	2.609	0.153	**0.36**	**0.51**
12	bw1	0.30	0.60	0.15	0.12	3.32	17.19	0.007	0.01	1.23	7.98	0.017	2.500	0.200	**0.05**	**0.19**
13	bw1	0.30	0.60	0.15	0.11	3.32	17.19	0.007	0.00	1.30	8.22	0.017	2.655	0.188	**0.04**	**0.15**

Table A-8

Analysis of Individual Gauge for Rubble Structure

Setup	Gauge	H_s(m)	T_s(s)	H_{mo}(m)	T_p(s)	K_t	Setup	Gauge	H_s(m)	T_s(s)	H_{mo}(m)	T_p(s)	K_t
Test1 Layout 0° H_i=0.080m T_c=1.60s	1	0.103	1.42	0.091	1.42		Test2 Layout 0° H_i=0.110m T_c=1.88s	1	0.147	1.70	0.126	2.13	
	2	0.108	1.47	0.101	1.59			2	0.147	1.65	0.129	1.59	
	3	0.105	1.48	0.098	1.59			3	0.147	1.68	0.128	1.81	
	4	0.100	1.44	0.094	1.43			4	0.143	1.76	0.124	2.12	
	5	0.112	1.48	0.105	1.55			5	0.144	1.66	0.129	1.60	
	Average	**0.106**	**1.46**	**0.098**	**1.52**	**0.479**			**0.146**	**1.69**	**0.127**	**1.85**	**0.432**
	3D-BDM			**0.094**	**1.60**	**0.489**		**3D-BDM**			**0.120**	**1.82**	**0.450**
	6	0.047	1.33	0.043	1.55			6	0.060	1.54	0.051	1.82	
	7	0.047	1.21	0.050	1.59			7	0.064	1.46	0.061	1.60	
	8	0.046	1.25	0.047	1.55			8	0.060	1.44	0.054	1.81	
	9	0.055	1.33	0.049	1.55			9	0.066	1.48	0.057	1.60	
	10	0.043	1.26	0.045	1.54			10	0.056	1.40	0.052	1.80	
	Average	**0.048**	**1.28**	**0.047**	**1.56**				**0.061**	**1.46**	**0.055**	**1.73**	
	3D-BDM			**0.046**	**1.60**			**3D-BDM**			**0.054**	**1.97**	
Test3 Layout 0° H_i=0.140m T_c=2.12s	1	0.183	2.02	0.163	2.21		Test6 Layout 0° H_i=0.140m T_c=1.50s	1	0.135	1.35	0.121	1.45	
	2	0.154	1.87	0.131	2.13			2	0.129	1.38	0.118	1.50	
	3	0.165	1.91	0.142	2.13			3	0.126	1.38	0.115	1.51	
	4	0.177	2.02	0.163	2.20			4	0.129	1.35	0.117	1.46	
	5	0.152	1.84	0.140	2.04			5	0.133	1.41	0.124	1.51	
	Average	**0.166**	**1.93**	**0.148**	**2.14**	**0.401**			**0.130**	**1.37**	**0.119**	**1.49**	**0.462**
	3D-BDM			**0.132**	**2.13**	**0.424**		**3D-BDM**			**0.112**	**1.51**	**0.464**
	6	0.064	1.79	0.057	2.18			6	0.055	1.26	0.052	1.47	
	7	0.069	1.57	0.065	2.13			7	0.056	1.14	0.062	1.50	
	8	0.066	1.65	0.059	2.13			8	0.052	1.23	0.054	1.49	
	9	0.069	1.74	0.056	2.11			9	0.061	1.29	0.056	1.47	
	10	0.061	1.59	0.057	2.10			10	0.049	1.26	0.051	1.46	
	Average	**0.066**	**1.67**	**0.059**	**2.14**				**0.055**	**1.24**	**0.055**	**1.48**	
	3D-BDM			**0.056**	**2.13**			**3D-BDM**			**0.052**	**1.97**	
Test25 Layout 30° H_i=0.140m T_c=2.12s	1	0.195	1.93	0.175	1.95		Test30 Layout 30° H_i=0.140m T_c=1.50s	1	0.154	1.36	0.143	1.43	
	2	0.146	1.77	0.123	1.83			2	0.144	1.36	0.136	1.36	
	3	0.178	1.89	0.157	1.94			3	0.148	1.39	0.136	1.51	
	4	0.178	1.97	0.163	2.02			4	0.146	1.34	0.138	1.34	
	5	0.176	1.92	0.159	1.95			5	0.143	1.40	0.133	1.60	
	Average	**0.175**	**1.90**	**0.155**	**1.94**	**0.378**			**0.147**	**1.37**	**0.137**	**1.45**	**0.418**
	3D-BDM			**0.144**	**1.97**	**0.424**		**3D-BDM**			**0.130**	**1.42**	**0.438**
	6	0.059	1.42	0.055	1.97			6	0.051	1.16	0.054	1.53	
	7	0.057	1.30	0.058	1.97			7	0.052	1.13	0.054	1.53	
	8	0.057	1.41	0.057	1.96			8	0.051	1.15	0.056	1.49	
	9	0.071	1.56	0.063	1.96			9	0.061	1.25	0.063	1.51	
	10	0.061	1.43	0.061	1.96			10	0.054	1.11	0.060	1.51	
	Average	**0.061**	**1.42**	**0.059**	**1.96**				**0.054**	**1.16**	**0.057**	**1.51**	
	3D-BDM			**0.061**	**1.97**			**3D-BDM**			**0.057**	**1.42**	
Test57 Layout 50° H_i=0.140m T_c=2.12s	1	0.182	1.83	0.163	1.97		Test62 Layout 50° H_i=0.140m T_c=1.50s	1	0.161	1.38	0.146	1.47	
	2	0.147	1.77	0.126	1.97			2	0.134	1.32	0.125	1.35	
	3	0.165	1.82	0.144	2.02			3	0.148	1.38	0.135	1.50	
	4	0.179	1.92	0.161	2.03			4	0.144	1.38	0.134	1.47	
	5	0.165	1.87	0.143	2.02			5	0.141	1.42	0.132	1.51	
	Average	**0.168**	**1.84**	**0.147**	**2.00**	**0.381**			**0.146**	**1.38**	**0.134**	**1.46**	**0.411**
	3D-BDM			**0.140**	**1.97**	**0.407**		**3D-BDM**			**0.127**	**1.42**	**0.425**
	6	0.057	1.49	0.054	1.99			6	0.048	1.07	0.051	1.60	
	7	0.049	1.23	0.051	1.97			7	0.048	1.03	0.054	1.57	
	8	0.055	1.29	0.056	1.97			8	0.051	1.13	0.054	1.65	
	9	0.075	1.64	0.064	2.06			9	0.062	1.33	0.059	1.52	
	10	0.061	1.42	0.056	1.97			10	0.056	1.32	0.058	1.53	
	Average	**0.059**	**1.41**	**0.056**	**1.99**				**0.053**	**1.18**	**0.055**	**1.57**	
	3D-BDM			**0.057**	**1.97**			**3D-BDM**			**0.054**	**1.51**	

Table A-9

Analysis of Individual Gauge for Smooth Structure

Setup	Gauge	H_s(m)	T_s(s)	H_{mo}(m)	T_p(s)	K_t	Setup	Gauge	H_s(m)	T_s(s)	H_{mo}(m)	T_p(s)	K_t
Test1 **Layout 0°** **H_i=0.080m** **T_c=1.60s**	1	0.093	1.56	0.092	1.70		**Test2** **Layout 0°** **H_i=0.110m** **T_c=1.88s**	1	0.142	1.79	0.129	1.77	
	2	0.093	1.52	0.093	1.55			2	0.139	1.74	0.125	2.21	
	3	0.089	1.55	0.089	1.56			3	0.134	1.75	0.120	1.94	
	4	0.090	1.59	0.090	1.70			4	0.136	1.79	0.123	1.78	
	5	0.088	1.53	0.090	1.54			5	0.129	1.72	0.115	2.31	
	Average	**0.091**	**1.55**	**0.091**	**1.61**	**0.531**			**0.136**	**1.76**	**0.122**	**2.00**	**0.495**
	3D-BDM			**0.085**	**1.60**	**0.565**		**3D-BDM**			**0.118**	**1.71**	**0.508**
	6	0.043	1.09	0.046	1.61			6	0.060	1.40	0.058	1.84	
	7	0.047	1.09	0.051	1.52			7	0.060	1.26	0.063	1.83	
	8	0.045	1.06	0.049	1.52			8	0.059	1.28	0.061	1.89	
	9	0.047	1.09	0.049	1.66			9	0.067	1.35	0.062	1.90	
	10	0.042	1.07	0.046	1.66			10	0.056	1.30	0.059	1.88	
	Average	**0.045**	**1.08**	**0.048**	**1.59**				**0.060**	**1.32**	**0.061**	**1.87**	
	3D-BDM			**0.048**	**1.51**			**3D-BDM**			**0.060**	**1.83**	
Test3 **Layout 0°** **H_i=0.140m** **T_c=2.12s**	1	0.181	1.92	0.158	2.21		**Test6** **Layout 0°** **H_i=0.140m** **T_c=1.50s**	1	0.142	1.48	0.133	1.70	
	2	0.181	1.98	0.152	2.13			2	0.139	1.44	0.13	1.55	
	3	0.170	1.91	0.149	2.13			3	0.133	1.48	0.127	1.55	
	4	0.178	1.88	0.146	2.20			4	0.138	1.48	0.127	1.61	
	5	0.161	1.94	0.138	2.04			5	0.131	1.47	0.126	1.50	
	Average	**0.174**	**1.93**	**0.149**	**2.14**	**0.468**			**0.137**	**1.47**	**0.129**	**1.58**	**0.467**
	3D-BDM			**0.138**	**1.97**	**0.478**		**3D-BDM**			**0.121**	**1.60**	**0.479**
	6	0.073	1.67	0.065	2.14			6	0.057	1.19	0.056	1.60	
	7	0.070	1.5	0.070	2.13			7	0.058	1.18	0.062	1.60	
	8	0.069	1.54	0.073	2.13			8	0.057	1.18	0.060	1.60	
	9	0.077	1.61	0.070	2.13			9	0.062	1.19	0.061	1.60	
	10	0.065	1.44	0.066	1.99			10	0.053	1.16	0.061	1.61	
	Average	**0.071**	**1.55**	**0.070**	**2.13**				**0.057**	**1.18**	**0.060**	**1.60**	
	3D-BDM			**0.066**	**1.97**			**3D-BDM**			**0.058**	**1.60**	
Test25 **Layout 30°** **H_i=0.140m** **T_c=2.12s**	1	0.177	1.89	0.162	1.91		**Test30** **Layout 30°** **H_i=0.140m** **T_c=1.50s**	1	0.147	1.40	0.143	1.50	
	2	0.178	1.90	0.154	2.06			2	0.144	1.37	0.137	1.45	
	3	0.174	1.90	0.152	2.05			3	0.141	1.39	0.136	1.47	
	4	0.175	1.90	0.159	1.91			4	0.148	1.40	0.142	1.42	
	5	0.171	1.87	0.151	1.97			5	0.142	1.40	0.136	1.47	
	Average	**0.175**	**1.89**	**0.156**	**1.98**	**0.402**			**0.144**	**1.39**	**0.139**	**1.46**	**0.395**
	3D-BDM			**0.150**	**2.13**	**0.387**		**3D-BDM**			**0.133**	**1.51**	**0.391**
	6	0.058	1.38	0.060	2.11			6	0.050	1.15	0.051	1.47	
	7	0.053	1.21	0.060	1.96			7	0.048	0.96	0.052	1.39	
	8	0.059	1.42	0.057	2.1			8	0.051	1.11	0.053	1.40	
	9	0.075	1.57	0.071	2.11			9	0.064	1.23	0.062	1.43	
	10	0.063	1.38	0.065	1.95			10	0.054	1.13	0.056	1.35	
	Average	**0.062**	**1.39**	**0.063**	**2.05**				**0.053**	**1.12**	**0.055**	**1.41**	
	3D-BDM			**0.058**	**1.83**			**3D-BDM**			**0.052**	**1.42**	
Test57 **Layout 50°** **H_i=0.140m** **T_c=2.12s**	1	0.187	1.94	0.175	2.14		**Test62** **Layout 50°** **H_i=0.140m** **T_c=1.50s**	1	0.145	1.38	0.141	1.50	
	2	0.183	1.84	0.161	1.97			2	0.153	1.37	0.144	1.50	
	3	0.187	1.94	0.166	2.14			3	0.143	1.37	0.135	1.50	
	4	0.176	1.97	0.165	2.20			4	0.140	1.38	0.136	1.42	
	5	0.183	1.96	0.161	2.19			5	0.143	1.38	0.134	1.42	
	Average	**0.183**	**1.93**	**0.166**	**2.13**	**0.306**			**0.145**	**1.38**	**0.138**	**1.47**	**0.328**
	3D-BDM			**0.158**	**1.97**	**0.323**		**3D-BDM**			**0.132**	**1.42**	**0.333**
	6	0.045	1.09	0.046	2.14			6	0.040	0.91	0.043	1.46	
	7	0.044	1.02	0.046	1.95			7	0.039	0.91	0.040	1.48	
	8	0.048	1.11	0.050	1.97			8	0.041	0.88	0.043	1.59	
	9	0.057	1.33	0.060	2.13			9	0.049	1.01	0.052	1.46	
	10	0.052	1.21	0.051	1.97			10	0.042	0.89	0.048	1.59	
	Average	**0.049**	**1.15**	**0.051**	**2.03**				**0.042**	**0.92**	**0.045**	**1.52**	
	3D-BDM			**0.051**	**1.97**			**3D-BDM**			**0.044**	**1.42**	

BDM Analysis on Energy Distribution (1)

Table A-10 (Leeside of Rubble Structure)

Test	Set-up				Measured Incident		H_t	f_p	$1.5f_p$	f_{max}	f_{max}/f_p	E_{total}	$E_{1.5fp\text{-}max}$	S_{op}	K_t	Percent
No.	R_c	H_i (m)	T_s (s)	f_p	H_i	f_p	(m)					(10^{-4})	(10^{-4})			(%)
1	0.00	0.08	1.60	0.624	0.094	0.625	0.05	0.625	0.938	1.992	3.2	1.312	0.534	0.024	0.49	**40.7**
2	0.00	0.11	1.88	0.533	0.120	0.547	0.054	0.625	0.938	1.953	3.1	1.814	0.660	0.023	0.45	**36.4**
3	0.00	0.14	2.12	0.472	0.132	0.469	0.056	0.469	0.704	1.914	4.1	1.971	0.912	0.019	0.42	**46.3**
4	0.00	0.08	1.13	0.883	0.063	0.820	0.032	0.820	1.230	2.656	3.2	0.657	0.209	0.027	0.51	**31.8**
5	0.00	0.11	1.33	0.753	0.095	0.742	0.046	0.703	1.055	2.305	3.3	1.316	0.440	0.033	0.48	**33.4**
6	0.00	0.14	1.50	0.668	0.112	0.664	0.052	0.703	1.055	2.031	2.9	1.682	0.550	0.032	0.46	**32.7**
7	0.00	0.14	2.12	0.472	0.134	0.469	0.057	0.469	0.704	1.875	4.0	2.049	0.916	0.019	0.43	**44.7**
8	0.00	0.14	1.50	0.668	0.127	0.625	0.057	0.625	0.938	2.070	3.3	2.038	0.790	0.032	0.45	**38.8**
9	0.05	0.07	1.50	0.668	0.083	0.625	0.026	0.625	0.938	2.070	3.3	0.423	0.169	0.021	0.31	**40.0**
10	0.05	0.09	1.70	0.589	0.096	0.625	0.031	0.625	0.938	2.383	3.8	0.609	0.269	0.024	0.32	**44.2**
11	0.05	0.11	1.88	0.533	0.109	0.586	0.035	0.625	0.938	2.461	3.9	0.748	0.338	0.024	0.32	**45.2**
12	0.05	0.07	1.06	0.944	0.060	0.938	0.014	0.938	1.407	2.266	2.4	0.124	0.016	0.034	0.23	**12.9**
13	0.05	0.09	1.20	0.833	0.079	0.938	0.021	0.781	1.172	2.461	3.2	0.278	0.078	0.044	0.27	**28.1**
14	0.05	0.11	1.33	0.753	0.095	0.742	0.028	0.781	1.172	2.461	3.2	0.475	0.163	0.033	0.29	**34.3**
15	-0.05	0.09	1.70	0.589	0.094	0.625	0.061	0.625	0.938	1.719	2.8	2.340	0.713	0.024	0.65	**30.5**
16	-0.05	0.13	2.04	0.490	0.131	0.508	0.075	0.508	0.762	1.756	3.5	3.520	1.590	0.022	0.57	**45.2**
17	-0.05	0.17	2.33	0.428	0.157	0.469	0.081	0.469	0.704	1.641	3.5	4.090	1.720	0.022	0.52	**42.1**
18	-0.05	0.09	1.20	0.833	0.076	0.703	0.052	0.820	1.230	1.875	2.3	1.710	0.695	0.024	0.68	**40.6**
19	-0.05	0.13	1.44	0.693	0.106	0.703	0.065	0.703	1.055	1.641	2.3	2.660	0.792	0.034	0.61	**29.8**
20	-0.05	0.17	1.65	0.606	0.144	0.664	0.077	0.664	0.996	1.797	2.7	3.690	1.050	0.041	0.53	**28.5**
21	0.00	0.08	1.60	0.624	0.095	0.625	0.042	0.625	0.938	2.109	3.4	1.110	0.375	0.024	0.44	**33.8**
22	0.00	0.11	1.88	0.533	0.127	0.586	0.053	0.586	0.879	2.070	3.5	1.760	0.779	0.028	0.42	**44.3**
23	0.00	0.11	1.88	0.533	0.129	0.547	0.050	0.547	0.821	2.070	3.8	1.550	0.731	0.025	0.39	**47.2**
24	0.00	0.11	1.88	0.533	0.120	0.586	0.054	0.586	0.879	1.992	3.4	1.830	0.8	0.026	0.45	**43.7**
25	0.00	0.14	2.12	0.472	0.144	0.508	0.061	0.508	0.762	1.992	3.9	2.310	1.15	0.024	0.42	**49.8**
26	0.00	0.08	1.13	0.883	0.072	0.898	0.034	0.898	1.347	2.617	2.9	0.715	0.214	0.037	0.47	**29.9**
27	0.00	0.11	1.33	0.753	0.103	0.820	0.048	0.82	1.230	2.305	2.8	1.420	0.344	0.044	0.47	**24.2**
28	0.00	0.11	1.33	0.753	0.110	0.820	0.045	0.742	1.113	2.344	3.2	1.280	0.419	0.047	0.41	**32.7**
29	0.00	0.11	1.33	0.753	0.103	0.781	0.05	0.781	1.172	2.188	2.8	1.540	0.401	0.040	0.49	**26.0**
30	0.00	0.14	1.50	0.668	0.130	0.703	0.057	0.703	1.055	2.188	3.1	2.060	0.684	0.041	0.44	**33.2**
31	0.00	0.14	2.12	0.472	0.144	0.469	0.064	0.508	0.762	1.953	3.8	2.520	1.28	0.020	0.44	**50.8**
32	0.00	0.14	1.50	0.668	0.131	0.664	0.059	0.664	0.996	1.914	2.9	2.200	0.799	0.037	0.45	**36.3**
33	0.00	0.14	1.50	0.668	0.123	0.664	0.059	0.664	0.996	1.953	2.9	2.190	0.765	0.035	0.48	**34.9**
34	0.00	0.14	1.50	0.668	0.133	0.664	0.062	0.664	0.996	2.109	3.2	2.440	0.840	0.038	0.47	**34.4**
35	0.05	0.07	1.50	0.668	0.080	0.625	0.019	0.703	1.055	2.070	2.9	0.214	0.030	0.020	0.24	**14.0**
36	0.05	0.09	1.70	0.589	0.096	0.586	0.023	0.625	0.938	2.383	3.8	0.343	0.109	0.021	0.24	**31.8**
37	0.05	0.11	1.88	0.533	0.120	0.508	0.030	0.547	0.821	2.305	4.2	0.550	0.243	0.020	0.25	**44.2**
38	0.05	0.11	1.88	0.533	0.114	0.508	0.026	0.586	0.879	2.422	4.1	0.434	0.179	0.019	0.23	**41.2**
39	0.05	0.11	1.88	0.533	0.116	0.547	0.032	0.547	0.821	2.344	4.3	0.656	0.309	0.022	0.28	**47.1**
40	0.05	0.07	1.06	0.944	0.060	0.898	0.012	0.898	1.347	1.953	2.2	0.087	0.004	0.031	0.20	**4.5**
41	0.05	0.09	1.20	0.833	0.084	0.820	0.018	0.781	1.172	2.422	3.1	0.211	0.045	0.036	0.21	**21.3**
42	0.05	0.11	1.33	0.753	0.099	0.781	0.024	0.703	1.055	2.227	3.2	0.353	0.099	0.039	0.24	**28.0**

Table A-11

BDM Analysis on Energy Distribution (2)
(Leeside of Rubble Structure)

Test	Set-up				Measured Incident		H_t	f_p	$1.5f_p$	f_{max}	f_{max}/f_p	E_{total}	$E_{1.5fp\text{-}max}$	S_{op}	K_t	Percent
No.	R_c	H_i (m)	T_s (s)	f_p	H_i	f_p	(m)					(10^{-4})	(10^{-4})			(%)
43	-0.05	0.09	1.70	0.589	0.102	0.625	0.065	0.625	0.938	1.719	2.8	2.610	0.762	0.026	0.64	**29.2**
44	-0.05	0.13	2.04	0.490	0.136	0.508	0.078	0.547	0.821	1.719	3.1	3.800	1.530	0.022	0.57	**40.3**
45	-0.05	0.13	2.04	0.490	0.135	0.508	0.073	0.469	0.704	1.914	4.1	3.290	1.640	0.022	0.54	**49.8**
46	-0.05	0.13	2.04	0.490	0.132	0.469	0.08	0.508	0.762	1.719	3.4	4.030	1.810	0.019	0.61	**44.9**
47	-0.05	0.17	2.33	0.428	0.165	0.469	0.084	0.469	0.704	1.836	3.9	4.370	1.970	0.023	0.51	**45.1**
48	-0.05	0.09	1.20	0.833	0.083	0.820	0.055	0.898	1.347	2.109	2.3	1.880	0.384	0.036	0.66	**20.4**
49	-0.05	0.13	1.44	0.693	0.123	0.703	0.068	0.703	1.055	1.914	2.7	2.880	0.772	0.039	0.55	**26.8**
50	-0.05	0.13	1.44	0.693	0.120	0.703	0.066	0.703	1.055	2.070	2.9	2.690	0.842	0.038	0.55	**31.3**
51	-0.05	0.13	1.44	0.693	0.124	0.781	0.074	0.742	1.113	1.875	2.5	3.430	0.921	0.048	0.60	**26.9**
52	-0.05	0.17	1.65	0.606	0.146	0.625	0.079	0.625	0.938	1.875	3.0	3.900	1.290	0.037	0.54	**33.1**
53	0.00	0.08	1.60	0.624	0.093	0.664	0.044	0.664	0.996	2.031	3.1	1.220	0.377	0.026	0.47	**30.9**
54	0.00	0.11	1.88	0.533	0.120	0.586	0.053	0.547	0.821	2.031	3.7	1.780	0.789	0.026	0.44	**44.3**
55	0.00	0.11	1.88	0.533	0.117	0.586	0.05	0.547	0.821	1.922	3.5	1.530	0.659	0.026	0.43	**43.1**
56	0.00	0.11	1.88	0.533	0.123	0.547	0.057	0.547	0.821	1.992	3.6	2.050	0.798	0.024	0.46	**38.9**
57	0.00	0.14	2.12	0.472	0.140	0.508	0.057	0.580	0.870	1.953	3.4	2.020	0.985	0.023	0.41	**48.8**
58	0.00	0.08	1.13	0.883	0.072	0.859	0.033	0.859	1.289	2.539	3.0	0.688	0.179	0.034	0.46	**26.0**
59	0.00	0.11	1.33	0.753	0.103	0.781	0.047	0.703	1.055	2.266	3.2	1.370	0.458	0.040	0.46	**33.4**
60	0.00	0.11	1.33	0.753	0.100	0.781	0.042	0.781	1.172	2.266	2.9	1.080	0.314	0.039	0.42	**29.1**
61	0.00	0.11	1.33	0.753	0.099	0.781	0.047	0.781	1.172	2.227	2.9	1.400	0.370	0.039	0.47	**26.4**
62	0.00	0.14	1.50	0.668	0.127	0.703	0.054	0.703	1.055	2.019	2.9	1.830	0.630	0.040	0.43	**34.4**
63	0.00	0.14	2.12	0.472	0.131	0.469	0.057	0.469	0.704	1.950	4.2	2.050	1.050	0.018	0.44	**51.2**
64	0.00	0.14	1.50	0.668	0.131	0.664	0.057	0.664	0.996	2.070	3.1	2.030	0.801	0.037	0.44	**39.5**
65	0.00	0.14	1.50	0.668	0.129	0.664	0.057	0.664	0.996	2.070	3.1	2.030	0.801	0.036	0.44	**39.5**
66	0.00	0.14	1.50	0.668	0.125	0.664	0.057	0.664	0.996	2.070	3.1	2.010	0.778	0.035	0.46	**38.7**
67	0.05	0.07	1.50	0.668	0.079	0.625	0.02	0.664	0.996	1.445	2.2	0.255	0.031	0.020	0.25	**12.2**
68	0.05	0.09	1.70	0.589	0.097	0.625	0.027	0.625	0.938	2.031	3.2	0.465	0.124	0.024	0.28	**26.7**
69	0.05	0.11	1.88	0.533	0.119	0.547	0.029	0.547	0.821	2.109	3.9	0.544	0.203	0.023	0.24	**37.3**
70	0.05	0.11	1.88	0.533	0.112	0.547	0.027	0.547	0.821	2.031	3.7	0.461	0.139	0.021	0.24	**30.2**
71	0.05	0.11	1.88	0.533	0.114	0.508	0.031	0.547	0.821	2.266	4.1	0.606	0.258	0.019	0.27	**42.6**
72	0.05	0.07	1.06	0.944	0.061	0.977	0.013	0.977	1.466	2.031	2.1	0.113	0.005	0.037	0.21	**4.5**
73	0.05	0.09	1.20	0.833	0.082	0.820	0.019	0.820	1.230	1.797	2.2	0.217	0.016	0.035	0.23	**7.4**
74	0.05	0.11	1.33	0.753	0.095	0.820	0.024	0.664	0.996	2.148	3.2	0.367	0.087	0.041	0.25	**23.7**
75	-0.05	0.09	1.70	0.589	0.104	0.625	0.068	0.625	0.938	1.719	2.8	2.890	0.849	0.026	0.65	**29.4**
76	-0.05	0.13	2.04	0.490	0.124	0.508	0.076	0.508	0.762	1.641	3.2	3.630	1.620	0.020	0.61	**44.6**
77	-0.05	0.13	2.04	0.490	0.133	0.547	0.075	0.547	0.821	1.758	3.2	3.500	1.420	0.025	0.56	**40.6**
78	-0.05	0.13	2.04	0.490	0.132	0.508	0.077	0.469	0.704	1.797	3.8	3.730	1.850	0.022	0.58	**49.6**
79	-0.05	0.17	2.33	0.428	0.157	0.430	0.077	0.430	0.645	1.797	4.2	3.720	1.800	0.019	0.49	**48.4**
80	-0.05	0.09	1.20	0.833	0.084	0.898	0.056	0.781	1.172	2.031	2.6	1.980	0.456	0.043	0.67	**23.0**
81	-0.05	0.13	1.44	0.693	0.123	0.742	0.071	0.703	1.055	1.953	2.8	3.120	0.873	0.043	0.58	**28.0**
82	-0.05	0.13	1.44	0.693	0.120	0.703	0.065	0.664	0.996	1.914	2.9	2.660	0.895	0.038	0.54	**33.6**
83	-0.05	0.13	1.44	0.693	0.124	0.742	0.072	0.703	1.055	1.914	2.7	3.280	0.869	0.044	0.58	**26.5**
84	-0.05	0.17	1.65	0.606	0.157	0.664	0.079	0.664	0.996	1.992	3.0	3.860	1.290	0.044	0.50	**33.4**

Table A-12

BDM Analysis on Energy Distribution (1)
(Leeside of Smooth Structure)

Test No.	Set-up R_c	Set-up H_i (m)	Set-up T_s (s)	Set-up f_p	Measured Incident H_i	Measured Incident f_p	H_t (m)	f_p	$1.5f_p$	f_{max}	f_{max}/f_p	E_{total} (10^{-4})	$E_{1.5fp\text{-}max}$ (10^{-4})	S_{op}	K_t	Percent (%)
1	0.00	0.08	1.60	0.624	0.085	0.625	0.048	0.664	0.996	2.305	3.5	1.440	0.553	0.021	0.56	**38.4**
2	0.00	0.11	1.88	0.533	0.118	0.586	0.060	0.547	0.821	1.914	3.5	2.270	0.857	0.026	0.51	**37.8**
3	0.00	0.14	2.12	0.472	0.138	0.508	0.066	0.508	0.762	1.758	3.5	2.720	0.969	0.023	0.48	**35.6**
4	0.00	0.08	1.13	0.883	0.065	0.781	0.030	0.820	1.230	2.969	3.6	0.572	0.205	0.025	0.46	**35.8**
5	0.00	0.11	1.33	0.753	0.092	0.742	0.044	0.742	1.113	2.344	3.2	1.210	0.371	0.032	0.48	**30.7**
6	0.00	0.14	1.50	0.668	0.121	0.625	0.058	0.625	0.938	2.031	3.2	2.11	0.726	0.030	0.48	**34.4**
7	0.00	0.14	2.12	0.472	0.136	0.430	0.072	0.43	0.645	1.680	3.9	3.22	1.450	0.016	0.53	**45.0**
8	0.00	0.14	1.50	0.668	0.124	0.625	0.060	0.625	0.938	1.875	3.0	2.23	0.717	0.031	0.48	**32.2**
9	0.05	0.07	1.50	0.668	0.082	0.625	0.030	0.664	0.996	2.773	4.2	0.548	0.278	0.021	0.37	**50.7**
10	0.05	0.09	1.70	0.589	0.096	0.547	0.040	0.625	0.938	2.422	3.9	1.010	0.454	0.018	0.42	**45.0**
11	0.05	0.11	1.88	0.533	0.113	0.547	0.047	0.547	0.821	2.188	4.0	1.390	0.641	0.022	0.42	**46.1**
12	0.05	0.07	1.06	0.944	0.060	0.781	0.016	0.781	1.172	3.320	4.3	0.156	0.095	0.023	0.27	**60.9**
13	0.05	0.09	1.20	0.833	0.079	0.742	0.026	0.742	1.113	3.008	4.1	0.419	0.216	0.028	0.33	**51.6**
14	0.05	0.11	1.33	0.753	0.098	0.742	0.036	0.703	1.055	2.617	3.7	0.795	0.357	0.035	0.37	**44.9**
15	-0.05	0.09	1.70	0.589	0.110	0.586	0.072	0.586	0.879	1.953	3.3	3.220	1.320	0.024	0.65	**41.0**
16	-0.05	0.13	2.04	0.490	0.150	0.469	0.087	0.469	0.704	1.719	3.7	4.690	1.930	0.021	0.58	**41.2**
17	-0.05	0.17	2.33	0.428	0.185	0.469	0.091	0.430	0.645	1.602	3.7	5.140	1.920	0.026	0.49	**37.4**
18	-0.05	0.09	1.20	0.833	0.085	0.781	0.055	0.820	1.230	2.500	3.0	1.860	0.878	0.033	0.65	**47.2**
19	-0.05	0.13	1.44	0.693	0.132	0.703	0.070	0.664	0.996	2.148	3.2	3.070	1.05	0.042	0.53	**34.2**
20	-0.05	0.17	1.65	0.606	0.163	0.586	0.086	0.586	0.879	1.914	3.3	4.580	1.590	0.036	0.53	**34.7**
21	0.00	0.08	1.60	0.624	0.094	0.625	0.044	0.625	0.938	2.383	3.8	1.190	0.458	0.024	0.47	**38.5**
22	0.00	0.11	1.88	0.533	0.122	0.586	0.053	0.586	0.879	2.188	3.7	1.780	0.68	0.027	0.43	**38.2**
23	0.00	0.11	1.88	0.533	0.123	0.547	0.048	0.508	0.762	2.266	4.5	1.420	0.666	0.024	0.39	**46.9**
24	0.00	0.11	1.88	0.533	0.124	0.547	0.057	0.547	0.821	2.188	4.0	2.010	0.792	0.024	0.46	**39.4**
25	0.00	0.14	2.12	0.472	0.150	0.469	0.058	0.469	0.704	1.914	4.1	2.100	0.864	0.021	0.39	**41.1**
26	0.00	0.08	1.13	0.883	0.079	0.859	0.030	0.82	1.230	2.968	3.6	0.570	0.189	0.037	0.38	**33.2**
27	0.00	0.11	1.33	0.753	0.105	0.781	0.042	0.703	1.055	2.500	3.6	1.130	0.376	0.041	0.40	**33.3**
28	0.00	0.11	1.33	0.753	0.107	0.742	0.039	0.703	1.055	2.500	3.6	0.934	0.315	0.038	0.36	**33.7**
29	0.00	0.11	1.33	0.753	0.104	0.781	0.047	0.703	1.055	2.500	3.6	1.380	0.471	0.041	0.45	**34.1**
30	0.00	0.14	1.50	0.668	0.133	0.664	0.052	0.703	1.055	2.305	3.3	1.660	0.506	0.038	0.39	**30.5**
31	0.00	0.14	2.12	0.472	0.147	0.508	0.060	0.469	0.704	1.641	3.5	2.230	0.795	0.024	0.41	**35.7**
32	0.00	0.14	1.50	0.668	0.140	0.703	0.054	0.704	1.056	2.188	3.1	1.820	0.519	0.044	0.39	**28.5**
33	0.00	0.14	1.50	0.668	0.139	0.664	0.053	0.664	0.996	2.188	3.3	1.780	0.558	0.039	0.38	**31.3**
34	0.00	0.14	1.50	0.668	0.135	0.664	0.052	0.625	0.938	2.266	3.6	1.720	0.604	0.038	0.39	**35.1**
35	0.05	0.07	1.50	0.668	0.086	0.625	0.027	0.664	0.996	2.734	4.1	0.447	0.224	0.022	0.31	**50.1**
36	0.05	0.09	1.70	0.589	0.107	0.586	0.036	0.703	1.055	2.617	3.7	0.812	0.326	0.024	0.34	**40.1**
37	0.05	0.11	1.88	0.533	0.122	0.547	0.043	0.586	0.879	2.383	4.1	1.140	0.519	0.023	0.35	**45.5**
38	0.05	0.11	1.88	0.533	0.125	0.547	0.038	0.547	0.821	2.539	4.6	0.893	0.428	0.024	0.30	**47.9**
39	0.05	0.11	1.88	0.533	0.122	0.547	0.046	0.547	0.821	2.305	4.2	1.320	0.645	0.023	0.38	**48.9**
40	0.05	0.07	1.06	0.944	0.065	0.898	0.015	0.898	1.347	3.516	3.9	0.140	0.079	0.034	0.23	**56.4**
41	0.05	0.09	1.20	0.833	0.084	0.898	0.024	0.742	1.113	3.047	4.1	0.352	0.179	0.043	0.29	**50.9**
42	0.05	0.11	1.33	0.753	0.105	0.781	0.032	0.703	1.055	2.734	3.9	0.629	0.283	0.041	0.30	**45.0**

Table A-13

BDM Analysis on Energy Distribution (2)
(Leeside of Smooth Structure)

Test	Set-up				Measured Incident		H_t	f_p	$1.5f_p$	f_{max}	f_{max}/f_p	E_{total}	$E_{1.5fp\text{-}max}$	S_{op}	K_t	Percent
No.	R_c	H_i (m)	T_s (s)	f_p	H_i	f_p	(m)					(10^{-4})	(10^{-4})			(%)
43	-0.05	0.09	1.70	0.589	0.117	0.625	0.065	0.586	0.879	2.109	3.6	2.650	1.090	0.029	0.56	**41.1**
44	-0.05	0.13	2.04	0.490	0.155	0.469	0.073	0.508	0.762	1.836	3.6	3.2900	1.310	0.022	0.47	**39.8**
45	-0.05	0.13	2.04	0.490	0.153	0.469	0.067	0.508	0.762	1.992	3.9	2.840	1.130	0.022	0.44	**39.8**
46	-0.05	0.13	2.04	0.490	0.157	0.508	0.08	0.430	0.645	1.875	4.4	3.950	1.930	0.026	0.51	**48.9**
47	-0.05	0.17	2.33	0.428	0.194	0.430	0.081	0.469	0.704	1.680	3.6	4.150	1.310	0.023	0.42	**31.6**
48	-0.05	0.09	1.20	0.833	0.097	0.781	0.054	0.82	1.230	2.539	3.1	1.820	0.599	0.038	0.56	**32.9**
49	-0.05	0.13	1.44	0.693	0.143	0.742	0.063	0.664	0.996	2.227	3.4	2.460	0.873	0.050	0.44	**35.5**
50	-0.05	0.13	1.44	0.693	0.139	0.703	0.059	0.664	0.996	2.266	3.4	2.140	0.801	0.044	0.42	**37.4**
51	-0.05	0.13	1.44	0.693	0.133	0.703	0.069	0.664	0.996	2.031	3.1	2.870	1.000	0.042	0.52	**34.8**
52	-0.05	0.17	1.65	0.606	0.178	0.664	0.075	0.625	0.938	2.070	3.3	3.530	1.140	0.050	0.42	**32.3**
53	0.00	0.08	1.60	0.624	0.093	0.664	0.035	0.664	0.996	2.695	4.1	0.772	0.332	0.026	0.38	**43.0**
54	0.00	0.11	1.88	0.533	0.131	0.547	0.044	0.586	0.879	2.383	4.1	1.200	0.495	0.025	0.34	**41.3**
55	0.00	0.11	1.88	0.533	0.131	0.586	0.038	0.586	0.879	2.461	4.2	0.891	0.378	0.029	0.29	**42.4**
56	0.00	0.11	1.88	0.533	0.122	0.547	0.05	0.586	0.879	2.266	3.9	1.570	0.628	0.023	0.41	**40.0**
57	0.00	0.14	2.12	0.472	0.158	0.508	0.051	0.580	0.870	2.148	3.7	1.630	0.688	0.026	0.32	**42.2**
58	0.00	0.08	1.13	0.883	0.073	0.859	0.024	0.859	1.289	3.359	3.9	0.352	0.156	0.034	0.33	**44.3**
59	0.00	0.11	1.33	0.753	0.106	0.820	0.036	0.703	1.055	2.930	4.2	0.813	0.335	0.046	0.34	**41.2**
60	0.00	0.11	1.33	0.753	0.104	0.820	0.030	0.742	1.113	3.047	4.1	0.563	0.25	0.045	0.29	**44.4**
61	0.00	0.11	1.33	0.753	0.107	0.742	0.042	0.742	1.113	2.539	3.4	1.080	0.371	0.038	0.39	**34.4**
62	0.00	0.14	1.50	0.668	0.132	0.703	0.044	0.703	1.055	2.539	3.6	1.190	0.416	0.042	0.33	**35.0**
63	0.00	0.14	2.12	0.472	0.146	0.508	0.048	0.469	0.704	2.148	4.6	1.440	0.661	0.024	0.33	**45.9**
64	0.00	0.14	1.50	0.668	0.127	0.742	0.044	0.703	1.055	2.656	3.8	1.220	0.453	0.045	0.35	**37.1**
65	0.00	0.14	1.50	0.668	0.129	0.703	0.045	0.703	1.055	2.695	3.8	1.240	0.457	0.041	0.35	**36.9**
66	0.00	0.14	1.50	0.668	0.129	0.664	0.045	0.625	0.938	2.578	4.1	1.240	0.528	0.036	0.35	**42.6**
67	0.05	0.07	1.50	0.668	0.092	0.742	0.015	0.742	1.113	3.477	4.7	0.132	0.08	0.032	0.16	**60.6**
68	0.05	0.09	1.70	0.589	0.119	0.547	0.021	0.547	0.821	3.086	5.6	0.265	0.145	0.023	0.18	**54.7**
69	0.05	0.11	1.88	0.533	0.146	0.547	0.027	0.586	0.879	2.773	4.7	0.442	0.209	0.028	0.18	**47.3**
70	0.05	0.11	1.88	0.533	0.146	0.586	0.019	0.586	0.879	3.086	5.3	0.216	0.113	0.032	0.13	**52.3**
71	0.05	0.11	1.88	0.533	0.136	0.547	0.034	0.508	0.762	2.578	5.1	0.722	0.388	0.026	0.25	**53.7**
72	0.05	0.07	1.06	0.944	0.071	0.977	0.007	0.820	1.230	3.945	4.8	0.034	0.025	0.043	0.10	**73.2**
73	0.05	0.09	1.20	0.833	0.093	0.781	0.012	0.820	1.230	3.672	4.5	0.088	0.057	0.036	0.13	**64.8**
74	0.05	0.11	1.33	0.753	0.115	0.820	0.017	0.742	1.113	3.477	4.7	0.172	0.095	0.050	0.15	**55.2**
75	-0.05	0.09	1.70	0.589	0.115	0.664	0.062	0.625	0.938	2.344	3.8	2.370	1.150	0.032	0.54	**48.5**
76	-0.05	0.13	2.04	0.490	0.160	0.508	0.067	0.508	0.762	2.070	4.1	2.840	1.370	0.026	0.42	**48.2**
77	-0.05	0.13	2.04	0.490	0.159	0.469	0.061	0.742	1.113	2.227	3.0	2.340	1.220	0.022	0.38	**52.1**
78	-0.05	0.13	2.04	0.490	0.158	0.508	0.076	0.508	0.762	1.914	3.8	3.590	1.630	0.026	0.48	**45.4**
79	-0.05	0.17	2.33	0.428	0.200	0.439	0.072	0.469	0.704	2.031	4.3	3.280	1.480	0.025	0.36	**45.1**
80	-0.05	0.09	1.20	0.833	0.095	0.781	0.052	0.781	1.172	2.500	3.2	1.690	0.655	0.037	0.55	**38.8**
81	-0.05	0.13	1.44	0.693	0.138	0.664	0.061	0.664	0.996	2.383	3.6	2.360	1.04	0.039	0.44	**44.1**
82	-0.05	0.13	1.44	0.693	0.143	0.703	0.055	0.703	1.055	2.656	3.8	1.880	0.880	0.045	0.38	**46.8**
83	-0.05	0.13	1.44	0.693	0.137	0.703	0.067	0.742	1.113	2.188	2.9	2.830	0.952	0.043	0.49	**33.6**
84	-0.05	0.17	1.65	0.606	0.182	0.664	0.067	0.586	0.879	2.227	3.8	2.840	1.230	0.051	0.37	**43.3**

APPENDIX B

Figures of layouts and cross sections

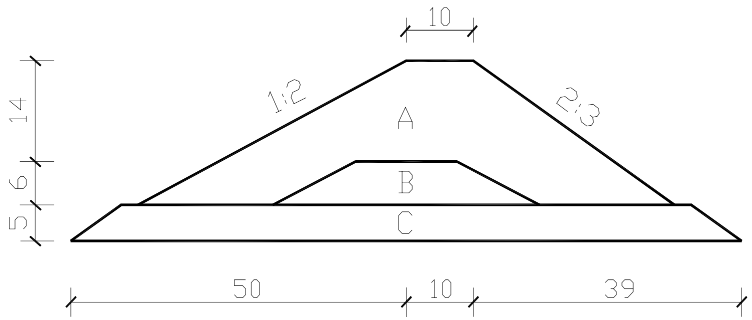

Figure B-1 Cross-section of rubble structure

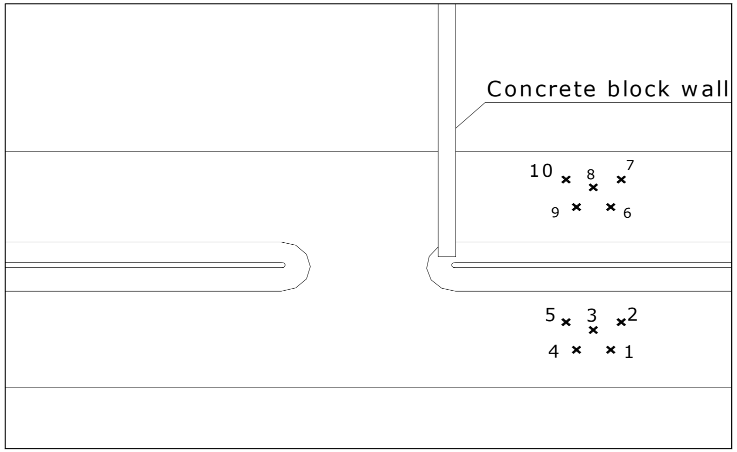

Figure B-2 Rubble structure layout with 0º

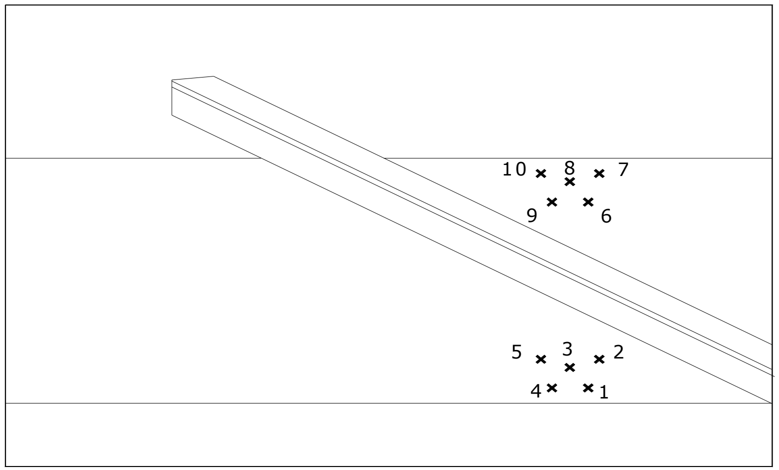

Figure B-3 Rubble structure layout with30º

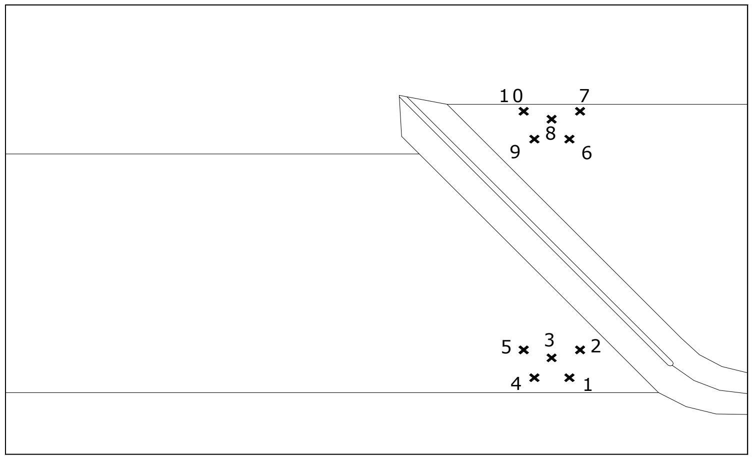

Figure B-4 Rubble structure layout with 50º

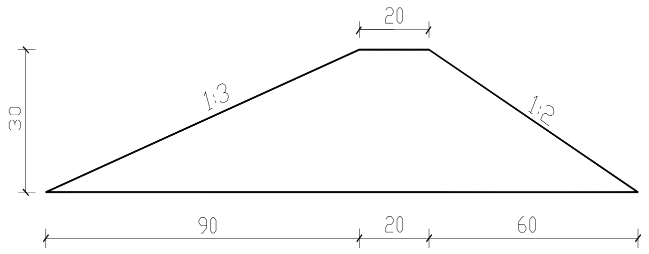

Figure B-5 Cross-section of smooth structure

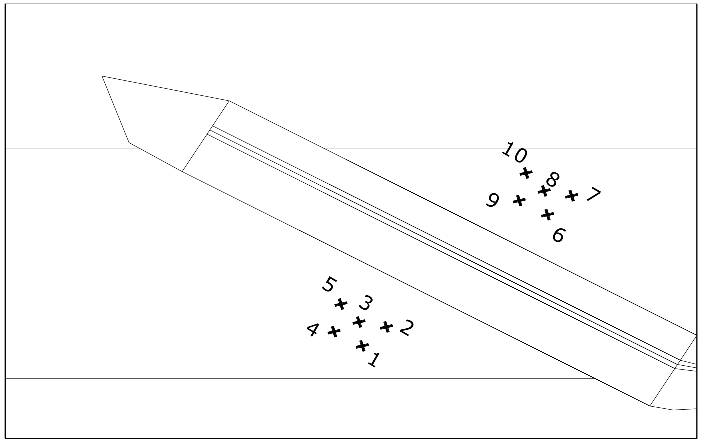

Figure B-6 Smooth structure layout with 0º

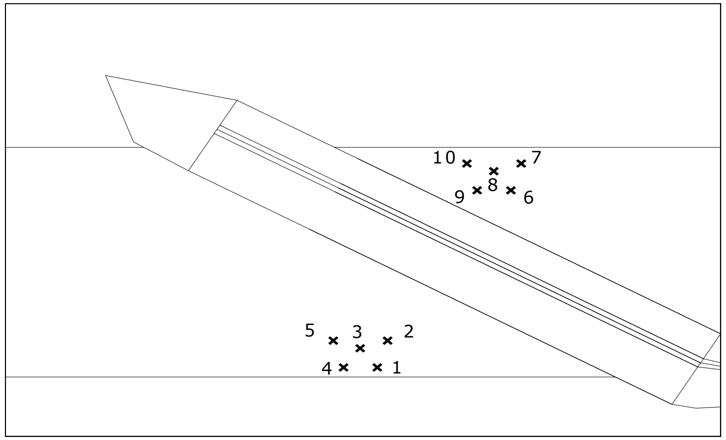

Figure B-7 Smooth structure layout with30º

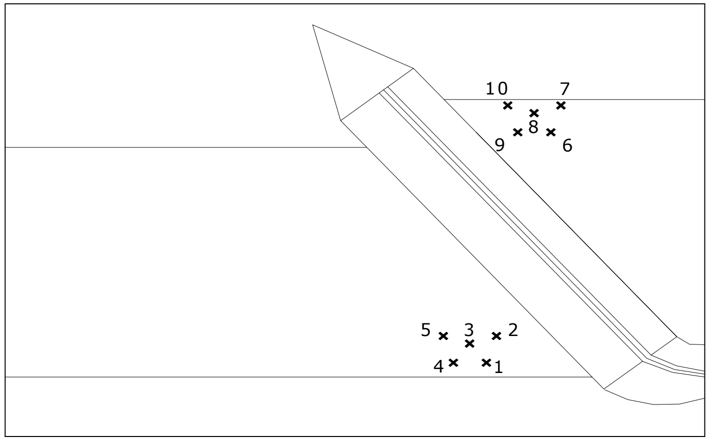

Figure B-8 Smooth structure layout with 50º

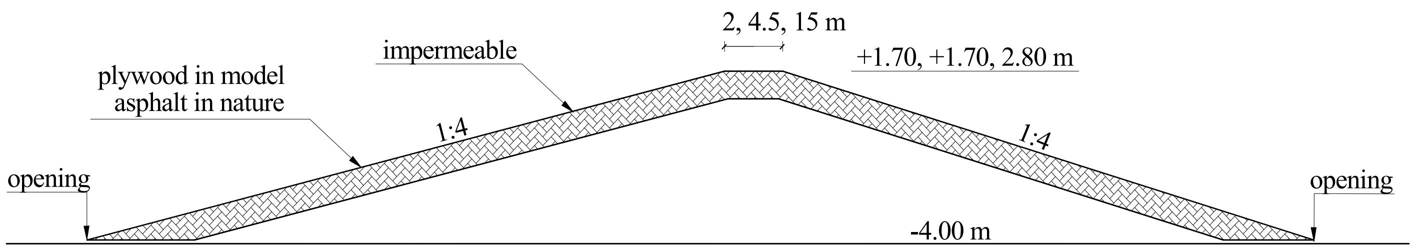

Figure B-9 Cross-section of smooth structure (Infram)

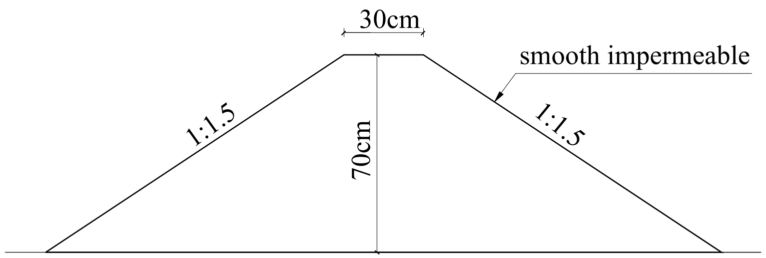

Figure B-10 Cross section of smooth structure (Seeling bw1)

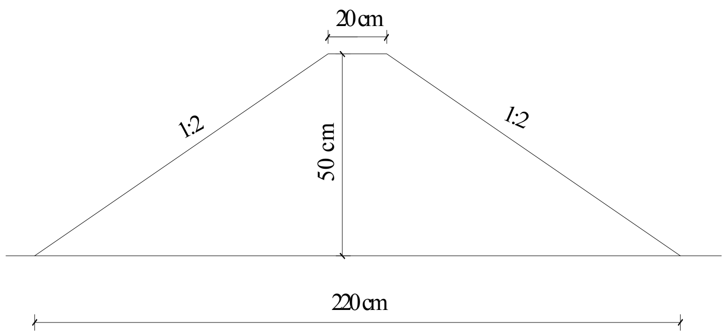

Figure B-11 Cross section of smooth structure (Daka)

APPENDIX C

Figures for Chapter 5

Figure C-1

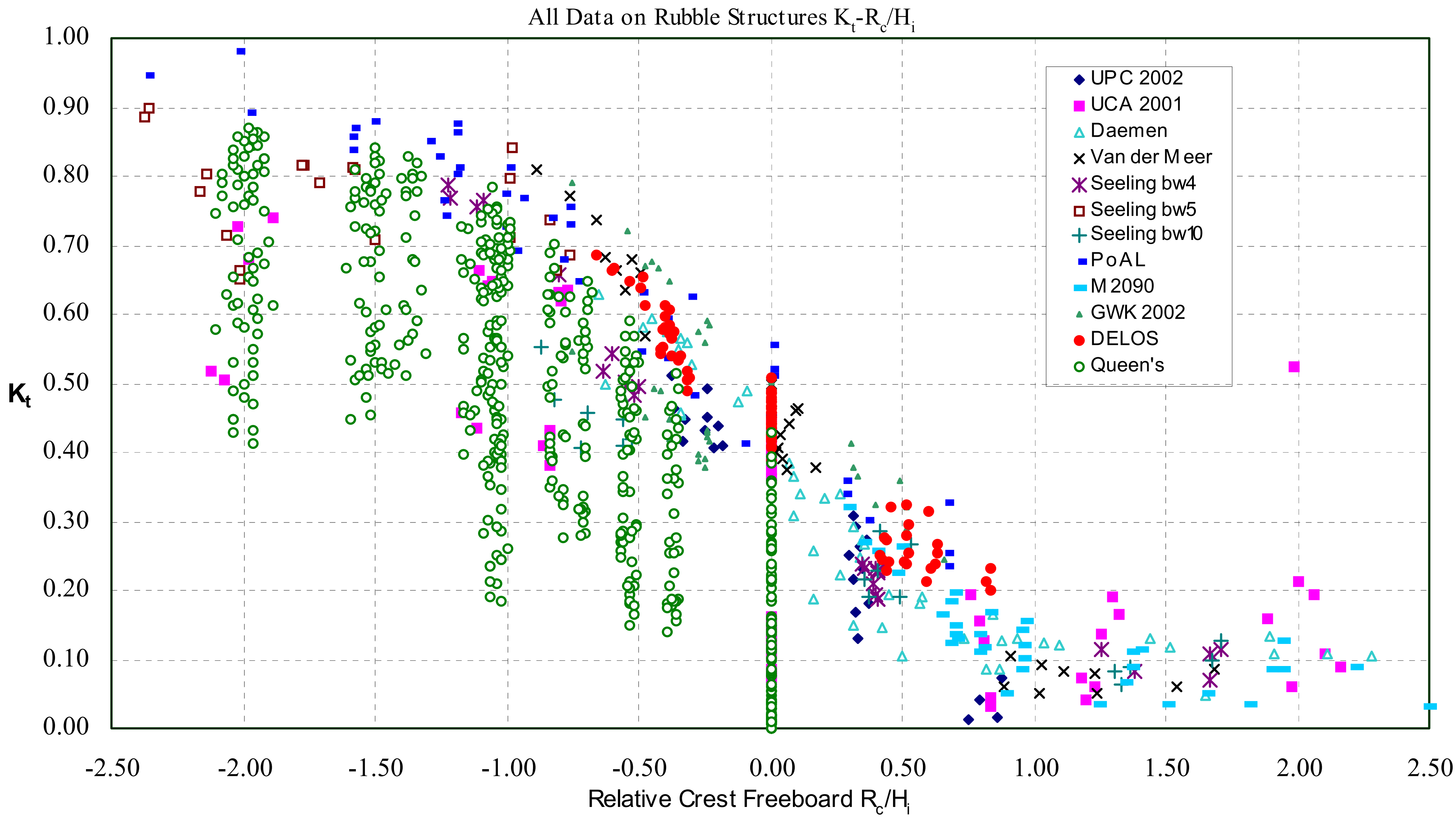
All Data on Rubble Structures Kt-Rc/Hi
1.00
0.90
0.80
0.70
0.60
0.50
0.40
0.30
0.20
0.10
0.00
Kt
-2.50
-2.00
-1.50
-1.00
-0.50
0.00
0.50
1.00
1.50
2.00
2.50
Relative Crest Freeboard Rc/Hi
UPC 2002
UCA 2001
Daemen
Van der Meer
Seeling bw4
Seeling bw5
Seeling bw10
PoAL
M 2090
GWK 2002
DELOS
Queen's

Figure C-2

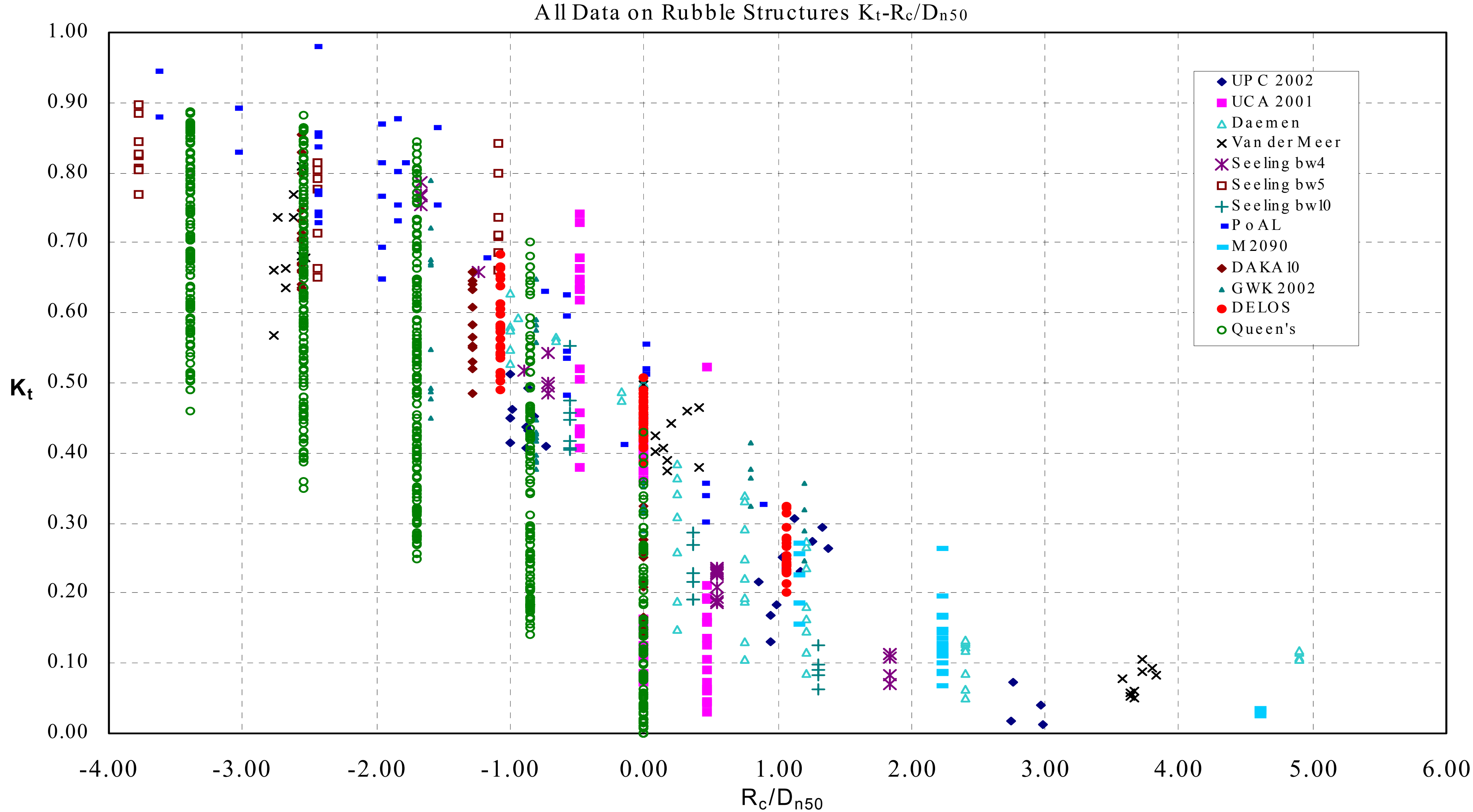
All Data on Rubble Structures Kt-Rc/Dn50
1.00
0.90
0.80
0.70
0.60
0.50
0.40
0.30
0.20
0.10
0.00
Kt
-4.00
-3.00
-2.00
-1.00
0.00
1.00
2.00
3.00
4.00
5.00
6.00
Rc/Dn50
UPC 2002
UCA 2001
Daemen
Van der Meer
Seeling bw4
Seeling bw5
Seeling bw10
PoAL
M2090
DAKA 10
GWK 2002
DELOS
Queen's

Figure C-3

All Data on Smooth Structures

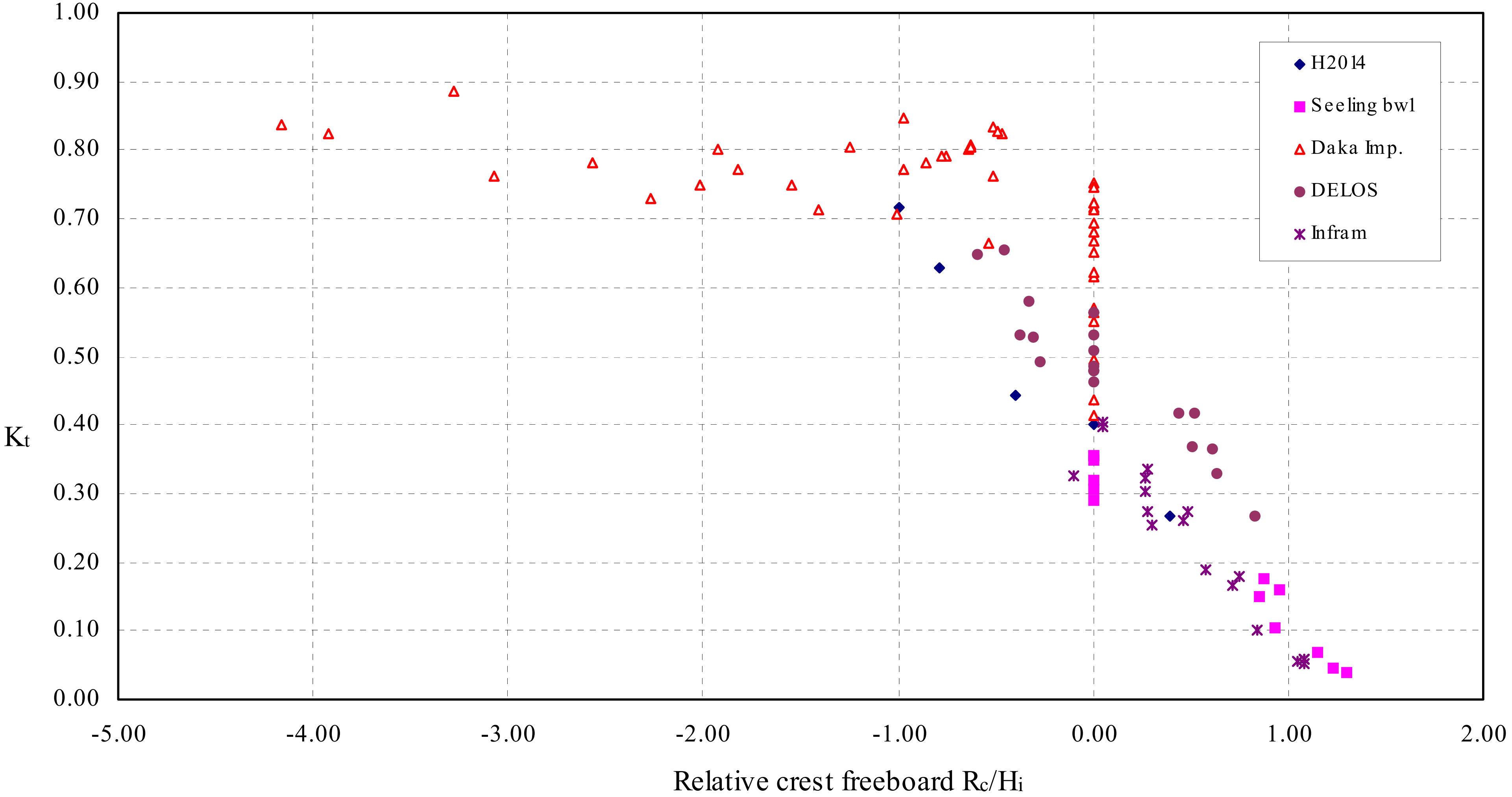

Figure C-4

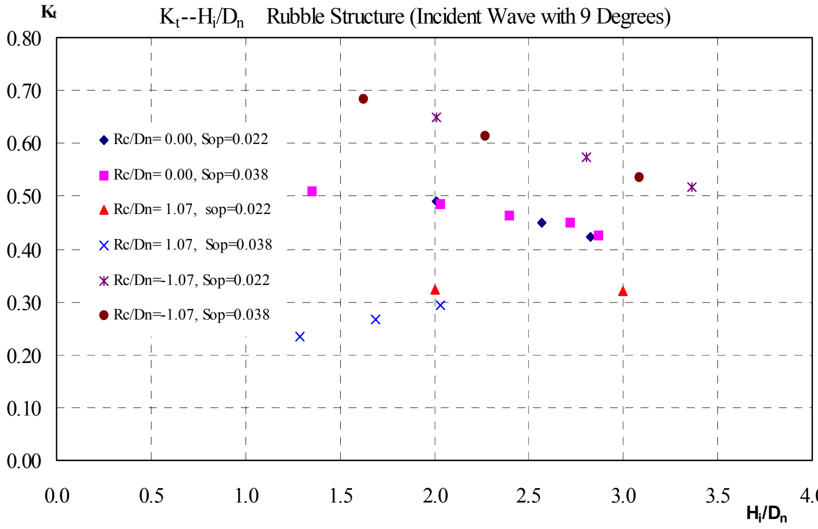

Figure C-5

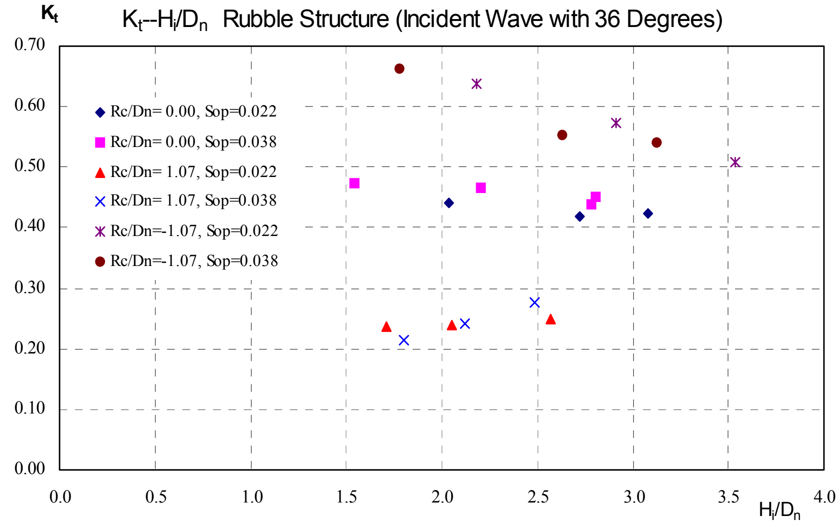

Figure C-6

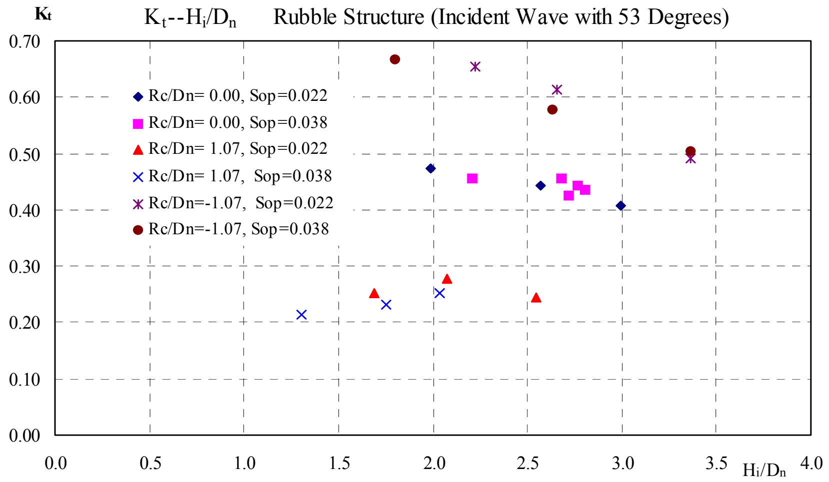

Figure C-7

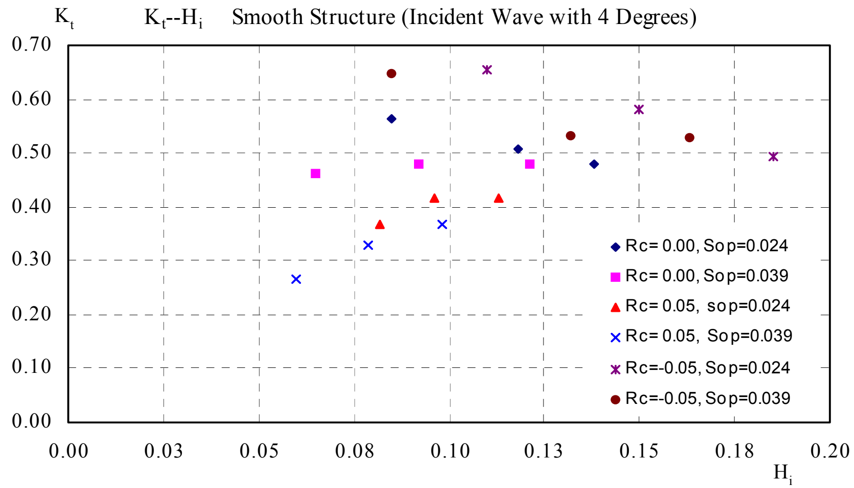

Figure C-8

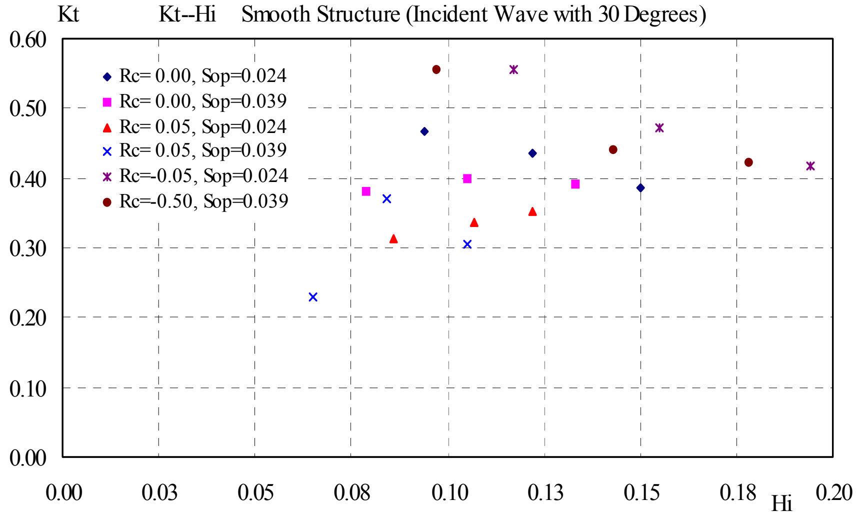

Figure C-9

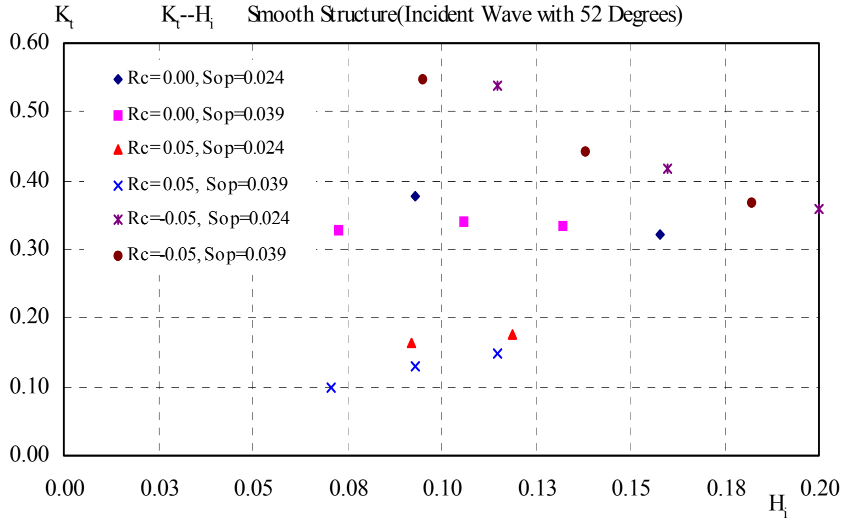

Figure C-10

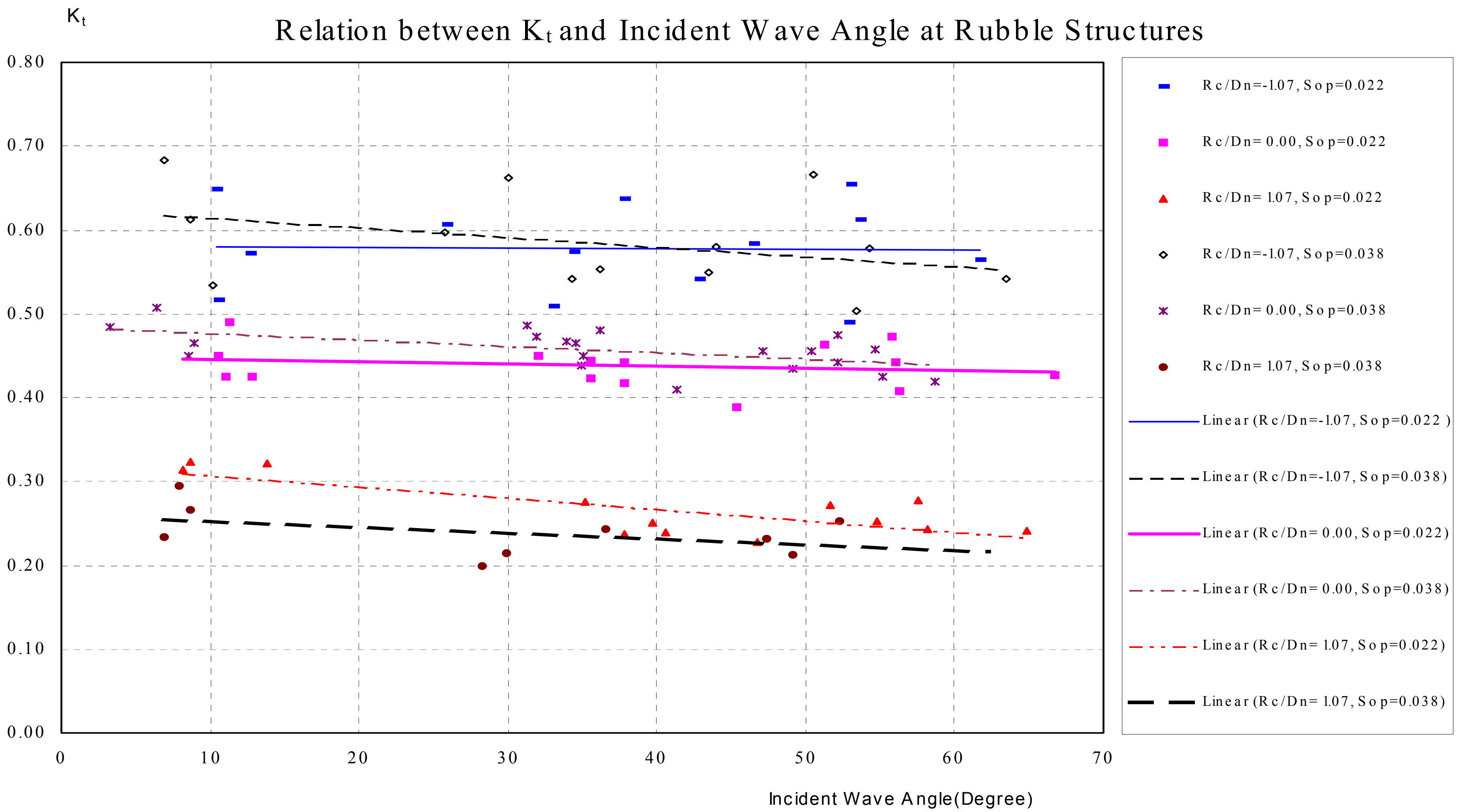

K_t
Relation between K_t and Incident Wave Angle at Rubble Structures
0.80
0.70
0.60
0.50
0.40
0.30
0.20
0.10
0.00
0
10
20
30
40
50
60
70
Incident Wave Angle(Degree)
Rc/Dn=-1.07, Sop=0.022
Rc/Dn= 0.00, Sop=0.022
Rc/Dn= 1.07, Sop=0.022
Rc/Dn=-1.07, Sop=0.038
Rc/Dn= 0.00, Sop=0.038
Rc/Dn= 1.07, Sop=0.038
Linear (Rc/Dn=-1.07, Sop=0.022)
Linear (Rc/Dn=-1.07, Sop=0.038)
Linear (Rc/Dn= 0.00, Sop=0.022)
Linear (Rc/Dn= 0.00, Sop=0.038)
Linear (Rc/Dn= 1.07, Sop=0.022)
Linear (Rc/Dn= 1.07, Sop=0.038)

Figure C-11

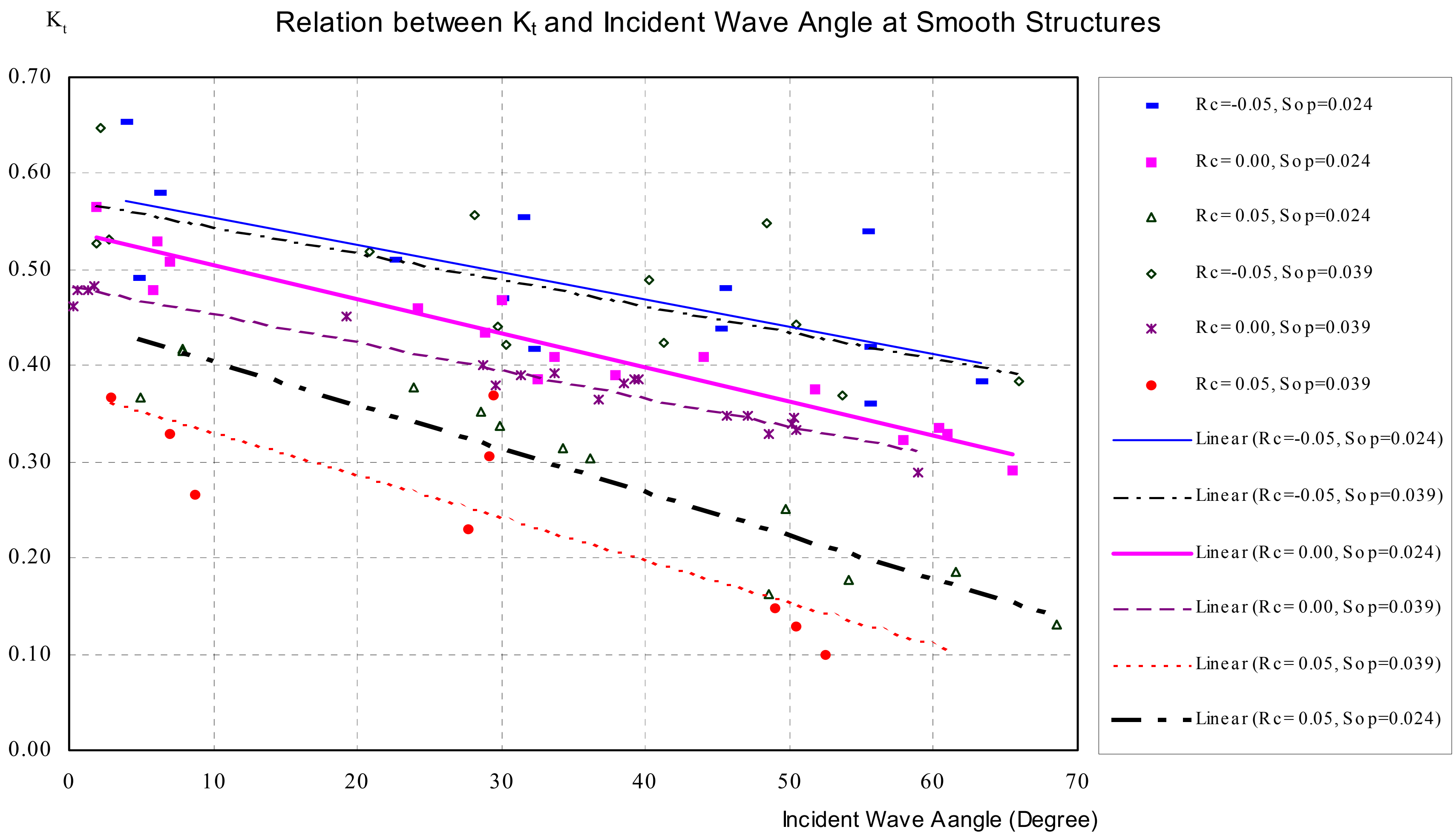

Relation between Kt and Incident Wave Angle at Smooth Structures
Kt
0.70
0.60
0.50
0.40
0.30
0.20
0.10
0.00
0
10
20
30
40
50
60
70
Incident Wave Aangle (Degree)
Rc=-0.05, Sop=0.024
Rc= 0.00, Sop=0.024
Rc= 0.05, Sop=0.024
Rc=-0.05, Sop=0.039
Rc= 0.00, Sop=0.039
Rc= 0.05, Sop=0.039
Linear (Rc=-0.05, Sop=0.024)
Linear (Rc=-0.05, Sop=0.039)
Linear (Rc= 0.00, Sop=0.024)
Linear (Rc= 0.00, Sop=0.039)
Linear (Rc= 0.05, Sop=0.039)
Linear (Rc= 0.05, Sop=0.024)

Figure C-12

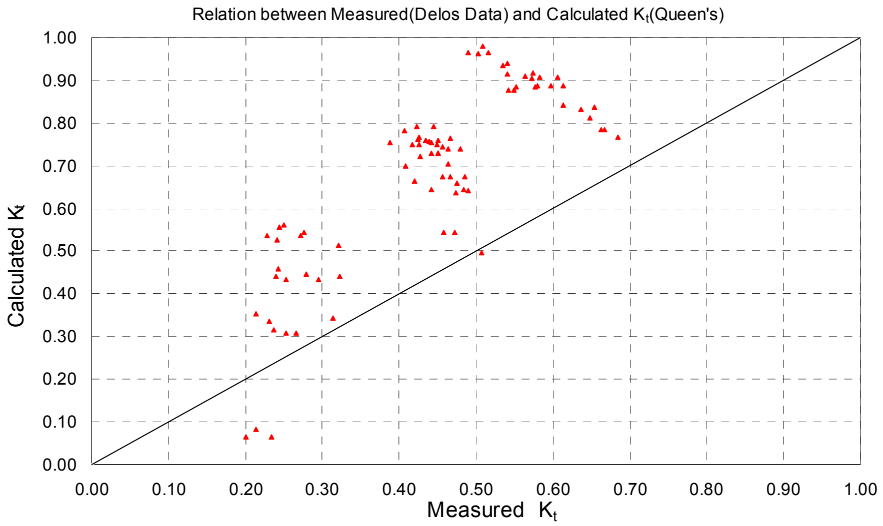

Figure C-13

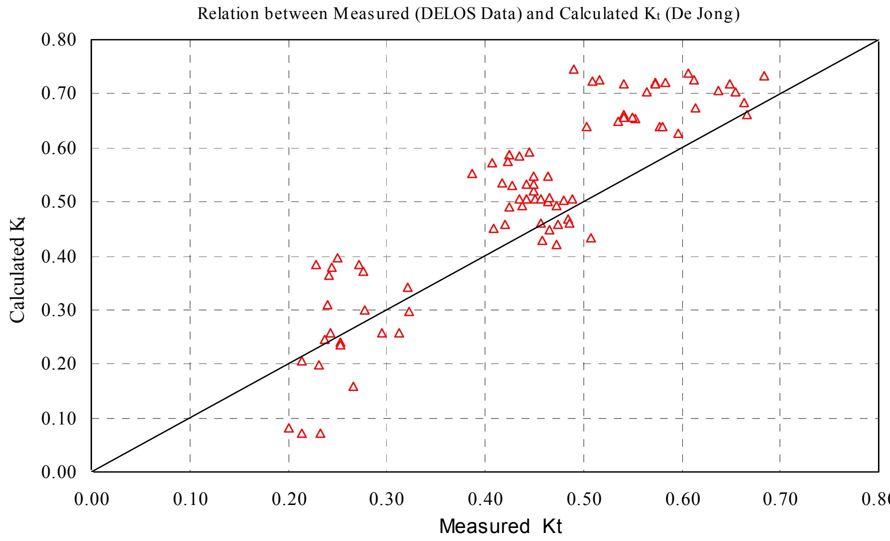

Figure C-14

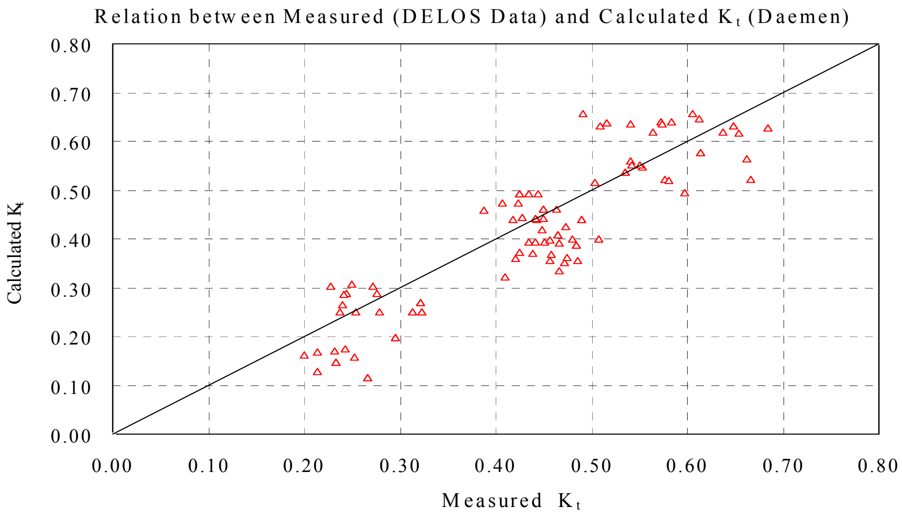

Figure C-15

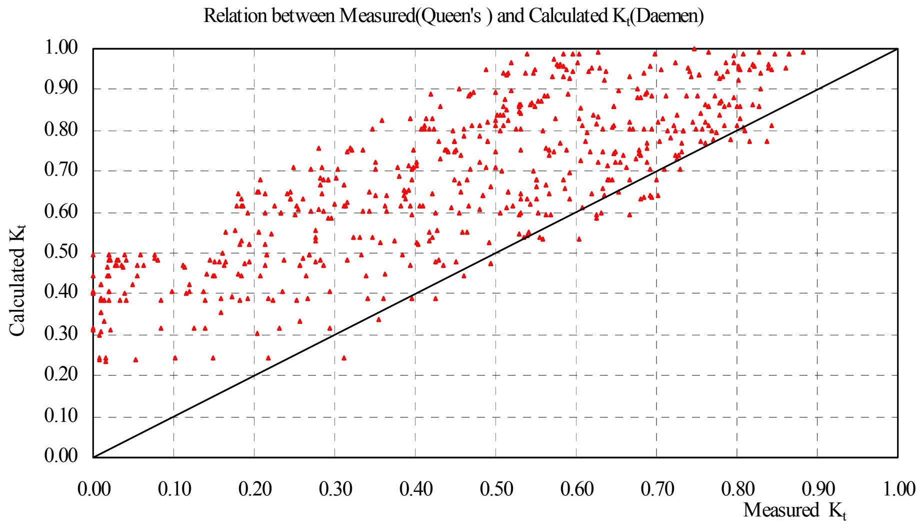

Figure C-16

Relation between Measured and Calculated K_t (De Jong) at Smooth Structures

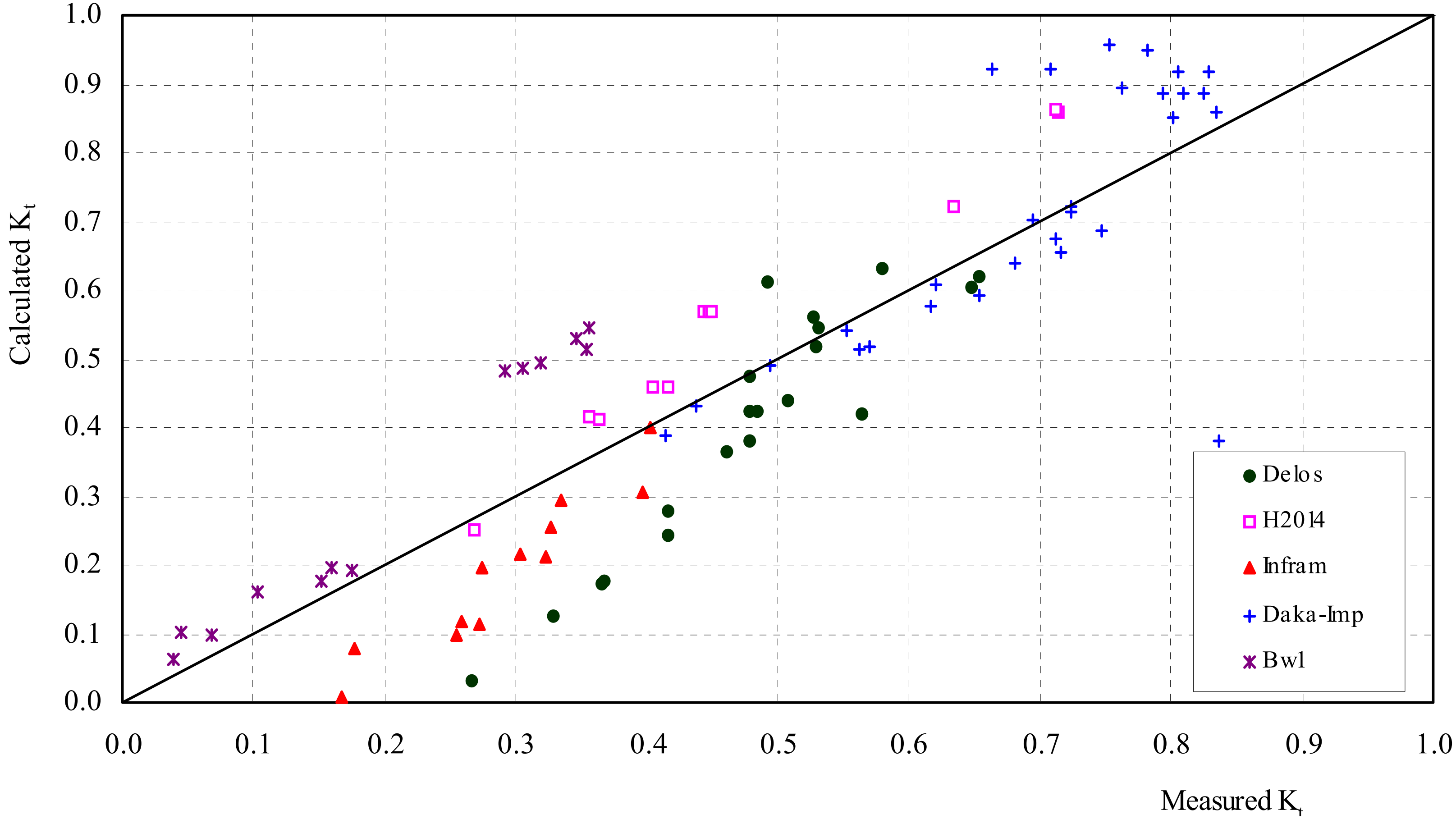

Figure C-17

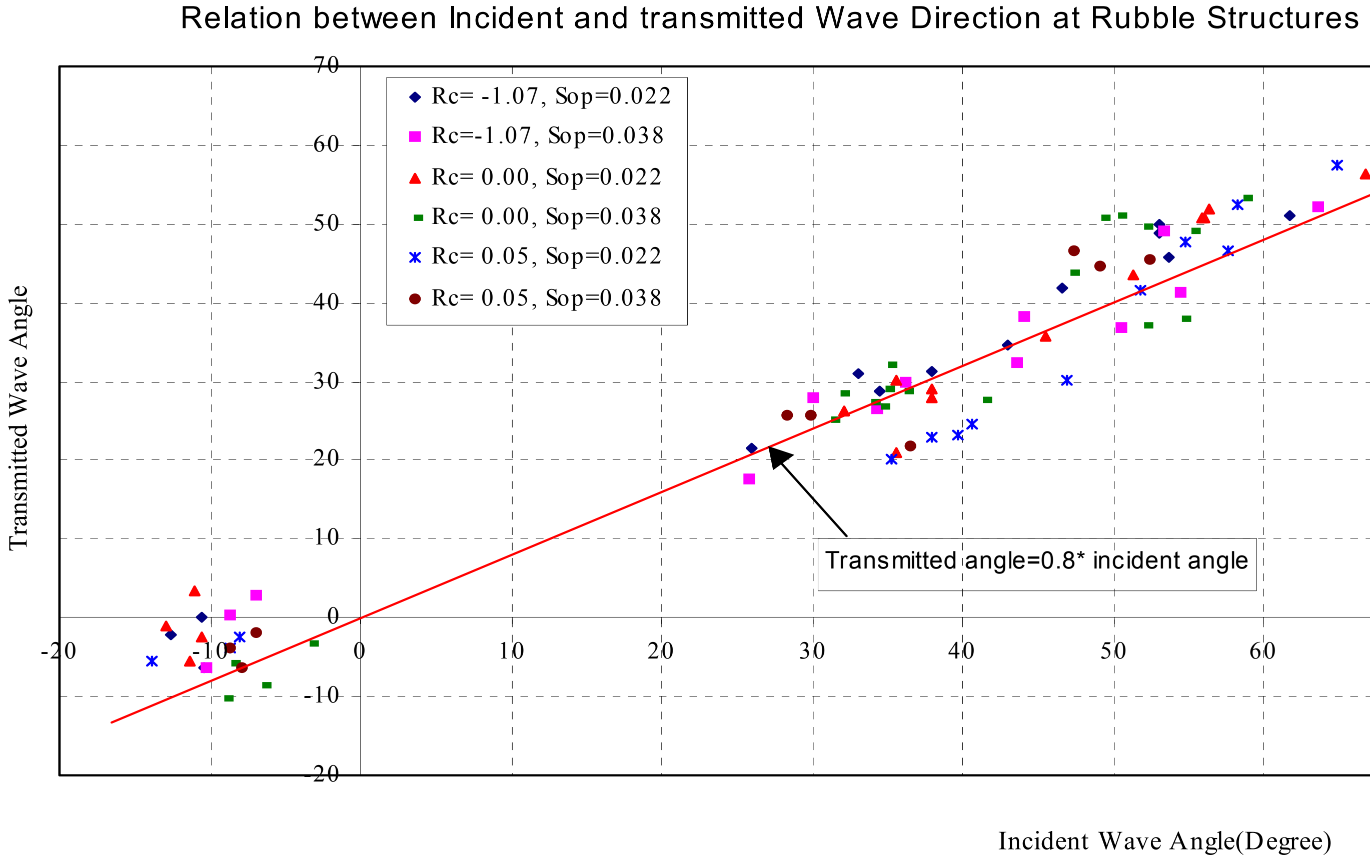
Relation between Incident and transmitted Wave Direction at Rubble Structures
Rc= -1.07, Sop=0.022
Rc=-1.07, Sop=0.038
Rc= 0.00, Sop=0.022
Rc= 0.00, Sop=0.038
Rc= 0.05, Sop=0.022
Rc= 0.05, Sop=0.038
Transmitted angle=0.8* incident angle
Transmitted Wave Angle
Incident Wave Angle(Degree)
70
60
50
40
30
20
10
0
-10
-20
-20
-10
0
10
20
30
40
50
60
70

Figure C-18

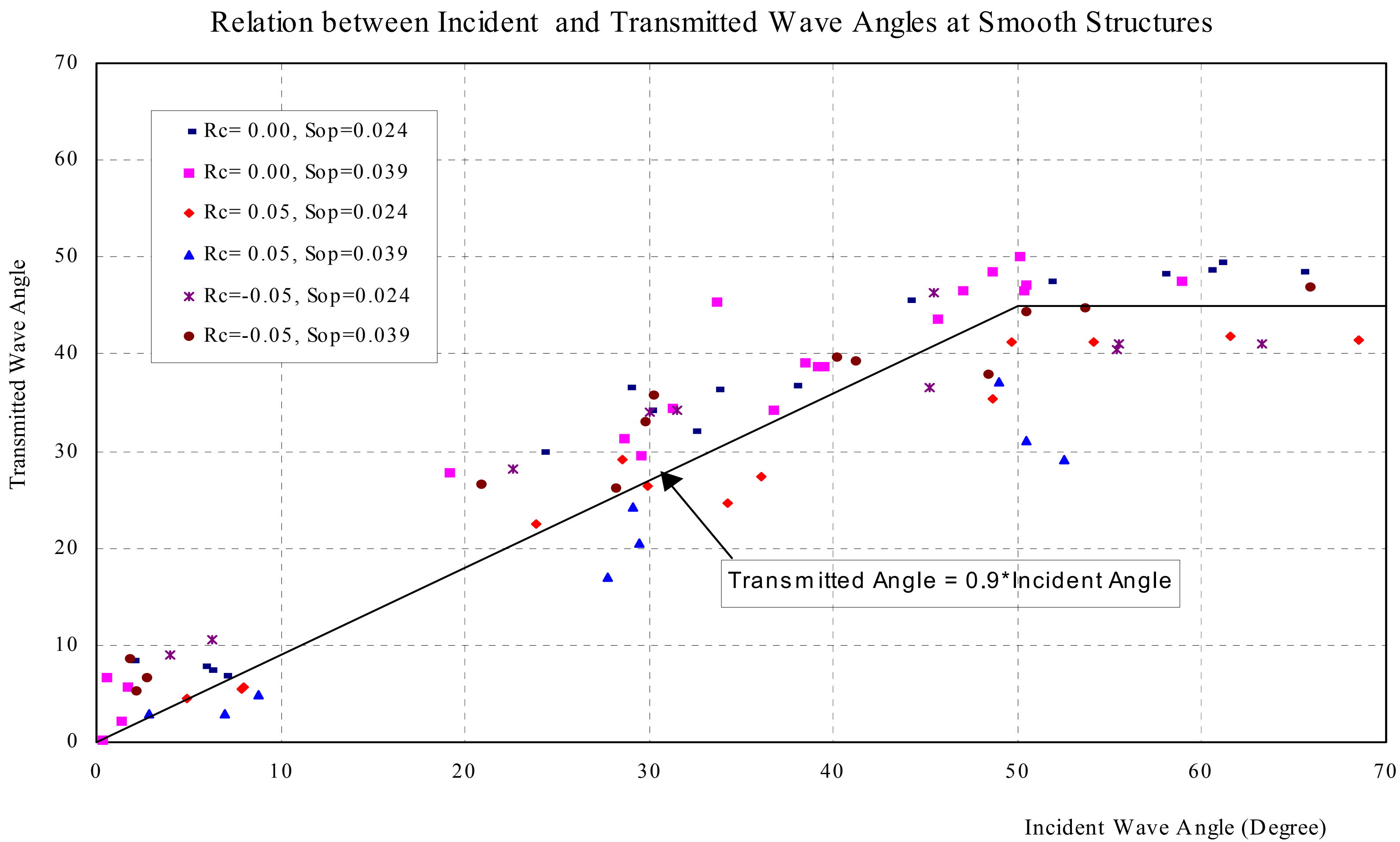
Relation between Incident and Transmitted Wave Angles at Smooth Structures
Transmitted Wave Angle
Incident Wave Angle (Degree)
Rc= 0.00, Sop=0.024
Rc= 0.00, Sop=0.039
Rc= 0.05, Sop=0.024
Rc= 0.05, Sop=0.039
Rc=-0.05, Sop=0.024
Rc=-0.05, Sop=0.039
Transmitted Angle = 0.9*Incident Angle
0
10
20
30
40
50
60
70

Figure C-19

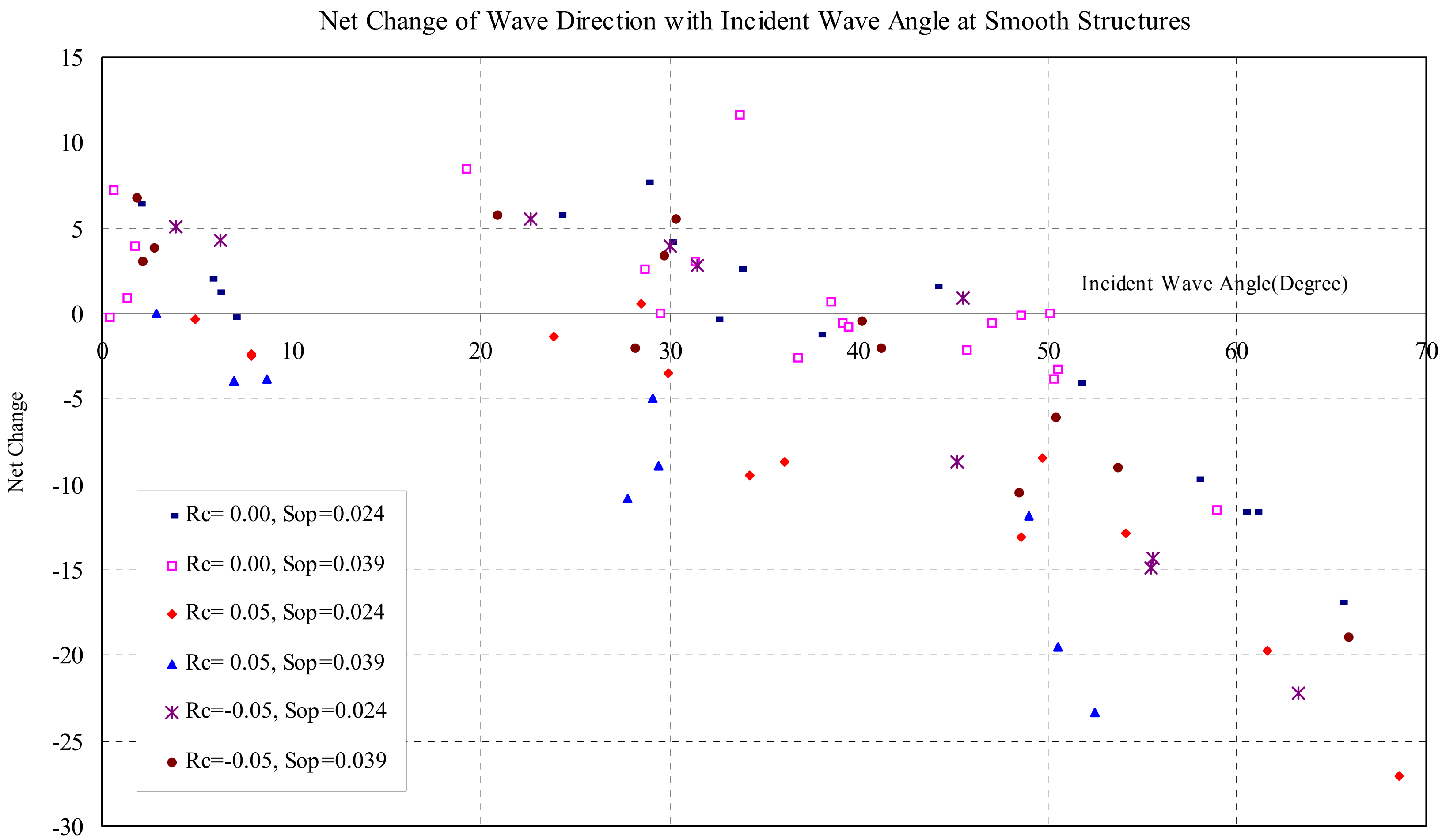
Net Change of Wave Direction with Incident Wave Angle at Smooth Structures
15
10
5
0
-5
-10
-15
-20
-25
-30
Net Change
0
10
20
30
40
50
60
70
Incident Wave Angle(Degree)
Rc= 0.00, Sop=0.024
Rc= 0.00, Sop=0.039
Rc= 0.05, Sop=0.024
Rc= 0.05, Sop=0.039
Rc=-0.05, Sop=0.024
Rc=-0.05, Sop=0.039

APPENDIX D

Figures for Chapter 6

Figure D-1

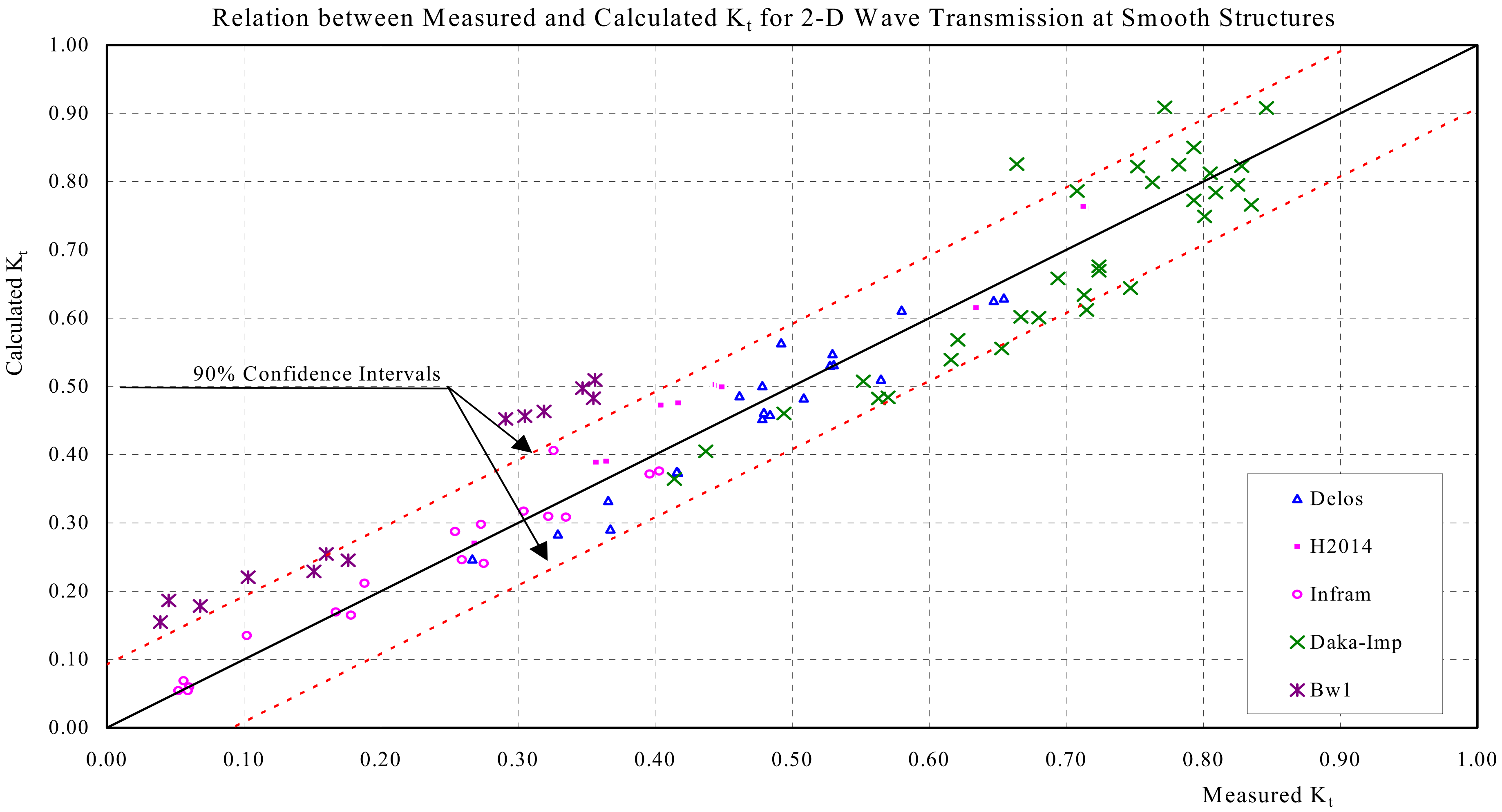

Relation between Measured and Calculated K_t for 2-D Wave Transmission at Smooth Structures
Calculated K_t
Measured K_t
90% Confidence Intervals
1.00
0.90
0.80
0.70
0.60
0.50
0.40
0.30
0.20
0.10
0.00
0.00
0.10
0.20
0.30
0.40
0.50
0.60
0.70
0.80
0.90
1.00
Delos
H2014
Infram
Daka-Imp
Bw1

Figure D-2

Relation between Measured and Calculated K_t for all Data at Smooth Structures

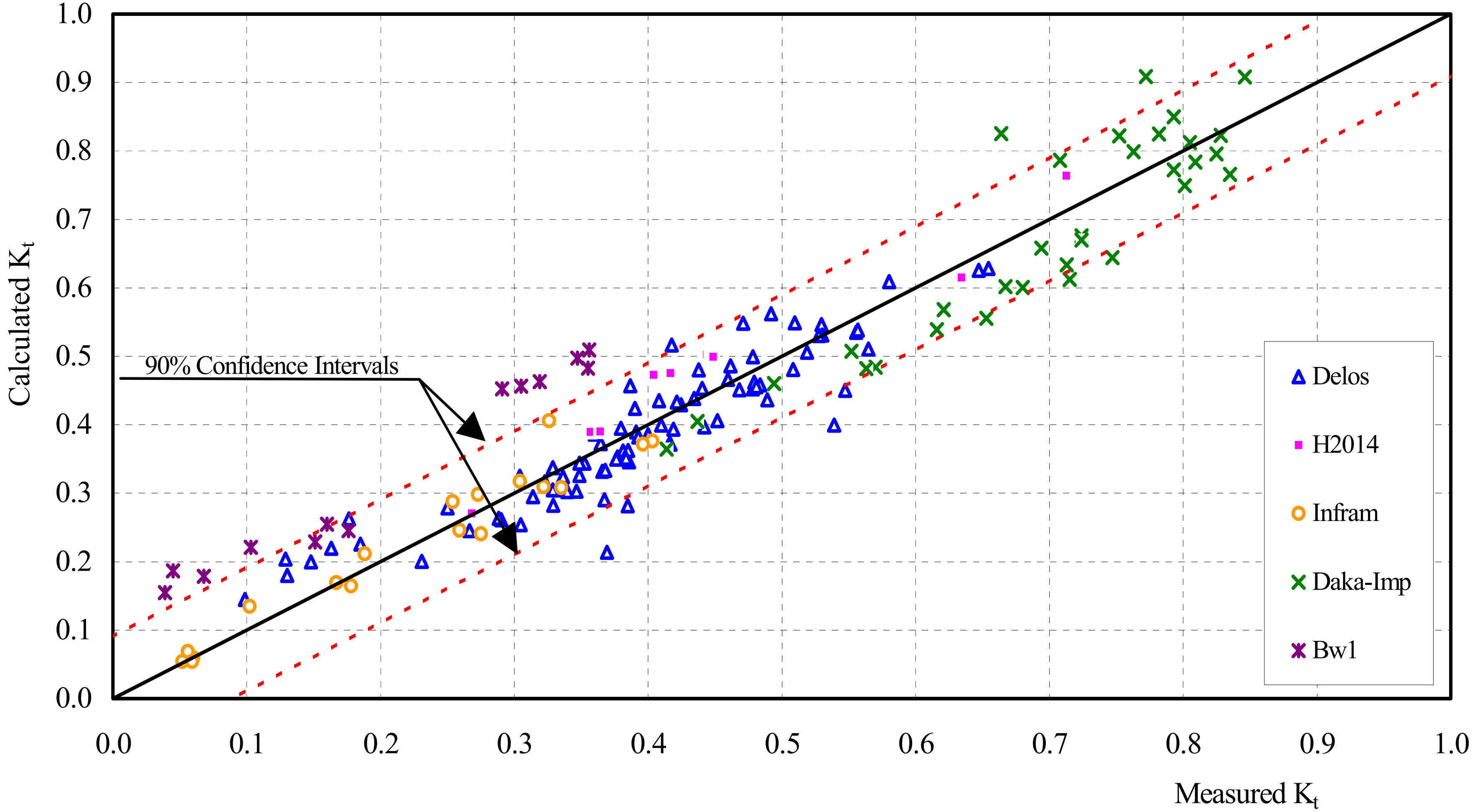

APPENDIX E

Figures for Chapter 7

Figure E-1

Relation between f_{pt}/f_{pi} and f_{pi} at Rubble Structures

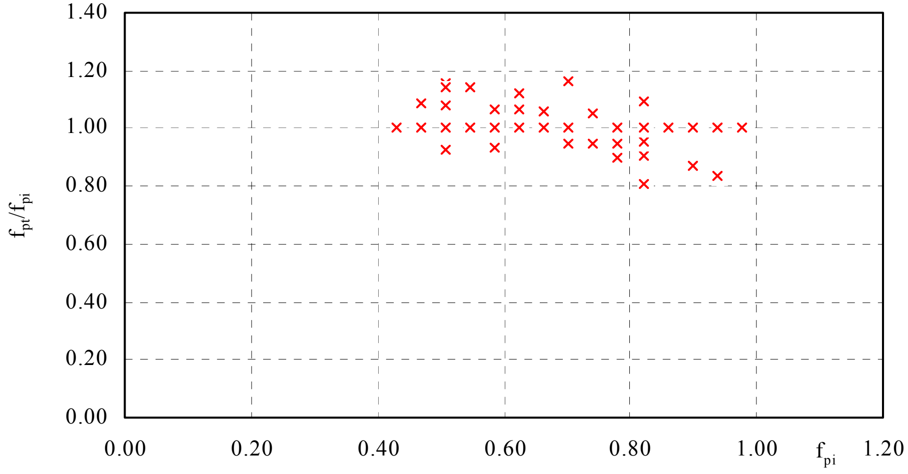

Figure E-2

Relation between f_{pt}/f_{pi} and K_t at Rubble Structures

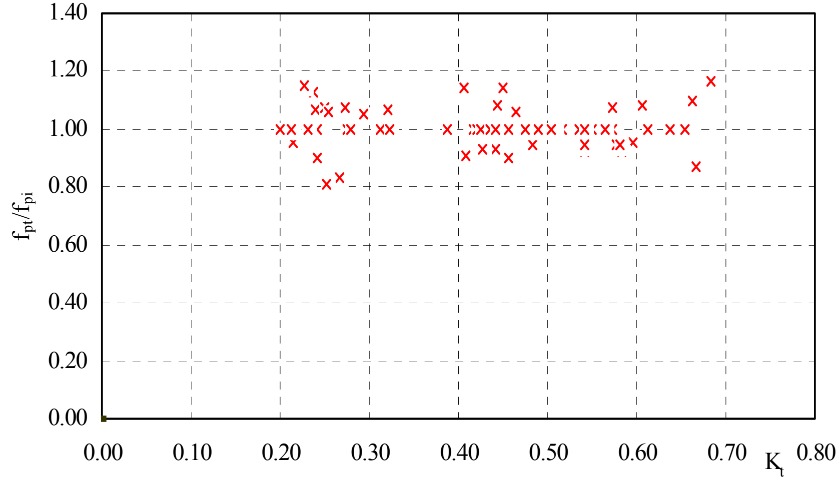

Figure E-3

Relation between f_{pt}/f_{pi} and s_{op} at Rubble Structures

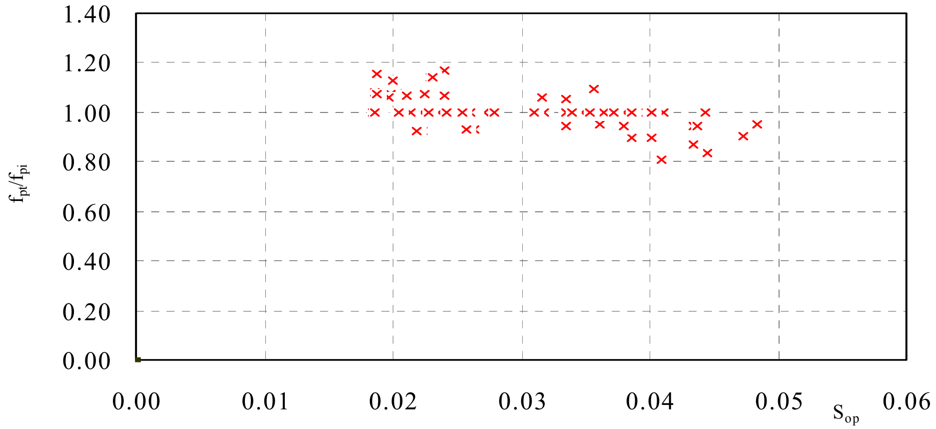

Figure E-4

Relation between f_{pt}/f_{pi} and f_{pi} at Smooth Structures

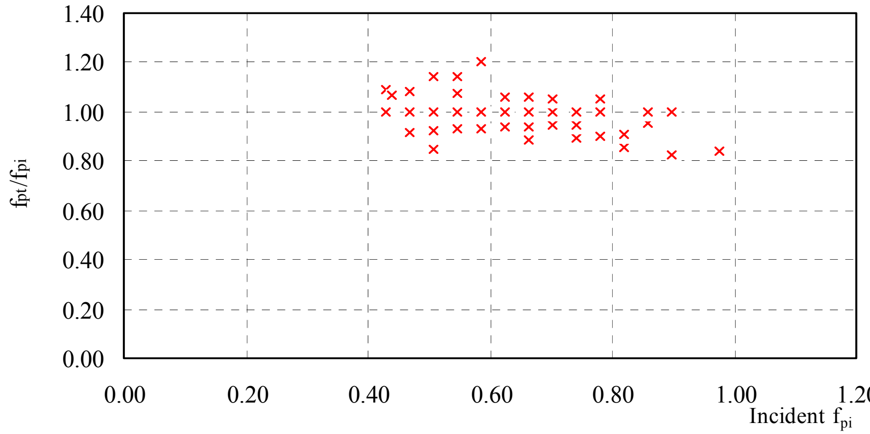

Figure E-5

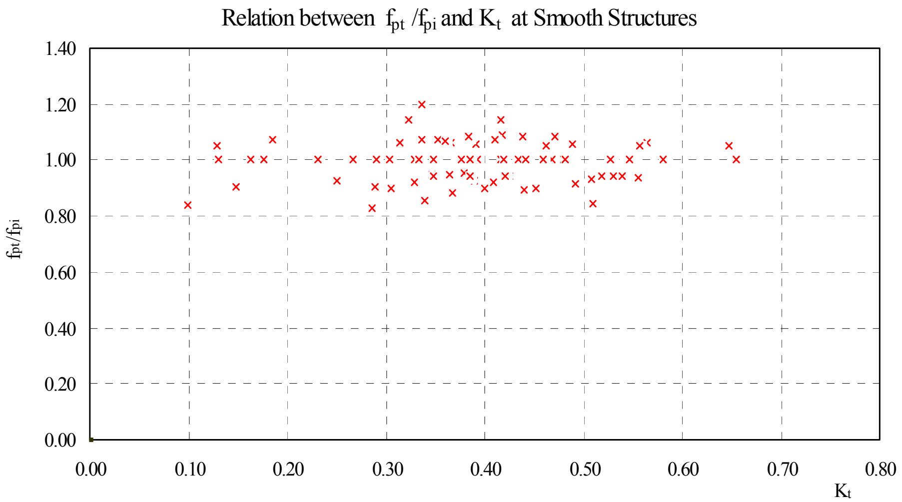

Figure E-6

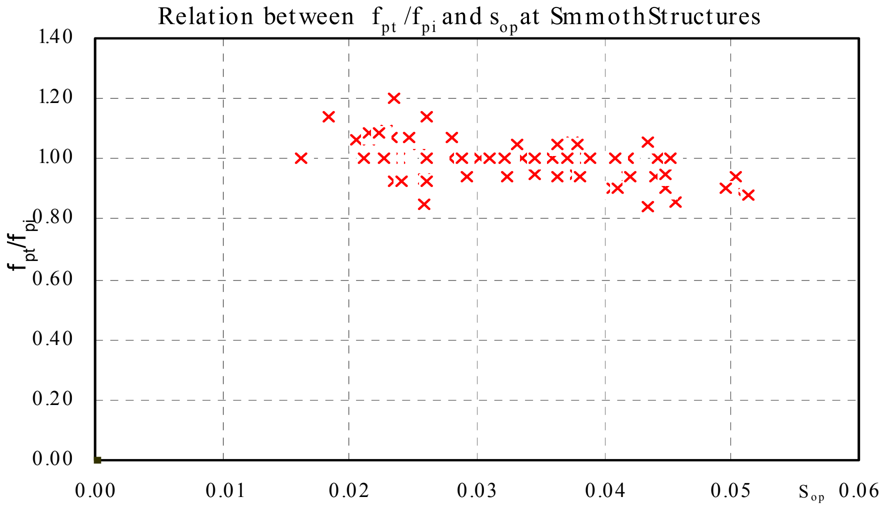

Figure E-7

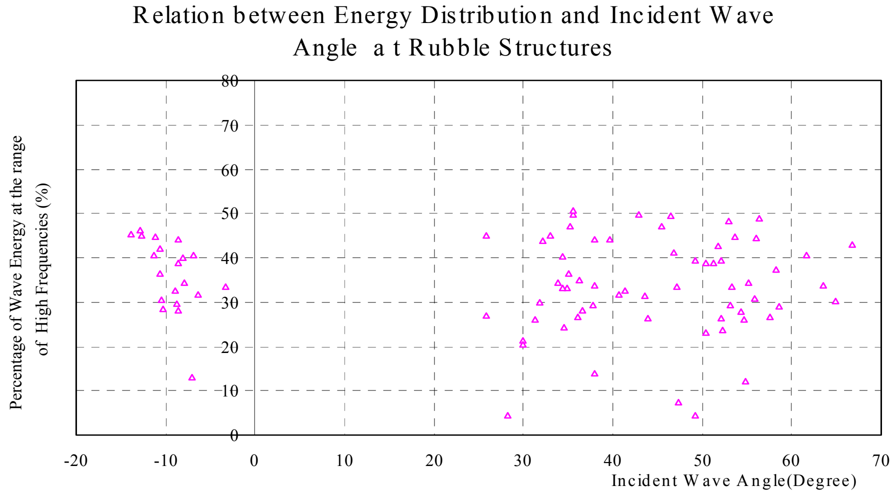

Figure E-8

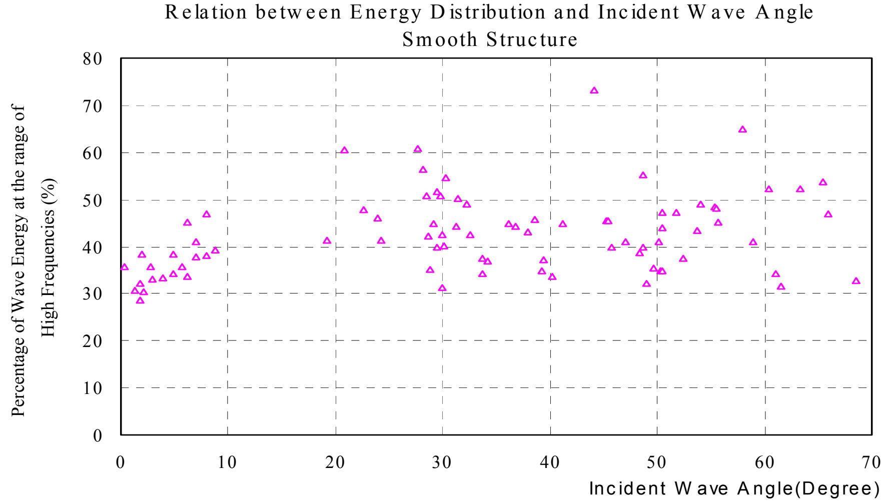

Figure E-9

Relation between f_{max}/fp and Incident Wave Angle at Rubble Structures

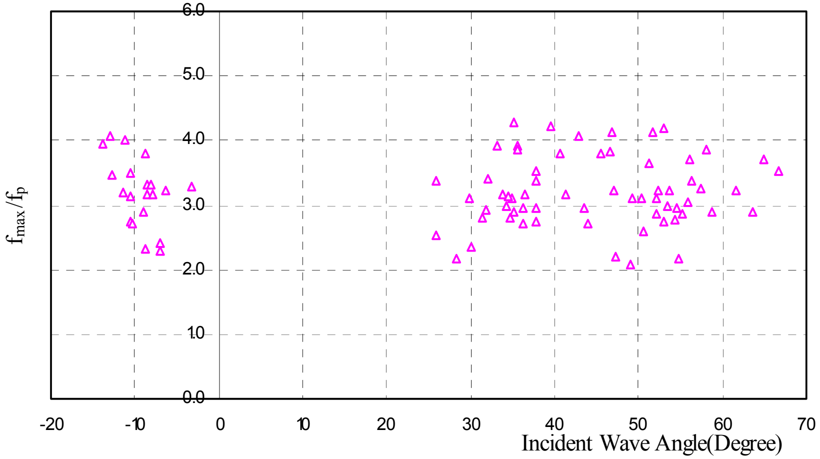

Figure E-10

Relation between f_{max}/fp and Incident Wave Angle at Smooth Structures

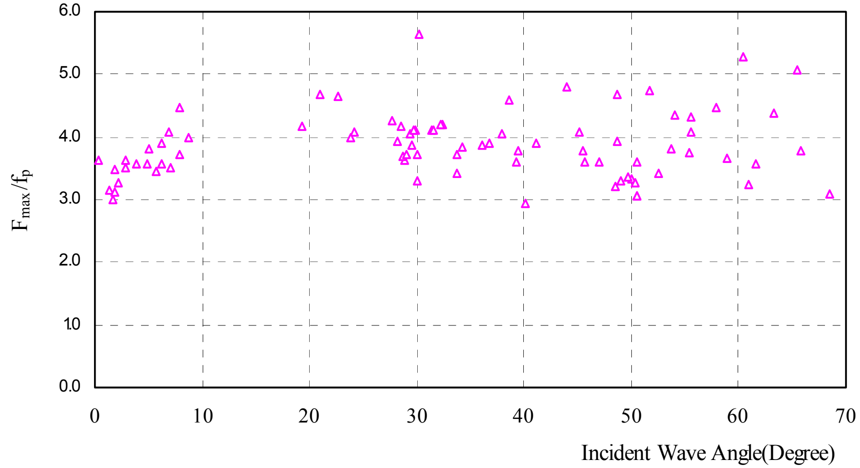

Figure E-11

f_{max}/f_p-R_c/Hi at Rubble Structures

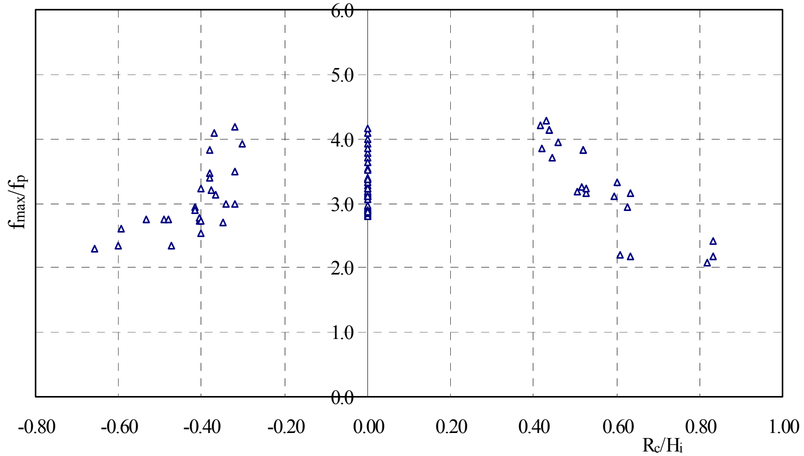

Figure E-12

f_{max}/f_p-R_c/H_i at Smooth Structures

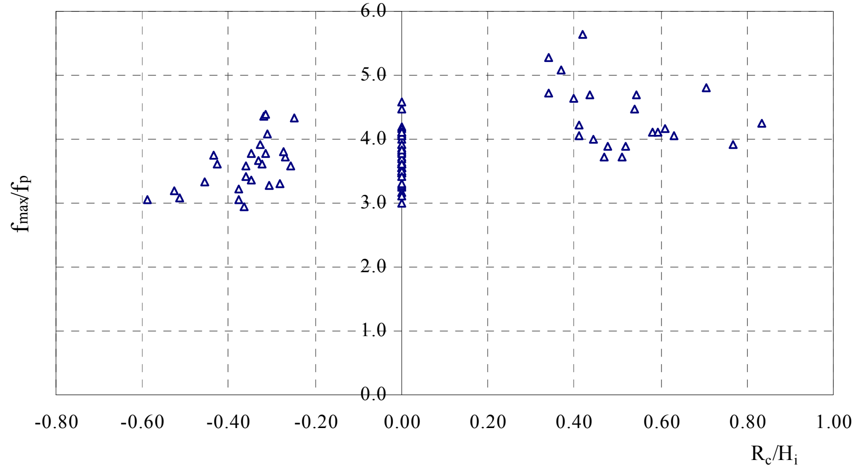

Figure E-13

Relation between s_{op} and Percentage of Total Energy at High Frequency Range for Rubble Structures

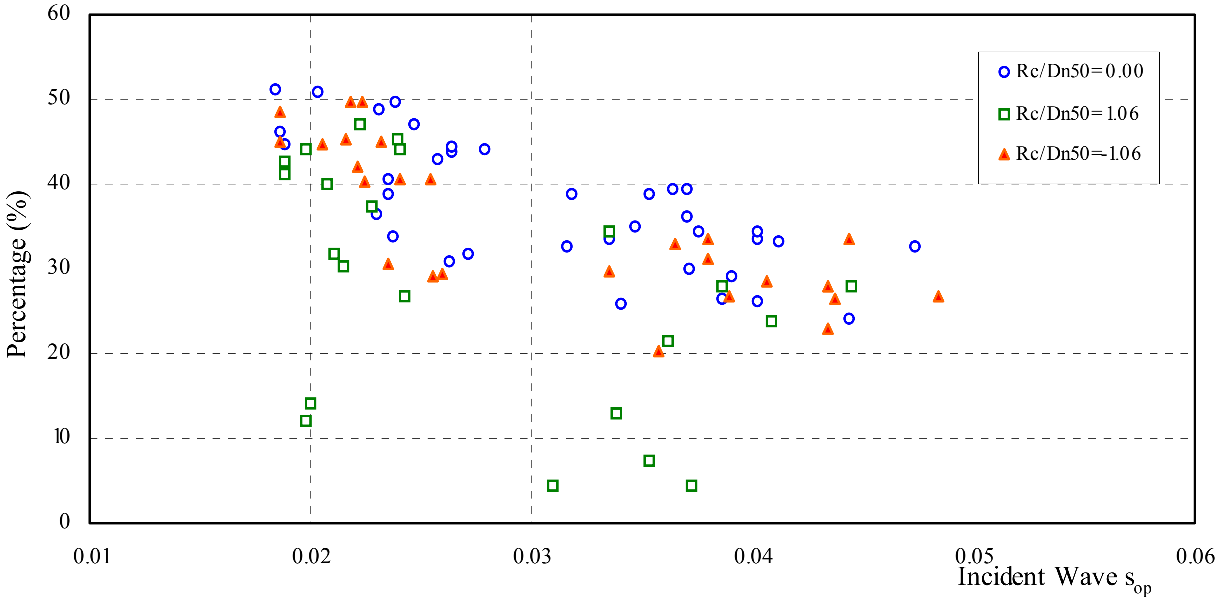

Figure E-14

Relation between K_t and Percentage of Total Energy at High Frequency Range for Smooth Structures